UNIVERSITY OF CALIFORNIA, SAN DIEGO

Biosynthesis of polybrominated aromatic molecules by marine bacteria

A dissertation submitted in partial satisfaction of the
requirements for the Degree Doctor of Philosophy

in

Marine Biology

by

Abrahim Abbas El Gamal

Committee in charge:

Professor Bradley S. Moore, Chair
Professor Lihini I. Aluwihare
Professor Peter C. Dorrestein
Professor Amro Hamdoun
Professor Chambers C. Hughes

2016

The dissertation of Abrahim Abbas El Gamal is approved, and it is acceptable in quality and form for publication on microfilm and electronically:

_____

_____

_____

_____

_____

Chair

University of California, San Diego

2016

Dedication

For nana

Table of Contents

Signature Page ..... **iii**

Dedication ..... **iv**

Table of Contents ..... **v**

List of Figures ..... **vi**

List of Tables ..... **x**

Acknowledgements ..... **xi**

Vita ..... **xiii**

Abstract of the Dissertation ..... **xiv**

Chapter 1: Introduction **1**

Chapter 2: Biosynthesis of polybrominated aromatic molecules by marine bacteria **25**

Chapter 3: Biosynthesis of coral settlement cue tetrabromopyrrole in marine bacteria by a uniquely adapted brominase-thioesterase enzyme pair **91**

Chapter 4: An alkylhydroperoxidase-like debrominase is an enzymatic switch in the biosynthesis of pentabromopseudilin **124**

Chapter 5: Opportunities in halopyrrole biosynthesis **170**

References **186**

List of Figures

Figure 1.1: Halogens matter. Examples of natural products whose biological is demonstrated to be influenced by halogenations..…….. **2**
Figure 1.2: Schematic for MCD assay for detection of electrophilic halogen species. …. **5**
Figure 1.3: Representative diversity of halogenated natural products..…….. **7**
Figure 1.4: Flavin-dependent halogenases...……...…… **9**
Figure 1.5: Mechanistic proposal for halogenation-mediated atropo-selective N-C coupling in the biosynthesis of Marinopyrrole A..…….…….. **17**
Figure 1.7: A modular polybrominated pyrrole/phenol (Bmp) biosynthetic pathway from marine bacteria..…… **18**
Figure 1.8: A modular polybrominated pyrrole/phenol (Bmp) biosynthetic pathway from marine bacteria..…… **20**
Figure 1.9: A dehalogenase switch in pentabromopseudilin biosynthesis..……. **22**
Figure 1.10: A metagenomics approach toward elucidation of pyrrole-imidazole alkaloid biosynthesis..……. **24**
Figure 2.1: Structures and sources of marine polybrominated natural products..…… **27**
Figure 2.2: Genetic basis of the Bmp pathway..……... **28**
Figure 2.3: In vitro reconstitution of activity for brominase Bmp2..…… **28**
Figure 2.4: Biosynthesis of bromophenols by flavin-dependent decarboxylase-brominase Bmp5..……... **29**
Figure 2.5: Enzymatic synthesis of polybrominated biphenyls and OH-BDEs…… **30**
Figure 2.6: Bi-modular scheme for the biosynthesis of polybrominated marine natural products by the bmp pathway..……. **31**
Supplementary Figure 2.1: Production of signature polybrominated molecules 1–3 by marine bacteria…….. **45**
Supplementary Figure 2.2: High-resolution mass spectra for selected polybrominated metabolites from an organic extract of *P. luteoviolacea* 2ta16……..……. **46**
Supplementary Figure 2.3: Chemical logic for the biosynthesis of halogenated pyrrole moieties in natural products…….. **47**
Supplementary Figure 2.4: pGAL-*bmp1–7* yeast/*E. coli* shuttle vector……... **48**
Supplementary Figure 2.5: Chemotype for bmp7 deletion. 49
Supplementary Figure 2.6: Plasmids for co-expression of *bmp1* with *bmp3*…….... **50**
Supplementary Figure 2.7: MS2 product ions corresponding to phosphopantetheine, phosphopantetheine acylated with pyrrole, and subsequent brominated states of the pyrrole……... **51**
Supplementary Figure 2.8: Enzymatic synthesis of pyrrolyl-*S*-Bmp1(ACP) by Bmp3 and Bmp4……. **52**
Supplementary Figure 2.9: ^{1}H NMR spectrum for 16…….. **54**
Supplementary Figure 2.10: Hydrolysis of model esterase substrate *p*-nitrophenyl acetate (pNPA) by Bmp1(TE)……... **55**
Supplementary Figure 2.11: Chemotype for heterologous expression of *bmp1–7* omitting bmp8……. **56**
Supplementary Figure 2.12: Spectral characteristics of CYP450 Bmp7 and spectrophotometric determination of substrate tolerance……. **57**

Supplementary Figure 2.13: *In vitro* Bmp7 reaction products with 6 (black, top curve) and 7 (bottom, red curve) as substrates……. **58**
Supplementary Figure 2.14: Characterization of 2 generated by Bmp7 *in vitro* reaction with 6 as a substrate…….. **59**
Supplementary Figure 2.15: Characterization of 7 generated by Bmp7 *in vitro* reaction with 6 as a substrate…….. **61**
Supplementary Figure 2.16: Purification of recombinant Bmp5 and time course for the change in concentrations of the substrate, intermediate and product species as shown in Fig. 4a……..… **62**
Supplementary Figure 2.17: Mass spectra for 8 and 4, and in vivo production of 4 and 5 by Bmp5…… **63**
Supplementary Figure 2.18: Negative control reactions demonstrate the requirement of KBr and NADPH for catalysis by Bmp5…….. **64**
Supplementary Figure 2.19: Comparison of retention times and NMR spectra of polybrominated biphenyl products 1 and 10 generated by Bmp7 *in vitro* with authentic synthetic standards…… **65**
Supplementary Figure 2.20: Mass spectrometric analysis of the polybrominated biphenyls, and OH-BDE products generated by Bmp7……..…….. **67**
Supplementary Figure 2.21: ^{1}H NMR spectrum for 11…… **68**
Supplementary Figure 2.22: Identification of 2′-OH-BDE-68 (13) as a reaction product generated by Bmp7……... **69**
Supplementary Figure 2.23: HPLC detection of products generated by Bmp7 using 5 as a substrate…… **70**
Supplementary Figure 2.24: MS and MS/MS profiles for 14, produced enzymatically by reaction of Bmp7 with 5……... **71**
Supplementary Figure 2.25: Mass spectrometric analysis of the biphenyl and hydroxylated diphenyl ether products formed by Bmp7 reaction with 17……... **72**
Supplementary Figure 2.26: Characterization of 3 generated by Bmp7 in an *in vitro* reaction with 4 and 6 as substrates…… **73**
Supplementary Figure 2.27: Characterization of 15 generated by Bmp7 in an in vitro reaction with 4 and 6 as substrates……..... **75**
Supplementary Figure 2.28: Production of iodinated bromophenols by heterologous host E. coli expressing bmp1–8 grown in the presence of KI…….. **77**
Supplementary Figure 2.29: Mass spectrometry based characterization of a polybrominated phenol-pyrrole ether product generated by Bmp7 […]…….. **79**
Supplementary Figure 2.30. Primary sequence analysis identifies Bmp5 to be homologous to flavin-dependent monooxygenases. Primary sequence of Bmp5 was provided as an input to the NCBI BLAST program and analyzed against the 'Non-reduntant protein sequence (nr)' dataset. All homologs of Bmp5 […]…… **81**
Figure 3.1: Structures and biosynthesis of halopyrrole natural products……. **93**
Figure 3.2: A genetic basis for production of 1…… **93**
Figure 3.3: Enzymatic synthesis of 1…… **94**
Figure 3.4: Preparation of 8 and *in vitro* conversion to 1 by Bmp2 and Bmp1(TE)…..... **94**
Figure 3.5: Scheme for bromination-dependent pyrrole offloading and decarboxylation……. **95**

Figure 3.6: Structural basis for tetrahalogenation activity of Bmp2…… **96**
Figure S3.1: LC/MS comparisons of *in vivo* and *in vitro* EICSs to those of authentic standards of 1, 6, and 7…….. **105**
Figure S3.2: Confirmation of CoA extension and loading of pyrrole substrates onto ACPs…….. **106**
Figure S3.3: Bioinformatic identification and *in vitro* confirmation of catalytic Ser202 of Mm_Bmp1(TE) with a model chromogenic substrate, p-nitrophenyl acetate (pNPA). A. […]……. **107**
Figure S3.4: Non-enzymatic hydrolysis of proposed ACP-bound tetrabrominated intermediate yields 1…….. **108**
Figure S3.5: Interrogation of the potential of 2,3,4-tribromopyrrole 6 and 7 to serve as intermediates in the biosynthesis of 1…… **109**
Figure S3.6: Reductive debromination of 1 by NADPH yields 6…….. **110**
Figure S3.7: FAD-bound holo structures of pyrrolyl-*S*-ACP flavin-dependent halogenases from this study…… **111**
Figure S3.8: Lack of chlorination activity for Bmp2-TM…….. **112**
Figure S3.9: *In vivo* coexpression of *Mm_bmp1*, *Mm_bmp3*, and *Mm_bmp4* with wildtype *Mm_bmp2* (*Mm_bmp2-wt*) or *Mm_bmp2* triple mutant (*Mm_bmp2-TM*)…….. **113**
Figure S3.10: ^{1}H NMR spectrum of 1 ($CDCl_3$, 500 MHz)…… **114**
Figure S3.:11: ^{1}H NMR spectrum of 7 ($CDCl_3$, 500 MHz)…… **114**
Figure S3.12: ^{13}C NMR spectrum of 7 ($CDCl_3$, 125 MHz)…… **115**
Figure S3.13. Scheme for the synthesis of 9…….. **115**
Figure S3.14: ^{1}H NMR spectrum of Boc-protected S1 ($CDCl_3$, 500 MHz)…….. **116**
Figure S3.15: ^{1}H NMR spectrum of 9 (d_6-DMSO, 500 MHz)…….. **116**
Figure S3.16: ^{13}C NMR spectrum of 9 (d_6-DMSO, 150 MHz)…….. **117**
Figure S3.17: DQF-COSY spectrum of 9 (d_6-DMSO, 600 MHz)…….. **117**
Figure S3.18: HSQC spectrum of 9 (d_6-DMSO, 600 MHz)…….. **118**
Figure S3.19: HMBC spectrum of 9 (d_6-DMSO, 600 MHz)…….. **118**
Figure S3.20: Sequence alignments of Bmp2 homologs…… **119**
Figure 4.1: Bmp biosynthetic pathway…… **127**
Figure 4.2: Debromination of bromopyrroles by Bmp8…….. **130**
Figure 4.3: Redox state of Bmp8-CXXC…….. **133**
Figure 4.4: Biochemical interrogation of Bmp8-CXXC…….. **138**
Figure 4.5: Biochemical interrogation of the conserved CXYCXXH of Mm_Bmp8 and a distant homolog 2ta16_Bmp8-H…… **140**
Figure 4.6: Bmp8 mechanistic proposal…….. **142**
Figure S4.1: Affinity purification of N-His6-Bmp8 by co-expression with Bmp1(TE), and cleavage of N-His6 affinity tag…….. **154**
Figure S4.2: Dechlorination of 2,3,4,5-tetrachloropyrrole catalyzed by Bmp8……. **155**
Figure S4.3: Bmp8 homologs from (meta)genomic datasets…….. **156**
Figure S4.4: Bmp8-CXXC is reduced in enzyme as-purified…… **157**
Figure S4.5: Conserved Bmp8 Cys57 and Cys163 do not play a direct role in Bmp8 reaction mechanism…… **158**

Figure S4.6: Whole-protein mass spectra for wildtype Bmp8 and Bmp8 Cys to Ala mutants under various conditions……... **159**
Fig. S4.7: A distant Bmp8 homolog from *P. luteovioalcea* 2ta16, 2ta16_Bmp-H……. **160**
Fig. S4.8: Functional characterization for Bmp8 homologs from Bmp pathways harbored by two additional marine bacteria……... **160**
Figure S4.9: Bmp8 selectively debrominates a differentially halogenated pyrrole substrate…….. **161**
Figure S4.10: Mass spectra for Bmp8 products…….. **162**
Figure S4.12: Regeneration of Bmp8…….…… **163**
Figure S4.13: Oxygen sensitivity of Bmp8……. **164**
Figure S4.14: Reductive dehalogenation of tetrabromopyrrole (Br4Py, 3) by Bmp8 […] ……. **165**
Figure S4.15: Non-enzymatic aqueous reductive dehalogenation of tetrabromopyrrole (Br4Py, 3) by reducing agents…… **166**
Figure S4.16: Whole-protein mass spectrometry of Bmp8-C82A with other halogenated pyrrole substrates…… **167**
Figure 5.1: Packing a punch with parsimony. Complex PIAs are thought to arise from universal achiral building blocks…… **172**
Figure 5.2: Palau'amine: simplicity in complexity. As per biosynthetic proposal, clathrodin moiety (red) and clathrodin sub-unit 3-amino-1-(2-amino imidazolyl) prop-1-ene moiety (green)…….. **173**
Figure 5.3: Scheme for metagenomic approach for elucidation of PIA biosynthesis… **174**
Figure 5.4: Chemical diversity of *S. massa*. Representative structure of alkaloids furnished by extracts of the sponge *S. massa*……. **176**
Figure 5.5: LC-MS validation of production of oroidin and cylcooroidin compounds from *S. massa* collected in Guam…… **177**
Figure 5.6: Comparison of phylum-level prokaryotic diversity of *A. tubulata* and *S. massa*…….. **178**
Figure 5.7: Return of the halopyrrole biosynthetic handle……. **179**
Figure 5.8: Phylogeny of putative *A. tubulata* pyrrole halogenase……. **180**
Figure 5.9: Putative "PIA" cluster from the *A. tubulata metagenome*…… **182**

List of Tables

Supplementary Table 2.1: High-resolution MS used for determination of molecular formulae of polybrominated metabolites from extract of *P. luteoviolacea* 2ta16.... **83**
Supplementary Table 2.2: *P. luteoviolacea* 2ta16 bmp gene cluster annotation…….. **84**
Supplementary Table 2.3: Primers used to generate overlapping fragments for yeast assembly of yeast/E. coli shuttle vector pGAL-bmp1–7…….. **85**
Supplementary Table 2.4: Primers used to generate gene deletions from pETDuet-bmp. ……... **86**
Supplementary Table 2.5: Co-transformations of E. coli BL21(DE3) for heterologous expression of bmp cluster and derivatives…… **87**
Table S3.1: Bmp homology…… **120**
Table S3.2. Data collection and refinement statistics for Mpy16, Bmp2, and Bmp2-TM structures……. **121**
Table S4.1. Mass shift calculation from whole-protein mass spectrometry analysis…. **164**

Acknowledgements

Many thanks to my advisor Bradley S. Moore, for taking me on as a Ph.D. student and providing me with a rigorous and forgiving environment in which to grow as a researcher, mentor, and person. Many thanks to Kazuya Yamanaka who was my first teacher of molecular biology in the laboratory and who provided me with the foundations and tools to become an independent researcher. Many thanks to Vinayak Agarwal who was my first teach in biochemistry in the laboratory, and with whom I have enjoyed a close and productive collaboration for the major part of my Ph.D. Bradley Moore, Kazuya Yamanaka, and Vinayak Agarwal have truly lead by example with their patience and remarkable mentoring skills, and have made this Ph.D. an enriching, stimulating, and worthwhile experience.

Chapter 2, in full, is a reprint of materials as it appears in "Biosynthesis of polybrominated aromatic molecules by marine bacteria" in *Nature Chemical Biology*, 2014, Agarwal V., El Gamal A., Yamanaka K., Poth D., Kersten R. D., Schorn M., Allen E. E., and Moore, B. S., The dissertation author was one of two equally contributing primary investigators and authors of this paper.

Chapter 3, in full, is a reprint of materials as it appears in "Biosynthesis of a coral chemical cue tetrabromopyrrole in marine bacteria by a uniquely adapted brominase-thioesterase enzyme pair" in *Proceedings of the National Academy of Sciences U.S.A.*, 2016. El Gamal A., Agarwal V., Diethelm S., Rahman I., Schorn M., Sneed J.M., Louie G.V., Whalen, K.E., Mincer T.J., Noel J.P., Paul V.J., and Moore B.S. The dissertation author was one of two equally contributing primary investigators and authors of this paper.

Chapter 4, in full, is currently being prepared for submission of the material. El Gamal A., Agarwal V., Rahman I., and Moore B.S. The dissertation author is the primary investigator and author of this paper.

Vita

2011 – 2016 Ph.D., University of California, San Diego

2009 – 2011 M.S., Stanford University

2005 – 2009 B.S., Stanford University

Publications

2016 El Gamal A., Agarwal V., Rahman I., and Moore B.S. An akylpoeroxidase-like reductive dehalogenase is an enzymatic switch in the biosynthesis of polybrominated pyrroles by marine bacteria. *In preparation*.

El Gamal A., Agarwal V., Diethelm S., Rahman I., Schorn M., Sneed J.M., Louie G.V., Whalen, K.E., Mincer T.J., Noel J.P., Paul V.J., and Moore B.S. Biosynthesis of a coral chemical cue tetrabromopyrrole in marine bacteria by a uniquely adapted brominase-thioesterase enzyme pair. *Proceedings of the National Academy of Sciences, U.S.A.* Online 21 March 2016, doi: 10.1073/pnas.1519695113.

Harvey E.L., Deering R.W., Rowley D.C., El Gamal A., Schorn M., Moore B.S., Johnson M.D., Mincer T.J., and Whalen K.E. A bacterial quorum-sensing precursor induced mortality in the Marine Coccolithophore, *Emiliana huxleyi*. *Frontiers in Microbiology*. 7(Art. 59), 2016.

2014 Agarwal V., El Gamal A., Yamanaka K., Poth D., Kersten R. D., Schorn M., Allen E. E., and Moore, B. S. Biosynthesis of polybrominated aromatic organic compounds by marine bacteria. *Nature Chemical Biology*. 10(8): 640-647, 2014.

Abstract of the Dissertation

Biosynthesis of polybrominated aromatic molecules by marine bacteria

by

Abrahim Abbas El Gamal

Doctor of Philosophy in Marine Biology

University of California, San Diego, 2016

Professor Bradley S. Moore, Chair

Nature produces a plethora of bioactive secondary metabolites with diverse hydrocarbon scaffolds and bioactivities. These natural products serve as signaling and defense molecules in their physiological settings, and as inspiration for therapeutics in the clinic. Natural product scaffolds are elaborated with functional groups that influence their biological activities. One such chemical functionality found in thousands of natural product molecules is halogenation. Reflective of the structural diversity of halogenated natural products (halometabolites), biology has evolved an equally diverse set of enzyme catalysts using numerous strategies for activating halides for addition onto various oxidation states of carbon. The last two decades have witnessed a renaissance in the discovery of mechanistically diverse halogenating

enzymes due to the unprecedented opportunity to study them in the context of halometabolite biosynthetic pathways afforded by advancements in nucleic acid sequencing technologies and computational biology. Despite the fact that the majority of halometabolites are brominated compounds derived from the marine environment, the majority of halogenting enzymes characterized to date are involved in chlorination of terrestrial microbial metabolites. Chapter 2 of this thesis describes the biosynthesis of the highly brominated pyrrole-phenol marine bacterial metabolite pentabromopseudilin by the brominated marine pyrrole/phenol (Bmp) biosynthetic pathway, which revealed the first two examples of brominating enzymes—pyrrole and phenol halogenases—from a confirmed biosynthetic context. Chapter 3 provides an in-depth investigation of regiopromiscuous pyrrole halogenase Bmp2 in contrast to canonical regioselective pyrrole chlorinases. In addition to enzymes involved in the addition of halogen atoms to the aromatic building blocks, the Bmp pathway was found to contain a dehalogenating enzyme (Bmp8) that partially undoes the work of the Bmp2 to allow a free bromopyrrole moiety to participate in the final step of pentabromopseudilin biosynthesis. Chapter 4 describes the activity and mechanism of Bmp8 as the first example of a dehalogenating tailoring enzyme from the confirmed context of a halometabolite biosynthetic pathway. Chapter 5 of this thesis concludes with an exploration of additional opportunities in the study of natural products containing halogenated pyrrole moieties, describing a strategy for the elucidation of the biosynthesis of the bioactive pyrrole-imidazole alkaloid class of sponge secondary metabolites.

Chapter 1: Introduction

1.1 Halogenated natural products: questions and opportunities

Nature synthesizes a remarkable diversity of bioactive halogenated organic compounds ranging from simple aliphatic and aromatic molecules to complex terpenoids, polyketides, oligopeptides, and alkaloids[1,2]. Halogenation is of critical importance to the bioactivities of natural products used in the clinic, under clinical trial, and in their native physiological contexts[3-6]. For example, the "antibiotic of last resort" vancomycin exhibits a drop to 70% of its activity against a model strain of *Bacillus subtilis* following the removal of one of the two chlorines decorating its glycopeptide core, and a 50% reduction in activity when both chlorines are eliminated (**Fig. 1.1**)[4]. In a natural physiological context, tetraiodinated thyroid hormone (T_4), a modulator of mammalian metabolism, is activated upon enzymatic deiodination to T_3, and is rendered inactive by a second round of enzymatic deiodination[7]. Halogenation plays a direct role in the mechanism of action of the γ-lactam-β-lactone natural product salinosporamide A in clinical trial for the treatment of cancer, which forms a covalent adduct with the active site threonine residue of the 20S proteasome facilitated by a chlorine leaving group[6,8]. In addition to halogenation, halogen identity also affects the potency of halogenated natural products. For example, replacing the two chlorines of balhimycin, a differently glycosylated variant of vancomycin, to bromines profoundly alters its antimicrobial profile[5]. Furthermore, fluorination, while exceedingly rare in biology is a well-proven strategy for increasing the efficacy of pharmaceuticals[9,10].

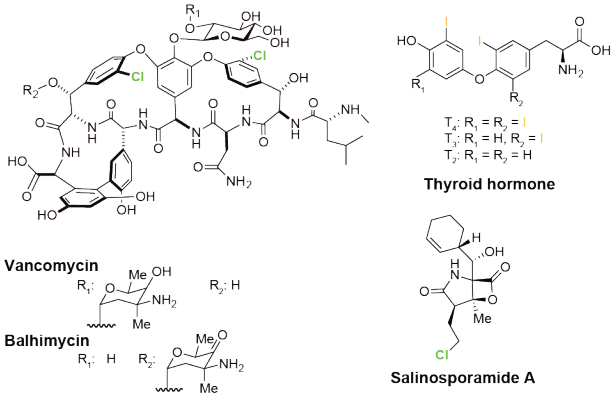

Figure 1.1: Halogens matter. Examples of natural products whose biological is demonstrated to be influenced by halogenations.

Despite the wealth of halogenated natural products discovered to date (>4,000 compounds) and their recognized importance as potential therapeutic agents, an understanding of the biosynthesis of these compounds has lagged behind their discovery largely because relatively few biosynthetic gene loci encoding their biosyntheses have been identified and characterized. However, with the rapid growth in genetic information made available by advancements in nucleic acid sequencing, along with the development of increasingly sophisticated tools to interpret this genetic information, understanding of bacterial natural product biosynthesis is on an unprecedented upswing[11,12]. Paralleling the structural diversity of organohalogen natural products, the study of their biosynthesis has, in short order, revealed an equally diverse array of halogenation biocatalysts[13-15]. Unlike traditional synthetic approaches for halogenation that utilize harsh conditions, and often add halogens in a non-regioselective manner, halogenation enzyme catalysts operate in aqueous solution under ambient conditions and can be highly regioselective, and even halogen specific[16,17].

From the discovery of the earliest halogenation biocatalyst, a promiscuous fungal chloroperoxidase (CPO) fifty years ago, to the more recent discovery of exquisitely O_2-dependent halogenases over thirty years later, halogenation biocatalysts have been enthusiastically explored for their potential biotechnological applications through extensive study of their substrate scope and the scalability of the reactions they catalyze[18,19]. An additional lesser-explored area of biotechnological interest from both the perspectives of synthetic chemistry and bioremediation of organohalogen pollutants, is the discovery of novel biocatalysts that perform dehalogenation either in the context of biosynthetic tailoring enzymes, or from the degradation pathways of natural organohalogens[20-22]. This chapter will provide a brief overview of the state of the art of understanding of organohalogen biosynthesis with an emphasis on the questions and opportunities arising from the study of enzymatic transformations involving halogens from within biosynthetic contexts, and concluding with motivations for the study of the biosynthesis of polybrominated aromatic molecules by marine bacteria that is the subject of this thesis.

1.2 The inorganic halogen pool

Halogens are biologically available in the environment as halides (Cl^-, Br^-, F^-, and I^-). The majority of organohalogen natural products are brominated or chlorinated with fewer examples of iodinated compounds, and even rarer examples of fluorinated compounds[2]. While chlorination is represented in both marine and terrestrial environments, bromination is almost exclusively a feature of marine natural products due to the relatively high bioavailability of bromide in seawater[2,23]. Remarkably, despite the fact that brominated natural products outnumber their chlorinated

counterparts, chloride occurs in seawater at a concentration nearly three orders of magnitude greater than that of bromide, hinting at the predominance of oxidative strategies in organohalogen natural product biosynthesis as bromide is more readily oxidized than chloride[15,24]. Moreover, biological fluorination is exceedingly rare despite the great natural abundance fluorine likely due to the extreme electronegativity of fluorine[24]. On the other hand, the scarcity of organoiodine natural products (~110 reported), that still outnumber their organofluorine counterparts by over tenfold, is explained by the extremely low natural availability of iodide rather than redox potential[10,24,25]. In line with the widespread distribution of natural organohalogens, emerging studies have suggested a native role for microbial dehalogenation as part of a biogeochemical halogen cycle in marine and terrestrial environments[20-22]. However, in contrast to the abundance of reported halogenated natural products, the biochemical transformations leading to their natural formation and degradation remain largely unexplored, providing a vast untapped source of novel biocatalysts.

1.3 Biological halogenation strategies: as diverse as the scaffolds they modify

The first halogenating biocatalyst reported nearly fifty years ago was an H_2O_2/ heme-dependent chloroperoxidase (CPO) secreted from the terrestrial fungus *Caldariomyces fumago*, and implicated in the biosynthesis of halogenated cylclopentanediol fungal halometabolite caldariomycin[26-28]. CPO has since been thoroughly studied and even marketed as an electrophilic halogenating reagent with broad substrate specificty[29]. The initial characterization of CPO introduced a spectrophotometric assay to monitor electrophilic halogenation activity utilizing a

chromophoric analog of caldariomycin, monochlorodimedone (MCD), that exhibits a loss in absorption at 277 nm following electrophilic halogenation[26]. The MCD assay relies on the ability of a candidate enzyme to oxidize a halide substrate (X^-: Cl^-, Br^-, and I^-) to form a diffusable hypohalite species (i.e., utilizing an oxidative 'X^+' strategy), and hence inherently selects for promiscuous oxidative halogenation enzyme catalysts (**Fig. 1.2**)[30]. Utilizing the MCD assay, numerous haloperoxidases were discovered, including an additional class of vanadium-dependent haloperoxidases found in seaweeds some twenty years after the initial report of the first CPO[31].

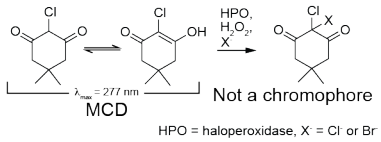

Figure 1.2: Schematic for MCD assay for detection of electrophilic halogen species. The MCD assay monitors a decrease in the absorbance at 277 nm upon electrophilic addition of a halogen to MCD to form the dihalogenated species.

The paucity of alternative biological halogenation enzymes and strategies discovered over the decades that followed the discovery of haloperoxidases, led to the assumption that haloperoxidases were the predominant means of halogenation underlying the biosynthesis of halometabolites—in other words, absence of evidence became evidence for absence[32]. Indeed, at the time of the discovery of the first CPO, this argument was helped by the fact that biological halogenation was largely considered to be an accident of biology, as only thirty halogenated natural products had been described[33]. However, with the subsequent discovery of thousands of bioactive natural products bearing halogens attached to both electron rich and

aliphatic scaffolds in apparently regiospecific configurations, it has become clear that halogenation is not a mere accident of Nature (**Fig. 1.3**)[1,2]. Moreover, the discovery of fluorinated natural products, despite the inability of any known haloperoxidase to accept fluoride as a substrate further challenged the notion that these enzymes were the sole strategy for biological halogenation[10]. Hence, the broad structural diversity of organohalogen natural products signaled a wealth of substrate-specific biocatalysts utilizing alternative halogenation strategies beyond promiscuous haloperoxidases[30]. One of the main obstructions to the discovery new halogenation biocatalysts has been the inability to link enzymes with their natural substrates. However, disruptive advancements in genome sequencing and computational biology over the last two decades have lead to a renaissance in the discovery of natural product biosynthetic pathways and tailoring enzymes[34].

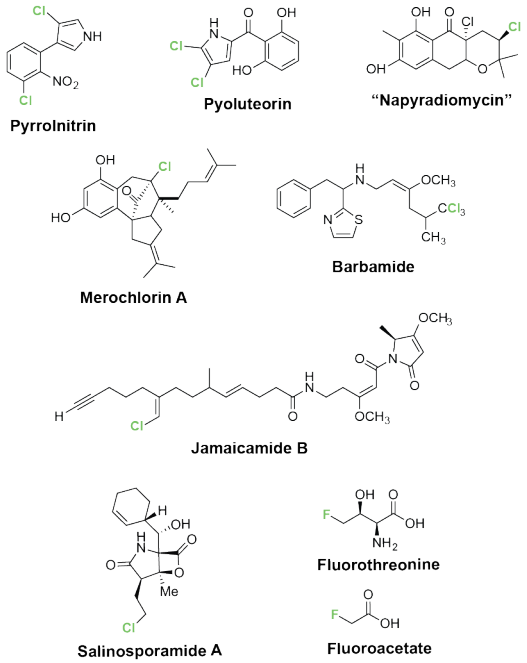

Figure 1.3: Representative diversity of halogenated natural products. Halogens decorate a diversity of natural product scaffolds that foretell diverse biological halogenation strategies.

Nearly forty years after the discovery of the first haloperoxidase, a new class of regioselective O_2/flavin-dependent electrophilic halogenases was described[35]. This enzyme, PrnA from the biosynthesis of the anti-fungal pyrrolonitrin, was shown to catalyze a regioselective chlorination at the 7-position of L-tryptophan. PrnA is related to two-component flavin-dependent monooxygenases, so-named because they require an external NAD(P)H-dependent flavin reductase redox partner (**Fig. 1.4A,B**)[35-37]. Based on structural studies of tryptophan 7-halogenases PrnA and RebH from the biosynthesis of the indolocarbazole natural product rebeccamycin, a mechanism for flavin-dependent halogenases akin to their monooxygenase counterparts has been proposed. The reaction sequence is initiated by the attack of molecular oxygen on the C_{4a} position of isoalloxazine moiety of the flavin co-factor

to generate a flavin peroxide (FAD-C_{4a}-O-OH) which is then attacked by a halide (X^-) to release water and form a flavin hypohalite (FAD-C_{4a}-O-X) that is subsequently resolved to a diffusable hypohalous acid, the same reactive intermediate proposed for haloperoxidases[36]. Subsequent to its release, the hypohalous acid is proposed to react directly with a conserved lysine residue amine side chain to form a chloramine intermediate that confers control to the halogenation reaction taking place in the substrate-binding pocket[36,38]. Despite strong evidence for formation of an apparent "long-lived" chloramine intermediate, the identity of this adduct is disputed on the grounds that such an intermediate might be too unreactive to halogenate tryptophan[39]. In addition to tryptophan 7-halogenases, trytophan 5- and 6- halogenases from the biosyntheses of the bacterial natural products pyrrindomycin and thienodolin, respectively, have also been described (**Fig. 1.4B**)[40,41]. More recently a pair of flavin-dependent halogenases, KtzQ and KtzR, were shown to perform serial halogenations, respectively, of the 6- and 7- positions of L-tryptophan in the biosynthesis of the cyclic depsipeptide kutznerides (**Fig. 1.4B**)[42]. The discovery of a series of tryptophan halogenases catalyzing a range of regioselective halogen additions has provided an opportunity for studying the molecular basis of halogenation regioselectivity. Indeed, comparative structure-guided mutagenesis of tryptophan halogenases exhibiting different regioselectivities has lead to the identification a molecular basis for the exquisite regioselectivity exhibited by these halogenating biocatalysts[43].

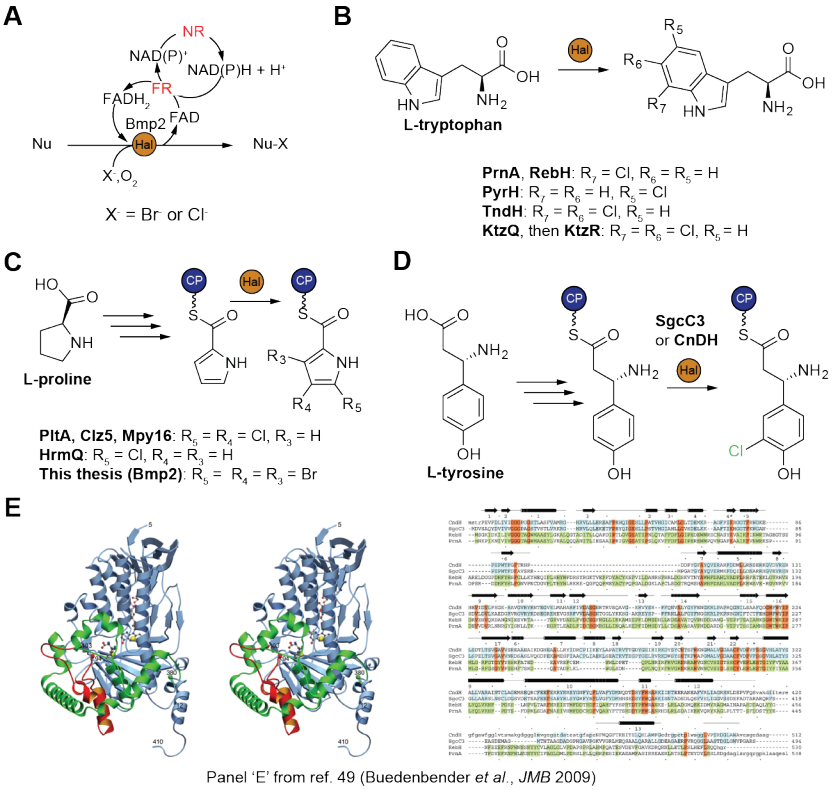

Panel 'E' from ref. 49 (Buedenbender *et al.*, *JMB* 2009)

Figure 1.4: Flavin-dependent halogenases. (**A**) The catalytic cycle for typical 2-component flavin-dependent halogenases (Nu = nucleophile, FR = flavin-reductase, NR = NAD(P)+-reductase). (**B**)-(**D**) Transformations catalyzed by (**B**) Tryptophan halogenases, (**C**) pyrrolyl-*S*-carrier protein(CP) halogenases, and (**D**) tyrosyl-*S*-CP halogenases. (**E**) Left hand side shows ribbon structure of CndH in blue with "insertions" from PrnA/RebH shown in red and green, and the right hand side shows primary amino acid sequence alignments of tyrolsyl-*S*-CP halogenases (top two lines) with RebH and PrnA (bottom two lines) from ref. 49.

Following the discovery of flavin-dependent halogenases that act on a free amino (i.e. L-tryptophan), regioselective flavin-dependent halogenases acting on L-proline-derived pyrrolyl- and L-tyrosine-derived tyrosyl-*S*-carrier-protein substrates were also described, adding to the versatility of flavin-dependent halogenases (**Fig. 1.4C,D**)[44-48]. Based on comparison of the crystal structure of tryptophan halogenase PrnA to that of a putative tryrosyl-*S*-carrier protein halogenase (CndH from the biosynthesis of chondrochlorens), a preliminary means of distinguishing between

flavin-dependent halogenases acting on free versus thiotemplated substrates was proposed based on primary sequence motifs (**Fig. 1.4E**)[49]. Prior to the work described in this thesis, several examples of flavin-dependent pyrrole 4,5-dichlorinases[44-46] and one example of a pyrrole 5-chlorinase[47] acting on carrier protein-bound substrates were described. Chapters 2 and 3 of this thesis characterize a pyrrole brominase that exhibits total loss of halogenation regiocontrol to afford fully brominated 2,3,4,5-tetrabromopyrrole via decarboxylative tetrabromination of a carrier protein-bound pyrrole. The availability of pyrrole halogenases displaying a series of regioselectivies from mono- through tetra- halogenation affords a unique opportunity to investigate a molecular basis for regiocontrol in halogenases acting on thiotemplated substrates, which is exploited in Chapter 3 of this thesis.

Incidentally, the scope of reactions catalyzed by flavin-dependent halogenase may extend beyond halogenation for halogenation's sake. A pair of putative flavin-dependent halgoenasaes, Mpy10 and Mpy11, was implicated in the atropo-selective N-C coupling reaction of two monomers of monodeoxypyoluteorin in the final step of the biosynthesis of the marine natural product marinopyrrole A[45]. While this mechanism has not yet been demonstrated, Yamanaka *et al.* propose that biaryl coupling is activated by cryptic C or N halogenation resulting in the loss of a halide leaving group (**Fig. 1.5**). Notably the marinopyrrole biosynthetic pathway also contains a flavin-dependent pyrrole dichlorinase, which regiospecifically installs two chlorine atoms on an ACP-bound pyrrole substrate. Hence, marinopyrrole A biosynthesis may provide an example of the use of halogenation by flavin-dependent enzyme catalysts as both a means to an ends and means in and of itself.

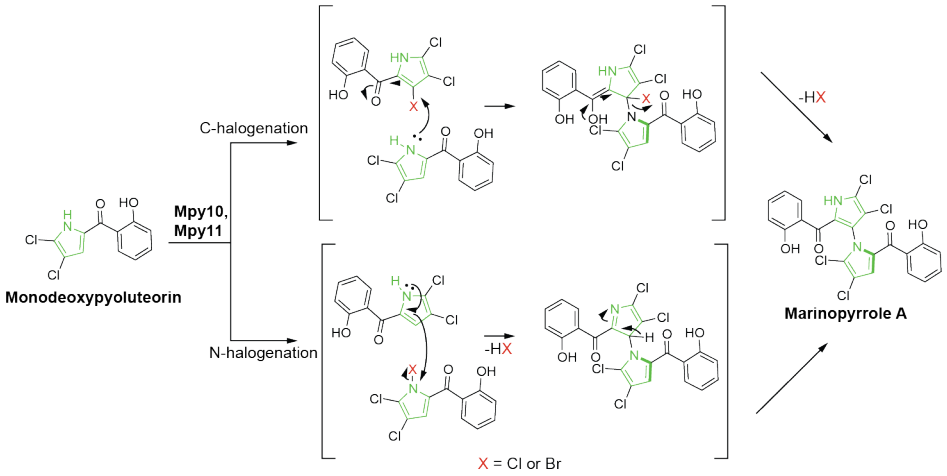

Figure 1.5: Mechanistic proposal for halogenation-mediated atropo-selective N-C coupling in the biosynthesis of Marinopyrrole A. The coupling of monodeoxypyoluteorin is proposed to occur via either C- or N- halogenation involving putative flavin-dependent halogenases Mpy10 and Mpy11. Scheme adapted from ref. 45 (Yamanaka *et al*., *J. Am. Chem. Soc.* 2012).

The discovery of flavin-dependent halogenases led to reactionary claims that this class of enzyme rather than the haloperoxidases was the truly dominant regioselective electrophilic halogenation catalyst[30,37]. While numerous examples of natural products gene clusters encoding flavin-dependent halogenases have been reported[19,44-47,50,51], these absolutist claims have been quickly tempered by the subsequent discovery of bacterial H_2O_2/vanadium-dependent haloperoxidases catalyzing highly selective chlorination reactions in confirmed biosynthetic contexts[52-55]. These enzymes are the first examples of vanadium-dependent peroxidases of bacterial origin and appear to have evolved from bacterial acid phosphatases[52]. The first bacterial vanadium-dependent haloperoxidase characterized was the chloroperoxidase NapHI from the biosynthesis of the polyketide-terpenoid (meroterpenoid) antibiotic napyradiomycin that catalyzes a site-specific chlorination-cyclization reaction[54]. Another recently described vanadium-dependent

chloroperoxidase Mcl24 catalyzes a regioselective chlorination/oxidative dearomatization/cyclization reaction sequence in the biosynthesis of the meroterpenoids merochlorins A and B[55]. Notably, the use of an electrophilic halogenation strategy would not have been immediately apparent from inspection of the structures of these meroterpenoid natural products, which bear halogens on aliphatic carbons. Hence, the discovery of regiospecific haloperoxidases delineates the importance of studying halogenating enzymes in their biosynthetic contexts.

The existence of organohalogen natural products bearing halogens on unactivated carbons foretold a radical halogenation strategy[56,57]. Several years after the discovery of flavin-dependent halogenases, another O_2-dependent class of halogenase related to Fe^{II}/α-ketoglutarate(α-KG)-dependent dioxygenases was reported from the biosyntheses of the non-ribosomal peptides syringomycin A and the barbamides, and the non-proteinogenic amino acid armentomycin[58-60]. These non-heme O_2/Fe^{II}/α-KG-dependent halogenases generate a halogen radical from chloride (i.e. an '$X^{\bullet}$' strategy) to halogenate methyl groups of carrier protein-tethered amino acids[13]. Interestingly the kutzernide biosynthetic pathway contains both flavin-dependent halogenases and a non-heme O_2/Fe^{II}/α-KG-dependent halogenases. As previously mentioned, the former are involved in the tandem dichlorination of tryptophan, while the latter was shown to catalyze a "cryptic" C-H activating chlorination reaction leading to cyclopropane ring formation in the biosynthesis of the non-proteinogenic amino acid building block derived from L-isoleucine[61]. Hence the kutzernide biosynthetic pathway demonstrates Nature's capacity to combine multiple halogenation strategies, using halogens to manipulate both reactivity and bioactivity.

Likely due to the electronegativity of fluorine, no known oxidative or radical strategy for its incorporation into natural product scaffolds has been discovered. Hence, the halogenation strategy implied by the existence of fluorinated natural products is a nucleophilic halogenation strategy that directly utilizes fluoride. Indeed, shortly after the discovery of the the first flavin-dependent halogenases, a *S*-adenosyl methionine (SAM)-dependent nucleophilic fluorinase was reported from the soil bacterium *Streptomyces catteleya* known to produce the fluorometabolites fluoroacetate and 4'-fluorothreonine[62]. An additional SAM-dependent nucleophilic halogenase was later described from the biosynthesis of the chlorinated marine natural product salinosporamide A[63]. SAM-dependent halogenases directly utilize halides (i.e. X^-: F^- or Cl^-) which perform a substitution reaction at the C-5' position of SAM, attacking the nucleophilic sulfonium center, and releasing a neutral L-methionine leaving group[64]. The resultant halogenated nucleoside is then metabolized to precursors that are incorporated into the final natural product. As such, nucleophilic halogenation by SAM-dependent halogenases is a remarkable feat of Nature, but is also a highly specialized halogenation strategy. Nonetheless, fluorine, which is commonly used to enhance efficacy of clinical drugs, is by far the most well-represented halogen in pharmaceuticals, and hence novel fluorinated natural products and associated fluorinating strategies should continue to be sought[9].

By the start of the decade four additional classes of halogenating enzymes utilizing halides via three distinct strategies—oxidative, radical, and nucleophilic—had been discovered. Remarkably, in a paradigm shift from the biased MCD assay used to screen for haloperoxidases, the true substrates for all of these new

halogenation biocatalysts are known thanks to their systematic study in their biosynthetic contexts[34]. Moreover, the improved capacity for prediction of biosynthetic gene loci from natural product scaffolds has enabled the appreciation of halogenating biocatalysts in their physiological contexts, and afforded the opportunity for engineering of these biocatalysts for altered regioselectivity and substrate scope[18,19]. The fact that halogenating enzymes like all enzymes of secondary metabolism evolved from primary metabolism hints that many more unique halogenation biocatalysts remain to be discovered[13,65]. Indeed, halogenated natural products are already being linked to genetic contexts which lack annotations for known halogenating enzymes. For example, a putative N-oxidase-like enzyme-BrtJ has been proposed to be the halogenase involved in the biosynthesis of the recently described cyanobacterial aromatic glycolipid natural product bartolosides[66]. Further, the extensive natural product cataloging efforts of prior decades have endowed enzymologists with an inventory of natural products as a springboard for generating biosynthetic hypotheses, while sequencing, computational biology, molecular biology, metabolic engineering, analytical chemistry, and synthetic chemistry have teamed up to provide a direct basis for interrogation of these hypotheses[2,67].

1.4 Comment on the "haloperoxidase doctrine"

In light of the renaissance in halogenation enzymology, it is curious to note the persistence of the notion in the scientific literature that haloperoxidases are responsible for the bulk of marine halogenation[13,68]. Apart from a few recent examples in which bacterial haloperoxidases found in the contexts of biosynthetic gene clusters have been shown to be directly involved in specific reactions, the main

drivers for the "haloperoxidase doctrine" are studies that rely on transformations of putative precursors for natural products for which no genetic information is known[68]. An additional *ad ignorantium* argument that has persisted in the literature is the notion that haloperoxidases are responsible for the majority of brominated natural products due to the prevalence of vanadium-dependent bromoperoxidases found in red algae that are also an abundant source of bromophenol metabolites[32,69]. Indeed, the first two examples of marine brominases from a physiological context described in chapters 2-3 of this thesis are substrate-specific flavin-dependent halogenases and not haloperoxidases[50]. Moreover, another notion challenged by this thesis is the dichotomy that flavin-dependent halogenases are regioselective, while haloperoxidases are regiopromiscuous[30]. This thesis describes an "aberrant" regiopromiscuous flavin-dependent halogenation that exhibits complete loss of halogenation regiocontrol with respect to an ACP-bound pyrrole substrate. This loss in regiocontrol in turn serves as a means for elimination of the proline-derived α-carboxylate, which is otherwise retained in lesser halogenated halopyrrole-containing natural products[16]. Indeed, it seems the only generalization that can be drawn about halogenating enzymes, or for that matter any biosynthetic tailoring enzyme, is that they are uniquely evolved to influence functional outcomes specified in the contexts of biosynthetic pathways.

1.5 Biological dehalogenation: a new frontier in natural products biosynthesis

While the major part of this chapter has discussed Nature's strategies for adding halogens to hydrocarbon scaffolds, another frontier for biocatalysis is the

discovery of enzymes that remove halogen atoms from organic substrates. Enzymatic dehalogenation is of particular interest in the remediation of highly brominated persistent pollutants of which many have analogs in natural products[70]. While studies have been performed to probe the capacities of microbial communities for dehalogenation of man-made compounds, thus far none has looked toward the biosyntheses and degradation of highly halogenated microbial natural products as an inspiration for the discovery for new dehalogenating biocatalysts[71]. Apart from the few examples of dehalogenations taking place in the course of transformations involving cryptic halogenation reactions, in which a halogen installed by a halogenating enzyme serves as a leaving group, no example of a dedicated dehalogenase tailoring enzyme has been described from the context of a natural product biosynthetic pathway[45,61,72,73]. Moreover, despite a recognition of Nature's capacity to degrade halogenated natural products, no enzyme involved in the natural degradation of organohalogen natural products has been identified from an environmental context[20-22]. An illustrative example of the wealth of enzymology arising from the formation and metabolism of a halogenated natural product comes from the study of thyroid hormone biosynthesis, which has afforded three new classes of enzymes—a halogenating enzyme and two classes of deiodinases (flavoprotein and selenoprotein) involved in activation-inactivation of thyroid hormone and reclamation of scarce iodide[7,74]. Chapter 4 of this thesis describes the discovery and elucidation of a novel class of dehalogenase, Bmp8, providing the first example of a dehalogenase tailoring enzyme from the context of a natural product biosynthetic pathway.

1.6 In this thesis**: motivations for the study of the biosynthesis of pentabromopseudilin**

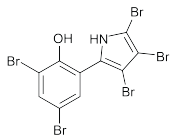

Figure 1.6: Pentabromopseudilin. The compact highly brominated structure of the marine microbial natural product pentabromopseudilin is packed with biosynthetic opportunity.

Pentabromopseudilin is the first reported marine microbial natural product, isolated in 1966 by Burkholder and colleagues from the marine bacterium *Pseudoalteromonas bromoutilis*[75]. Apart from its place in history, the compact structure of pentabromopseudilin which consists of a tribromopyrrole moiety coupled to a dibromophenol moiety via a C-C bond is packed with opportunity from a biosynthetic standpoint (**Fig. 1.6**). From the perspective of novel enzymology, no brominating enzyme from the confirmed context of a natural product biosynthetic pathway had been reported when this study was begun five years ago—the structure of pentabromopseudilin suggests at least two brominating enzymes. In addition to motivations deriving from biosynthetic novelty, our attention was drawn to the biosynthesis of pentabromopseudilin by analogy of both of its brominated aromatic moieties to polybrominated aromatic bipyrrole and biphenyl compounds that accumulate up the marine food chain[70]. While bioaccumulative polyhalogenated bipyrroles are strictly of natural origin, the hydroxylated polybrominated diphenyl ethers (OH-BDEs) are thought to be of mixed natural and anthropogenic origin[2]. However, claims of the natural origin of OH-BDEs at the time of this study were based exclusively on circumstantial evidence[76,77]. Hence, an unfulfilled need remained for a genetic or biosynthetic logic with which to mine environmental

metagenomes as means of understanding the distribution of sources of natural OH-BDEs. Critically, the ability to identify a molecular origin for the biosynthesis of OH-BDEs has the potential to dramatically influence the discussion regarding our small molecule interaction with the environment, as most biomonitoring programs ignore OH-BDEs altogether, assuming them to be metabolic products of anthropogenic polybrominated diphenyl ethers (PBDEs)[78,79]. The remainder of this thesis will describe the enzymatic and chemical diversity afforded by the total *in vitro* reconstitution of the biosynthesis of pentabromopseudilin, as well as questions and opportunities arising from the study thereof. This introductory chapter concludes with a synopsis of the remaining chapters.

1.6.1 Chapter 2: Biosynthesis of polybrominated aromatic molecules by marine bacteria

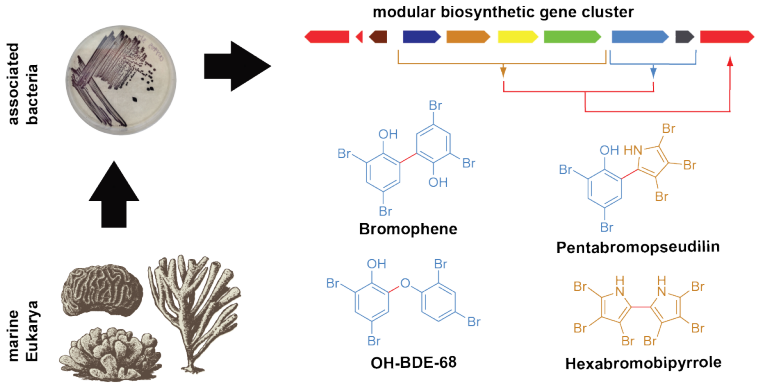

Figure 1.7: A modular polybrominated pyrrole/phenol (Bmp) biosynthetic pathway from marine bacteria. Pentabromopseudilin biosynthesis is encoded by the modular Bmp biosynthetic gene cluster that additionally affords combinatorically C-C and C-O coupled homo- and hetero- coupled bromo- pyrroles and phenols.

This published chapter (Agarwal and El Gamal *et al.*, *Nat. Chem. Biol.*, 2014) consists of the initial description of the brominated marine pyrrole/phenol (Bmp) biosynthetic pathway found across several species and genera of host-associated marine γ-proteobacteria (**Fig. 1.7**). In this study several genomes of marine γ-

proteobacteria confirmed to produce pentabromopseudilin were sequenced, and interrogated using genes from the biosynthesis of the halopyrrole moiety of pyoluteorin[44]. This query lead to the identification of a modular biosynthetic gene locus, which was heterologously expressed and functionally interrogated *in vivo* and *in vitro*. This study confirmed the hypothesis that the bromopyrrole moiety of pentabromopseudilin arises from a conserved halopyrrole biosynthetic logic. Additionally, this chapter describes the first two examples of marine brominating enzymes from the confirmed context of a natural product biosynthetic pathway. The pyrrole halogenase Bmp2 is homologous to previously described flavin-dependent pyrrole halogenases and is demonstrated to catalyze an unprecedented three brominations on an ACP-bound pyrrole substrate. The phenol halogenase Bmp5 employs a decarboxylative halogenation mechanism to convert *p*-hydroxybenzoic acid to 2,4-dibromophenol. The architecture of Bmp5 is unique among flavin-dependent halogenases characterized to date in that its protein sequence resembles that of single-component monooxygenases, meaning that it does not require an external NAD(P)H-dependent flavin reductase and contains sequence motifs for binding both flavin and a NAD(P)H. It was also revealed that these marine brominating enzymes are selective for bromide and exclude chloride, providing a basis for comparing flavin-dependent chlorinases (accept Cl^-, Br^-) to brominases (accept on Br^-) toward understanding the fundamental question of halogen specificity of halogenating enzymes. Also characterized in the chapter is the versatile cytochrome P450 Bmp7 that forms the basis for combinatorial C-C and C-O coupling of the bromopyrrole and bromophenol building blocks produced by the Bmp pathway

to afford an astonishing chemical diversity consisting of fifteen metabolites, several of which are new chemical entities. Notably, OH-BDEs were found to be among the metabolites synthesized by the Bmp pathway. This initial report provided the near complete *in vitro* reconstitution of the pentabromopseudilin biosynthetic pathway, but left unanswered the enzymes and reaction sequence leading to the offloading and decarboxylation of the bromopyrrole moiety. The elucidation of these transformation and associated enzymes form the basis for chapter 3 and 4 of this thesis.

1.6.2 Chapter 3: Biosynthesis of the coral larval settlement cue tetrabromopyrrole in marine bacteria by a uniquely adapted brominase-thioesterase enzyme pair

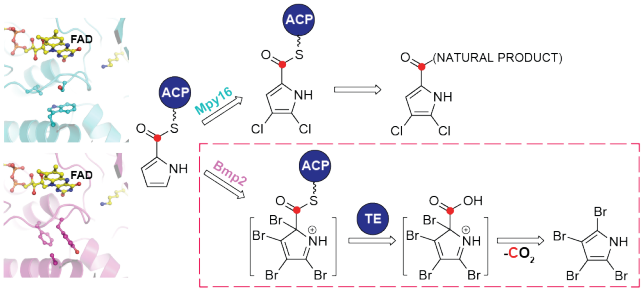

Figure 1.8: A modular polybrominated pyrrole/phenol (Bmp) biosynthetic pathway from marine bacteria. Pentabromopseudilin biosynthesis is encoded by the modular Bmp biosynthetic gene cluster that additionally affords combinatorically C-C and C-O coupled homo- and hetero- coupled bromo- pyrroles and phenols.

This published chapter (El Gamal and Agarwal *et al.*, *Proc. Natl. Acad. Sci. USA*, 2016) focuses on the unusual mechanism of offloading and decarboxylation of the bromopyrrole moiety of pentabromopseudilin. This study was originally motivated by another related bromopyrrole natural product, tetrabromopyrrole, which is a coral larval settlement cue produced by marine bacteria that form biofilms on coral substrates[80]. In the initial elucidation of the the biosynthesis of

pentabromopseudilin, asymmetric tribromopyrrole—not tetrabromopyrrole—was identified as the substrate for the bromo- phenol/pyrrole coupling enzyme Bmp7. However, this finding stood at odds with a symmetric pyrrole intermediate implied by shuffling with respect to C-C coupling in earlier isotope feeding studies of pentabromopseudilin biosynthesis[81]. Hence, studying the biosynthesis of tetrabromopyrrole had the potential to address two biosynthetic questions. Firstly, the presence of a bromine in place of the anticipated proline-derived α-carboxylate in tetrabromopyrrole implied a brominative decarboxylation mechanism. Secondly, the elucidation of the tetrabromopyrrole biosynthetic pathway offered to address the question of the identity of the symmetric intermediate implied in the biosynthesis of pentabromopseudilin. Sequencing of two tetrabromopyrrole-producing bacteria and querying with Bmp biosynthetic genes revealed that only the bromopyrrole module of the Bmp pathway was present in their genomes. Further, this study revealed that the pyrrole front-end of the Bmp pathway produced tetrabromopyrrole as its sole enzymatic product. Moreover, it was demonstrated that the pyrrole halogenase Bmp2 catalyzes a fourth halogenation of the carrier protein-bound pyrrole scaffold that triggers the thioesterase-mediated release of the pyrrole, and leads to spontaneous decarboxylation to tetrabromopyrrole (**Fig. 1.8**). Hence, the decarboxylative halogenation mechanism of Bmp2 mirrors that of the *p*-hydroxybenzoic acid brominase/decarboxylase Bmp5. Notably, Bmp2 provides the first example of a flavin-dependent halogenase exhibiting a complete loss of regiocontrol. While previously characterized pyrrole halogenases catalyze up to two regiospecific halogenation on carrier protein-bound pyrrole scaffolds, Bmp2 catalyzed an

unprecedented four halogenations. To interrogate a molecular basis for halogenation regiospecificity, high-resolution crystal structures were generated for the pyrrole dichlorinase Mpy16 from the biosynthesis of marinopyrrole A[45] and tetrabrominase Bmp2. Structure-guided mutagenesis of the active site of Bmp2 to resemble that of Mpy16 lead to a reduction in the degree of halogenation catalyzed from four down to one. The discovery of tetrabromopyrrole as the enzymatic product of the bromopyrrole biosynthetic "module" of the Bmp pathway, leads to the natural follow-on question as to the mechanism for the conversion of symmetric tetrabromopyrrole to the asymmetric Bmp7-substrate tribromopyrrole in the biosynthesis of pentabromopseudilin. The elucidation of an unusual dehalogenase tailoring enzyme-Bmp8 catalyzing this transformation forms the basis for Chapter 4 of this thesis.

1.6.3 Chapter 4: An alkylhydroperoxidase-like debrominase is an enzymatic switch in the biosynthesis of pentabromopseudilin

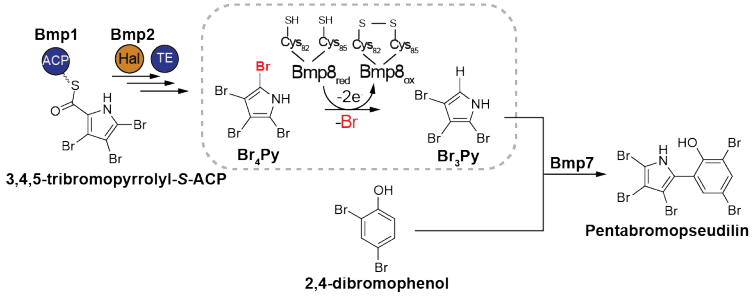

Figure 1.9: A dehalogenase switch in pentabromopseudilin biosynthesis. Dehalogenase-Bmp8 utilizes a cofactor-independent redox thiolate mechanism to transforms 2,3,4,5-tetrabromopyrrole (Br_4Py) to 3,4,5-tribromopyrrole (Br_3Py) to permit coupling with 2,4-bromophenol in the formation of pentabromopseudilin.

This chapter describes a new class of co-factor independent reductive-dehalogenases. We show that Bmp8 catalyzes the transformation of tetrabromopyrrole to the Bmp7-substrate tribromopyrrole, reconciling the

pentabromopseudilin biosynthetic scheme with earlier isotope feeding studies and the biosynthesis of tetrabromopyrrole. This chapter describes the mass-spectrometry-driven elucidation of Bmp8, which revealed that Bmp8 utilizes a redox active cysteine residue side chain thiol in its reaction mechanism. Mining publically available databases with the primary sequence of Bmp8 revealed hundreds of homologs from different biosynthetic contexts bearing a simple conserved motif that could be used to predict for the ability to dehalogenate bromopyrroles. Homology-guided mutagenesis was further performed to identify residues in the motif that are critical to the activity of Bmp8. To the best of our knowledge, Bmp8 is the first reported example of a dehalogenating tailoring enzyme from the context of a biosynthetic pathway. Additionally, Bmp8 is only the second example of a reductive dehalogenase that utilizes a cofactor-independent mechanism (the other is a mammalian selenoprotein deiodinase that uses a similar mechanism that likely exemplifies a case of convergent evolution), as well as the only other physiologically confirmed dehalogenating enzyme described in biology (**Fig. 1.9**)[7]. Hence, this chapter concludes the total *in vitro* characterization of the biosynthesis of pentabromopseudilin.

1.6.4 Chapter 5: Opportunities in halopyrrole biosynthesis

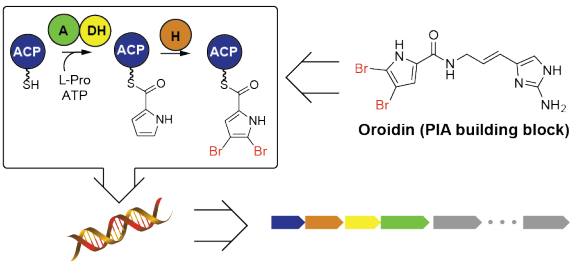

Figure 1.10: A metagenomics approach toward elucidation of pyrrole-imidazole alkaloid biosynthesis. A conserved halopyrrole biosynthetic logic may serve as a handle to mine for pyrrole-imidazole alkaloid biosynthetic gene loci, unlocking the biosynthesis of a diverse class of bioactive natural products.

One of the key challenges in the identification of gene clusters encoding the biosyntheses of non-canonical natural products (i.e. neither NRPS nor PKS) is the lack of an appropriate query with which to search genomic datasets. One strategy for going after chemical moieties that lack biosynthetic precedents is to identify natural products that wed the familiar to the exotic. For example, in the case of the hybrid pyrrole-phenol structure of pentabromopseudilin (Chapter 2), the familiar halopyrrole moiety served as a biosynthetic hook with which to extract the biosynthesis of the bromophenol moiety. Chapter 5 explores the application of the same halopyrrole biosynthetic probe toward the elucidation of the biosynthesis of the pyrrole-imidazole alkaloid (PIA) class of sponge natural products. This intriguing class of bioactive natural products consists of over 150 chemical structures ranging in complexity from the simplest achiral building block oroidin to the awe-inspiring oroidin dimer palau'amine whose hexacyclic core consists of eight contiguous stereocenters[82]. This chapter will describe an approach toward the identification of a genetic basis for PIA biosynthesis from sponge metagenomes, along with insights gained from an initial application of this approach to two metagenomes of sponges harboring PIAs (**Fig. 1.10**).

Chapter 2: Biosynthesis of polybrominated aromatic molecules by marine bacteria

ARTICLE
PUBLISHED ONLINE: 29 JUNE 2014 | DOI: 10.1038/NCHEMBIO.1564

Biosynthesis of polybrominated aromatic organic compounds by marine bacteria

Vinayak Agarwal[1,6], Abrahim A El Gamal[1,6], Kazuya Yamanaka[2,5], Dennis Poth[2], Roland D Kersten[2,5], Michelle Schorn[2], Eric E Allen[1-3] & Bradley S Moore[1,2,4]*

Polybrominated diphenyl ethers (PBDEs) and polybrominated bipyrroles are natural products that bioaccumulate in the marine food chain. PBDEs have attracted widespread attention because of their persistence in the environment and potential toxicity to humans. However, the natural origins of PBDE biosynthesis are not known. Here we report marine bacteria as producers of PBDEs and establish a genetic and molecular foundation for their production that unifies paradigms for the elaboration of bromophenols and bromopyrroles abundant in marine biota. We provide biochemical evidence of marine brominases revealing decarboxylative-halogenation enzymology previously unknown among halogenating enzymes. Biosynthetic motifs discovered in our study were used to mine sequence databases to discover unrealized marine bacterial producers of organobromine compounds.

Halogenation, particularly bromination, is a diagnostic feature of marine natural products. Although bromide is present in only trace amounts terrestrially, its greater natural abundance in seawater provides a substrate reservoir for halogenating enzymes evolved to selectively activate and transfer bromide to organic molecules. Marine organisms, including bacteria, algae and invertebrates, are prolific sources of organobromine compounds that number over 2,200 reported molecules with a wide range of biological properties[1,2]. These brominated natural products range from simple volatile polybromoalkanes[3] to highly complex alkaloids[4]. Yet, our understanding of the biosynthesis of brominated natural products has lagged far behind their discovery, largely because few biosynthetic gene loci have been identified and characterized. Herein we report a pervasive marine bacterial pathway to polybrominated aromatic compounds that accounts for a diverse suite of common polybrominated pyrrole and phenol-based natural products.

In their hydroxylated (OH-BDE) and methoxylated (MeO-BDE) forms, PBDEs are abundant across all trophic levels of marine life ranging from marine plants[5], algae[6–8] and invertebrates[9–12] to marine mammals at the apex of the food chain[13–15]. OH-BDEs and MeO-BDEs detected in marine biota were once thought to be derived from chemical transformation of anthropogenically produced polybrominated flame-retardant chemicals of similar structure[16]. However, derivatives such as 2′-MeO-BDE-47, a metabolite widely detected in the marine metabolome (**Fig. 1a**), were shown through $\Delta^{14}C$ measurements to be of natural origin[15]. Despite the mounting evidence for the biosynthesis of OH-BDEs in the natural metabolome, no natural producer of these potential toxins that target mammalian nuclear hormone mediated signaling pathways[17] has been confirmed.

An abundance of PBDEs at all trophic levels of marine Eukarya suggests lower-trophic-level sources for their genesis. This hypothesis is supported by the production of chemically similar polybrominated molecules, such as 3,3′,5,5′-tetrabromo-2,2′-biphenyldiol (**1**) (ref. 18), hexabromo-2,2′-bipyrrole (**2**) (ref. 19) and the hybrid bromophenol-bromopyrrole pentabromopseudilin (**3**) (refs. 19,20) (**Fig. 1a**), by *Pseudoalteromonas* spp., marine γ-proteobacteria often associated with eukaryotic hosts[21]. Although **1** and **2** are not industrially synthesized, their methylated analogs are extensively detected in marine mammals[14,22] (**Fig. 1a**). Notably, in contrast to the microbial biosynthesis of polybrominated biphenyls and bipyrroles, production of PBDEs has not been confirmed from marine bacterial sources.

Herein we report the discovery of a conserved biosynthetic gene cluster in marine bacteria responsible for the synthesis of widespread polybrominated aromatic compounds and describe two flavin-dependent brominases involved in the synthesis of universal polybromophenol- and polybromopyrrole-based metabolites. For what is to our knowledge the first time, our findings establish marine bacteria as sources of OH-BDEs, and we provide the first report and biochemical characterization of a flavin-dependent decarboxylative-brominase enzyme using an inferred enzyme architecture not previously realized among halogenases.

RESULTS

A genetic basis for bromination in marine bacteria

In our search for marine prokaryotic sources of polybrominated molecules, we focused on the cosmopolitan marine genus *Pseudoalteromonas* spp., previously shown to produce **1**–**3**. Specifically, we queried the small-molecule natural products synthesized by coral-associated *Pseudoalteromonas luteoviolacea* 2ta16 isolated in the Florida Keys[23] and by planktonic *Pseudoalteromonas phenolica* O-BC30 isolated off the coast of Japan[18]. We analyzed organic extracts of liquid cultures of these marine bacteria grown in the presence of bromide by high performance LC/MS/MS. Among numerous polybrominated molecules present in the culture extract of both bacteria, we confirmed the production of **1**–**3** by MS and NMR spectroscopy of isolated compounds (**Fig. 1b** and **Supplementary Results, Supplementary Figs. 1** and **2** and

[1]Center for Oceans and Human Health, Scripps Institution of Oceanography, University of California–San Diego, La Jolla, California, USA. [2]Center for Marine Biotechnology and Biomedicine, Scripps Institution of Oceanography, University of California–San Diego, La Jolla, California, USA. [3]Division of Biological Sciences, University of California–San Diego, La Jolla, California, USA. [4]Skaggs School of Pharmacy and Pharmaceutical Sciences, University of California–San Diego, La Jolla, California, USA. [5]Present address: JNC Corporation, Yokohama Research Center, Yokohama, Japan (K.Y.); Salk Institute for Biological Studies, San Diego, California, USA (R.D.K.). [6]These authors contributed equally to this work. *e-mail: bsmoore@ucsd.edu

NATURE CHEMICAL BIOLOGY DOI: 10.1038/NCHEMBIO.1564 ARTICLE

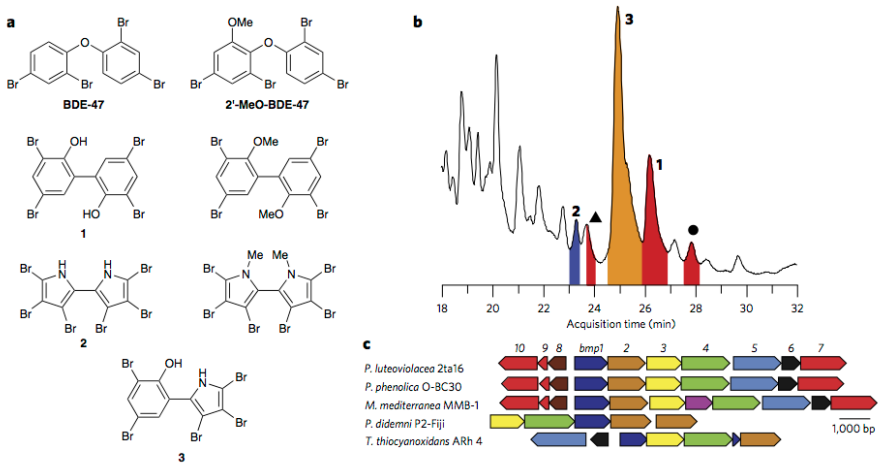

Figure 1 | Structures and sources of marine polybrominated natural products. (**a**) Representative structures of polybrominated molecules produced anthropogenically (BDE-47) or microbially (**1**–**3**) and their derivatives detected in the environment. (**b**) TIC (black curve) from LC/MS/MS analysis of an organic extract of *P. luteoviolacea* 2ta16 demonstrating production of the **1**–**3**. Peaks labeled with the solid circle and solid triangle were later correlated to OH-BDEs **11** and **12**, respectively (described below). (**c**) Organization of *bmp* gene loci in marine bacteria. *M. mediterranea* MMB-1 encodes a putative permease between *bmp3* and *bmp4*.

Supplementary Table 1). Additionally, we confirmed the production of a large series of bromophenol and bromopyrrole monomeric molecules, including 2,4-dibromophenol (**4**); 2,4,6-tribromophenol (**5**); 2,3,4-tribromopyrrole (**6**); and 2,3,4,5-tetrabromopyrrole (**7**) on the basis of their MS spectra and comparison to synthetic standards (**Supplementary Fig. 2** and **Supplementary Table 1**).

Having established experimentally tractable marine bacterial sources for the production of **1**–**7**, we next sought to determine the genetic basis for the production of these polybrominated small-molecule marine natural products. Toward this aim, we sequenced the genomes of *P. luteoviolacea* 2ta16 and *P. phenolica* O-BC30, resulting in draft 6.36-Mb and 4.76-Mb genomes, respectively. We hypothesized that the bromopyrroles and, by extension, the bromopyrrole moieties of heterodimeric molecules such as **3** are derived in a manner analogous to the biosynthesis of the dichlorinated pyrrole moiety of the antifungal natural product pyoluteorin[24], consistent with prior isotope feeding studies tracing the source of the pyrrole moiety of **3** to L-proline[25] (**Supplementary Fig. 3**). Hence, we queried the genomes of *P. luteoviolacea* 2ta16 and *P. phenolica* O-BC30 for the proline dehydrogenase (PltE) and the pyrrole halogenase (PltA) enzymes from pyoluteorin biosynthesis. This analysis successfully led to the identification of the brominated marine pyrroles/phenols (*bmp*) biosynthetic gene locus in both bacteria. Homologs of *pltE* and *pltA* (*bmp3* and *bmp2*, respectively; **Fig. 1c**) were found clustered together with genes putatively encoding an acyl carrier protein (ACP)-thioesterase (TE) di-domain protein (*bmp1*), proline adenyltransferase (*bmp4*), flavin-dependent oxygenase (*bmp5*), chorismate lyase (*bmp6*), cytochrome P450 (CYP450, *bmp7*), ferredoxin (*bmp9*) and ferredoxin reductase (*bmp10*), and a carboxymuconolactone decarboxylase homolog (*bmp8*). The primary sequence similarity of Bmp ORFs to pyoluteorin biosynthetic enzymes is provided in **Supplementary Table 2**.

To confirm the contribution of the *bmp* gene cluster to the biosynthesis of **1**–**7**, we constructed an expression vector and heterologously expressed *P. luteoviolacea* 2ta16 genes *bmp1*–*8* in *Escherichia coli* (**Supplementary Fig. 4** and **Supplementary Tables 3** and **5**). In the presence of bromide, we observed the heterologous production of **1**–**7** (**Fig. 2a**,**b**). Notably, the complexity of the culture extract precluded a concomitant visual representation of all of the polybrominated molecules within a single total ion chromatogram (TIC). We next explored the individual functions of the *bmp1*–*8* genes by expressing the *bmp* cluster with individual gene deletions (**Supplementary Table 5**). As postulated by homology to the pyoluteorin pyrrole dichlorinase enzyme PltA and consistent with its assignment as a pyrrole brominase, deletion of *bmp2* abolished the production of bromopyrroles **2**, **3**, **6** and **7** (**Fig. 2a**). In contrast, deletion of *bmp5* eliminated **1**, **3** and all of the other bromophenol-containing species, leading to the proposed role of Bmp5 as a phenol brominase. We further identified *bmp7* as a coupling enzyme as its deletion led to the abolishment of the dimers **1**–**3**, whereas monomers **4**–**6** could still be detected; **7** was a notable exception (**Supplementary Fig. 5**). These experiments established what is to our knowledge the first genetic link to the production of polybrominated aromatic molecules in nature.

We next analyzed genomic data sets for the presence of orphan gene loci related to the *bmp* gene cluster. Indeed, we identified a highly conserved gene cluster in the melanogenic marine bacterium *Marinomonas mediterranea* MMB-1 (ref. 26), with an insertion of a putative permease between *bmp3* and *bmp4* (**Fig. 1c**). As expected, we confirmed the production of brominated molecules **1**–**3** by *M. mediterranea* MMB-1 (**Supplementary Fig. 1**), providing halogenated natural products from this genus that commonly associates with sea grass. Indeed, the methylated variant of **7** (2,3,4,5-tetrabromo-1-methylpyrrole) and MeO-BDEs such as 2′-MeO-BDE-68 (described below) have been detected in the sea grass *Halophila ovalis*[5] and obligate marine herbivores such as dugongs[13]. We also identified a truncated gene cluster in the *Lissoclinum patella* tunicate metagenomic data set for the marine cyanobacterial symbiont *Prochloron didemni* P-2 Fiji[27] (**Fig. 1c**). Additionally, we found a highly similar gene locus in the sulfur-oxidizing γ-proteobacterium *Thioalkalivibrio thiocyanoxidans* ARh 4 (ref. 28) that, notably, was missing CYP450 *bmp7* and CYP450 electron transfer partners *bmp9* and *bmp10* (**Fig. 1c**).

ARTICLE NATURE CHEMICAL BIOLOGY DOI: 10.1038/NCHEMBIO.1564

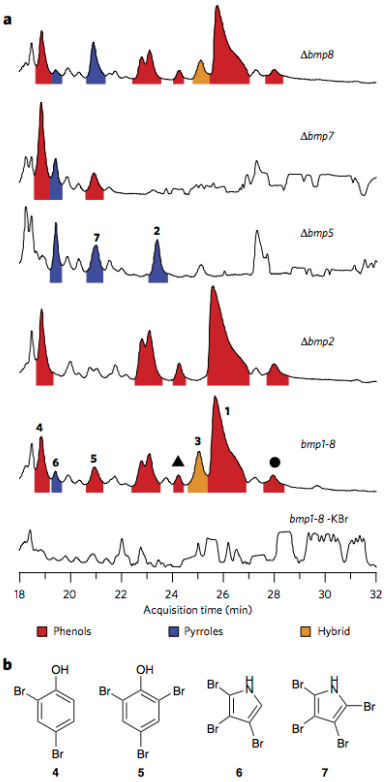

Figure 2 | Genetic basis of the Bmp pathway. (**a**) TICs for organic extracts of *E. coli* expressing the *P. luteoviolacea* 2ta16 *bmp* gene cluster and selected gene deletions. **2** is only present in high abundance in the absence of *bmp5* as *E. coli* expressing both *bmp5* and *bmp7* preferentially produce **1** and other coupled bromophenols. Retention times of **5** and **7** are nearly identical; hence, for the sake of clarity, the more abundant species is highlighted in chromatograms where both are present (i.e., *bmp1–8* and *Δbmp7*). In addition to **1**–**7**, the *bmp1–8* extract contains other polybrominated phenol species. Peaks labeled with the solid circle and solid triangle were later correlated to OH-BDEs **11** and **12** (described below). TIC for an organic extract of *E. coli* expressing *bmp1–8* cultured in the absence of bromide is shown as a negative control. (**b**) Chemical structures of bromophenol and bromopyrrole monomers **4**–**7**.

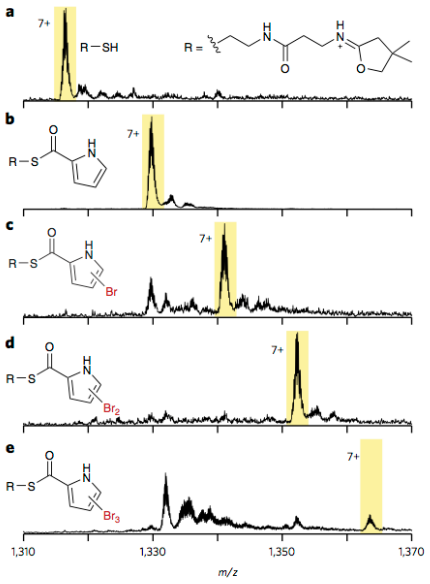

Figure 3 | *In vitro* reconstitution of activity for brominase Bmp2. (**a**–**e**) Assay for the activity of Bmp2 relies on the detection of MS1 ions for tryptic peptide fragments of Bmp1 corresponding to holo-*S*-Bmp1 (**a**), pyrrolyl-*S*-Bmp1 (**b**), monobromopyrrolyl-*S*-Bmp1 (**c**), dibromopyrrolyl-*S*-Bmp1 (**d**) and tribromopyrrolyl-*S*-Bmp1 (**e**). All MS1 ions (**a**–**e**, shaded in yellow) bear a +7 charge, as identified by their isotopic distributions. MS/MS fragmentation of the shaded MS1 ions generates distinct diagnostic MS2 ions that are shown by their corresponding chemical structures. The dehydrated cyclopantetheinyl MS2 ion for **a** is abbreviated for clarity in **b**–**e**. Upon transfer of pyrrolyl-*S*-CoA (**16**) to apo-*S*-Bmp1(ACP) by the *B. subtilis* phosphopantetheinyl transferase Sfp (Online Methods), pyrrolyl-*S*-Bmp1 is generated that is mono-, di- and tribrominated by Bmp2 in the presence of NADPH, KBr and *E. coli* flavin-reductase SsuE. Calculation for MS1 peptide masses and peptide identification protocol, as inspired by prior reports[24,50], is described in detail in **Supplementary Note 1**. The expression of Bmp1 in *E. coli* generates a mixture of apo-Bmp1 and holo-*S*-Bmp1. Of these, only apo-Bmp1 participates in the Bmp2 assay owing to its amenability for acylation catalyzed by the Sfp transferase. Holo-*S*-Bmp1 remains unmodified, as shown in **a**.

Brominase Bmp2 catalyzes pyrrole tribromination

We next sought biochemical confirmation for individual enzymatic transformations in the Bmp pathway, suggested by proline-based halopyrrole biosynthetic logic and gene deletion experiments. As characterized for the biosynthesis of pyrrole moieties in numerous alkaloid natural products[29], the proline adenyltransferase Bmp4, together with the flavin-dependent dehydrogenase Bmp3, catalyzed the near-stoichiometric conversion of holo-Bmp1 to pyrrolyl-*S*-Bmp1 (**Supplementary Figs. 6–8**; detailed analytical protocols are described in **Supplementary Note 1**). Enzymatic conversion was abolished in the absence of either ATP or L-proline, whereas reduced conversion was observed in the absence of Mg^{2+}. These observations were consistent with the proposed reaction scheme for adenyltransferases proceeding via an adenylated amino acid intermediate that is subsequently transferred to the phosphopantetheine sulfhydryl of the ACP with the concomitant release of AMP.

Bmp2 is homologous to canonical flavin-dependent halogenases that use ACP-tethered substrates[30] (**Supplementary Fig. 30**). These enzymes require an exogenous supply of reduced flavin cofactor ($FADH_2$), typically provided *in situ* by a flavin reductase that catalyzes the reduction of the flavin cofactor with the concomitant oxidation of NAD(P)H[24,31]. In the presence of *E. coli* flavin reductase SsuE[32], NADPH and bromide, Bmp2 catalyzed the bromination of pyrrolyl-*S*-Bmp1(ACP) to mono-, di- and tribromopyrrolyl-*S*-Bmp1(ACP) (**Fig. 3**). This result established the *in vitro* reconstitution of a flavin-dependent halogenase with physiological bromination activity involved in natural product biosynthesis. Assignment of Bmp2 as a brominase is further supported by the observation that no incorporation of chloride was detected[33].

NATURE CHEMICAL BIOLOGY DOI: 10.1038/NCHEMBIO.1564 ARTICLE

Although numerous bromopyrrole containing marine natural products have been identified[4,34], **2** and **3** bear a distinct chemical signature in that all three available positions on the pyrrole ring are brominated, as opposed to mono- or di- bromination, which is more commonly observed in brominated alkaloids with the 3-position of the pyrrole being universally unmodified.

Chemical logic for the biosynthesis of **2** and **3** using enzyme functionalities present within the *bmp* gene locus dictates that an ACP-bound tribromopyrrole intermediate is released by the TE domain of Bmp1 and decarboxylated by Bmp8 to give **6**. Although the esterase activity of Bmp1 TE domain could indeed be confirmed by the hydrolysis of the model esterase substrate *p*-nitrophenylacetate (**Supplementary Fig. 10**), biochemical investigations into the formation of **6** by Bmp8 were precluded by our inability to generate soluble recombinant Bmp8 protein. However, the expression of *bmp1–7* in *E. coli* excluding *bmp8* resulted in altered levels of bromopyrroles, thus supporting a role of Bmp8 in bromopyrrole biosynthesis (**Fig. 2a** and **Supplementary Fig. 11**).

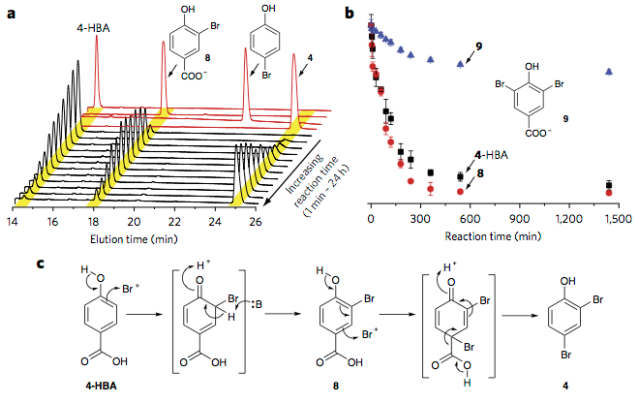

Figure 4 | Biosynthesis of bromophenols by flavin-dependent decarboxylase-brominase Bmp5. (**a**) Bmp5 was incubated with 4-HBA, KBr, NADPH and FAD at 30 °C in 20 mM Tris-HCl (pH 8.0) buffer. At the indicated time points, a 40-µl assay volume was withdrawn and quenched by the addition of 16 µl MeCN plus 0.35% TFA. HPLC separation of the substrate, intermediate and products of the Bmp5 reaction are shown as black traces after the following reaction times: 1 min, 5 min, 10 min, 30 min, 60 min, 90 min, 120 min, 180 min, 240 min, 360 min, 540 min and 1,440 min. HPLC traces corresponding to synthetic standards analyzed under identical chromatographic conditions are shown in red. (**b**) Time-dependent conversion of **8** to **4** and of **9** to **5** was monitored in an identical fashion, and the area under the substrate peaks was integrated and plotted against reaction time to compare the relative rates for the consumption of 4-HBA, **8** and **9** by Bmp5. Experiments were conducted in triplicate; data represent mean values ± s.d. (**c**) A proposed reaction scheme for the conversion of 4-HBA to **4** catalyzed by Bmp5.

Bmp5, a decarboxylating phenol brominase

In contrast to assembly of bromopyrroles, the biosynthetic logic for the assembly of bromophenols and thereafter of PBDEs and polybrominated biphenyls could not be readily anticipated. Previous isotope feeding experiments[35] and the presence of a chorismate lyase (Bmp6) in the gene cluster suggested 4-hydroxybenzoic acid (4-HBA) as the precursor for the bromophenol moiety of **3**. Although the *bmp5* deletion experiments postulated its role as the phenol brominase, the lack of sequence similarity of the flavoenzyme Bmp5 to canonical flavin-dependent halogenases, which includes Bmp2, led to uncertainty in this assignment. Moreover, incorporation of 4-HBA into bromophenols necessitates decarboxylation, a transformation not previously associated with flavin-dependent halogenases. Hence, we undertook a detailed *in vitro* characterization of the activity of Bmp5. Upon incubation of 4-HBA with recombinant Bmp5 in the presence of bromide, NADPH and FAD, we observed a time-dependent formation of one major product via a stable intermediate (**Fig. 4a** and **Supplementary Fig. 16**). The identity of the intermediate as 3-bromo-4-hydroxybenzoic acid (**8**) and of the product as **4** was confirmed by MS and retention time comparison to authentic synthetic standards (**Fig. 4a** and **Supplementary Fig. 17**). Bmp5 could use **8** as a substrate for the synthesis of **4**, further establishing **8** as the physiological intermediate for the reaction (**Fig. 4b**). Bmp5 also generated **5** when expressed in *E. coli* in the presence of bromide (**Supplementary Fig. 17**). Although production of **5** could not be detected *in vitro*, this observation is consistent with the acceptance of 3,5-dibromo-4-hydroxybenzoic acid (**9**) as a poor substrate by Bmp5 as compared to 4-HBA and **8** (**Fig. 4b**). Bmp5 activity was abolished in the absence of either bromide or NADPH, whereas a partial reduction in activity was observed upon omission of FAD, consistent with the partial occupancy of FAD in Bmp5 as purified (**Supplementary Fig. 18**). Consistent with prior characterization of halide specificity of aromatic halogenases[33], Bmp5 could use iodide *in vivo*, leading to the formation of iodophenols, whereas no chloride incorporation was observed (**Supplementary Fig. 28**).

In contrast to the flavin-dependent halogenases described to date, Bmp5 did not require the addition of a flavin reductase to regenerate $FADH_2$ *in situ*. This finding is consistent with sequence homology of Bmp5 to single-component flavin-dependent oxygenases (**Supplementary Fig. 30**). Consistent with the formation of electrophilic peroxo intermediates by flavin-dependent oxygenases and halonium intermediates by flavin-dependent halogenases[36], a putative reaction scheme catalyzed by Bmp5 can be discerned (**Fig. 4c**). To the best of our knowledge, Bmp5 represents the first example of a decarboxylating flavin-dependent halogenase. The stability of benzoic acids distinguishes the Bmp5 decarboxylation activity from the extensively sampled marine haloperoxidases[37] that participate in the decarboxylative degradation of labile halogenated derivatives of 3-oxo carboxylic acids and acyl homoserine lactones[38,39].

Bmp7 catalyzed coupling of bromophenols and bromopyrroles

We next investigated whether the bromophenol products of Bmp5 could be accepted as substrates by CYP450 Bmp7. In the presence of ferredoxin (Bmp9), ferredoxin reductase (Bmp10) and NADH, Bmp7 catalyzed the coupling of **4** to at least six distinct products that could be identified by LC/MS/MS (**Fig. 5a**). Characterization of Bmp7 products provided by MS/MS, NMR and comparison to authentic standards is detailed in **Supplementary Note 2**. We confirmed polybrominated biphenyls previously isolated from *Pseudoalteromonas* spp., **1** (ref. 18) and 3,5,5′-tribromo-2,2′-biphenyldiol (**10**) (ref. 40) as Bmp7 products (**Fig. 5** and **Supplementary Figs. 19** and **20**). Additionally, a tribromo-biphenyldiol isomer of **10** (**Fig. 5a**) was detected as a Bmp7 product but could not be isolated in sufficient quantities for comprehensive structure elucidation.

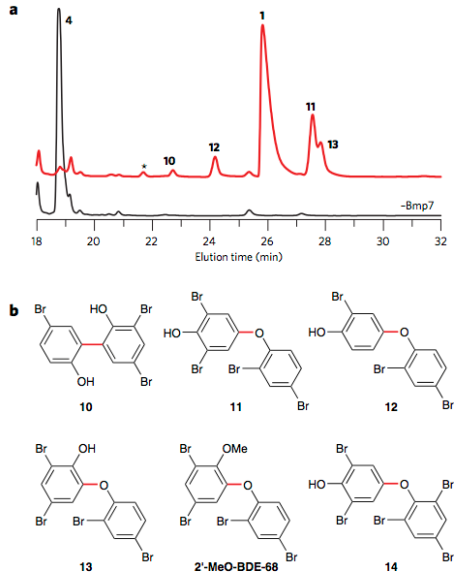

Figure 5 | Enzymatic synthesis of polybrominated biphenyls and OH-BDEs. (**a**) CYP450 Bmp7 dimerizes two molecules of **4** to generate biphenyls **1** and **10** and OH-BDEs **11**–**13** (red curve). The curve in black represents the negative control in the absence of the enzyme. Asterisk represents a likely tribrominated biphenyl coupling product that could not be isolated in quantities sufficient for comprehensive structural characterization. (**b**) Chemical structures of polybrominated biphenyls and OH-BDEs generated by the *bmp* pathway, as identified in this study. Coupling bonds generated by Bmp7 are shown in red. Also shown is 2′-MeO-BDE-68, the methoxylated derivative of **13**.

Guided by differential MS/MS fragmentation of polybrominated biphenyls and OH-BDEs[41], we further characterized three OH-BDE products, namely 2,6-dibromo-4-(2,4-dibromophenoxy) phenol (**11**), 2-bromo-4-(2,4-dibromophenoxy)phenol (**12**) and 4,6-dibromo-2-(2,4-dibromophenoxy)phenol (2′-OH-BDE68, **13**) (**Fig. 5**, **Supplementary Note 2** and **Supplementary Figs. 20**–**22**). The OH-BDE products have two distinct chemical signatures, namely, *para* (**11** and **12**) and *ortho* coupling (**13**) with respect to the hydroxyl group (**Fig. 5b**). Guided by our *in vitro* identification of OH-BDEs, we analyzed organic extracts of *P. luteoviolacea* 2ta16 as well as *E. coli* expressing *bmp1–8* and confirmed the *in vivo* production of **11** and **12** (**Figs. 1b** and **2a**). This observation provides what is to our knowledge the first confirmation for marine bacterial biosynthesis of OH-BDEs. **11** and **13** are isomeric with **1** and have very similar retention times to each other. Moreover, in contrast to the diagnostic MS2 patterns for polybrominated biphenyls and *para*-OH-BDEs (**Supplementary Note 2**), the structural characterization of **13** relied on comparison to an authentic synthetic standard (**Supplementary Fig. 22**). These findings highlight some of the technical challenges inherent with the characterization of isomeric polybrominated biphenyl and OH-BDE products from whole-cell culture extracts.

Bmp7 could also dimerize two molecules of **5**, albeit with reduced catalytic efficiency, to generate the OH-BDE product 2,6-dibromo-4-(2,4,6-tribromophenoxy)phenol (**14**) (**Fig. 5b** and **Supplementary Figs. 23** and **24**). Bmp7 converted chlorinated phenolic substrates as well, catalyzing the dimerization of 2,4-dichlorophenol to three isomeric products, corresponding to chlorinated counterparts to the polybrominated products **1**, **11** and **13** generated with **4** (**Supplementary Fig. 25**). The MS-based prediction of the polychlorinated products is described in detail in **Supplementary Note 2**.

Proceeding on the basis of the biosynthetic logic for the hydrolytic offloading of tribromopyrrole carboxylic acid by Bmp1 TE domain and its decarboxylation by Bmp8, we propose **6** as the physiological substrate for Bmp7, which is supported by a typical substrate-induced UV-visible absorbance shift (**Supplementary Fig. 12**). *In vitro* activity assays of Bmp7 in the presence of redox partners Bmp9–10 and NADH with **6** as a substrate generated **2** and **7** as major products (**Supplementary Figs. 13**–**15**). The identity of the reaction products was confirmed by comparison to authentic standards. A final demonstration for the biosynthetic versatility for Bmp7 was provided by an *in vitro* reaction involving the heterodimerization of **4** and **6**. We confirmed the enzymatic synthesis of **3** and 2,3,5,7-tetrabromobenzofuro[3,2-*b*] pyrrole (**15**)[40] by comparison to authentic standards isolated from *P. luteoviolacea* 2ta16 (**Fig. 6a** and **Supplementary Figs. 26**–**27**). Additionally, we detected an isomer of **3** as a minor product generated by Bmp7 during the *in vitro* coupling of **4** and **6**, which could also be detected in the culture extracts of the three producer strains. Though a comprehensive structural characterization by NMR spectroscopy could not be realized, a characteristic hydroxytribromopyrrole MS/MS product ion suggests a polybrominated phenol-pyrrole ether, a class of marine natural product not previously described (**Supplementary Fig. 29**).

DISCUSSION

Although several Bmp pathway products identified in this study were previously isolated from marine bacteria (**1**–**3** (refs. 18–20), **7** (ref. 19), **10** and **15** (ref. 40)), with **3** being reported in 1966, the genetic and molecular bases for their biosyntheses have remained elusive until now. In this study, we identified a conserved gene locus in marine γ-proteobacteria encoding the biosynthesis of at least 15 polybrominated aromatic marine natural products containing ubiquitous bromopyrrole and bromophenol building blocks. A near-complete *in vitro* reconstitution of all of the enzymatic steps within the Bmp pathway provides the basis for a bimodular biosynthetic scheme (**Fig. 6a**).

The bromopyrrole and bromophenol biosynthetic modules function independently and are united through the action of CYP450 Bmp7. CYP450-catalyzed phenol coupling reactions have extensive biochemical precedents, and the formation of polybrominated biphenyls **1** and **10** and OH-BDEs **11**–**14** are expected to follow accepted biradical mechanisms (**Fig. 6b**). A similar mechanism can be envisaged for coupling of bromopyrroles, consistent with CYP450-catalyzed coupling in indolocarbazole antibiotics[42]. The modularity of the Bmp pathway is reflected in the preservation of only the bromopyrrole biosynthetic module in the marine symbiotic cyanobacterium *P. didemni* P2-Fiji[27] (**Fig. 1c**). As the bromophenol module is absent, it is likely that *P. didemni* P2-Fiji produces only halogenated pyrroles. Furthermore, a homologous gene locus identified in *T. thiocyanoxidans* ARh 4 lacks a gene coding for a coupling CYP450 (**Fig. 1c**). It is conceivable that an even wider applicability of the chemical logic described here for the biosynthesis of marine bromophenols and bromopyrroles is limited only by the availability of genomic data.

The discovery of flavoenzyme Bmp5 as a phenol brominase was unexpected. Bmp5 is homologous to flavin-dependent oxygenases[43] rather than flavin-dependent halogenases. Primary sequence motifs for binding both the flavin cofactor as well as the nicotinamide electron donor can be readily discerned within the primary sequence of Bmp5 (**Supplementary Fig. 30**). Indeed,

NATURE CHEMICAL BIOLOGY DOI: 10.1038/NCHEMBIO.1564 ARTICLE

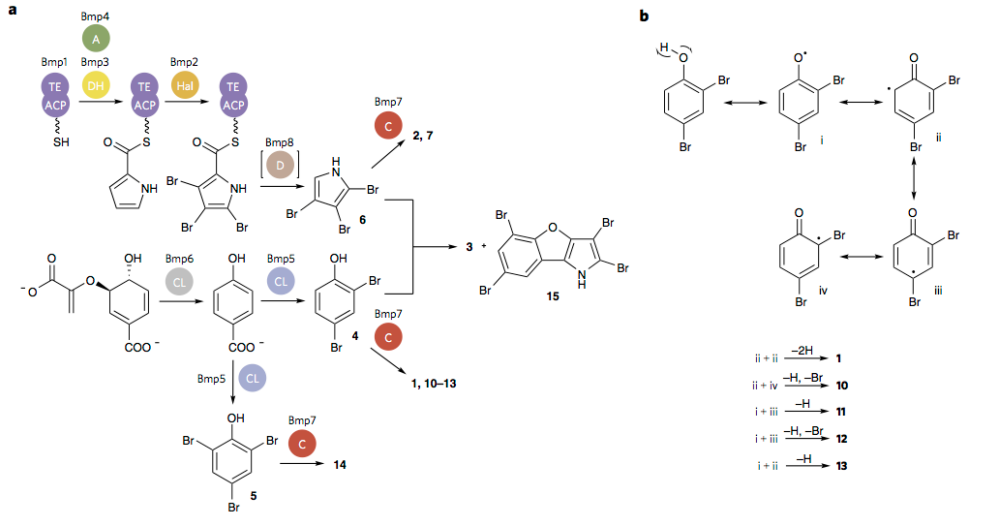

Figure 6 | Bi-modular scheme for the biosynthesis of polybrominated marine natural products by the *bmp* pathway. (**a**) Chorismate, the precursor for bromophenols, is converted to 4-HBA by chorismate lyase (CL) Bmp6 and then to **4** and **5** by flavin-dependent halogenase (Hal) Bmp5. The CYP450 coupling (C) enzyme Bmp7 generates a suite of diverse polybrominated biphenyls (**1** and **10**) and OH-BDEs (**11**–**14**) from **4** and **5**. The electron transfer partners for Bmp7, Bmp9 and Bmp10 are omitted for clarity. The bromopyrroles are derived from L-proline. Acylation of L-proline to the ACP domain of Bmp1 by the proline adenyltransferase (A) Bmp4 initiates its oxidation by the flavin-dependent dehydrogenase (DH) Bmp3 and tribromination by the flavin-dependent halogenase (Hal) Bmp2. The TE domain of Bmp1 most likely catalyzes the offloading of a carboxylic acid intermediate that is decarboxylated (D) by carboxymuconolactone decarboxylase homolog Bmp8 to **6**. **6** can be dimerized by Bmp7 to generate **2**, or it can be dimerized with **4** to generate heterodimers such as **3** and **15**. During the homodimerization of **6**, we also observed the formation of **7**. The coloring scheme is consistent with that in **Figure 1c**. (**b**) Proposed steps for radical generation (i), rearrangement (ii–iv) and coupling of **4** by Bmp7 to generate biphenyls and OH-BDEs.

bmp5 homologs in the biosynthetic gene clusters identified in *M. mediterranea* MMB-1 and *T. thiocyanoxidans* ARh 4 are annotated as flavin-dependent oxygenases (**Fig. 1c**). Although decarboxylation was until now an unrealized activity within the catalytic repertoire of flavin-dependent halogenases, *ortho*-hydroxylation of 4-HBA[44] as well as *para*-decarboxylative hydroxylation of 4-HBA[45] have been reported for flavin-dependent oxygenases, leading to a proposal for a two-step reaction scheme for Bmp5 (**Fig. 4c**). The collective action of an electron-donating phenol hydroxyl and electron-withdrawing carboxyl group would first direct electrophilic bromonium addition at the *ortho* position, and subsequent proton abstraction by a catalytic base would result in the formation of **8**. This intermediate would then undergo a second bromonium addition *para* to the hydroxyl, followed by decarboxylation to generate **4**. The Bmp5 reaction is regiospecific in that *ortho* bromination is the first half-reaction, followed by decarboxylative-bromination at the *para* position. This assertion for the strictly directed two-step Bmp5 reaction scheme is supported by 4-bromophenol not being detected as an intermediate or as a product of the Bmp5 reaction (**Fig. 4a**). Furthermore, the Bmp5 active site most likely sterically occludes bromonium addition at one of the *ortho* positions of the aryl ring, thus biasing the second half-reaction toward decarboxylative-bromination at the *para* position, rather than a second *ortho* bromination to yield **9** as a second intermediate. This postulate is supported by the observation that under identical experimental conditions, rates of decrease of 4-HBA and **8** in an *in vitro* reaction with Bmp5 are nearly identical, whereas **9** is a poor substrate for Bmp5 (**Fig. 4b**). Consequently, **5** is a minor product generated by Bmp5 that could not be detected *in vitro* but is only detected to be produced *in vivo* when Bmp5 is heterologously expressed in *E. coli* in the presence of bromide in the culture medium (**Supplementary Fig. 17**). Additionally, Bmp5 could use iodide but not chloride *in vivo* (**Supplementary Fig. 28**).

It is notable that neither bromophenol monomers nor OH-BDEs had previously been isolated from marine bacterial sources. Bromophenols and OH-BDEs identified in this study (and their methylated derivatives) have instead been extensively detected in marine eukaryotes, ranging from autotrophs and invertebrates, to apex predators[5–15,46]. Although sponge-associated symbiotic cyanobacteria were hinted as producers of OH-BDEs[10], a definite genetic basis for OH-BDE biosynthesis had not been established. Furthermore, in the absence of definitive genetic evidence for algal biosynthesis of OH-BDEs, a contribution of associated bacteria toward the production of OH-BDEs sourced from marine algae cannot be discounted[8,12]. It is thus noteworthy that all three marine bacteria harboring the Bmp pathway as identified in this study also belong to genera commonly associated with marine eukaryotes. Identification of the *bmp* gene locus should henceforth aid the computational mining of marine metagenomic data sets for the identification of bacterial as well as potential eukaryotic OH-BDE producers using similar motifs. Together with **1** (**Fig. 1a**), the methoxylated derivative for **13** (2′-MeO-BDE-68; **Fig. 5b**) is extensively detected in marine mammals and even humans[14,15], suggesting that bromophenols and OH-BDEs identified in this study bioaccumulate in the marine food web and are transferred to humans via trophic connections. Furthermore, methylation of OH-BDEs and, by extension, of polybrominated biphenyls and bipyrroles (**Fig. 1a**) seems to be a facile biochemical transformation consistent with a positive correlation between the existence of OH-BDEs and MeO-BDEs in marine environmental matrices[16,47].

OH-BDEs, such as those characterized in this study, commonly feature two distinct chemical signatures in which the hydroxyl group is positioned either *ortho* or *para* to the ether linkage. Of the two regioisomers, *para*-OH-BDEs are potent inhibitors of thyroid hormone signaling[48], with **14** having a higher affinity for binding to the thyroid hormone transport protein than its physiological substrates[49]. Hence, the detection of *para*-OH-BDEs such as **11** and **12** and, specifically, **14** puts into perspective the toxic potential of the metabolites generated by the Bmp pathway. As the synthesis of biphenyls and diphenyl ethers could also be confirmed for Bmp7 using polychlorinated and polyiodinated phenolic substrates (**Supplementary Figs. 25** and **28**), other naturally occurring polyhalogenated aryl compounds may also be derived from analogous enzymatic pathways with differing halogen specificities of the halogenases. As the industrial production of polybrominated flame-retardant chemicals continues to be phased out in recognition of their persistence and toxicity, we anticipate that naturally produced marine bacterial PBDEs will take a center stage in informing our small molecule–mediated interactions with the environment.

Received 15 December 2013; accepted 19 May 2014;
published online 29 June 2014

METHODS

Methods and any associated references are available in the online version of the paper.

Accession codes. GenBank. Sequence data for *P. luteoviolacea* 2ta16 and *P. phenolica* O-BC30 has been deposited under accession codes AUSV00000000 (accession code for contig containing the *bmp* locus: AUSV01000133.1) and KF540211 (*bmp* locus accession code KF540211.1), respectively.

References

1. Gribble, G.W. The natural production of organobromine compounds. *Environ. Sci. Pollut. Res. Int.* **7**, 37–47 (2000).
2. Gribble, G.W. *Naturally Occurring Organohalogen Compounds—a Comprehensive Update*. Vol. 91 (Springer Vienna, 2010).
3. Liu, Y.N. *et al.* Spatial and temporal distributions of bromoform and dibromomethane in the Atlantic Ocean and their relationship with photosynthetic biomass. *J. Geophys. Res.–Oceans* **118**, 3950–3965 (2013).
4. Al-Mourabit, A., Zancanella, M.A., Tilvi, S. & Romo, D. Biosynthesis, asymmetric synthesis, and pharmacology, including cellular targets, of the pyrrole-2-aminoimidazole marine alkaloids. *Nat. Prod. Rep.* **28**, 1229–1260 (2011).
5. Gaul, S. *et al.* Identification of the natural product 2,3,4,5-tetrabromo-1-methylpyrrole in Pacific biota, passive samplers and seagrass from Queensland, Australia. *Mar. Pollut. Bull.* **62**, 2463–2468 (2011).
6. Kitamura, M., Koyama, T., Nakano, Y. & Uemura, D. Corallinafuran and Corallinaether, novel toxic compounds from crustose coralline red algae. *Chem. Lett.* **34**, 1272–1273 (2005).
7. Kuniyoshi, M., Yamada, K. & Higa, T. A biologically-active diphenyl ether from the green-alga *Cladophora fascicularis*. *Experientia* **41**, 523–524 (1985).
8. Malmvärn, A., Zebuhr, Y., Kautsky, L., Bergman, K. & Asplund, L. Hydroxylated and methoxylated polybrominated diphenyl ethers and polybrominated dibenzo-*p*-dioxins in red alga and cyanobacteria living in the Baltic Sea. *Chemosphere* **72**, 910–916 (2008).
9. King, G.M., Giray, C. & Kornfield, I. Biogeographical, biochemical and genetic differentiation among North-American *Saccoglossids* (*Hemichordata, Enteropneusta, Harrimaniidae*). *Mar. Biol.* **123**, 369–377 (1995).
10. Unson, M.D., Holland, N.D. & Faulkner, D.J. A brominated secondary metabolite synthesized by the cyanobacterial symbiont of a marine sponge and accumulation of the crystalline metabolite in the sponge tissue. *Mar. Biol.* **119**, 1–11 (1994).
11. Calcul, L. *et al.* NMR strategy for unraveling structures of bioactive sponge-derived oxy-polyhalogenated diphenyl ethers. *J. Nat. Prod.* **72**, 443–449 (2009).
12. Löfstrand, K. *et al.* Brominated phenols, anisoles, and dioxins present in blue mussels from the Swedish coastline. *Environ. Sci. Pollut. Res. Int.* **17**, 1460–1468 (2010).
13. Vetter, W., Scholz, E., Gaus, C., Müller, J.F. & Haynes, D. Anthropogenic and natural organohalogen compounds in blubber of dolphins and dugongs (*Dugong dugon*) from northeastern Australia. *Arch. Environ. Contam. Toxicol.* **41**, 221–231 (2001).
14. Marsh, G. *et al.* Identification, quantification, and synthesis of a novel dimethoxylated polybrominated biphenyl in marine mammals caught off the coast of Japan. *Environ. Sci. Technol.* **39**, 8684–8690 (2005).
15. Teuten, E.L., Xu, L. & Reddy, C.M. Two abundant bioaccumulated halogenated compounds are natural products. *Science* **307**, 917–920 (2005).
16. Wan, Y. *et al.* Origin of hydroxylated brominated diphenyl ethers: natural compounds or man-made flame retardants? *Environ. Sci. Technol.* **43**, 7536–7542 (2009).
17. Ren, X.M. & Guo, L.H. Molecular toxicology of polybrominated diphenyl ethers: nuclear hormone receptor mediated pathways. *Environ. Sci. Process. Impacts* **15**, 702–708 (2013).
18. Isnansetyo, A. & Kamei, Y. MC21-A, a bactericidal antibiotic produced by a new marine bacterium, *Pseudoalteromonas phenolica* sp. nov. O-BC30^{T}, against methicillin-resistant *Staphylococcus aureus*. *Antimicrob. Agents Chemother.* **47**, 480–488 (2003).
19. Andersen, R.J., Wolfe, M.S. & Faulkner, D.J. Autotoxic antibiotic production by a marine chromobacterium. *Mar. Biol.* **27**, 281–285 (1974).
20. Burkholder, P.R., Pfister, R.M. & Leitz, F.H. Production of a pyrrole antibiotic by a marine bacterium. *Appl. Microbiol.* **14**, 649–653 (1966).
21. Holmström, C. & Kjelleberg, S. Marine *Pseudoalteromonas* species are associated with higher organisms and produce biologically active extracellular agents. *FEMS Microbiol. Ecol.* **30**, 285–293 (1999).
22. Vetter, W. Polyhalogenated alkaloids in environmental and food samples. *Alkaloids Chem. Biol.* **71**, 211–276 (2012).
23. Rypien, K.L., Ward, J.R. & Azam, F. Antagonistic interactions among coral-associated bacteria. *Environ. Microbiol.* **12**, 28–39 (2010).
24. Dorrestein, P.C., Yeh, E., Garneau-Tsodikova, S., Kelleher, N.L. & Walsh, C.T. Dichlorination of a pyrrolyl-*S*-carrier protein by FADH2-dependent halogenase PltA during pyoluteorin biosynthesis. *Proc. Natl. Acad. Sci. USA* **102**, 13843–13848 (2005).
25. Peschke, J.D., Hanefeld, U. & Laatsch, H. Biosynthesis of the marine antibiotic pentabromopseudilin. 2. The pyrrole ring. *Biosci. Biotechnol. Biochem.* **69**, 628–630 (2005).
26. Lucas-Elío, P. *et al.* Complete genome sequence of the melanogenic marine bacterium *Marinomonas mediterranea* type strain (MMB-1^{T}). *Stand. Genomic Sci.* **6**, 63–73 (2012).
27. Donia, M.S., Fricke, W.F., Ravel, J. & Schmidt, E.W. Variation in tropical reef symbiont metagenomes defined by secondary metabolism. *PLoS ONE* **6**, e17897 (2011).
28. Sorokin, D.Y., Tourova, T.P., Lysenko, A.M., Mityushina, L.L. & Kuenen, J.G. *Thioalkalivibrio thiocyanoxidans* sp. nov. and *Thioalkalivibrio paradoxus* sp. nov., novel alkaliphilic, obligately autotrophic, sulfur-oxidizing bacteria capable of growth on thiocyanate, from soda lakes. *Int. J. Syst. Evol. Microbiol.* **52**, 657–664 (2002).
29. Walsh, C.T., Garneau-Tsodikova, S. & Howard-Jones, A.R. Biological formation of pyrroles: nature's logic and enzymatic machinery. *Nat. Prod. Rep.* **23**, 517–531 (2006).
30. Buedenbender, S., Rachid, S., Muller, R. & Schulz, G.E. Structure and action of the myxobacterial chondrochloren halogenase CndH: a new variant of FAD-dependent halogenases. *J. Mol. Biol.* **385**, 520–530 (2009).
31. van Pée, K.H. Enzymatic chlorination and bromination. *Methods Enzymol.* **516**, 237–257 (2012).
32. Eichhorn, E., van der Ploeg, J.R. & Leisinger, T. Characterization of a two-component alkanesulfonate monooxygenase from *Escherichia coli*. *J. Biol. Chem.* **274**, 26639–26646 (1999).
33. Blasiak, L.C. & Drennan, C.L. Structural perspective on enzymatic halogenation. *Acc. Chem. Res.* **42**, 147–155 (2009).
34. Gribble, G.W. Occurrence of halogenated alkaloids. *Alkaloids Chem. Biol.* **71**, 1–165 (2012).
35. Hanefeld, U., Floss, H.G. & Laatsch, H. Biosynthesis of the marine antibiotic pentabromopseudilin. 1. The benzene-ring. *J. Org. Chem.* **59**, 3604–3608 (1994).
36. Walsh, C.T. & Wencewicz, T.A. Flavoenzymes: versatile catalysts in biosynthetic pathways. *Nat. Prod. Rep.* **30**, 175–200 (2013).
37. Hewson, W.D. & Hager, L.P. Bromoperoxidases and halogenated lipids in marine-algae. *J. Phycol.* **16**, 340–345 (1980).
38. Borchardt, S.A. *et al.* Reaction of acylated homoserine lactone bacterial signaling molecules with oxidized halogen antimicrobials. *Appl. Environ. Microbiol.* **67**, 3174–3179 (2001).
39. Beissner, R.S., Guilford, W.J., Coates, R.M. & Hager, L.P. Synthesis of brominated heptanones and bromoform by a bromoperoxidase of marine origin. *Biochemistry* **20**, 3724–3731 (1981).
40. Fehér, D., Barlow, R., McAtee, J. & Hemscheidt, T.K. Highly brominated antimicrobial metabolites from a marine *Pseudoalteromonas* sp. *J. Nat. Prod.* **73**, 1963–1966 (2010).
41. Mas, S. *et al.* Comprehensive liquid chromatography-ion-spray tandem mass spectrometry method for the identification and quantification of eight hydroxylated brominated diphenyl ethers in environmental matrices. *J. Mass Spectrom.* **42**, 890–899 (2007).

42. Makino, M. *et al.* Crystal structures and catalytic mechanism of cytochrome P450 StaP that produces the indolocarbazole skeleton. *Proc. Natl. Acad. Sci. USA* **104**, 11591–11596 (2007).
43. Ballou, D.P., Entsch, B. & Cole, L.J. Dynamics involved in catalysis by single-component and two-component flavin-dependent aromatic hydroxylases. *Biochem. Biophys. Res. Commun.* **338**, 590–598 (2005).
44. Eppink, M.H., Cammaart, E., Van Wassenaar, D., Middelhoven, W.J. & van Berkel, W.J. Purification and properties of hydroquinone hydroxylase, a FAD-dependent monooxygenase involved in the catabolism of 4-hydroxybenzoate in *Candida parapsilosis* CBS604. *Eur. J. Biochem.* **267**, 6832–6840 (2000).
45. Eppink, M.H., Boeren, S.A., Vervoort, J. & van Berkel, W.J. Purification and properties of 4-hydroxybenzoate 1-hydroxylase (decarboxylating), a novel flavin adenine dinucleotide-dependent monooxygenase from *Candida parapsilosis* CBS604. *J. Bacteriol.* **179**, 6680–6687 (1997).
46. Blunt, J.W., Copp, B.R., Keyzers, R.A., Munro, M.H. & Prinsep, M.R. Marine natural products. *Nat. Prod. Rep.* **30**, 237–323 (2013).
47. Wiseman, S.B. *et al.* Polybrominated diphenyl ethers and their hydroxylated/methoxylated analogs: environmental sources, metabolic relationships, and relative toxicities. *Mar. Pollut. Bull.* **63**, 179–188 (2011).
48. Ucán-Marin, F., Arukwe, A., Mortensen, A.S., Gabrielsen, G.W. & Letcher, R.J. Recombinant albumin and transthyretin transport proteins from two gull species and human: chlorinated and brominated contaminant binding and thyroid hormones. *Environ. Sci. Technol.* **44**, 497–504 (2010).
49. Meerts, I.A. *et al.* Potent competitive interactions of some brominated flame retardants and related compounds with human transthyretin in vitro. *Toxicol. Sci.* **56**, 95–104 (2000).
50. Dorrestein, P.C. & Kelleher, N.L. Dissecting non-ribosomal and polyketide biosynthetic machineries using electrospray ionization Fourier-Transform mass spectrometry. *Nat. Prod. Rep.* **23**, 893–918 (2006).

Acknowledgments

We thank our colleagues E. Frick for preliminary *in vitro* studies with Bmp6, B.M. Duggan for assistance in NMR data collection, P.A. Jordan for NMR data analysis, Y. Su for MS data collection and L.I. Aluwihare for useful discussions. This work was jointly supported by the US National Science Foundation (OCE-1313747) and the US National Institute of Environmental Health Sciences (P01-ES021921) through the Oceans and Human Health program, the Gordon and Betty Moore Foundation Marine Microbial Sequencing Project, the Helen Hay Whitney Foundation postdoctoral fellowship to V.A., the US National Institutes of Health (NIH) Marine Biotechnology Training Grant predoctoral fellowship to A.A.E. (T32-GM067550) and an NIH instrument grant (S10-RR031562).

Author contributions

V.A., A.A.E., E.E.A. and B.S.M. designed research; V.A., A.A.E. and K.Y. performed genetic experiments; V.A., A.A.E. and R.D.K. performed *in vitro* experiments; M.S. and E.E.A. generated sequencing data; D.P. contributed new analytical reagents; and V.A., A.A.E., E.E.A. and B.S.M. analyzed data and wrote the manuscript.

Competing financial interests

The authors declare no competing financial interests.

Additional information

Supplementary information and chemical compound information is available in the online version of the paper. Reprints and permissions information is available online at http://www.nature.com/reprints/index.html. Correspondence and requests for materials should be addressed to B.S.M.

Supplementary Information for

Biosynthesis of polybrominated aromatic organic compounds by marine bacteria

Vinayak Agarwal, Abrahim A. El Gamal, Kazuya Yamanaka, Dennis Poth, Roland D. Kersten, Michelle Schorn, Eric E. Allen, Bradley S. Moore

SUPPLEMENTARY RESULTS

Supplementary Note 1

Detection of dehydrogenation and halogenation of L-proline acylated to Bmp1.

Trypsin-digested N-His_6-Bmp1(ACP) was analyzed by LC-MS/MS. 10 µL of the trypsin-digested assay mixture was injected onto a reverse phase C_4 column (Vydac 5 µm, 4.6 mm × 250 mm). Water + 0.1% formic acid was used as solvent A, and MeCN + 0.1% formic acid was used as solvent B. The elution profile was as follows (0.7 mL/min): 10% B for 10 min, linear increase to 30% B across 5 min, linear increase to 70% B across 40 min, linear decrease to 10% B across 5 min, linear increase to 100% B across 1 min followed by 2 min at 100% B, decrease to 10% B across 1 min, 10% B for 2 min and 5 min of post-time equilibration. The assay relies on the detection of MS2 product ions **i–v** as shown in **Supplementary Fig. 7**. Briefly, ion **i** would be generated by collision-induced disassociation for holo-N-His_6-Bmp1(ACP) and ion **ii** by pyrrolyl-*S*-N-His_6-Bmp1(ACP). Ions **iii–v** correspond to brominated variants for phosphopantetheinylated halo-pyrrole ions as previously described in the literature[1-2]. Expression of N-His_6-Bmp1(ACP) in *E.* coli should provide a mixture of apo-N-His_6-Bmp1(ACP), and holo-N-His_6-Bmp1(ACP) as a result of crosstalk with fatty acid biosynthesis. The side chain hydroxyl of the serine residue at the carboxy terminus of the α-2 helix for the Bmp1(ACP) should be post-translationally esterified with phosphopantetheine for holo-N-His_6-Bmp1(ACP), but not for apo-N-His_6-Bmp1(ACP). By sequence homology, this serine residue was identified to be Ser35 for Bmp1. Holo-N-His_6-Bmp1(ACP) will not participate further in the assay, as acylation by Sfp (*B. subtilis* phosphopantetheinyl transferase) requires the presence of a non-esterified Ser35 side chain. The presence of holo-N-His_6-Bmp1(ACP) was confirmed by detection of MS2 ion **i**. As a second means of independent verification, the MS2 ion **i** was traced back to a MS1

peptide fragment of N-His_6-Bmp1(ACP) that bears the Ser35 residue. For peptide mapping, the mass of the holo-peptide fragment was calculated based on the mass of the monoisotopic peak for the peptide, and its charge state (z). For calculation of the mass of the apo-peptide fragment, the mass corresponding to ion **vi** was subtracted from it. The mass of the apo-peptide fragment thus determined could be traced to the peptide fragment generated by trypsin digestion of His_6-Bmp1(ACP) as shown in **Fig. 3** and **Supplementary Fig. 8**. The equations for calculation of the apo-peptide fragment mass corresponding to holo-N-His_6-Bmp1(ACP) as identified in **Supplementary Fig. 8** are as follows:

$$z = 1/(mass\ difference\ between\ successive\ isotope\ peaks)$$

$$apo\ peptide\ mass = [(parent\ ion\ \times z) - (z\ \times 1.00728)] - 340.0858$$

Upon transfer of **16** to apo-N-His_6-Bmp1(ACP), MS2 ion **ii** could be detected, and upon mono- di-, and tri-halogenation by Bmp2, ejection ions corresponding to **iii–v** could be detected. The apo-peptide fragments generating these MS2 ions were mapped back to Bmp1(ACP) by subtraction of the mass of ions **viii–x** (**Supplementary Fig. 7**) from the respective holo-peptide masses.

Using this assay methodology, we could generate N-His_6-pyrrolyl-*S*-Bmp1(ACP) by loading **16** onto the apo-N-His_6-Bmp1(ACP). Upon addition of Bmp2, SsuE (*E. coli* flavin reductase), NADPH and KBr, mono-, di-, and tri-brominated Bmp1(ACP) peptides could be detected, thus establishing tri-bromination of the pyrrole ring by Bmp2. No halogenation was observed when KBr was replaced with KCl or KI. Regiospecificity for bromination of the pyrrole ring by Bmp2 is assumed to be similar to the pyrrole chlorinase PltA due to high sequence similarity between the two enzymes.

Supplementary Note 2

Identification and characterization of polybrominated biphenyl and OH-BDE products generated by Bmp7 *in vitro*, and a mass spectrometry-based detection of OH-BDEs in culture extracts.

MS1 for the Bmp7 *in vitro* reaction analyte (**Supplementary Fig. 20**, panel **a**) led to determination of the molecular weights of different product species, and together with the typical isotopic distribution afforded by bromination, molecular formulae of the products could be discerned. With **4** as a substrate, three isomers each for the molecular formulae $C_{12}H_6O_2Br_4$ (**Supplementary Fig. 20**, panel **b**) and $C_{12}H_7O_2Br_3$ (**Supplementary Fig. 20**, panel **c**) could be reproducibly detected as the major products of the reaction. The most abundant isotope ion for each formula was then selected for targeted MS/MS by collision induced disassociation. An identical approach was used to analyze products of the reaction with 2,4-dichlorophenol (**17**) (described later). The molecular formulae for the major products, $C_{12}H_6O_2Br_4$ and $C_{12}H_7O_2Br_3$, could be putatively assigned to biphenyl products **1** and **10**, respectively, as both molecules have previously been isolated from *Pseudoalteromonas* species. Upon chromatographic analysis of authentic synthetic standards of **1** and **10** (**Supplementary Fig. 19**), we could assign one of the isomers for $C_{12}H_6O_2Br_4$ as **1**, and one of the isomers for $C_{12}H_7O_2Br_3$ as **10**. These assignments were further confirmed by preparative scale purification of these two products from large scale *in vitro* Bmp7 reactions, and comparison of ^{1}H NMR spectra against values reported in literature[3-4]. While the mechanism for synthesis of **1** from **4** is expected to be analogous to bi-radical aryl coupling reactions[5-6], the production of **10** would additionally entail dehalogenation that has been reported in literature for aryl-coupling enzymes employing radical intermediates[7].

MS/MS analysis for **1** and **10** showed $[M\text{-}Br^-]^-$ and $[M\text{-}2Br^-]^-$ MS2 product ions (**Supplementary Fig. 20**, panels **d–e**, and panel **f** respectively), as would be expected for polybrominated biphenyls. Another isomer for $C_{12}H_7O_2Br_3$ also showed $[M\text{-}Br^-]^-$ MS2 product ions (**Supplementary Fig. 20**, panel **f**), leading to its assignment as a biphenyl (denoted by * in **Fig. 5a**). However, the molecule could not be isolated from large-scale Bmp7 reactions in sufficient quantities for comprehensive structure elucidation by NMR spectroscopy. As this species is isomeric with **10**, and is putatively a polybrominated biphenyl, we postulate its structure to be 3,3',5-tribromo-[1,1'-biphenyl]-2,4'-diol.

At this point, the identities of the other two isomers of $C_{12}H_6O_2Br_4$ and one isomer for $C_{12}H_7O_2Br_3$ were unknown. One of the isomers of $C_{12}H_6O_2Br_4$ (retention time ~ 28.2 min) showed MS2 product ions corresponding to dibromobenzoquinone (**Supplementary Fig. 20**, panel **g**). This ion could not be generated by a polybrominated biphenyl species, as scission of the carbon-carbon bond between the two aryl rings would lead to the formation of a dibromophenol ion, regardless of the positions of the bromines on the benzene ring. However, an OH-BDE molecule, in which scission of the ether bond occurs prior to the loss of bromine during MS/MS can generate a MS2 ion corresponding to dibromobenzoquinone as observed in panel **g**, and also reported in literature for para-OH-BDEs[8]. Hence, we putatively assigned this species as a para-OH-BDE. This hypothesis was supported by the observation that an isomeric OH-BDE to **1** should have a greater retention time than **1**, as one of the hydrophilic hydroxyl groups in **1** would be involved in ether bond formation in the OH-BDE. Preparative scale purification of this species from large scale Bmp7 reactions, and structure elucidation by NMR led to assignment of the structure as 2,6-dibromo-4-(2,4-dibromophenoxy)phenol (**11**) (**Supplementary Fig. 21**). Structure assignments for OH-BDEs are based upon ^{1}H NMR, HSQC, HMBC, and H2BC experiments. ^{13}C NMR shifts, deduced from HSQC, HMBC and H2BC correlations, are listed in the figure below. Specifically, **11**

was isolated by preparative HPLC separation of products from ethyl acetate extracts of large scale Bmp7 reactions with **4**. The solvent was removed *in vacuo*, and dried overnight to yield a white residue. The residue was dissolved in d_6-DMSO and NMR spectra collected using 600 MHz Varian NMR microprobe. Deduced structure of the molecule with proton shifts listed in red, and carbon shifts as deduced from HSQC and HMBC couplings listed in green is shown in panel **a** below. HSQC correlations are shown as thick bonds, HMBC correlations are shown as red arrows, and H2BC[11] correlations are shown as blue arrows in panel **b** below.

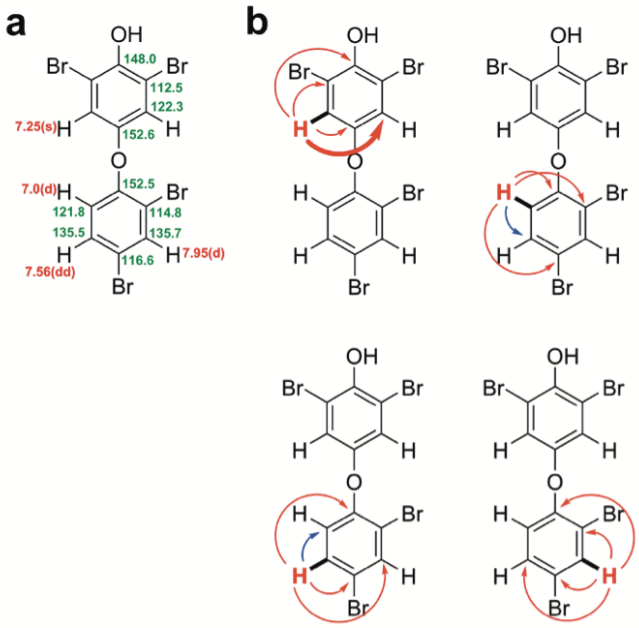

Note that the symmetry of one aryl ring is supported by the presence of a singlet in the ^{1}H NMR (**Supplementary Fig. 21**), and the HMBC coupling shown as a bold arrow that is identical to a HSQC coupling. Symmetry for the aryl rings is also supported by MS/MS fragmentation consistent with para-OH-BDE[8] (**Supplementary Fig. 20**). The isomeric ortho-OH-BDE (2′-OH-BDE-68) would have no symmetrical aryl ring. The ^{1}H and ^{13}C shifts

reported here for the non-symmetrical aryl ring are in agreement with those reported in literature[12].

One of the isomers for $C_{12}H_7O_2Br_3$ exhibiting MS2 product ions corresponding to monobromobenzoquinone (**Supplementary Fig. 20**, panel **h**), was isolated and its structure characterized by NMR spectroscopy to be 2-bromo-4-(2,4-dibromophenoxy)phenol (**12**). Specifically, **12** was isolated by preparative HPLC purification of ethyl acetate extracts of large scale Bmp7 reactions with **4**. The solvent was removed *in vacuo*, and dried overnight to yield a white residue. The residue was dissolved in d_6-DMSO and NMR spectra collected using 600 MHz Varian NMR microprobe. Deduced structure of the molecule with proton shifts listed in red and carbon shifts listed in green is shown panel **a** below. HSQC correlations are shown as thick bonds, HMBC correlations are shown as red arrows, and H2BC[11] correlations are shown as blue arrows in panel **b** below.

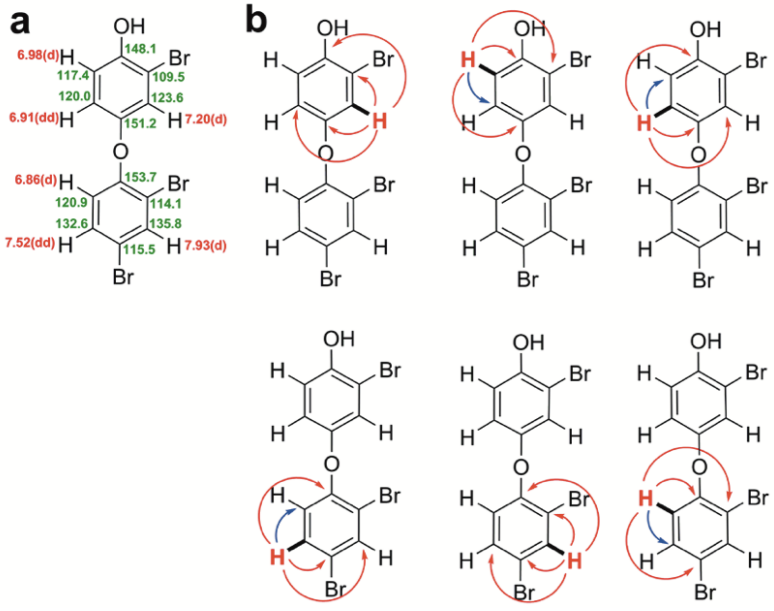

12: ^{1}H NMR (600 MHz, DMSO) δ 7.93 (d, *J* = 2.3 Hz, 1H), 7.52 (dd, *J* = 8.8, 2.4 Hz, 1H), 7.20 (d, *J* = 2.9 Hz, 1H), 6.98 (d, *J* = 8.8 Hz, 1H), 6.91 (dd, *J* = 8.8, 2.8 Hz, 1H), 6.86 (d, *J* = 8.8 Hz, 1H). The ^{1}H and ^{13}C shifts reported here for the aryl ring bearing two bromine atoms are in agreement with those reported in literature[12]. Overall, the NMR assignments are in agreement with previous report of **12** isolated from marine algae[13]. Structure assignment is also supported by MS/MS fragmentation consistent with para-OH-BDE[8] (**Supplementary Fig. 20**).

Hence, as this point, all three isomers for $C_{12}H_7O_2Br_3$ and two isomers for $C_{12}H_6O_2Br_4$ had been identified. Both **11** and **12** are para-OH-BDEs, in that the ether linkage is positioned para to the phenolic hydroxyl. The third, and as yet unidentified isomer for $C_{12}H_6O_2Br_4$, was also postulated to be an OH-BDE due to its higher retention time than **1**, and similar retention time as the OH-BDE **11**. However, this species demonstrated no major MS2 product ions. Envisaging a OH-BDE isomer for **11**, we rationalized the structure for this species to be 2,4-dibromo-6-(2,4-dibromophenoxy)phenol (2'-OH-BDE-68) (**13**). This hypothesis was confirmed by the successive addition of increasing amounts of commercially available synthetic **13** (AccuStandard, HBDE-4006S-CN) to the Bmp7 reaction extracts and by observation of an identical retention time of the Bmp7 reaction product to synthetic **13** standard (**Supplementary Fig. 22**). Hence, by a combination of LC-MS/MS, NMR spectroscopy and comparison to synthetic standards, all major products produced by the Bmp7 reaction could be identified. Notably, **13** is an ortho-OH-BDE, in that the ether linkage resides ortho to the phenolic hydroxyl. Differential MS/MS fragmentation of ortho- and para-OH-BDEs has been reported in literature[8]. The dibromobenzoquinone and monobromobenzoquinone MS2 ions for **11** and **12** respectively were used as signatures to mine the LC-MS/MS data for bacterial extracts, leading to the identification of **11** and **12** in the extracts of producer strains. It should be noted that the culture extracts contained more

than fifteen polybrominated aromatic organic molecules, in addition to other small molecules. This precluded a facile prior identification of OH-BDE molecules, as done for **1–3** from the culture extracts. Additionally, identification of ortho-OH-BDE relies on comparison to authentic synthetic standards as they do not possess a distinct MS/MS signature.

5 did not demonstrate a typical absorbance shift associated with substrate binding for Bmp7 (**Supplementary Fig. 12**). However, as **5** is a product generated by Bmp5 (**Supplementary Fig. 17**) and is present in the Δ*bmp7* extracts (**Supplementary Fig. 5**), we explored whether **5** could be used by Bmp7 as a substrate. Indeed, Bmp7 could use **5**, though substrate consumption was significantly lower as compared to that for **4** (**Supplementary Fig. 23**). A singular major product could be identified, with the MS1 predicted formula $C_{12}H_5Br_5O_2$ (**Supplementary Fig. 24**, panel **a**). As a dibromobenzoquinone MS2 product ion was observed (**Supplementary Fig. 24**, panel **b**), we postulated that the product of the reaction to be a para-OH-BDE. Preparative-scale purification of the product from large scale Bmp7 reactions with **5**, and subsequent NMR characterization led to the identification of the chemical structure of the product as 2,6-dibromo-4-(2,4,6-tribromophenoxy)phenol (**14**). Specifically, **14** was isolated by preparative HPLC separation of products from ethyl acetate extracts of large scale Bmp7 reactions with **5**. The solvent was removed *in vacuo*, and dried overnight to yield a white residue. The residue was dissolved in d_6-DMSO, NMR spectra collected using 600 MHz Varian NMR microprobe. Final deduced structure of the molecule, with the proton shifts listed in red, and the carbon shifts listed in green is shown in panel **a** below. HSQC correlations are shown as thick bonds, HMBC correlations in red arrows are shown in panel **b** below. No H2BC[11] correlations were observed.

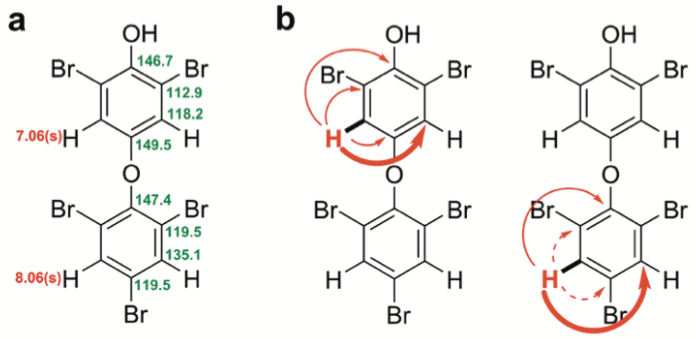

14: ^{1}H NMR (600 MHz, DMSO) δ 8.08 (s, 1H), 7.06 (s, 1H). Uncertainty in the assignment of two HMBC couplings is shown as dashed arrows, and is likely caused by the highly similar ^{13}C shifts of the two carbon atoms in the symmetrical ring. Note that the symmetry of both aryl rings is supported by the presence of only two singlets in the ^{1}H NMR, and the HMBC couplings shown in bold arrows that are identical to HSQC couplings. Symmetry for both rings is also supported by MS/MS fragmentation consistent with para-OH-BDEs[8] (**Supplementary Fig. 24**). A hypothetical isomeric ortho-OH-BDE would have only one symmetrical aryl ring.

Using the above discussion for products generated by Bmp7 using **4** and **5** as substrates, we could rationalize the products generated by Bmp7 using **17** as a substrate (**Supplementary Fig. 25**, panel **a**). It should be noted that **17** is not a physiological product generated by Bmp5 as Bmp5 does not incorporate chloride. LC-MS/MS analysis identifies three major isomeric product peaks with the molecular formula $C_{12}H_6Cl_4O_2$ (**Supplementary Fig. 25**, panel **b**). The first product peak showed $[M\text{-}Cl^-]^-$, $[M\text{-}2Cl^-]^-$, and $[M\text{-}3Cl^-]^-$ MS2 product ions (**Supplementary Fig. 25**, panels **c**, **d** and **e**, respectively). This lead to the assignment of this species as 4,4',6,6'-tetrachloro-2,2'-biphenol (**18**), a chlorinated analog of **1**. The second isomeric product peak demonstrated MS2 product ions corresponding to

dichlorobenzoquinone (**Supplementary Fig. 25**, panel **f**), leading to a putative assignment of its structure as 2,6-dichloro-4-(2,4-dichlorophenoxy)phenol (**19**). The third isomeric product did not show any major MS2 product ions. By analogy to Bmp7 brominated products, the structure for this species can be postulated to be 2,4-dichloro-6-(2,4-dichlorophenoxy)phenol (20). Though **18–20** are not as yet reported natural products, several million tons of **17** are industrially synthesized each year, and also generated by the degradation of the herbicide 2,4-dichlorophenoxyacetic acid. Hence, it is conceivable that **17** could exist in the marine microbial metabolome, owing to anthropogenic origins, or enzymatically synthesized by homologs of the Bmp5 enzymes. Consequently, **18–20**, and other reaction products of Bmp7 with **17** may already exist as halogenated marine natural products.

Supplementary Figures

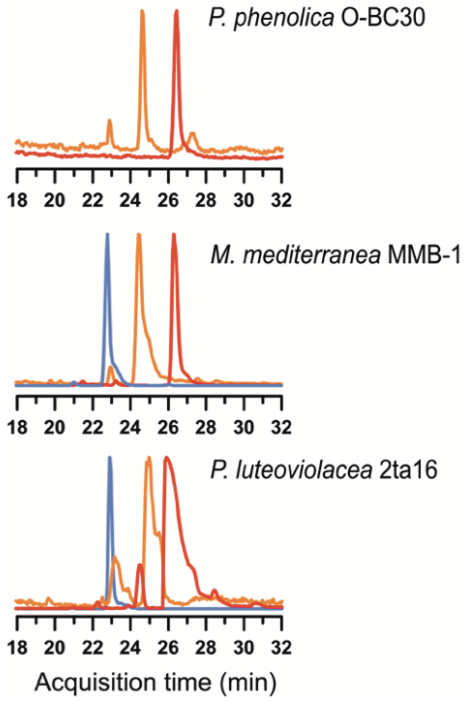

Supplementary Fig. 1. Production of signature polybrominated molecules 1–3 by marine bacteria. Extracted ion chromatograms (EICs) for extracts of *P. luteoviolacea* 2ta16, *P. phenolica* O-BC30, and *M. mediterranea* MMB-1 analyzed by LC-MS/MS demonstrating the production of **1** (red curves), **2** (violet curves), and **3** (orange curves). Bacteria were grown in Difco 2216 Marine Broth without additional supplementation of bromide. Extracts dissolved in MeOH were injected onto a reverse phase C_{18} column (Phenomenex Luna , 5 µm, 4.6 × 100 mm) operating on an Agilent 1260 HPLC in tandem to an Agilent 6530 Accurate Mass Q-TOF mass spectrometer. The solvents used for HPLC were water + 0.1% formic acid (A) and MeCN + 0.1% formic acid (B). The HPLC elution profile was as follows (flow rate 0.5 mL/min): 10% B for 5 min, linear gradient to 70% B across 10 min, linear increase to 100% B across 30 min, 100% B for 3 min, linear decrease to 10% B across 2 min, 10% B for 5 min. An identical LC-MS/MS profile has been used for all analytical scale heterologous culture extract analysis, Bmp7 reaction extracts, and for synthetic standards.

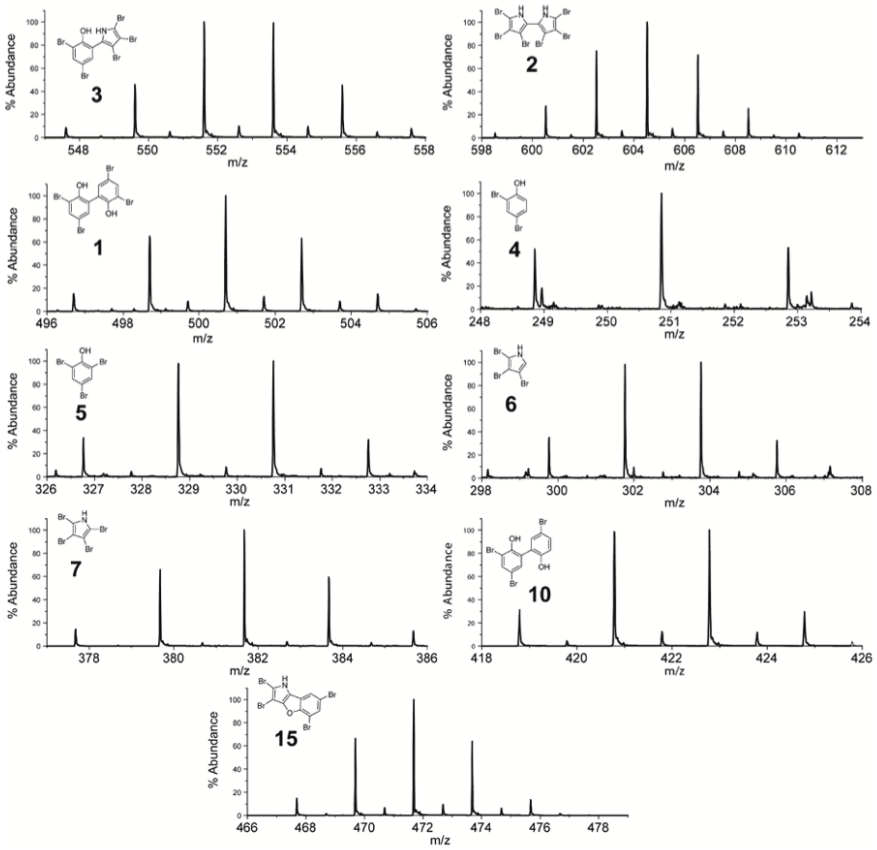

Supplementary Fig. 2. High-resolution mass spectra for selected polybrominated metabolites from an organic extract of *P. luteoviolacea* 2ta16. For accurate mass determination, an organic extract of *P. luteoviolacea* 2ta16 was analyzed by LC-ESI-MS in negative polarity on an Agilent 6230 Accurate Mass TOF-MS at the UCSD Chemistry and Biochemistry Molecular Mass Facility (La Jolla, CA). Isotope patterns for **1–7**, **10** and **15** identified in the culture extract of *P. luteoviolacea* 2ta16 are shown. See also **Supplementary Table 1** for error estimation in mass spectra.

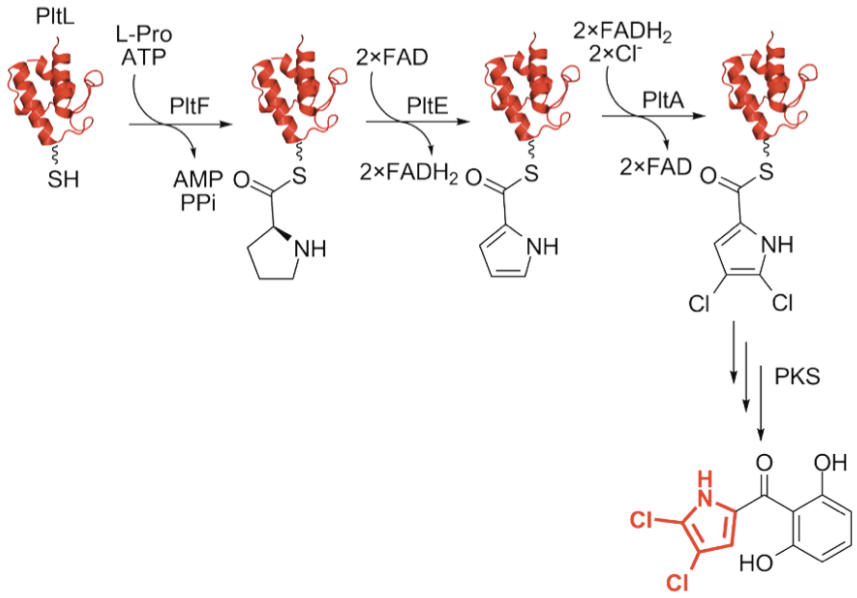

Supplementary Fig. 3. Chemical logic for the biosynthesis of halogenated pyrrole moieties in natural products. The scheme for the generation of dichlorinated pyrroles, tethered to an ACP molecule is shown as characterized for pyoluteorin biosynthesis[1,27]. The ACP (PltL) is phosphopantetheinylated to yield a free sulfhydryl moiety, which is then acylated to an amino acid (L-proline) by virtue of a thioester bond by an adenyltransferase PltF. This reaction requires the hydrolysis of a stoichiometric amount of ATP to AMP and PP_i. Subsequent to acylation, the pyrrolidine ring is dehydrogenated by PltE, with concomitant reduction of two FAD molecules to $FADH_2$. The pyrrole ring is then dichlorinated by the chlorinase PltA (5-position followed by 4-position). Halogenation requires reduced flavin cofactor, and appropriate halide ion in the presence of molecular oxygen. In the pyoluteorin biosynthetic scheme, the dichlorinated pyrrolyl-*S*-ACP then undergoes three rounds of polyketide extension, and subsequent release and aromatization. The dichlorinated pyrrole moiety in pyoluteorin is highlighted in red. The canonical four helix-bundle architecture of ACP (PltL) is shown in the red cartoon.

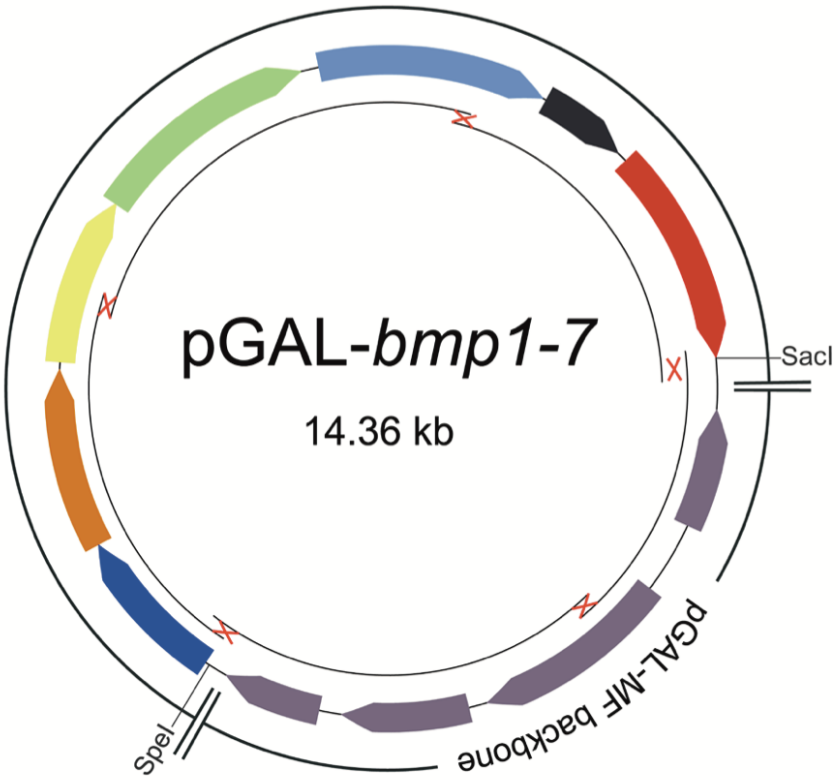

Supplementary Fig. 4. pGAL-*bmp1*–7 yeast/*E. coli* shuttle vector. pGAL-*bmp1–7* yeast/*E. coli* shuttle vector was assembled in *S. cerevisiae* BJ5465 from PCR amplified fragments (for primers see **Supplementary Table 3**).

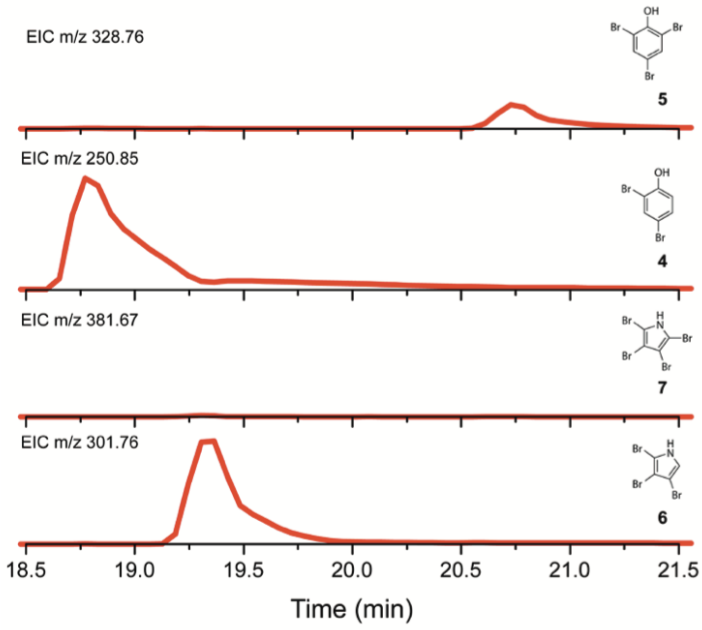

Supplementary Fig. 5. Chemotype for *bmp7* deletion. Deletion of *bmp7* from the heterologous expression vector pETDuet-*bmp1–7* results in accumulation of pyrrole and phenol monomers **4**–**6** in *E. coli*. Notably absent is **7**, which likely arises as a byproduct of dehalogenative radical coupling catalyzed by Bmp7. The figure shows EICs for the most abundant ions corresponding to each compound (the y-axis scale is identical for all plots).

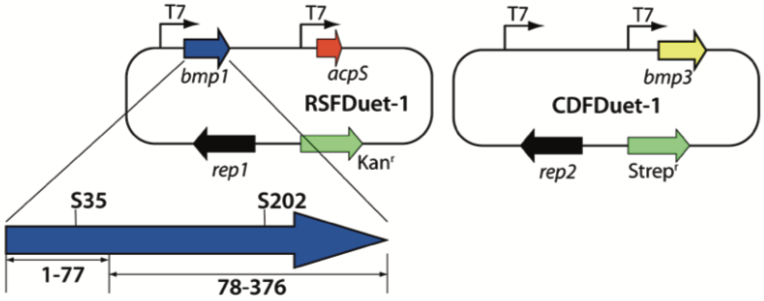

Supplementary Fig. 6. Plasmids for co-expression of *bmp1* with *bmp3*. Upon coexpression of the above two plasmids in *E. coli* BL21Gold(DE3), Bmp1(ACP) could be purified in complex with Bmp3. Purified Bmp1(ACP)-Bmp3 complex was subsequently used for assays with Bmp4 as described in **Supplementary Fig. 8**.

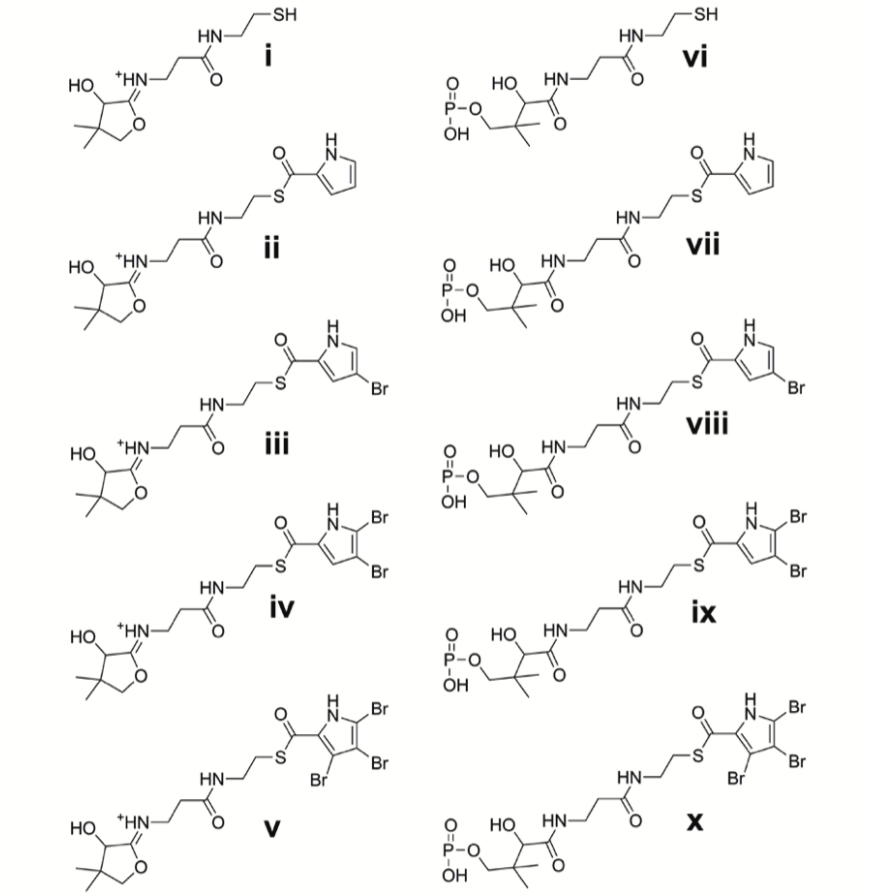

Supplementary Fig. 7. MS2 product ions corresponding to phosphopantetheine, phosphopantetheine acylated with pyrrole, and subsequent brominated states of the pyrrole. Note that the sites for the mono- and di-bromination for the pyrrole have been assumed as characterized for the pyrrole chlorinase PltA (**Supplementary Fig. 3**). The masses for the MS2 ions are listed. Under the experimental conditions in this study, MS2 product ions **i–v** were observed.

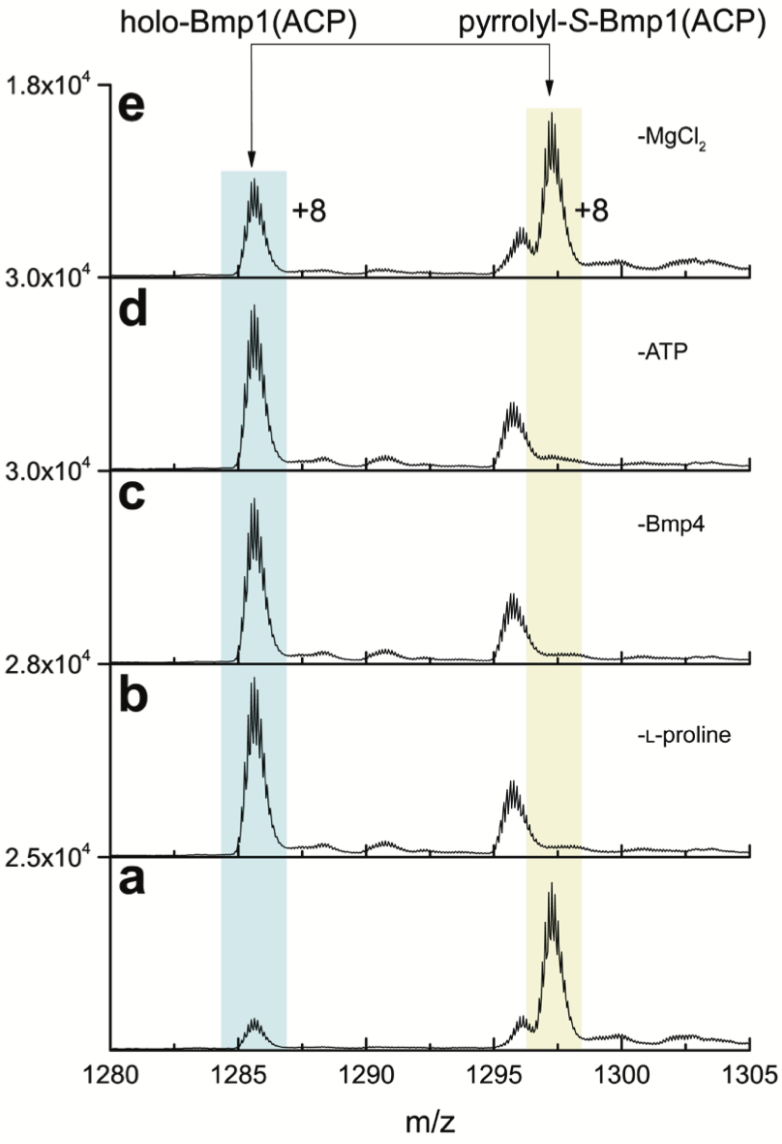

Supplementary Fig. 8. Enzymatic synthesis of pyrrolyl-*S*-Bmp1(ACP) by Bmp3 and Bmp4. (**a**) 40 μM of Bmp1(ACP)-Bmp3 complex, purified as described in **Supplementary Fig. 6** was incubated with 1 μM purified Bmp4, 4 mM L-proline, 2 mM ATP, 2 mM DTT and 10 mM $MgCl_2$ for 3 h at 30 °C in 100 mM potassium phosphate (pH 7.6) buffer.

Reaction components (**b**) ATP, (**c**) Bmp4, (**d**) L-proline, and (**e**) $MgCl_2$ were individually deleted and replaced with buffer. The assays were analyzed by LC-MS/MS. A peptide fragment corresponding to holo-Bmp1(ACP) (shaded blue) was identified by a diagnostic MS2 ion corresponding to species **i** as shown in **Supplementary Fig. 7**, while a peptide fragment corresponding to pyrrolyl-*S*-Bmp1(ACP) (shaded yellow) was identified by the diagnostic MS2 ion corresponding to species **ii** as shown in **Supplementary Fig. 7**. Both peptides were found to bear +8 charges as determined by their MS1 isotopic mass distribution. For illustrative purposes, MS1 spectra were summed over an identical 4 min time window during which both holo-Bmp1(ACP) and pyrrolyl-*S*-Bmp1(ACP) peptides were found to elute.

In the presence of all reaction components, Bmp4 and Bmp3 catalyzed the conversion of holo-Bmp1(ACP) to pyrrolyl-*S*-Bmp1(ACP) (panel **a**). Elimination of ATP, Bmp4 or L-proline abolished the formation of pyrrolyl-*S*-Bmp1(ACP). However, elimination of $MgCl_2$ (panel **e**) only led to a partial reduction in activity of Bmp4. These findings are consistent with the well-accepted reaction mechanism of adenyltransferase enzymes, such as Bmp4, in which the amino acid (L-proline for Bmp4) is activated by adenylation (derived from ATP), and subsequently transferred on to the terminal sulfhydryl of the phosphopantetheine arm of the holo-ACP.

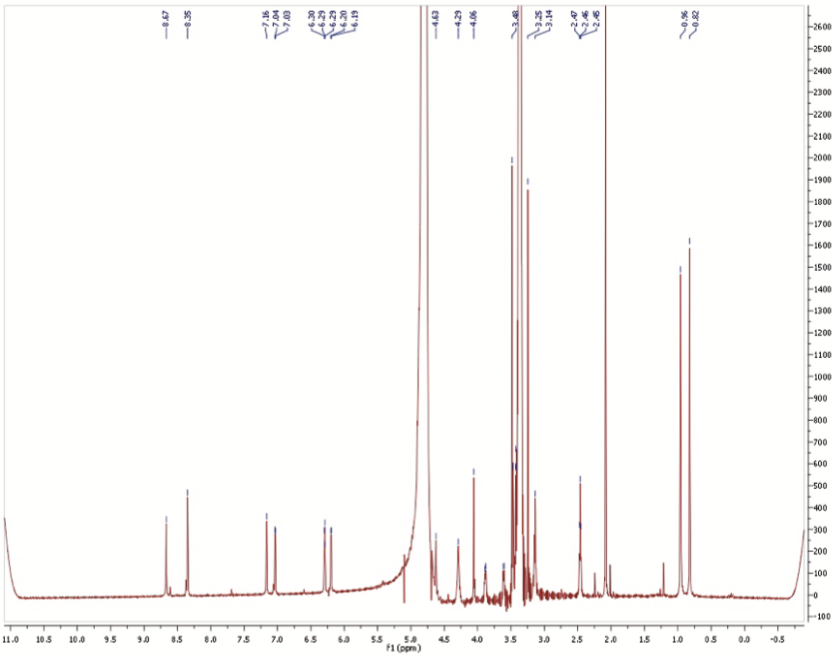

Supplementary Fig. 9. ^{1}H NMR spectrum for 16.

^{1}H NMR (600 MHz, D_2O) δ 8.67 – 8.63 (m, 1H), 8.33 (s, 1H), 7.16 – 7.12 (m, 1H), 7.15 (d, *J* = 7 Hz, 1H), 6.29 – 6.26 (m, 1H), 6.18 (d, *J* = 10 Hz 1H), 4.63-4.62 (m, 1H), 4.30 – 4.23 (m, 2H), 4.04 (s, 1H), 3.88 – 3.84 (m, 2H), 3.61 – 3.57 (m, 2H), 3.48 – 3.46 (m, 1H), 3.45-3.43 (m 1H) 3.41 (m, 1H), 3.23 (s, 1H), 3.12 (m, 1H), 2.44 (t, *J* = 10 Hz, 2H), 0.94 (s, 3H), 0.80 (s, 3H).

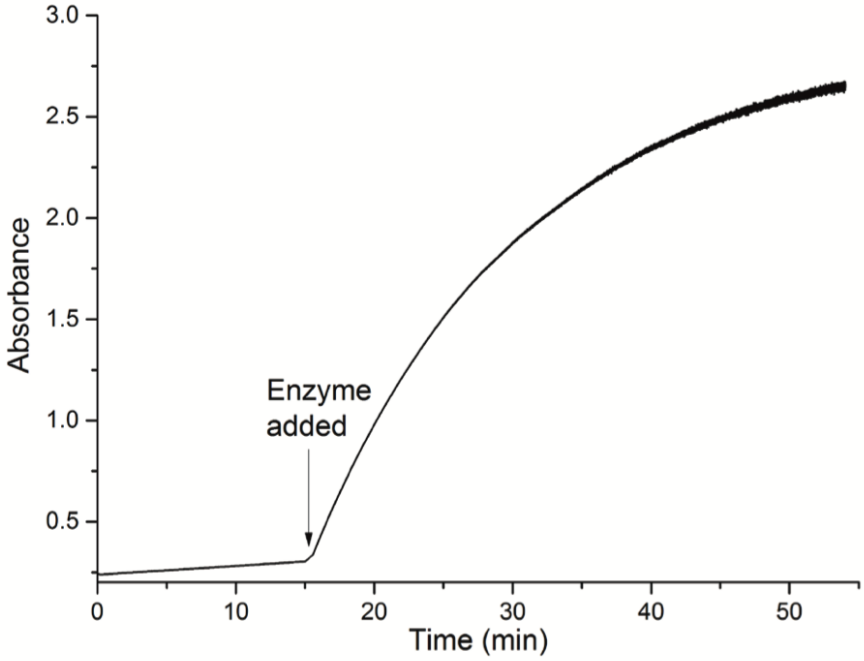

Supplementary Fig. 10. Hydrolysis of model esterase substrate p-nitrophenyl acetate (pNPA) by Bmp1(TE). 5 μM of purified Bmp1(TE) was used as the catalyst for the hydrolysis of 250 μM freshly prepared pNPA in 100 mM potassium phosphate (pH 7.6) buffer at room temperature. The reaction was monitored spectrophotometrically at wavelength of 400 nm in a quartz cuvette. Observed absorbance is plotted against time. Upon addition of enzyme, we observed significant increase in the hydrolysis of pNPA (denoted by the absorbance increase due to production of p-nitrophenol), implying that Bmp1(TE) catalyzed the hydrolysis of pNPA.

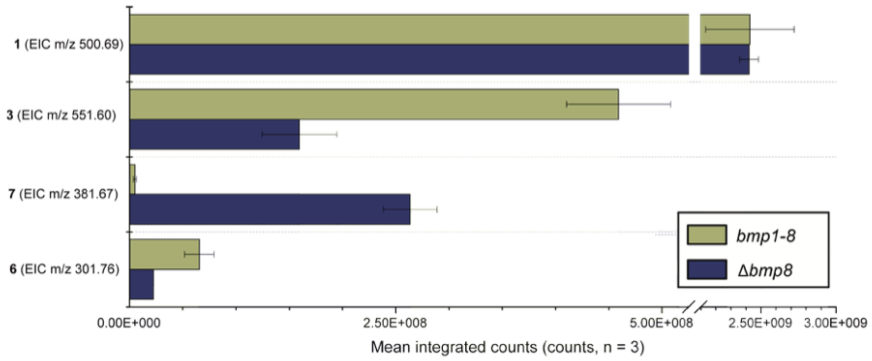

Supplementary Fig. 11. Chemotype for heterologous expression of *bmp1–7* omitting *bmp8*. Expression in *E. coli* of *bmp1-7* omitting *bmp8* results in decreased levels of **3** and **6** with a concomitant increase in **7**; **1** is shown as a control. Cultures of *E. coli* expressing the full *bmp* cluster or full *bmp* cluster excluding *bmp8* were grown in triplicate, extracted, and analyzed by LC-MS/MS as previously described. Levels of **3**, **6**, and **7** were quantified by peak integration of extracted ion chromatograms (EICs) corresponding to the most abundant ion for each compound. Means were calculated from each of three replicates for integrals taken from EICs for each ion and plotted, with the error bars representing standard deviations.

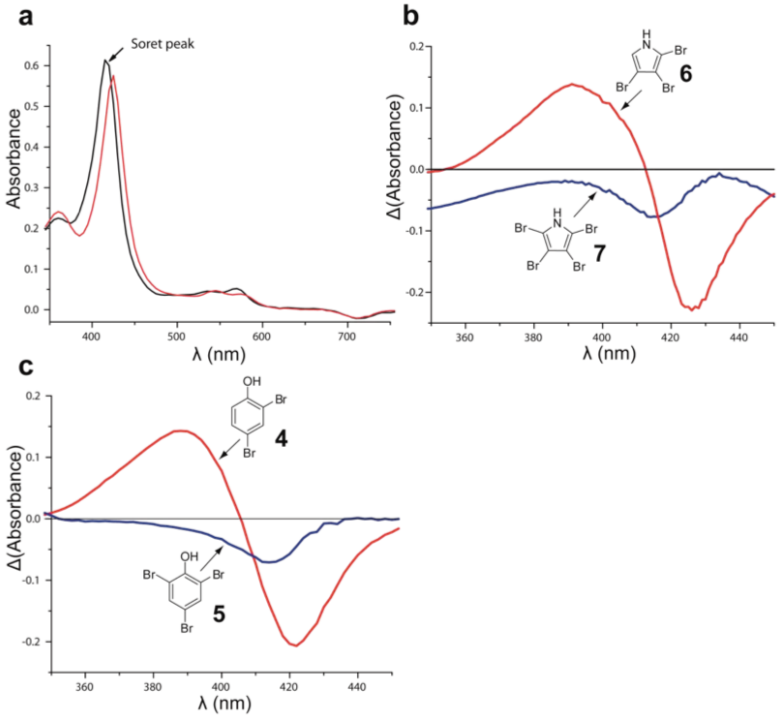

Supplementary Fig. 12. Spectral characteristics of CYP450 Bmp7 and spectrophotometric determination of substrate tolerance. (**a**) An absorbance scan for 5 μM purified Bmp7 in 100 mM potassium phosphate buffer (pH 7.6) was performed using a Cary-40 UV-Vis spectrophotometer in a quartz cuvette. Bmp7 demonstrates a typical CYP450 absorbance curve, with a Soret peak at 415 nm (black curve) upon addition of 1mM imidazole (red curve). (**b**) **6** was synthesized according to published protocols[10]. Difference absorbance spectra upon titration of Bmp7 with 200 μM **6** or **7** identify binding of **6** in a manner characteristic for substrates of CYP450 enzymes; note that **7** does not yield a similar absorbance change. (**c**) Similarly, a difference absorbance spectra upon titration of Bmp7 with **4** or **5** identifies binding of **4** characteristic for substrates of CYP450 enzymes.

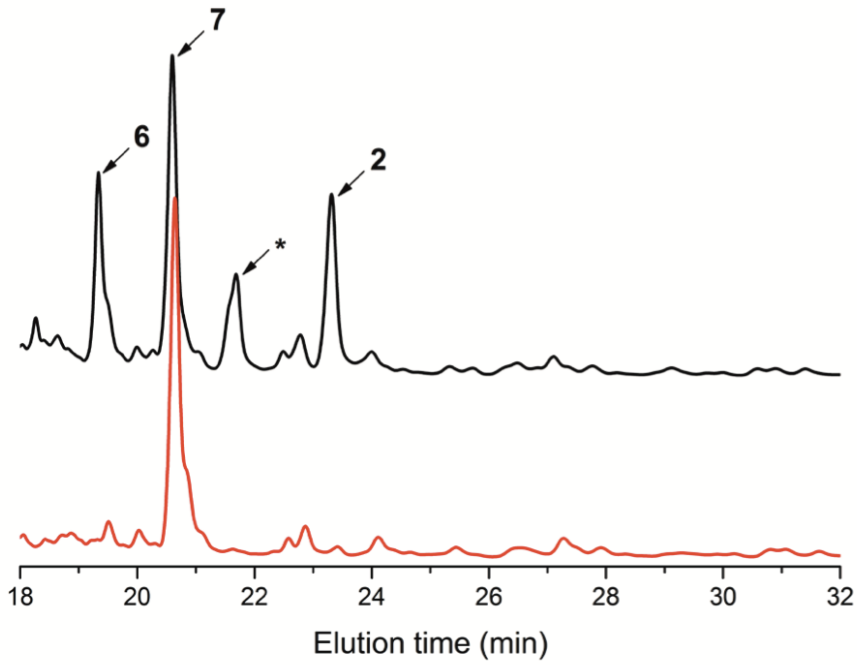

Supplementary Fig. 13. *In vitro* Bmp7 reaction products with 6 (black, top curve) and 7 (bottom, red curve) as substrates. With **6** as a substrate, Bmp7 generated three distinct products, **2**, **7**, and an uncharacterized species corresponding to pentabromo-bipyrrole (marked by *, having a molecular formula $C_8H_3Br_5N_2$ as predicted from MS1 spectrum). This product could not be generated in quantities sufficient for complete structure elucidation. The pentabromo-bipyrrole product can be rationalized on the basis of dehalogenated-aryl coupling polybrominated biphenyl and OH-BDE products **10**, **12** and **14** (*vide infra*). Upon reaction with **7**, no product peaks could be observed.

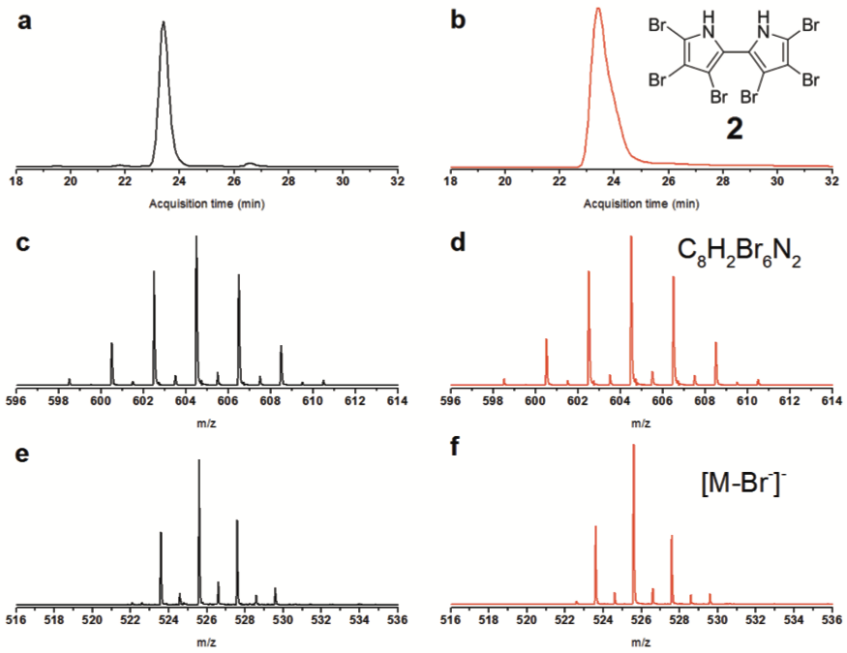

Supplementary Fig. 14. Characterization of 2 generated by Bmp7 *in vitro* reaction with 6 as a substrate. Extract of Bmp7 reaction (black curves) was compared to an authentic NMR characterized sample of **2** (red curves) isolated from *P. luteoviolacea* 2ta16. (**a**, **b**) Comparison of retention times. MS1 EIC corresponding to the most abundant isotope for the molecular formula $C_8H_2Br_6N_2$ (m/z =604.51, 10 ppm tolerance) for the Bmp7 reaction extract (**a**) and authentic standard of **2** (**b**) analyzed under identical chromatographic conditions. (**c**, **d**) Comparison of MS1 profiles. MS1 mass spectrum for species at retention time 23.4 min from the Bmp7 reaction extract (**c**) and authentic standard of **2** (**d**). (**e**, **f**) Comparison of MS/MS profiles. MS2 profile of the product ions generated from most abundant isotope MS1 ions corresponding to the molecular formula $C_8H_2Br_6N_2$ at identical retention times from the Bmp7 reaction extract (**e**) and authentic standard of **2** (**f**). Most abundant MS2 ions corresponded to the $[M\text{-}Br^-]^-$. Identical retention times, MS1 and MS/MS profiles as compared to a NMR characterized authentic standard lead to the characterization of the Bmp7 reaction product as **2**.

NMR spectra for **2** purified from preparative scale cultures of *P. luteoviolacea* 2ta16 and used as authentic standard in panels **b**, **d** and **f** above:

2: ^{1}H NMR: ($CDCl_3$) δ [ppm] 9.87 (bs, 1H); ^{13}C NMR: ($CDCl_3$) δ [ppm] 121.60, 115.37, 102.76, 100.98

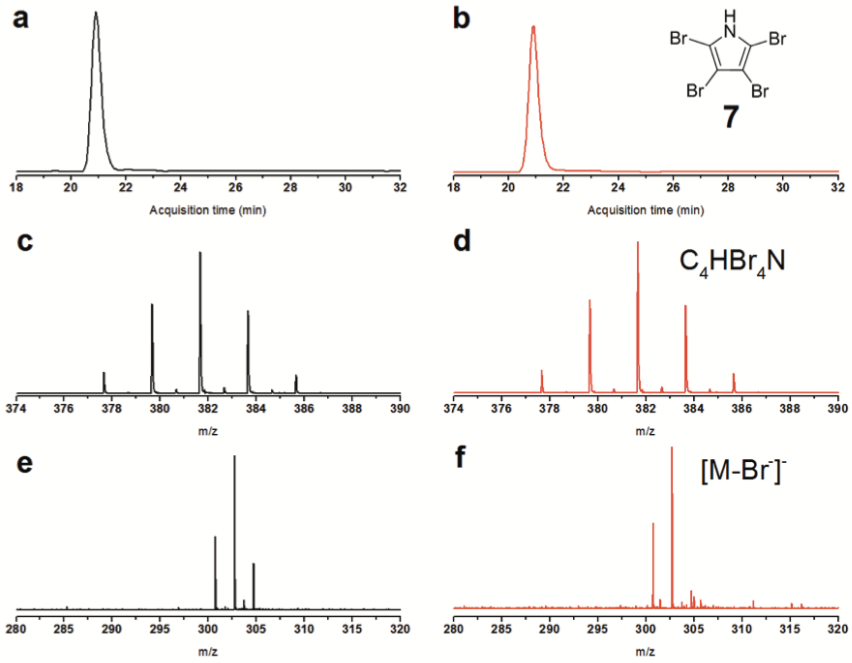

Supplementary Fig. 15. Characterization of 7 generated by Bmp7 *in vitro* reaction with 6 as a substrate. Extract of Bmp7 reaction (black curves) was compared to an authentic commercial synthetic standard of **7** (Sigma-Aldrich, L165042-50MG) (red curves). (**a**, **b**) Comparison of retention times. MS1 EIC corresponding to the most abundant isotope for the molecular formula C_4HBr_4N (m/z = 381.67, 10 ppm tolerance) for the Bmp7 reaction extract (**a**) and authentic standard of **7** (**b**) analyzed under identical chromatographic conditions. (**c**, **d**) Comparison of MS1 profiles. MS1 mass spectrum for species at retention time 20.8 min from the Bmp7 reaction extract (**c**) and authentic standard of **7** (**d**). (**e**, **f**) Comparison of MS/MS profiles. MS2 profile of the product ions generated from most abundant isotope MS1 ions corresponding to the molecular formula C_4HBr_4N at identical retention times from the Bmp7 reaction extract (**e**) and authentic standard of **7** (**f**). Most abundant MS2 ions corresponded to the $[M\text{-}Br^-]^-$. Identical retention times, MS1 and MS/MS profiles as compared to an authentic synthetic standard lead to the characterization of the Bmp7 reaction product as **7**.

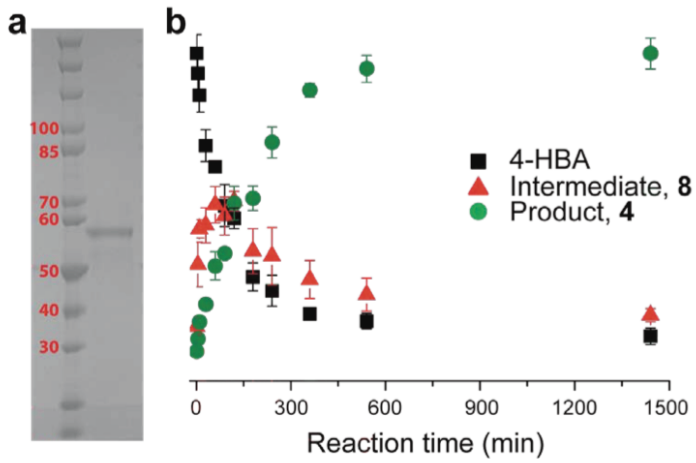

Supplementary Fig. 16. Purification of recombinant Bmp5 and time course for the change in concentrations of the substrate, intermediate and product species as shown in Fig. 4a. (**a**) Affinity chromatography purified Bmp5 is analyzed by SDS-PAGE, along with molecular weight marker (Fisher Scientific BP3602) with molecular weights listed in red in kDa. The expected molecular weight for N-His_6-Bmp5 is 61 kDa (**b**) Area under the substrate, intermediate and product peaks as shown in **Fig. 4a** were integrated, and mean values from three independent experiments were plotted against reaction time with error bars representing standard deviation. The intermediate and product were identified to be **8** and **4** respectively by high-resolution mass spectrometry and comparison of retention times to authentic synthetic standards.

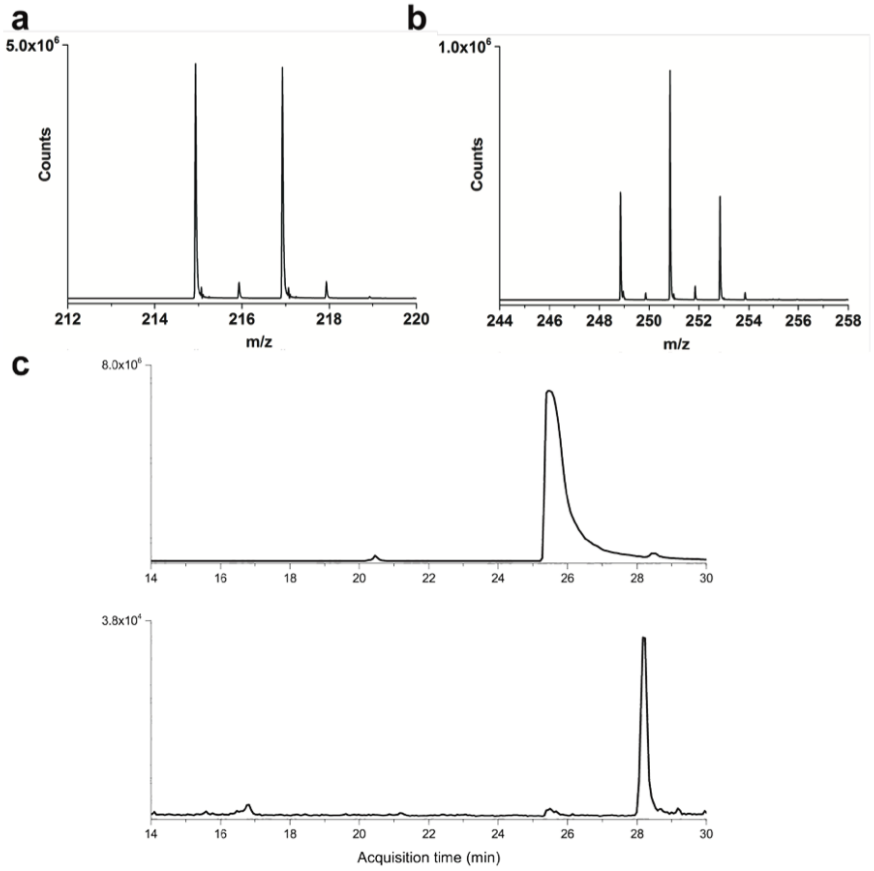

Supplementary Fig. 17: Mass spectra for 8 and 4, and *in vivo* production of 4 and 5 by Bmp5. The mass spectra for (**a**) Bmp5 intermediate **8** and (**b**) Bmp5 product **4** generated by *in vitro* reaction of Bmp5 with 4-HBA led to the assignment of the chemical formulae as $C_7H_5O_3Br$ and $C_6H_4OBr_2$ respectively. (**c**) MS1 EIC for m/z = 248.85 (10 ppm tolerance) and m/z = 326.766 (10 ppm tolerance) showing the production of **4** (top) and **5** (bottom) when Bmp5 was expressed in *E. coli* in LB media supplemented with 1 g/L KBr. Assuming identical ionization for **4** and **5**, it can be discerned that **4** is the major product generated by Bmp5.

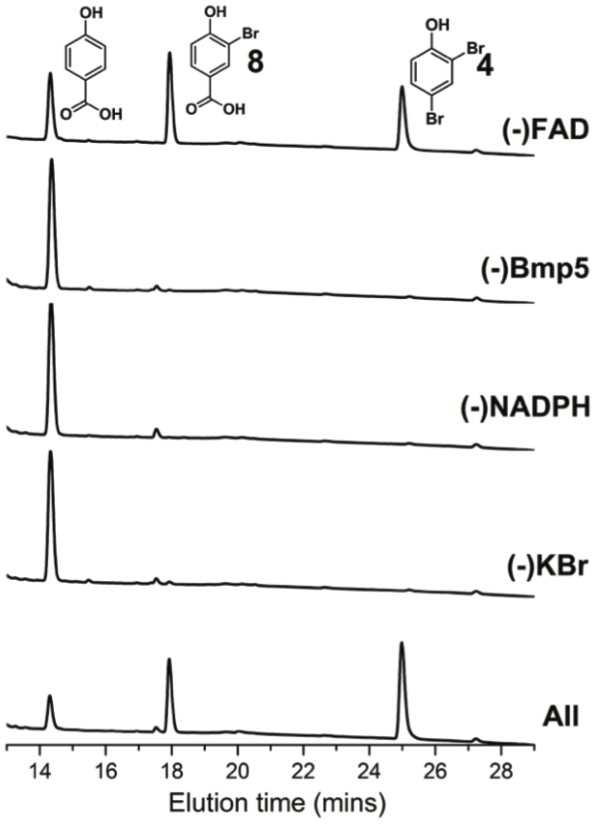

Supplementary Fig. 18. Negative control reactions demonstrate the requirement of KBr and NADPH for catalysis by Bmp5. No conversion of 4-HBA to **8** and **4** was observed when Bmp5, NADPH or KBr were omitted from the Bmp5 *in vitro* assay. Omission of FAD did not abolish enzyme activity, but lowered substrate turnover.

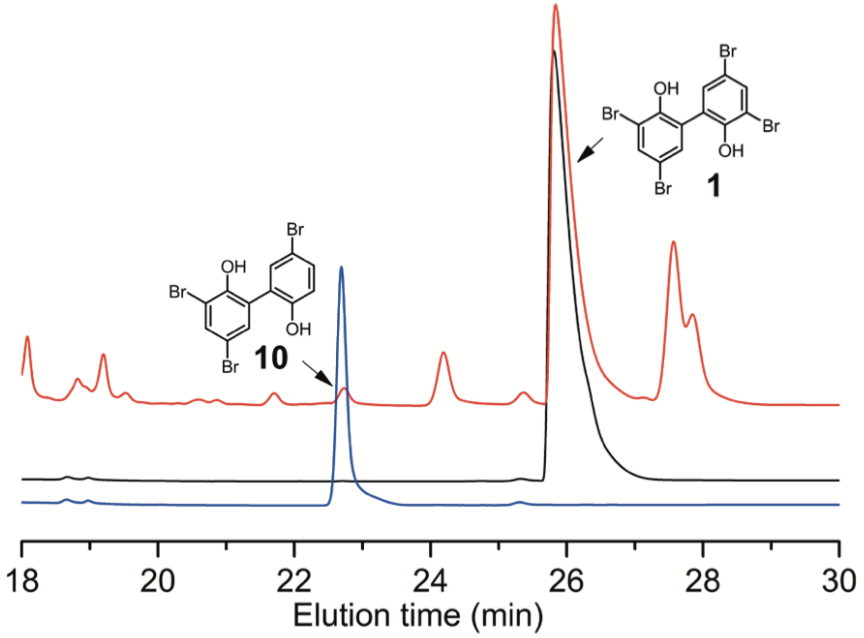

Supplementary Fig. 19. Comparison of retention times and NMR spectra of polybrominated biphenyl products 1 and 10 generated by Bmp7 *in vitro* with authentic synthetic standards. Extract of Bmp7 reaction with **4** (red curve) was analyzed using identical chromatographic conditions as for authentic synthetic standards of **1** (black curve) and **10** (blue curve). Note that retention times for authentic standards of **1** and **10** match those for two separate product peaks from the enzymatic reaction leading to the identification of the chemical structures of these species. Synthetic standard of **1** was obtained from Sigma-Aldrich (S842753-50MG) and dissolved in 1 mL DMSO. Analysis by LC-MS/MS identified two major peaks in roughly 80:20 relative abundance with respective molecular formulae as $C_{12}H_6O_2Br_4$ and $C_{12}H_7O_2Br_3$. Both products were purified by semi-preparative scale HPLC. After drying *in vacuo*, 500 µg of each product was dissolved in 50 µL DMSO, and ^{1}H NMR spectra were acquired. By molecular formulae, MS/MS fragmentation patterns, and comparison of NMR spectra to literature[3-4], the identity of the synthetic standard of **1** and for the synthetic standard of **10** can be discerned as shown above. This lead to the identification of **1** and **10** as products generated by Bmp7.

The ^{1}H NMR chemical shifts of the synthetic standards of **1** and **10**, which are in good agreement to literature values, are as follows:

1: ^{1}H NMR (600 MHz, $CDCl_3$) δ 7.65 (d, *J* = 2.3 Hz, 1H), 7.31 (d, *J* = 2.3 Hz, 1H).

10: ^{1}H NMR (600 MHz, $CDCl_3$) δ 7.67 (d, *J* = 2.3 Hz, 1H), 7.39 (dd, *J* = 8.6, 2.4 Hz, 1H), 7.37 (d, *J* = 2.3 Hz, 1H), 7.34 (d, *J* = 2.4 Hz, 1H), 6.90 (d, *J* = 8.6 Hz, 1H).

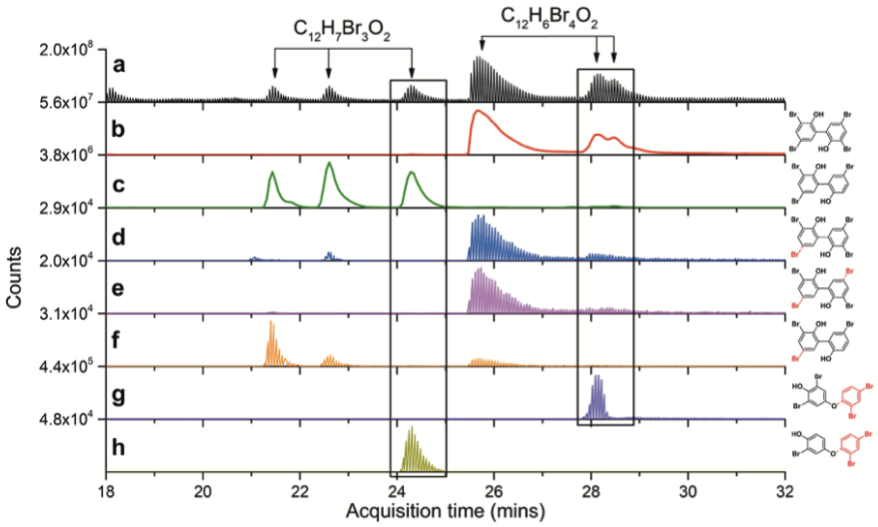

Supplementary Fig. 20. Mass spectrometric analysis of the polybrominated biphenyls, and OH-BDE products generated by Bmp7. (**a**) Total ion chromatogram (TIC) for the Bmp7 reaction extract. Peaks corresponding to the three isomers each for the major products corresponding to the molecular formulae $C_{12}H_7Br_3O_2$ and $C_{12}H_6Br_4O_2$ are indicated. (**b**) MS1 extracted ion chromatogram (EIC) corresponding to the most abundant ion for molecular formula $C_{12}H_6Br_4O_2$ (m/z = 500.69, 10 ppm tolerance) identifies a set of three distinct isomeric product peaks. Chemical structure for **1** is shown on the right. (**c**) MS1 EIC corresponding to the most abundant ion for molecular formula $C_{12}H_7Br_3O_2$ (m/z = 420.79, 10 ppm tolerance) identifies a second set of three distinct isomeric product peaks. The chemical structure for **10** is shown on the right. (**d**) EIC corresponding to MS2 product ion $[M\text{-}Br^-]^-$ from $C_{12}H_6Br_4O_2$ (m/z = 421.78, 10 ppm tolerance). (**e**) EIC corresponding to MS2 product ion $[M\text{-}2Br^-]^-$ from $C_{12}H_6Br_4O_2$ (m/z = 339.85, 10 ppm tolerance). (**f**) EIC corresponding to MS2 product ion $[M\text{-}Br^-]^-$ from $C_{12}H_7Br_3O_2$ (m/z = 340.86, 10 ppm tolerance). (**g**) EIC corresponding to dibromobenzoquinone MS2 product ion generated from $C_{12}H_6Br_4O_2$ (m/z = 265.84, 10 ppm tolerance). Chemical structure for **11** with the loss of dibromobenzene (in red) is shown on the right. (**h**) EIC corresponding to bromobenzoquinone MS2 product ion generated from $C_{12}H_7Br_3O_2$ (m/z = 185.93, 10 ppm tolerance). Chemical structure for **12** with the loss of dibromobenzene (in red) is shown on the right. Note that para-OH-BDEs (**11–12**) possess a MS/MS signature typified the detection of a bromobenzoquinone MS fragment ion, while ortho-OH-BDEs (**13**) are not fragmented.

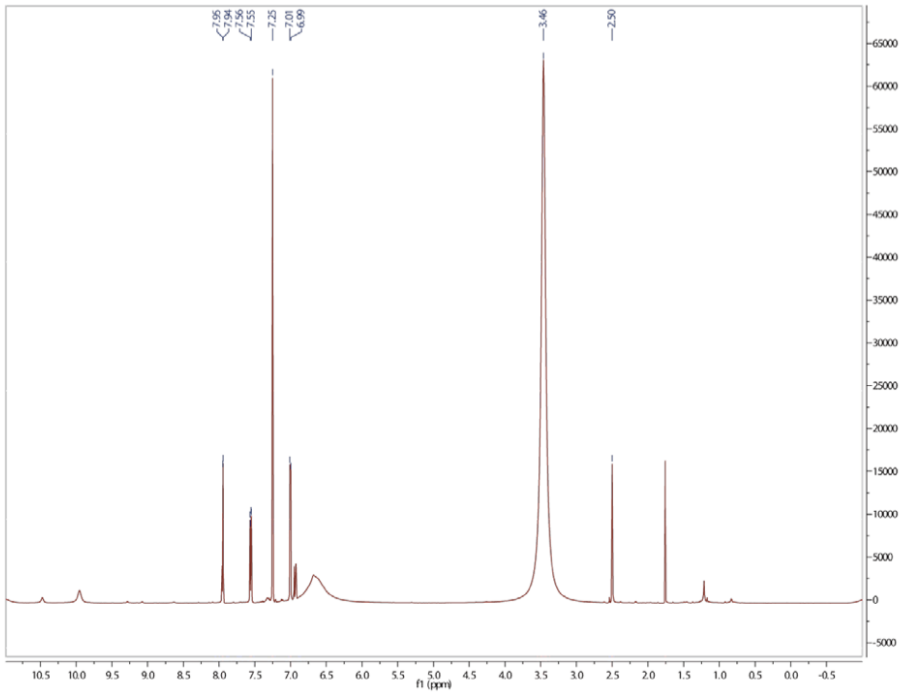

Supplementary Fig. 21. ^{1}H NMR spectrum for 11.

11: ^{1}H NMR (600 MHz, DMSO) δ 7.95 (d, *J* = 2.4 Hz, 1H), 7.56 (dd, *J* = 8.8, 2.3 Hz, 1H), 7.25 (s, 2H), 7.00 (d, *J* = 8.7 Hz, 1H).

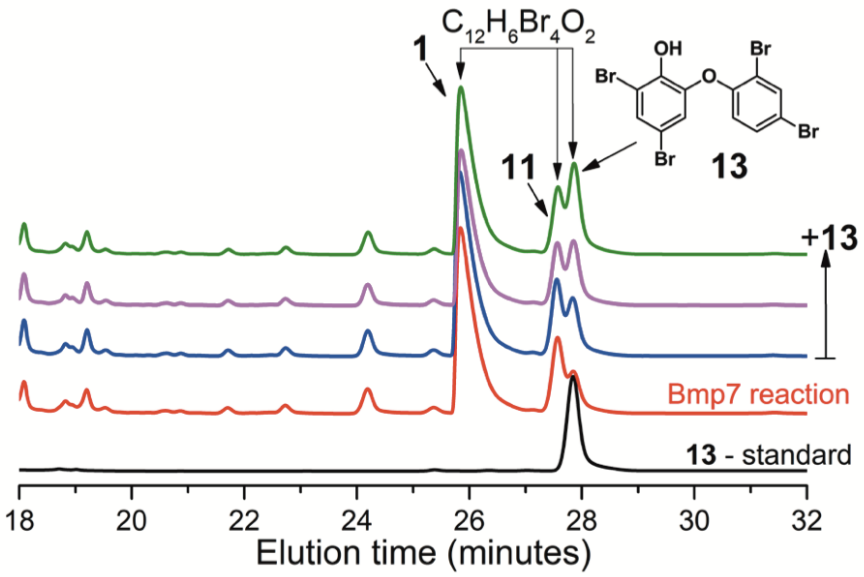

Supplementary Fig. 22. Identification of 2′-OH-BDE-68 (13) as a reaction product generated by Bmp7. Bmp7 produces three isomeric products of molecular formula $C_{12}H_6Br_4O_2$. Products **1** and **11** had been identified by comparison to authentic standard for **1** (**Supplementary Fig. 19**), and comprehensive structural characterization by NMR spectroscopy for **11** (**Supplementary Note 2** and **Supplementary Fig. 21**). Extract of *in vitro* reaction of Bmp7 with **4** (red trace) was supplemented with a synthetic standard of **13** in increments of 0.25 µg each. Note that of the three isomeric peaks with $C_{12}H_6Br_4O_2$ molecular formula, supplementation with authentic standard identifies the third peak with retention time ~ 27.8 min as **13**.

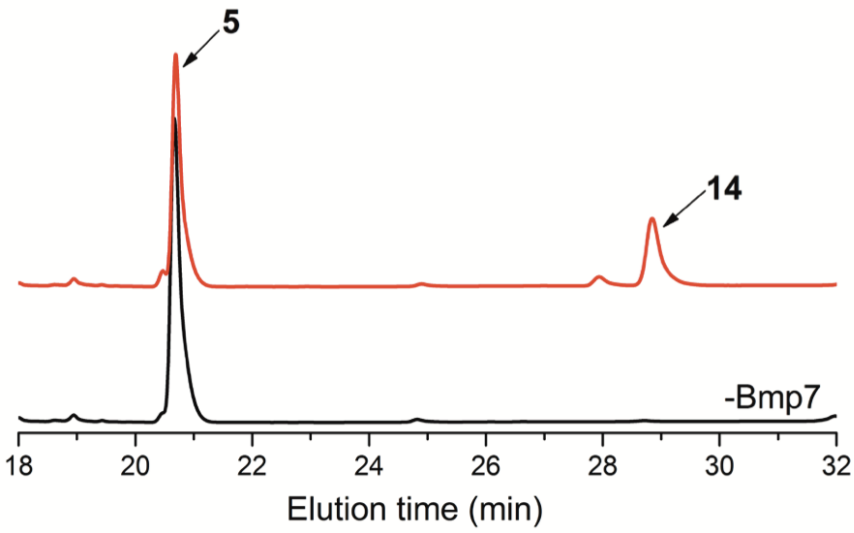

Supplementary Fig. 23. HPLC detection of products generated by Bmp7 using 5 as a substrate. Curve in black represents a negative control reaction in which Bmp7 was omitted. Only a single brominated product was identified (red curve). Note that the substrate (**5**) has only been partially consumed.

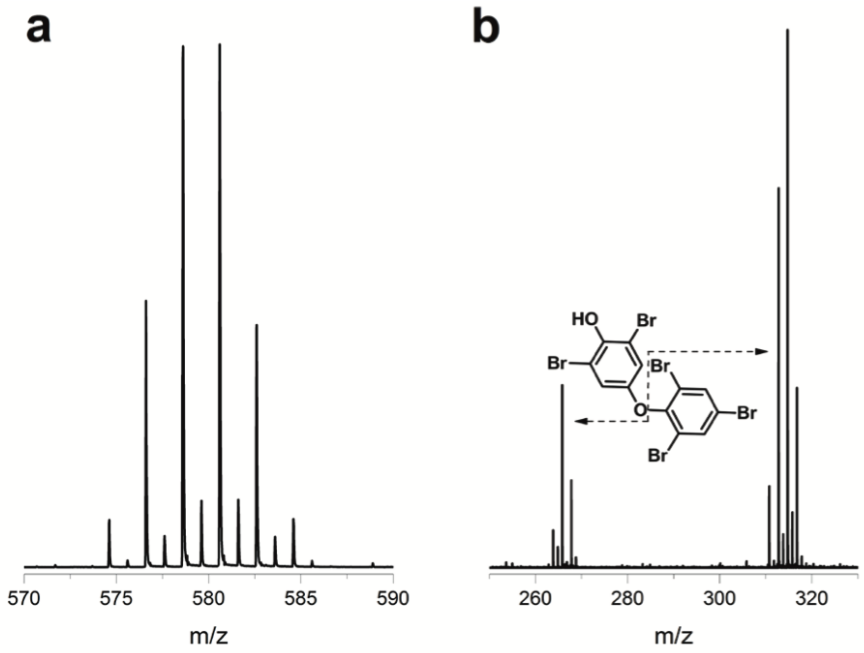

Supplementary Fig. 24. MS and MS/MS profiles for 14, produced enzymatically by reaction of Bmp7 with 5. (**a**) MS1 isotope distribution for **14**. The mass and isotope distribution correspondes to the molecular formula $C_{12}H_5Br_5O_2$. (**b**) MS2 ions corresponding to the scission of ether bond in the structure of **14**. Two distinct MS2 ions can be detected, corresponding to dibromobenzoquinone and tribromobenzene as shown. Detection of the dibromobenzoquinone MS2 ion is consistent with **14** being a para-OH-BDE[8], as discussed in the **Supplementary Note 2** and **Supplementary Fig. 20**. The final deduced structure of **14** is shown with the appropriate fragment ions.

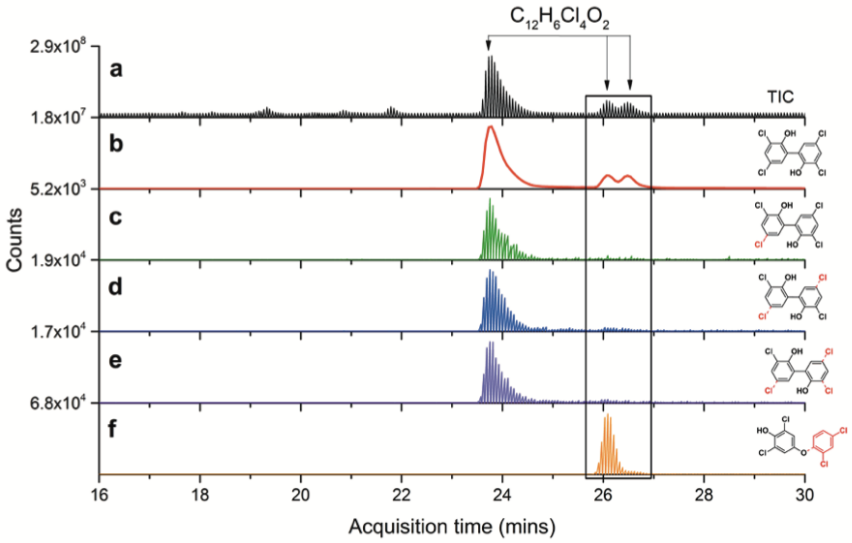

Supplementary Fig. 25. Mass spectrometric analysis of the biphenyl and hydroxylated diphenyl ether products formed by Bmp7 reaction with 17. (**a**) Total ion chromatogram (TIC) for the Bmp7 reaction extract. Peaks for the three isomeric major products corresponding to the molecular formulae $C_{12}H_6Cl_4O_2$ are indicated. (**b**) MS1 extracted ion chromatogram (EIC) corresponding to the most abundant ion for molecular formula $C_{12}H_6Cl_4O_2$ (m/z = 322.90, 10 ppm tolerance) identifies a set of three distinct isomeric product peaks. The postulated chemical structure for **18** is shown on the right. (**c**) MS2 EIC corresponding to $[M\text{-}Cl^-]^-$ (m/z = 286.92, 10 ppm tolerance). (**d**) MS2 EIC corresponding to $[M\text{-}2Cl^-]^-$ (m/z = 250.95, 10 ppm tolerance). (**e**) MS2 EIC corresponding to $[M\text{-}3Cl^-]^-$ (m/z = 222.95, 10 ppm tolerance). (**f**) MS2 EIC corresponding to dichlorobenzoquinone (m/z = 175.94, 10 ppm tolerance). The postulated chemical structure for **19** with the loss of dichlorobenzene (in red) is shown on the right. Note that of the three isomers, one isomers demonstrated the successive loss of chlorine atoms, leading to its postulated structure assignment as a polychlorinated biphenyl analogous to **1**. One of the isomers demonstrates a dichlorobenzoquinone MS2 product ion, leading to its postulated structure assignment as a para-hydroxyl diphenyl ether, analogous to **11**. The third isomer, with similar retention time to the para-hydroxy diphenyl ether, and not demonstrating any MS2 fragment ions is postulated to be an ortho-hydroxy diphenyl ether, analogous to **13**.

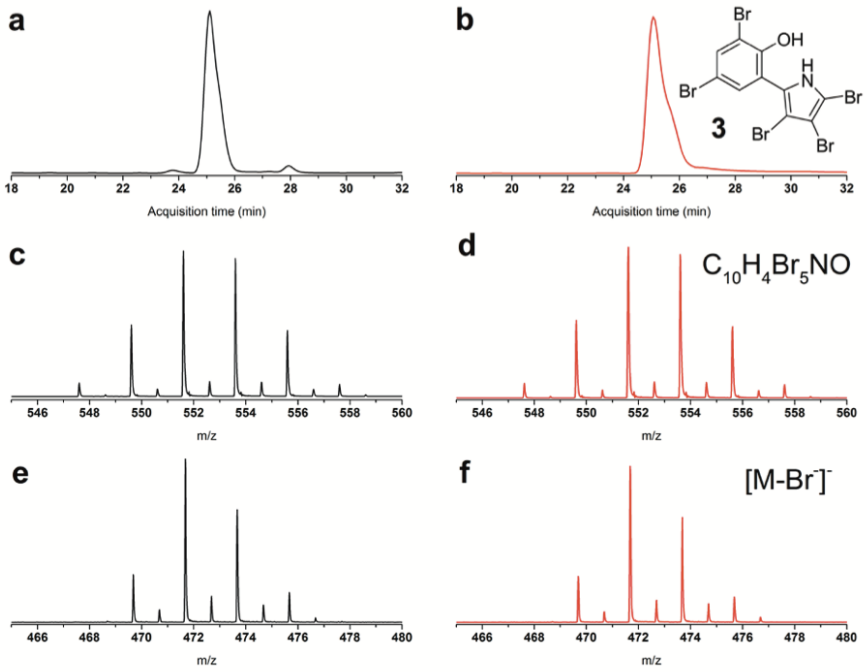

Supplementary Fig. 26. Characterization of 3 generated by Bmp7 in an *in vitro* reaction with 4 and 6 as substrates. Extract of Bmp7 reaction (black curves) was compared to an authentic NMR characterized sample of **3** (red curves) isolated from *P. luteoviolacea* 2ta16. (**a**, **b**) Comparison of retention times. MS1 EIC corresponding to the most abundant isotope for the molecular formula $C_{10}H_4Br_5NO$ (m/z = 551.60, 10 ppm tolerance) for the Bmp7 reaction extract (**a**) and authentic standard of **3** (**b**) analyzed under identical chromatographic conditions. (**c**, **d**) Comparison of MS1 profiles. MS1 mass spectrum for species at retention time 25.2 min from the Bmp7 reaction extract (**c**) and authentic standard of **3** (**d**). (**e**, **f**) Comparison of MS/MS profiles. MS2 profile of the product ions generated from most abundant isotope MS1 ions corresponding to the molecular formula $C_{10}H_3Br_4NO$ at identical retention times from the Bmp7 reaction extract (**e**) and authentic standard of **3** (**f**). Most abundant MS2 ions corresponded to the $[M-Br^-]^-$. Identical retention times, MS1 and MS/MS profiles as compared to a NMR characterized authentic standard lead to the characterization of the Bmp7 reaction product as **3**.

NMR spectrum for **3** purified from preparative scale cultures of *P. luteoviolacea* 2ta16 and used as authentic standard in panels **b**, **d** and **f** above:

3: ^{1}H NMR: ($CDCl_3$) δ [ppm] 9.54 (bs, 1H), 8.09 (d, J = 2.4 Hz, 1H), 7.58 (d, J = 2.4 Hz, 1H), 6.10 (bs, 1H)

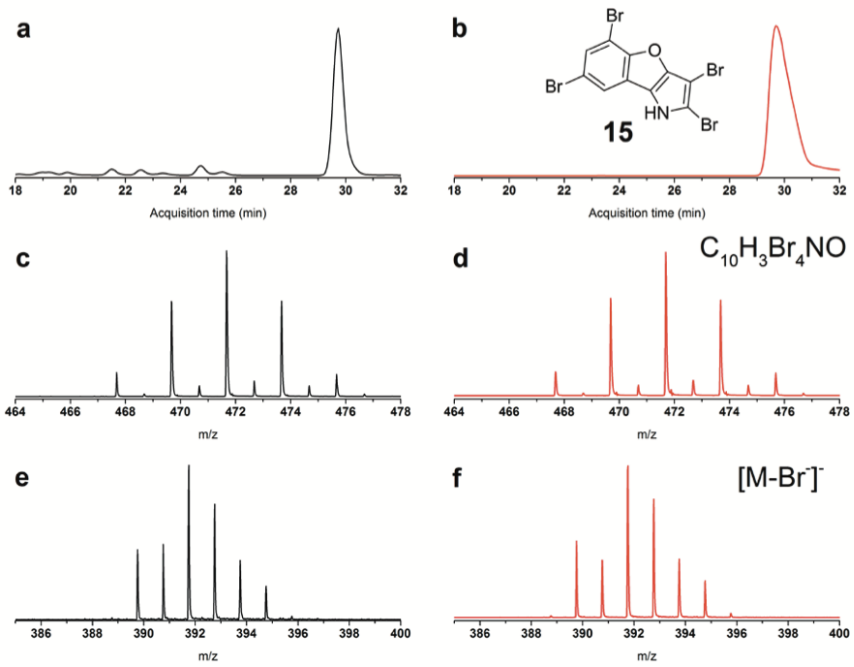

Supplementary Fig. 27. Characterization of 15 generated by Bmp7 in an *in vitro* reaction with 4 and 6 as substrates. Extract of Bmp7 reaction (black curves) was compared to an authentic NMR characterized sample of **15** (red curves) isolated from *P. luteoviolacea* 2ta16. (**a**, **b**) Comparison of retention times. MS1 EIC corresponding to the most abundant isotope for the molecular formula $C_{10}H_3Br_4NO$ (m/z = 471.68, 10 ppm tolerance) for the Bmp7 reaction extract (**a**) and authentic standard of **15** (**b**) analyzed under identical chromatographic conditions. (**c**, **d**) Comparison of MS1 profiles. MS1 mass spectrum for species at retention time 29.8 min from the Bmp7 reaction extract (**c**) and authentic standard of **15** (**d**). (**e**, **f**) Comparison of MS/MS profiles. MS2 profile of the product ions generated from most abundant isotope MS1 ions corresponding to the molecular formula $C_{10}H_3Br_4NO$ at identical retention times from the Bmp7 reaction extract (**e**) and authentic standard of **15** (**f**). Most abundant MS2 ions corresponded to the $[M\text{-}Br^-]^-$. Identical retention times, MS1 and MS/MS profiles as compared to a NMR characterized authentic standard lead to the characterization of the Bmp7 reaction product as **15**.

^{1}H NMR spectrum for **15** purified from preparative scale cultures of *P. luteoviolacea* 2ta16 and used as authentic standard in panels **b**, **d** and **f** above:

15: ^{1}H NMR ($CDCl_3$) δ [ppm] 8.79 (bs, 1H), 7.57 (d, J = 1.8 Hz, 1H), 7.54 (d, J = 1.8 Hz, 1H)

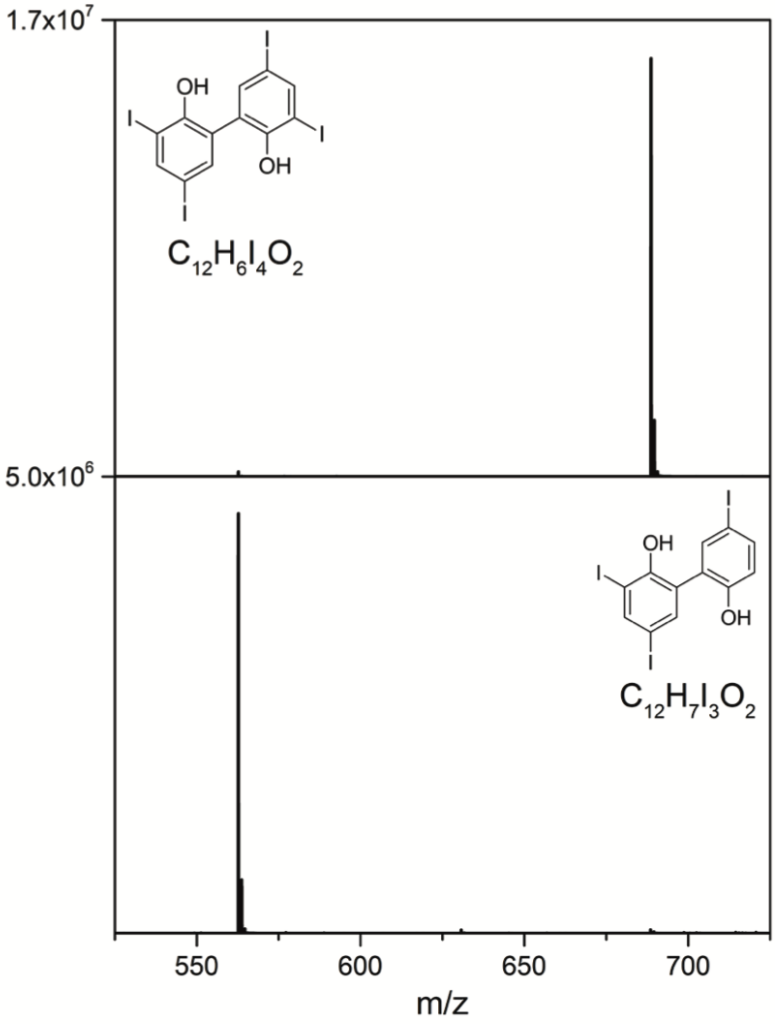

Supplementary Fig. 28. Production of iodinated bromophenols by heterologous host *E. coli* expressing *bmp1–8* grown in the presence of KI. When *E. coli* expressing *bmp1–8* was grown in the presence of 1 g/L KI (no KBr was present), we could detect MS1 signals corresponding to the molecular formulae $C_{12}H_6I_4O_2$ (top) (expected: 688.6474, found: 688.6472) and $C_{12}H_7I_3O_2$ (bottom) (expected: 562.7507, found: 562.7508). The molecular formula $C_{12}H_6I_4O_2$ corresponds to the iodinated analog of **1** (putative structure shown in top

panel), while $C_{12}H_7I_3O_2$ corresponds to the iodinated analog of **10** (putative structure shown in bottom panel). This result implies that Bmp5 could indeed accept iodide for incorporation to 4-HBA. Together with the dimerization of **17** as shown in **Supplementary Fig. 25**, this result demonstrates that Bmp7 is non-specific for the identity of halogens atoms present on the phenol ring to catalyze their coupling. Also note that during this experiment, 10 g/L chloride was present in the *E. coli* growth media. However, we could not detect the formation of any chlorinated phenol monomers or dimers.

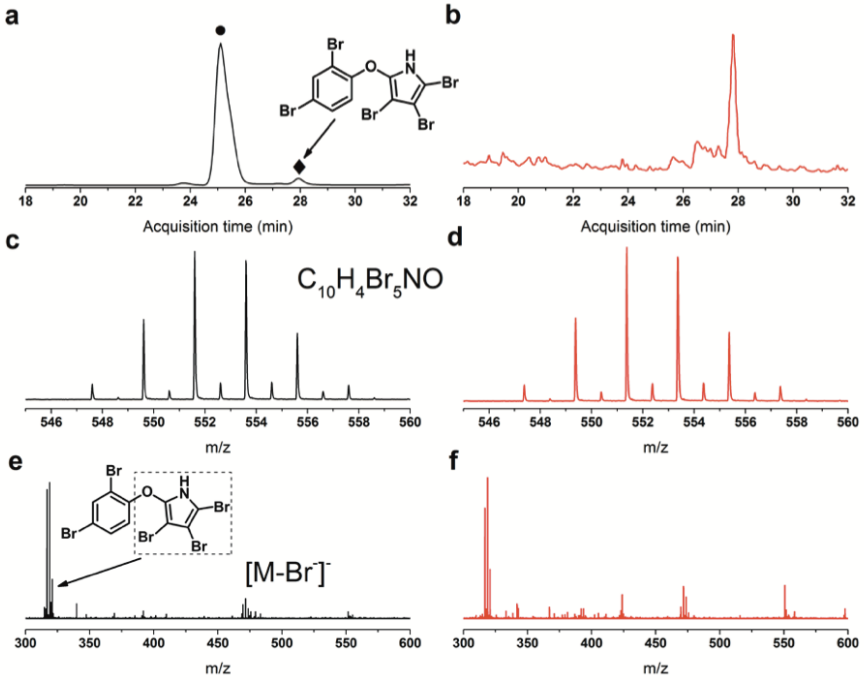

Supplementary Fig. 29. Mass spectrometry based characterization of a polybrominated phenol-pyrrole ether product generated by Bmp7 in an *in vitro* reaction with 4 and 6 as substrates, which is also detected in the culture extracts of *P. luteoviolacea* 2ta16. Extract of Bmp7 reaction (black curves) was compared to an extract of *P. luteoviolacea* 2ta16 (red curves). (**a**, **b**) Comparison of retention times. MS1 EIC corresponding to the most abundant isotope for the molecular formula $C_{10}H_4Br_5NO$ (m/z = 551.60, 10 ppm tolerance) for the Bmp7 reaction extract (**a**) and a MS2 EIC corresponding to m/z = 314.78, 10 ppm tolerance (*vide infra*) for an extract of *P. luteoviolacea* 2ta16 (**b**) analyzed under identical chromatographic conditions. Note that in (**a**), two isomeric molecules corresponding to the molecular formula $C_{10}H_4Br_5NO$ could be detected. Peak denoted by● corresponds to **3**, as shown in **Supplementary Fig. 26**. The peak corresponding to♦ is an isomer of **3**. (**c**, **d**) Comparison of MS1 profiles. MS1 mass spectrum for species at retention time 27.9 min from the Bmp7 reaction extract (**c**) and an extract of *P. luteoviolacea* 2ta16 (**d**). (**e**, **f**) Comparison of MS/MS profiles. MS2 profile of the product ions generated from most abundant isotope MS1 ions corresponding to the molecular formula $C_{10}H_3Br_4NO$ at identical retention times

from the Bmp7 reaction extract (**e**) and an extract of *P. luteoviolacea* 2ta16 (**f**). Most abundant MS2 ions (cluster around m/z = 314.78) corresponded to a hydroxytribromopyrrole moiety (shown in a dashed box in (**e**)), while a $[M\text{-}Br]^-$ MS2 product ion can also be detected. Detection of a hydroxytribromopyrrole MS2 ion leads us to postulate that the structure of this molecule could correspond to a polybrominated phenol-pyrrole ether as shown in (**a**).

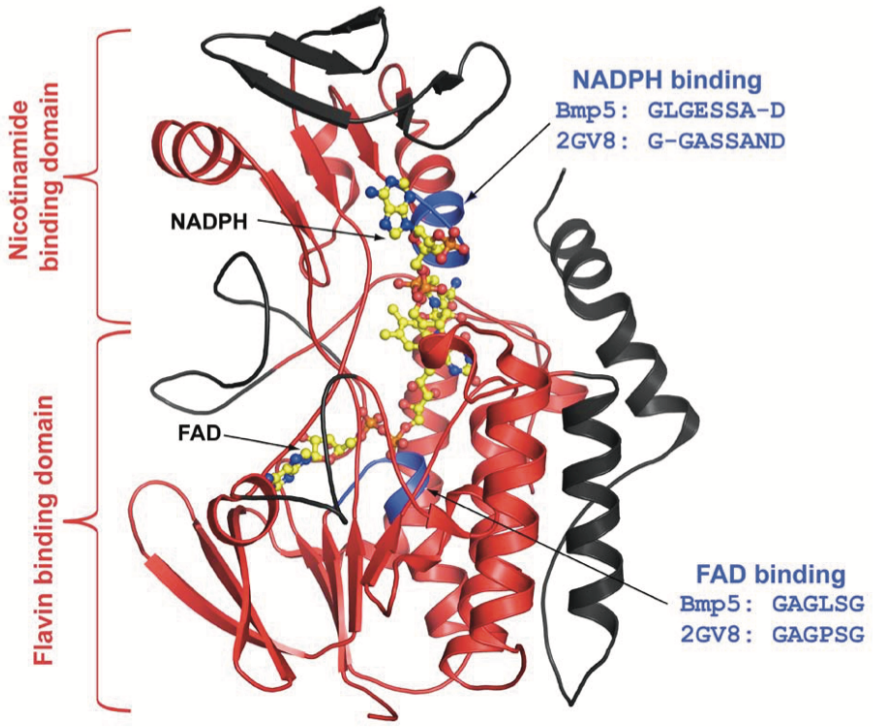

Supplementary Fig. 30. Primary sequence analysis identifies Bmp5 to be homologous to flavin-dependent monooxygenases. Primary sequence of Bmp5 was provided as an input to the NCBI BLAST program and analyzed against the 'Non-reduntant protein sequence (nr)' dataset. All homologs of Bmp5 identified using this analysis (apart *P. phenolica* O-BC30 and *M. mediterranea* MMB-1, as decribed in this study) were annotated as flavin-dependent dimethylaniline monooxygenases. However, as most of the sequences returned by the BLAST search were also annotated as hypothetical or predicted proteins with uncharacterized biochemical activities, a second BLAST search was performed against the 'Protein Data Bank (pdb)' database. The results of this search were more definitive, and are discussed here. The primary structural homologs for Bmp5 that had the most primary sequence coverage identified were:

1. PDB: 2GV8 and related structures. Flavin-dependent monooxygenase from *Schizosaccharomyces pombe*[14].

2. PDB: 2XVI and related structures. Flavin-dependent monooxygenase from *Methylophaga aminisulfidivorans*[15].

Further analysis reveals that the for both 2GV8 and 2XVI, homology to Bmp5 is divided into two distinct regions. The first region comprises of residues from the N-terminus of Bmp5 to residue 200 (identity/similarity = 28%/43% to 2GV8 and 27%/48% to 2XVI; henceforth referred to as *Motif 1*). The second region comprises of residues 315 to 426 (identity/similarity = 25%/47% to 2GV8 and 29%/46% to 2XVI; henceforth referred to as *Motif 2*). Upon mapping both regions back on to the structure 2GV8 (shown in cartoon representation above), it is evident that *Motif 1* and *Motif 2* (colored red in cartoon representation) comprise of all core secondary structural elements constututing the flavin binding and the nicotinamide binding domains. This includes the flavin binding GAGLSG sequence motif (colored blue), and the nicotinamide binding GLGESSAD sequence motif[14-15] (colored blue) identified in the primary sequence of Bmp5. Hence, the core structural elements in the structure of 2GV8 for both flavin binding, as well as nicotinamide binding can be identified in the primary sequence for Bmp5.

It is also noteworthy that the BLAST search for the primary sequence of Bmp5 against the PDB database did not return any hits for flavin-dependent halogenases, either of the PrnA[16]/RebH[17]/PyrH[18] (and an unpublished crystal structure PDB: 2PYX) type that utilize free substrates, or of the CmlS[19]/CndH[20] type that utilize substrates tethered to acyl carrier proteins. On the flip side, an identical BLAST search against the PDB database for the primary sequence of Bmp2 returns homology to CndH (31%/47%), CmlS (30%/45%) and an unpublished crystal structure PDB: 3NIX (28%/44%). A similar result is obtained for the following halogenases: chlorinase PltA[1] (CmlS: 30%/45%; CndH: 28%/46%; 3NIX: 27%/45%), chlorinase SgcC3[21] (CmlS: 36%/52%; CndH: 53%/66%; 3NIX: 32%/44%), chlorinase Mpy16[22] (CmlS: 30%/43%; CndH: 32%/49%; 3NIX: 26%/44%), chlorinase Clz5[23] (CmlS: 30%/43%; CndH: 32%/49%; 3NIX: 26%/44%), chlorinase Pyr29[24] (CmlS: 31%/45%; CndH: 30%/47%; 3NIX: 28%/44%), among other flavin-dependent halogenases that have been described in literature. Noteworthy here is the chlorinase ChlA[25]. Activity for ChlA was demonstrated for a substrate molecule not tetherred to an ACP molecule. However, ChlA demonstrates greatest homology to halogenases requiring ACP tethered substrates (CmlS: 25%/40%; CndH: 20%/38%; 3NIX was not returned as a homolog by BLAST). Expectedly, tryptophan chlorinases KtzQ and KtzR[26] display homology to PrnA/RebH/PyrH.

Supplementary Tables

Supplementary Table 1. High-resolution MS used for determination of molecular formulae of polybrominated metabolites from extract of *P. luteoviolacea* 2ta16.

Molecule	Molecular Formula	$[M-H]^-$ calculated (m/z)	$[M-H]^-$ measured (m/z)	Error (mmu)
1	$C_{12}H_6Br_4O_2$	496.7029	496.7029	0.0
2	$C_8H_2Br_6N_2$	598.5245	598.5244	0.1
3	$C_{10}H_4Br_5NO$	547.6137	547.6137	0.0
4	$C_6H_4Br_2O$	248.8556	248.8554	0.2
5	$C_6H_3Br_3O$	326.7661	326.7660	0.1
6	$C_4H_2Br_3N$	299.7665	299.7663	0.2
7	C_4HBr_4N	377.6770	377.6765	0.5
9	$C_{12}H_7Br_3O_2$	418.7923	418.7922	0.1
14	$C_{10}H_3Br_4NO$	467.6875	467.6874	0.1

Supplementary Table 2. ***P. luteoviolacea*** **2ta16** ***bmp*** **gene cluster annotation.**

Gene	Locus tag	Size [aa]	Proposed function	Homolog (%Similarity/%Identity) *functionally characterized	Accession number
bmp1	*Pl2ta16_01235*	77 (1–77)	Prolyl acyl carrier protein (N-terminal domain)	PltL, peptidyl carrier protein [*Pseudomonas protegens* pf-5] (60/34)*	YP_259898.1
bmp1	*Pl2ta16_01235*	280 (78–358)	Thioesterase (C-terminal domain)	α/β-hydrolase fold protein [*Krypidia tusciae* DSM 2912] (47/28)	YP_003588846
bmp2	*Pl2ta16_01236*	406	Pyrrole halogenase	PltA, $FADH_2$-dependent halogenase [*Pseudomonas protegens* Pf-5] (44/29)*	AAY92059.1
bmp3	*Pl2ta16_01237*	380	Proline dehydrogenase	PltE, acyl-CoA dehydrogenase [*Pseudomonas protegens* Pf-5] (62/45)*	AAY92063.1
bmp4	*Pl2ta16_01238*	518	L-Proline adenyl transferase	PltF, prolyl-AMP ligase [*Pseudomonas protegens* pf-5] (55/40)*	YP_259898.1
bmp5	*Pl2ta16_01239*	515	Flavin-dependent oxygenase	Dimethylaniline monooxygenase (N-Oxide forming) [*Myotis brandtii*] (50/33)	EPQ08634.1
bmp6	*Pl2ta16_01240*	202	Chorismate lyase	4-hydroxybenzoate synthetase [*Beggiatoa alba*] (60/41)	WP_002683800.1
bmp7	*Pl2ta16_01241*	491	Cytochrome P450	Cytochrome P450 [*Phalacrocorax carbo*] (50/30)	BAE93469.1
bmp8	*Pl2ta16_01234*	196	Carboxymuconolactone decarboxylase	Carboxymuconolactone decarboxylase [*Blastococcus saxobsidens* DD2] (58/42)	YP_005328578.1
bmp9	*Pl2ta16_01233*	106	Ferredoxin	Ferredoxin [*Idiomarina loihiensis* L2TR] (73/52)	YP_155277.1
bmp10	*Pl2ta16_01232*	415	Ferredoxin reductase	Ferredoxin reductase [*Pseudomonas* sp. 19-rlim] (70/53)	AEO27387.1

Supplementary Table 3. Primers used to generate overlapping fragments for yeast assembly of yeast/*E. coli* shuttle vector pGAL-*bmp1–7*. All primer sequences are listed from 5' to 3'.

Primer Name	Primer Sequence	Target
pGALbmp1F	AAGGTAAACAGGTAAGAGCTCGGTAATAACTG ATATAATTAAATTGAAG	pGAL-MF region1
pGALbmp1F	TGCAGTCTCTTGATAACTTTTTGCACTGTAGGTC CGTTAA	pGAL-MF region1
pGALbmp2F	TTAACGGACCTACAGTGCAAAAAGTTATCAAGA GACTGCA	pGAL-MF region2
pGALbmp2F	CTAGTCTGGCAATATTGTTAACACTAGTGACTC GCTGCGCTCGGTC	pGAL-MF region2
pGALbmp3F	ACCGAGCGCAGCGAGTCACTAGTGTTAACAATA TTGCCAGACTAGA	*bmp* cluster region1
pGALbmp3F	TTGGCCCAGGTAACCGAATTTAGCATTCGTAGT GGCATAC	*bmp* cluster region1
pGALbmp4F	GTATGCCACTACGAATGCTAAATTCGGTTACCT GGGCCAA	*bmp* cluster region2
pGALbmp4F	TGTGATCTTGTACTCAGTTTGCCAATGTTTCGTA TCGTAC	*bmp* cluster region2
pGALbmp5F	GTACGATACGAAACATTGGCAAACTGAGTACA AGATCACA	*bmp* cluster region3
pGALbmp5F	AATTTAATTATATCAGTTATTACCGAGCTCTTAC CTGTTTACCTTCGGGT	*bmp* cluster region3

Supplementary Table 4. Primers used to generate gene deletions from pETDuet-*bmp*. All primer sequences are listed from 5' to 3'.

Primer Name	Primer Sequence	ORF deleted
bmp2KO FWD	CATGGCATGAAGGAAAAGCACTGCGCTTTTCCTTCT AAGGGAAGGATTGATTATG	*bmp2*
bmp2KO REV	TGCTTTTCCTTCATGCCATGTCCACCTTAGTTAAGA AGTCTTCAACAACCCAGAC	
bmp5KO FWD	TGGTGCGTAAATAGTACGAGAAAGGACATGATTCG ATTGTCAGATGAAAGCCTGT	*bmp5*
bmp5KO REV	CTCGTACTATTTACGCACCACTTTGCACAGTATTAC TCCCGTGCCGTGGGCGAGT	
bmp7-XmaF	ACACCAGAATTATCAACCTTAGTCAGTGGGATTTG ACCACCCGGGGCTCACGGTAACTGATGCCG	*bmp7*
bmp7-XmaR	TAAGGATGGATGCAAAACCATCCTAAGTAGGATGG CCTTCCCGGGGGAACTTATGAGCTCAGCCA	

Supplementary Table 5. Co-transformations of *E. coli* BL21(DE3) for heterologous expression of *bmp* cluster and derivatives.

Strain name	Co-transformed plasmid 1	Co-transformed plasmid 2
bmp1–8	pETDuet-*bmp1–7*	pCOLADuet-*bmp8-ppt*
Δbmp2	pETDuet-*bmp1–7:Δbmp2*	pCOLADuet-*bmp8-ppt*
Δbmp5	pETDuet-*bmp1–7:Δbmp5*	pCOLADuet-*bmp8-ppt*
Δbmp7	pETDuet-*bmp1–7:Δbmp7*	pCOLADuet-*bmp8-ppt*
Δbmp8	pETDuet-*bmp1–7*	pCOLADuet-*ppt*

SUPPLEMENTARY REFERENCES

1 Dorrestein, P. C., Yeh, E., Garneau-Tsodikova, S., Kelleher, N. L. & Walsh, C. T. Dichlorination of a pyrrolyl-S-carrier protein by FADH2-dependent halogenase PltA during pyoluteorin biosynthesis. *Proc Natl Acad Sci U S A.* **102**, 13843-13848 (2005).

2 Dorrestein, P. C. *et al.* Facile detection of acyl and peptidyl intermediates on thiotemplate carrier domains via phosphopantetheinyl elimination reactions during tandem mass spectrometry. *Biochemistry.* **45**, 12756-12766 (2006).

3 Isnansetyo, A. & Kamei, Y. MC21-A, a bactericidal antibiotic produced by a new marine bacterium, *Pseudoalteromonas phenolica* sp. nov. O-BC30(T), against methicillin-resistant *Staphylococcus aureus*. *Antimicrob Agents Chemother.* **47**, 480-488 (2003).

4 Feher, D., Barlow, R., McAtee, J. & Hemscheidt, T. K. Highly brominated antimicrobial metabolites from a marine *Pseudoalteromonas* sp. *J Nat Prod.* **73**, 1963-1966 (2010).

5 Belin, P. *et al.* Identification and structural basis of the reaction catalyzed by CYP121, an essential cytochrome P450 in *Mycobacterium tuberculosis*. *Proc Natl Acad Sci U S A.* **106**, 7426-7431 (2009).

6 Zhao, B. *et al.* Binding of two flaviolin substrate molecules, oxidative coupling, and crystal structure of *Streptomyces coelicolor* A3(2) cytochrome P450 158A2. *J Biol Chem.* **280**, 11599-11607 (2005).

7 Dec, J., Haider, K. & Bollag, J. M. Release of substituents from phenolic compounds during oxidative coupling reactions. *Chemosphere.* **52**, 549-556 (2003).

8 Mas, S. *et al.* Comprehensive liquid chromatography-ion-spray tandem mass spectrometry method for the identification and quantification of eight hydroxylated brominated diphenyl ethers in environmental matrices. *J Mass Spectrom.* **42**, 890-899 (2007).

9 Li, D. B. *et al.* Chapter 19. In vitro studies of phenol coupling enzymes involved in vancomycin biosynthesis. *Methods Enzymol.* **458**, 487-509 (2009).

10 John, E. A., Pollet, P., Gelbaum, L. & Kubanek, J. Regioselective syntheses of 2,3,4-tribromopyrrole and 2,3,5-tribromopyrrole. *J Nat Prod.* **67**, 1929-1931 (2004).

11 Petersen, B. O. *et al.* H2BC: a new technique for NMR analysis of complex carbohydrates. *Carbohydr Res.* **341**, 550-556 (2006).

12 Calcul, L. *et al.* NMR strategy for unraveling structures of bioactive sponge-derived oxy-polyhalogenated diphenyl ethers. *J Nat Prod.* **72**, 443-449 (2009).

13 Kitamura, M., Koyama, T., Nakano, Y. & Uemura, D. Corallinafuran and Corallinaether, novel toxic compounds from crustose coralline red algae. *Chemistry Letters.* **34**, 1272-1273 (2005).

14 Eswaramoorthy, S., Bonanno, J. B., Burley, S. K. & Swaminathan, S. Mechanism of action of a flavin-containing monooxygenase. *Proc Natl Acad Sci U S A.* **103**, 9832-9837 (2006).

15 Cho, H. J. *et al.* Structural and functional analysis of bacterial flavin-containing monooxygenase reveals its ping-pong-type reaction mechanism. *J Struct Biol.* **175**, 39-48 (2011).

16 Dong, C. *et al.* Tryptophan 7-halogenase (PrnA) structure suggests a mechanism for regioselective chlorination. *Science.* **309**, 2216-2219 (2005).

17 Bitto, E. *et al.* The structure of flavin-dependent tryptophan 7-halogenase RebH. *Proteins.* **70**, 289-293 (2008).

18 Zhu, X. *et al.* Structural insights into regioselectivity in the enzymatic chlorination of tryptophan. *J Mol Biol.* **391**, 74-85 (2009).

19 Podzelinska, K. *et al.* Chloramphenicol biosynthesis: the structure of CmlS, a flavin-dependent halogenase showing a covalent flavin-aspartate bond. *J Mol Biol.* **397**, 316-331 (2010).

20 Buedenbender, S., Rachid, S., Muller, R. & Schulz, G. E. Structure and action of the myxobacterial chondrochloren halogenase CndH: a new variant of FAD-dependent halogenases. *J Mol Biol.* **385**, 520-530 (2009).

21 Lin, S., Van Lanen, S. G. & Shen, B. Regiospecific chlorination of (S)-beta-tyrosyl-S-carrier protein catalyzed by SgcC3 in the biosynthesis of the enediyne antitumor antibiotic C-1027. *J Am Chem Soc.* **129**, 12432-12438 (2007).

22 Yamanaka, K., Ryan, K. S., Gulder, T. A., Hughes, C. C. & Moore, B. S. Flavoenzyme-catalyzed atropo-selective N,C-bipyrrole homocoupling in marinopyrrole biosynthesis. *J Am Chem Soc.* **134**, 12434-12437 (2012).

23 Mantovani, S. M. & Moore, B. S. Flavin-linked oxidase catalyzes pyrrolizine formation of dichloropyrrole-containing polyketide extender unit in chlorizidine A. *J Am Chem Soc.* **135**, 18032-18035 (2013).

24 Zhang, X. & Parry, R. J. Cloning and characterization of the pyrrolomycin biosynthetic gene clusters from *Actinosporangium vitaminophilum* ATCC 31673 and *Streptomyces* sp. strain UC 11065. *Antimicrob Agents Chemother.* **51**, 946-957 (2007).

25 Neumann, C. S., Walsh, C. T. & Kay, R. R. A flavin-dependent halogenase catalyzes the chlorination step in the biosynthesis of *Dictyostelium* differentiation-inducing factor 1. *Proc Natl Acad Sci U S A.* **107**, 5798-5803 (2010).

26 Fujimori, D. G. *et al.* Cloning and characterization of the biosynthetic gene cluster for kutznerides. *Proc Natl Acad Sci U S A.* **104**, 16498-16503 (2007).

27 Thomas, M. G., Burkart, M. D. & Walsh, C. T. Conversion of L-proline to pyrrolyl-2-carboxyl-S-PCP during undecylprodigiosin and pyoluteorin biosynthesis. *Chem Biol.* **9**, 171-184 (2002).

Chapter 2, in full, is a reprint of materials as it appears in "Biosynthesis of polybrominated aromatic molecules by marine bacteria" in *Nature Chemical Biology*, 2014, Agarwal V., El Gamal A., Yamanaka K., Poth D., Kersten R. D., Schorn M., Allen E. E., and Moore, B. S., The dissertation author was one of two equally contributing primary investigators and authors of this paper.

V.A., A.A.E., E.E.A. and B.S.M. designed research; V.A., A.A.E. and K.Y. performed genetic experiments; V.A., A.A.E. and R.D.K. performed in vitro experiments; M.S. and E.E.A. generated sequencing data; D.P. contributed new analytical reagents; and V.A., A.A.E., E.E.A. and B.S.M. analyzed data and wrote the manuscript.

Chapter 3: Biosynthesis of coral settlement cue tetrabromopyrrole in marine bacteria by a uniquely adapted brominase-thioesterase enzyme pair

PNAS

Biosynthesis of coral settlement cue tetrabromopyrrole in marine bacteria by a uniquely adapted brominase–thioesterase enzyme pair

Abrahim El Gamal[a,1], Vinayak Agarwal[a,1], Stefan Diethelm[a], Imran Rahman[a], Michelle A. Schorn[a], Jennifer M. Sneed[b], Gordon V. Louie[c,d], Kristen E. Whalen[e], Tracy J. Mincer[e], Joseph P. Noel[c,d], Valerie J. Paul[b], and Bradley S. Moore[a,f,2]

[a]Center for Oceans and Human Health, Scripps Institution of Oceanography, University of California, San Diego, La Jolla, CA 92093; [b]Smithsonian Marine Station at Fort Pierce, Fort Pierce, FL 34949; [c]Howard Hughes Medical Institute, The Salk Institute for Biological Studies, La Jolla, CA 92037; [d]Jack H. Skirball Center for Chemical Biology and Proteomics, The Salk Institute for Biological Studies, La Jolla, CA 92037; [e]Marine Chemistry and Geochemistry, Woods Hole Oceanographic Institution, Woods Hole, MA 02543; and [f]Skaggs School of Pharmacy and Pharmaceutical Sciences, University of California, San Diego, La Jolla, CA 92093

Edited by Michael A. Fischbach, University of California, San Francisco, CA, and accepted by the Editorial Board February 24, 2016 (received for review October 4, 2015)

Halogenated pyrroles (halopyrroles) are common chemical moieties found in bioactive bacterial natural products. The halopyrrole moieties of mono- and dihalopyrrole-containing compounds arise from a conserved mechanism in which a proline-derived pyrrolyl group bound to a carrier protein is first halogenated and then elaborated by peptidic or polyketide extensions. This paradigm is broken during the marine pseudoalteromonad bacterial biosynthesis of the coral larval settlement cue tetrabromopyrrole (1), which arises from the substitution of the proline-derived carboxylate by a bromine atom. To understand the molecular basis for decarboxylative bromination in the biosynthesis of 1, we sequenced two *Pseudoalteromonas* genomes and identified a conserved four-gene locus encoding the enzymes involved in its complete biosynthesis. Through total in vitro reconstitution of the biosynthesis of 1 using purified enzymes and biochemical interrogation of individual biochemical steps, we show that all four bromine atoms in 1 are installed by the action of a single flavin-dependent halogenase: Bmp2. Tetrabromination of the pyrrole induces a thioesterase-mediated offloading reaction from the carrier protein and activates the biosynthetic intermediate for decarboxylation. Insights into the tetrabrominating activity of Bmp2 were obtained from the high-resolution crystal structure of the halogenase contrasted against structurally homologous halogenase Mpy16 that forms only a dihalogenated pyrrole in marinopyrrole biosynthesis. Structure-guided mutagenesis of the proposed substrate-binding pocket of Bmp2 led to a reduction in the degree of halogenation catalyzed. Our study provides a biogenetic basis for the biosynthesis of 1 and sets a firm foundation for querying the biosynthetic potential for the production of 1 in marine (meta)genomes.

natural products | biosynthesis | halogenation | enzymology

Marine bacteria of the genus *Pseudoalteromonas* produce numerous small molecule natural products with varied roles in marine chemical ecology (1–4). Recently, tetrabromopyrrole (**1**, Fig. 1) was established as a chemical cue produced by *Pseudoalteromonas* that induces larval settlement and metamorphosis in reef-building Caribbean coral species (3). Additionally, the chemical structure of **1** is notable for its degree of halogenation (one-to-one carbon-to-halogen ratio), unique among naturally occurring aromatic organohalogens (5).

Halopyrrole-containing microbial natural products are biosynthesized starting from L-proline. A highly conserved halopyrrole biosynthetic route involves oxidation of an acyl carrier protein (ACP)-loaded prolyl side chain and subsequent halogenation by a flavin-dependent halogenase (Fig. 1) (6). At this stage, two biosynthetic routes are possible. In the first route, the ACP-loaded halopyrrole is extended using modular assembly lines to yield nonribosomally synthesized peptide, or polyketide natural products (e.g., **2–4**, Fig. 1) (7–10). During the biosynthesis of **2–4**, and other related natural products, the halopyrrole carboxylic acid is transthioesterified to downstream ACPs during modular elongation reactions. Molecules arising from these modular biosynthetic pipelines are characterized by the preservation of the prolyl alpha-carboxyl carbon atom as a carbonyl, or embedded in the final natural product skeleton in varying oxidation states (in red, Fig. 1). In a recently discovered alternate route, the prolyl alpha-carboxyl carbon atom is lost during the biosynthesis of **1** and the cytotoxic marine bacterial natural product pentabromopseudilin (**5**, Fig. 1) (4, 11). Uniquely, **5** is biosynthesized via the coupling of 2,3,4-tribromopyrrole (**6**, Fig. 1) to 2,4-dibromophenol rather than via a modular assembly line. The molecular mechanism for the pyrrole offloading from the ACP and elimination of prolyl alpha-carboxyl carbon en route to the biosyntheses of **1** and **5–6** has not been determined. The structure of **1** poses an additional biosynthetic challenge due to the presence of a bromine atom in place of an acyl side chain. Although all previously described pyrrole halogenases

Significance

The majority of pharmaceuticals are inspired by natural product scaffolds that are functionalized by tailoring enzymes, such as halogenases. The degree of halogenation is an important determinant of natural product bioactivity, yet little is known regarding the molecular basis for the exquisite control exhibited by tailoring halogenases. Known pyrrole halogenases commonly perform up to two halogenations on the pyrrole. Our study of tetrabromopyrrole biosynthesis revealed a uniquely adapted halogenase–thioesterase enzyme pair that catalyzes an unprecedented series of halogenations on a pyrrole. Structural comparison of the pyrrole tetrahalogenase to a pyrrole dihalogenase revealed key residues involved in controlling the degree of halogenation. Our findings provide fundamental insights that might be applied in the rational design of biocatalysts toward directed biosynthesis of new chemicals.

Author contributions: A.E., V.A., and B.S.M. designed research; A.E., V.A., S.D., I.R., and M.A.S. performed research; S.D., J.M.S., G.V.L., K.E.W., T.J.M., J.P.N., and V.J.P. contributed new reagents/analytic tools; A.E., V.A., S.D., and B.S.M. analyzed data; and A.E., V.A., and B.S.M. wrote the paper.

The authors declare no conflict of interest.

This article is a PNAS Direct Submission. M.A.F. is a guest editor invited by the Editorial Board.

Data deposition: The sequences reported in this paper have been deposited in the Genbank database [accession nos. KR011923 (*Pseudoalteromonas* sp. PS5-derived bmp gene clusters) and KT808878 (*Pseudoalteromonas* sp. A757-derived bmp gene clusters)]. The atomic coordinates and structure factors have been deposited in the Protein Data Bank, www.rcsb.org (PDB ID codes 5BUK (Mpy16), 5BVA (Bmp2), and 5BUL (Bmp2-TM)].

[1]A.E. and V.A. contributed equally to this work.

[2]To whom correspondence should be addressed. Email: bsmoore@ucsd.edu.

This article contains supporting information online at www.pnas.org/lookup/suppl/doi:10.1073/pnas.1519695113/-/DCSupplemental.

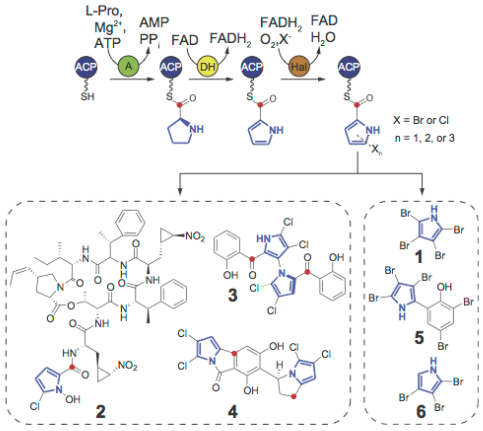

Fig. 1. Structures and biosynthesis of halopyrrole natural products. Halopyrrole biosynthesis starts from the loading of L-proline onto an ACP phosphopantetheine thiol by an adenylation (A) enzyme, followed by a 4e⁻ oxidation of the prolyl ring to a pyrrole (in blue) catalyzed by a dehydrogenase (DH) enzyme. Subsequent halogenation by a flavin-dependent halogenase (Hal) then installs one, two, or three halogens on the pyrrole ring. At this stage, the thiotemplated halopyrrole can proceed down assembly line biosynthetic routes to afford natural products, such as hormaomycin (**2**), marinopyrrole A (**3**), and chlorizidine A (**4**) (8–10). However, the biosyntheses of **1** and **5**–**6** do not entail modular assembly line extension of the L-proline–derived halopyrrole, but rather involve the loss of the prolyl alpha-carboxylate carbon atom (in red) via an unexplained mechanism.

catalyze one, two, or three halogen additions upon the ACP-loaded pyrrole ring, a halogenase capable of four halogenations on the pyrrole ring, as implied by the structure of **1**, has not been characterized. These open biosynthetic questions, together with the ecological significance of **1** in coral larval settlement, motivated us to explore the genetic and molecular logic for its biosynthesis in marine bacteria.

Herein, we establish the biosynthesis of **1** by the total in vitro enzymatic reconstitution of its biosynthetic machinery. We show that a single flavin-dependent brominase installs an unprecedented four halogens on an ACP-bound pyrrole required for the progression of thioesterase (TE)-mediated offloading and decarboxylation reactions. We also exploit an opportunity to structurally characterize and investigate via site-directed mutagenesis the molecular basis for a differential number of halogen additions catalyzed by flavin-dependent halogenases on aromatic substrates. Our structural comparison of a highly homologous pyrrole dihalogenase to the pyrrole tetrahalogenase reveals subtle variations in biocatalyst design that lead to divergent molecular outcomes.

Results

Genetic Basis for the Biosynthesis of 1. We recently reported that **1** produced by the marine bacterium *Pseudoalteromonas* sp. PS5 induces settlement of larvae associated with several Caribbean coral species (3). To investigate the genetic basis for the biosynthesis of **1**, we sequenced and assembled a 5.08-Mbp draft genome for *P.* sp. PS5. Querying the draft genome for the presence of the halopyrrole biosynthetic genes, we identified a gene locus in *P.* sp. PS5 with high homology to a subset of bromopyrrole biosynthetic genes present in the previously reported *bmp* gene locus from marine bacteria of the genera *Pseudoalteromonas* and *Marinomonas* (11) (Fig. 2*A* and *SI Appendix*, Table S1). The organization of the *bmp* homologs identified in the genome of *P.* sp. PS5 (*PS5_bmp*) is identical to that of the *bmp* gene cluster found in *Marinomonas mediterranea* MMB-1 *bmp* (*Mm_bmp*) and others (11). Notably, the *PS5_bmp* gene locus maintains the bromopyrrole biosynthetic module *Mm_bmp1–4* and the bromopyrrole/phenol coupling cytochrome P450 (CYP450) accessory genes *Mm_bmp9–10*, but lacks the genes associated with bromophenol biosynthesis (*Mm_bmp5–6*) and the CYP450-*Mm_bmp7* (Fig. 2*A*). In addition, we also sequenced and assembled a 5.13-Mbp draft genome for *Pseudoalteromonas* sp. A757 that also produces **1** (12). Querying the genome of *P.* sp. PS5 as before revealed a gene cluster with high homology to *PS5_bmp* (*A757_bmp*), providing a second example of a standalone bromopyrrole biosynthetic pathway from the genus *Pseudoalteromonas* (Fig. 2*A* and *SI Appendix*, Table S1).

To evaluate the role of *PS5_bmp1–4* genes in the production of **1**, we cloned and heterologously expressed *PS5_bmp1–4* in *Escherichia coli*. Only in the presence of bromide in the culture media, we observed robust heterologous production of **1** along with a minor amount of **6**, consistent with the product profile observed in organic extracts of cultures of *P.* sp. PS5 and *P.* sp. A757 (Fig. 2*B*). Although these results demonstrate that *bmp1–4* genes are necessary for the production of **1**, the molecular detail underlying the offloading of the L-proline–derived pyrrole moiety from the ACP, its timing relative to the bromination events, and the chemical logic for the loss of L-proline derived alpha-carboxyl was not discernible at this stage. Therefore, we next examined the biosynthetic pathway by total in vitro enzymatic reconstitution of the production of **1** using purified enzyme catalysts.

Decarboxylative Bromination of Thiotemplated Pyrrole. To examine the individual roles of Bmp1–4, we performed the total in vitro reconstitution of the biosynthesis of **1** (Fig. 3*A*). Due to the high sequence similarity of PS5_Bmp1–4 to Mm_Bmp1–4 (*SI Appendix*, Table S1), and production of **1** by both *P.* sp PS5 and *M. mediterranea* MMB-1 (11), we used recombinant Mm_Bmp1–4 proteins in our in vitro investigations. Bmp2 and Bmp4 were individually purified as N-His_6–tagged proteins whereas N-His_6–tagged apo-Bmp1 was purified in complex with untagged Bmp3 and converted to its pantetheine-loaded holo-form by the promiscuous *Bacillus subtilis* phosphopantetheinyl transferase Sfp (11, 13) (Fig. 3*A*). Incubation of L-proline and bromide with purified Bmp1–4 enzymes, along with flavin and nicotinamide cofactors (FAD and $NADP^+$) and cofactor regeneration enzymes (PtdH and SsuE), led to the formation of **1** as the major product (Fig. 3 and *SI Appendix*,

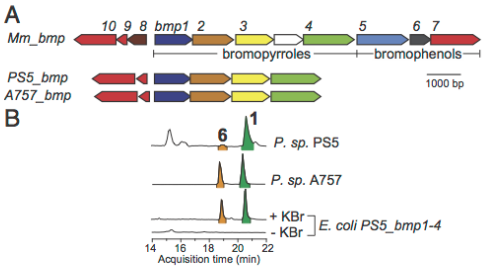

Fig. 2. A genetic basis for production of **1**. (*A*) *Mm_bmp*, *PS5_bmp*, and *A757_bmp* gene clusters with bromopyrrole and bromophenol biosynthetic genes indicated below the *Mm_bmp* gene cluster; a putative permease (uncolored) is inserted between *Mm_bmp3* and *Mm_bmp4*. Mm_Bmp1–4 are colored per their catalytic roles shown in Fig. 1. Note that *bmp1* encodes a di-domain protein with an ACP domain at the N terminus followed by a TE domain (11). (*B*) LC/MS extracted ion chromatograms (EICs) for $[M\text{-}H]^{1-}$ ions corresponding to **1** and **6** in organic extracts of *P.* sp. PS5, *P.* sp. A757, and *E. coli* expressing *PS5_bmp1–4* grown in media with (+) or without (–) bromide.

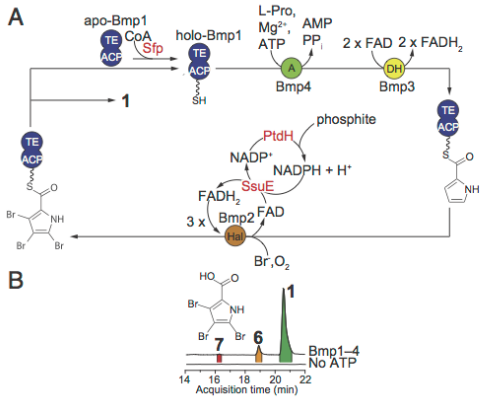

Fig. 3. Enzymatic synthesis of **1**. (*A*) Scheme for the total in vitro enzymatic synthesis of **1** starting from L-proline. Accessory enzymes not derived from the *Mm_bmp* gene cluster are indicated in red. $FADH_2$ required as a cofactor for Bmp2 was regenerated in situ by *E. coli* flavin reductase SsuE (32), which in turn oxidizes NADPH to $NADP^+$. $NADP^+$ was recycled to NADPH in situ using $NAD(P)^+$ reductase/phosphite dehydrogenase-PtdH (33). (*B*) EICs for $[M-H]^{1-}$ ions corresponding to **1**, **6**, and **7** for organic extracts of reactions described in *A*. Note that the production of **1**, **6**, and **7** was abolished in the absence of ATP.

Fig. S1). The production of **1** was abolished in the absence of ATP, which is required for the loading of L-proline onto the ACP domain of Bmp1 by Bmp4 (Fig. 3*B*). By comparison with authentic synthetic standards, we also confirmed the production of **6** and 3,4,5-tribromo-pyrrole-2-carboxylic acid (**7**) as minor products of the reaction (Fig. 3*B*).

Having established that Bmp1–4 enzymes are sufficient for the production of **1**, we next queried the timing and mechanism of the terminal bromination, offloading, and decarboxylation reactions. We previously established that Mm_Bmp2 converts pyrrolyl-*S*-Bmp1(ACP) to tribromopyrrolyl-*S*-Bmp1(ACP) (Fig. 3*A*), where the Bmp1(ACP) domain comprises residues 1–77 of Bmp1 (11). Therefore, we rationalized that 3,4,5-tribromopyrrolyl-*S*-Bmp1(ACP) (**8**, Fig. 4*A*) might be an intermediate en route to **1**. To test this hypothesis, we synthesized **8** following a recently described chemoenzymatic method (14). Briefly, synthetic **7**, generated by the bromination of pyrrole-2-carboxylic acid, was sequentially ligated to cysteamine and then to pantothenic acid to afford 3,4,5-tribromopyrrolyl-*S*-pantetheine **9** (Fig. 4*A* and *SI Appendix* for synthesis protocols and product characterization data). Compound **9** was then extended by the *E. coli* CoA biosynthetic enzymes CoaA, CoaD, and CoaE to generate 3,4,5-tribromopyrrolyl-*S*-CoA, which was used as the substrate for the in situ transfer of the 3,4,5-tribromopyrrolyl-*S*-phosphopantetheine moiety to the serine side chain hydroxyl of apo-Bmp1(ACP) by Sfp to yield **8** (Fig. 4*A* and *SI Appendix*, Fig. S2). We then expressed and purified the Bmp1 thioesterase domain, Bmp1 (TE), whose activity we previously confirmed using a model esterase substrate, *p*-nitrophenylacetate (11). Incubation of **8** with Bmp2, Bmp1(TE), bromide, $NADP^+$, FAD, and cofactor regeneration components led to formation of **1** as the major product, together with minor production of **6** and **7** (Fig. 4*B* and *SI Appendix*, Fig. S1). Exclusion of Bmp1(TE) from the reaction led to trace production of **1** (Fig. 4*B*). Additionally, we mapped the active site serine residue of Bmp1(TE) to Ser202 and confirmed that its mutation to alanine resulted in loss of esterase activity for the *p*-nitrophenylacetate substrate (*SI Appendix*, Fig. S3). Substitution of Bmp1(TE) with catalytically inactive Bmp1(TE)S202A mutant enzyme led to significantly reduced production of **1** (Fig. 4*B* and *SI Appendix*, Fig. S4). Finally, exclusion of Bmp2 from the reaction completely abolished the production of **1** (Fig. 4*B* and *SI Appendix*, Fig. S4). Similar levels of **7** were observed across all reactions, suggesting that it is likely an "off-pathway" product resulting from the hydrolysis of **8** (Fig. 4*B*). In support of **7** as a hydrolytic shunt product, no conversion of **7** to **1** or **6**, or to any new products, was observed upon its incubation with Bmp2, Bmp1 (TE), and bromide (*SI Appendix*, Fig. S5). These results provide two important findings. First, both catalysts, Bmp1(TE) and the halogenase Bmp2, are required to convert the intermediate **8** to **1**. Second, two enzymatic activities [that is, hydrolysis via thioesterase Bmp1(TE) and bromination via Bmp2] lead to three chemical events: (*i*) offloading of the pyrrole from Bmp1(ACP), (*ii*) the fourth bromination on the 2′-position of the pyrrole, and (*iii*) decarboxylative loss of the L-proline–derived alpha-carboxylate carbon atom.

We next evaluated the timing of formation of **6** relative to the formation of **1**. We thus incubated **6** with Bmp2, with and without Bmp1(TE), and cofactor-regenerating enzymes. We observed trace conversion of **6** to **1** only after prolonged reaction times, consistent with our hypothesis that **6** is a nonphysiological substrate for Bmp2 (*SI Appendix*, Fig. S5). Therefore, we propose that **6** might be a nonenzymatic reductive degradation byproduct of **1**. Indeed, incubation of synthetically prepared **1** with NADPH led to the conversion to **6** at levels comparable with total in vitro

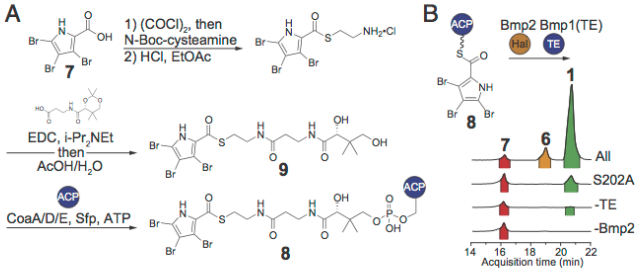

Fig. 4. Preparation of **8** and in vitro conversion to **1** by Bmp2 and Bmp1(TE). (*A*) Scheme showing generation of **8** by one-pot in vitro extension of synthetically prepared **9** using *E. coli* CoA biosynthetic enzymes, and loading onto holo-Bmp1(ACP) by Sfp. (*B*) Scheme for conversion of **8** to **1**, **6**, and **7** by Bmp2 and Bmp1(TE). Omitted for clarity are the cofactor regeneration systems for Bmp2, as shown in Fig. 3. Only trace, or no production, of **1** was observed when either Bmp2 or Bmp1 (TE) was omitted from the in vitro enzymatic reaction, or when the catalytically inactive Bmp1(TE)S202A enzyme was used.

reconstitution reactions (*SI Appendix*, Fig. S6). Together with our previous results, we propose that **7** and **6** are both off-pathway products arising, respectively, at stages preceding and after formation of **1** (Fig. 5).

In sum, our data support the Bmp2-catalyzed bromination of **8** leading to transient intermediate **i** as shown in Fig. 5, which would undergo transesterification to generate a Bmp1(TE) S202 side chain-bound oxoester **ii**, thus offloading the pyrrole from Bmp1(ACP). Hydrolytic offloading from Bmp1(TE) would generate the labile alpha-bromo acid **iii**. Driven by the rearomatization of the pyrrole ring, **iii** would spontaneously decarboxylate to **1**. Direct mass spectrometric evidence for **i** proved elusive, suggesting that **i** rapidly converts back to **8** via spontaneous debromination in the absence of Bmp1(TE). Therefore, the role of the Bmp1(TE) could be to trap the tetrabrominated pyrrole species by means of an irreversible transesterification step whereas the fourth bromination by Bmp2 activates the substrate for decarboxylation subsequent to hydrolytic offloading from Bmp1(TE).

Nonenzymatic hydrolysis of **i** may also lead to release of **iii** to afford **1**, consistent with our observation of low levels of **1** from reactions excluding Bmp1(TE) and with inactive Bmp1(TE)S202A. The observation of similar levels of **7** in all reactions further supports direct hydrolytic bypass of TE-mediated offloading. Furthermore, the fourth bromination of **8** by Bmp2, followed by transesterification and decarboxylation of **i**, neatly differentiates the biosynthesis of **1** from nonribosomal peptide synthetase- and polyketide synthase-derived pathways involving halopyrrole units in which the L-proline–derived alpha-carboxylate carbon atom is preserved in the mature natural product (Fig. 1).

Structural Basis for Unique Tetrahalogenating Activity of Bmp2. To realize the scheme shown in Fig. 5, the flavin-dependent brominase Bmp2 would need to halogenate all four positions of the pyrrole ring. This mechanistic requirement for the production of **1** is in stark contrast to all previously characterized pyrrole halogenases that halogenate the pyrrole ring only once or twice. To understand the structural basis for the tetrahalogenating activity of Bmp2, we determined the high-resolution crystal structure of FAD-bound holo-Bmp2 at a limiting resolution of 1.87 Å (Fig. 6*A*) and compared it with the FAD-bound holo-structure of dihalogenase Mpy16 participating in the biosynthesis of **3** that we determined at 1.95 Å resolution (Fig. 6*B* and *SI Appendix*, Table S2) (8). Bmp2 and Myp16 structures are highly homologous with all secondary structural elements in the vicinity of the active site strictly conserved between the two enzymes (*SI Appendix*, Fig. S7). Furthermore, the FAD cofactor isoalloxazine rings and the postulated active site lysine residues (15) (K74 for Bmp2, K72 for Mpy16) (Fig. 6 *A* and *B*) are superimposable. Although we could not determine a substrate pyrrolyl-*S*-ACP cocrystal structure for either Bmp2 or Mpy16, the position of the pyrrole binding sites for Bmp2 and Myp16 was inferred by a structural alignment of Bmp2 and Mpy16 with the crystal structures of substrate-bound forms of the flavin-dependent tryptophan-7-chlorinases PrnA (16) and RebH (17). Fittingly, the postulated pyrrole-binding site in Bmp2 and Mpy16 (Fig. 6 *A* and *B*) is in close proximity to the side chain of the catalytic lysine residue. An examination of the amino acids lining this putative pyrrole binding site in Bmp2 reveals a lack of conservation of three key sites (Y302, F306, and A345) that are otherwise strictly conserved among all pyrrolyl-*S*-ACP halogenases that selectively catalyze one [HrmQ (10)] or two [PltA (7), Mpy16 (8), Clz5 (9), and Pyr29 (18)] halogenations on the pyrrole ring (Fig. 6*D*). We thus mutated these three residues in Bmp2 to the corresponding residues in Mpy16 (Fig. 6*B*) to generate Bmp2-Y302S/F306V/A345W triple mutant enzyme (henceforth referred to as Bmp2-TM). We next investigated the effect of the triple mutation on the in vivo heterologous production of **1** in *E. coli*. Coexpression of *Mm_bmp1*, *Mm_bmp3*, and *Mm_bmp4*, with *Mm_bmp2-TM* in *E. coli*, led to a complete loss in the in vivo production of **1** in contrast to robust production with wild-type (WT) *Mm_bmp2* (*SI Appendix*, Fig. S9).

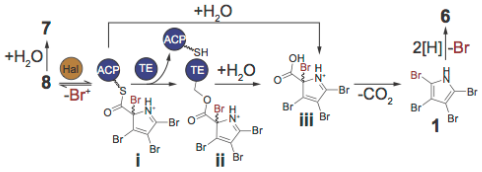

Fig. 5. Scheme for bromination-dependent pyrrole offloading and decarboxylation. Proposed reaction mechanisms for terminal bromination, offloading, and decarboxylation reactions with **8**; inferred intermediates are indicated by bold Roman numerals.

To explore the molecular basis for the in vivo loss in production of **1** by the Bmp2-TM enzyme, we compared the in vitro enzymatic activities of Bmp2, Mpy16, and Bmp2-TM enzymes. We chemoenzymatically synthesized pyrrolyl-*S*-Bmp1(ACP) and pyrrolyl-*S*-Mpy15, the requisite substrates for Bmp2 and Mpy16, respectively (8, 11, 14). Using a previously reported mass spectrometry-based proteomic assay that relies on detection of acyl-(cyclo)pantetheine MS2 product ions (14), we verified that WT Bmp2 enzyme catalyzed three brominations on the pyrrole ring (Fig. 6*E*) and that Mpy16 catalyzed no more than two chlorinations on the pyrrole ring acylated to Mpy15 (Fig. 6*F*) (14). Note that, although Bmp2 tetrabrominates the pyrrole ring as established by our previous findings, the assay used here detects only up to tribromination of pyrrolyl-*S*-Bmp1(ACP). In contrast to the WT Bmp2, Bmp2-TM could catalyze only a single bromination on the pyrrole ring (Fig. 6*G* and *SI Appendix*, Fig. S8), thereby precluding the synthesis of **1**.

Lastly, to eliminate the possibility that the reduced degree of halogenation catalyzed by Bmp2-TM was due to disruption of the enzyme active site by the three mutations, we determined the crystal structure of holo-Bmp2-TM at a resolution of 1.98 Å (Fig. 6*C*). Structural comparison of Bmp2-TM to Bmp2 and Mpy16 confirmed that the mutation of the three Bmp2 active site residues did not alter the positioning of the FAD isoalloxazine ring or the catalytic lysine side chain.

Discussion

In addition to characterizing the biosynthesis of a microbially produced coral settlement cue, our study reveals previously unidentified enzymology stemming from a biosynthetic motif ubiquitous among halopyrrole-containing natural products. Although our previous work had established tribromination of pyrrolyl-*S*-Bmp1(ACP) by Bmp2, the enzymatic activities responsible for the addition of the fourth bromine atom in **1** and offloading and decarboxylation of the pyrrolyl moiety from the ACP were unknown (11). Our current work demonstrates that a single halogenase, Bmp2, catalyzes the unprecedented tetrabromination of the ACP-bound pyrrole, which subsequently undergoes Bmp1(TE)-mediated offloading from the ACP and spontaneous decarboxylation. In light of the elucidation of the molecular and genetic details for the construction of **1**, we posit that **1** is an intermediate en route to the production of **5**, reconciling a previous report implicating an L-proline–derived symmetrical pyrrolic intermediate in the biosynthetic scheme for the production of **5** (19). Previously, based on primary sequence homology, we postulated that the enzyme Bmp8 (Fig. 2*A*) participates in the decarboxylation of **7** to produce **6** (11), a hypothetical route that is likely not operative in light of the biochemical data presented above. Therefore, the physiological transformations for the production of **6** en route to **5** remain to be elucidated. Furthermore, the previously reported production of **1** during the CYP450-Bmp7–mediated biradical homodimerization of **6** is likely an off-pathway route, with Bmp1–4 being the primary players in the production of **1**. Successive

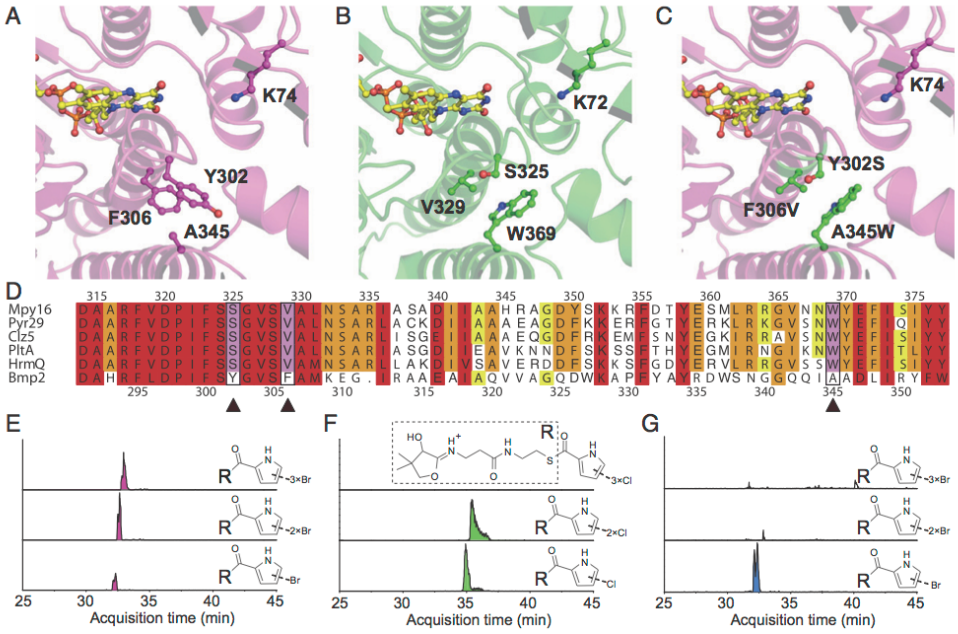

Fig. 6. Structural basis for tetrahalogenation activity of Bmp2. Comparison of the active sites of (*A*) holo-Bmp2, (*B*) holo-Mpy16, and (*C*) holo-Bmp2-TM. Note that side chains of Bmp2-TM residues S302, V306, and W345 in *C* structurally map to the corresponding side chains of Mpy16 residues S325, V329, and W369 shown in *B*. (*D*) Primary sequence alignments of tetrahalogenase Bmp2 with mono- and dihalogenating pyrrolyl-*S*-ACP halogenases demonstrate that the amino acids that were mutated on the basis of structural comparison with form Bmp2-TM (indicated by ▲) are conserved in all pyrrolyl-*S*-ACP halogenases but Bmp2 (see *SI Appendix*, Fig. S20 for alignment of Bmp2 homologs from different bacterial species). EICs for acyl-(cyclo)pantetheine MS2 product ions demonstrate that (*E*) WT Bmp2 generates mono-, di- and tribromopyrrolyl-*S*-Bmp1(ACP) products whereas (*F*) Mpy16 generates only mono- and dichloropyrrolyl-*S*-Mpy15, and (*G*) Bmp2-TM generates only monobromopyrrolyl-*S*-Bmp1(ACP) product.

biochemical studies promise to address these open questions to characterize all steps in the biosynthesis of **5** and assign physiological roles for each of the Bmp enzymes.

The complete in vitro reconstitution of the production of **1** using purified enzyme catalysts suggests a mechanism for the acyl-phosphopantetheine thioester to be sequestered and thereby inaccessible to Bmp1(TE) until the terminal fourth bromination. Sequestration of a pyrrole tethered to a type II peptidyl carrier protein (PCP) was recently demonstrated for a highly homologous PCP-PltL [57% amino acid similarity to Mm_Bmp1(ACP)] participating in the biosynthesis of the dichloropyrrole-containing natural product pyoluteorin (7, 20). By analogy, in the biosynthesis of **1**, it is possible that the terminal halogenation on the pyrrole partially liberates the sequestered substrate from the ACP, allowing access to the thioesterase. Therefore, the terminal fourth bromination by Bmp2 serves the dual role of triggering the release of the sequestered pyrrole moiety by presumably making the thioester susceptible to hydrolysis, in addition to activating the substrate for elimination of the L-proline–derived alpha-carboxyl. Activating halogenation reactions in natural product biosynthetic pathways has been demonstrated in the biosynthesis of NRPS-PKS hybrid curacin A, in which a cryptic halogenation catalyzed by α-ketoglutarate–dependent halogenase-CurA promotes cyclopropane ring formation (21), and in the biosynthesis of meroterpenoid merochlorins A and B, in which a dearomatization/terpene cyclization reaction cascade is initiated by a chlorination catalyzed by vanadium-dependent haloperoxidase-Mcl24 (22). Most analogously, paralleling the decarboxylative bromination strategy used by Bmp2, flavin-dependent brominase-Bmp5 catalyzes a bromination reaction that drives decarboxylation in the conversion of free *p*-hydroxybenzoic acid to 2,4-dibromophenol, the bromophenol building block of **5** (11).

The tetrabromination activity of Bmp2 is unprecedented among the flavin-dependent halogenases described to date that selectively add a specific number of halogen atoms to an aromatic substrate. In this study, we embraced the opportunity to interrogate the structural basis for this halogenation control in flavin-dependent pyrrolyl-*S*-ACP halogenases. Although the previously reported 2.1-Å crystal structure of putative tyrosyl-*S*-ACP flavin-dependent halogenase CndH highlighted the general differences in the architectures of flavin-dependent halogenases acting on free versus ACP-bound substrates (23), our study sheds mechanistic insight into the tuning of the enzyme active site in the context of confirmed biochemistry. Comparison of the putative substrate-binding cavities of the highly conserved structures of Bmp2 and Mpy16 resulted in a catalyst, Bmp2-TM, exhibiting an altered halogenation profile. Notably, the active site of Bmp2-TM exhibited no perturbation of the bound FAD cofactor with respect to WT Bmp2, nor did it lead to any apparent change in halogen binding properties of the enzyme, as demonstrated by conservation of its specificity for bromide. Already, for flavin-dependent tryptophan halogenases, it has been demonstrated that amino acid side chains that constitute the substrate binding site control the regiochemical outcomes for halogen additions (17, 24, 25). Our findings extend

this observation to flavin-dependent halogenases that catalyze halogenation of aromatic substrates acylated to ACPs in demonstrating that side chains of residues lining the putative halogenase active site play a role in controlling substrate access, and potentially in specifying the positions on the pyrrole ring that are accessible to halogenation. Unfortunately, in the case of Mpy16, efforts to alter the putative substrate-binding cavity to resemble that of Bmp2 resulted in insolubility of the mutant Mpy16 enzymes. Nonetheless, our results demonstrate that the active sites of otherwise highly homologous flavin-dependent halogenases are uniquely evolved to afford distinct product profiles. Biological activities of natural products are influenced by the number of halogens decorating their organic scaffolds (26, 27), and it would seem that Nature has taken note through the evolution of highly specialized halogenation catalysts.

In light of the existing literature and the findings of this study, several open questions remain regarding enzymatic halogenation (28). Of note is the question of the binding mode of both the ACP and the aromatic substrate by flavin-dependent halogenases that require acyl-*S*-ACP substrates. In addition, the primary question across all classes of halogenating enzymes is the structural determinant for halide specificity among these catalysts. Although Bmp2 and Mpy16 demonstrate different halide specificities, the amino acid side chains and the positioning of the FAD isoalloxazine ring relative to these side chains are remarkably conserved. Furthermore, the conservation of halide specificity in Bmp2-TM with respect to the WT enzyme raises the possibility that halide specificity in flavin-dependent halogenases is dictated not only by steric factors, such as halide ion radii, but also by the magnitude of the enthalpic penalty associated with desolvation of the halide ion in the halogenase active site before $2e^-$ oxidation to generate the electrophilic halonium. Furthermore, the contribution of the redox potential of the flavin isoalloxazine ring necessary to oxidize the halide, and the stability of the activated lysine-amine intermediate generated en route to the transfer of the halonium to the aromatic substrate should be considered (15). As such, the currently proposed halide binding site for flavin-dependent halogenases is itself debatable (29), thus underscoring the challenges associated with teasing apart the role of the enzymatic halogenase catalyst in each of the requisite mechanistic steps. Discovery and characterization of additional flavin-dependent halogenases promises to provide opportunities to answer these mechanistic questions, ultimately leading to engineerable toolkits to tailor the biosynthesis of halogenated natural products (30).

Materials and Methods

Detailed materials and methods are provided in *SI Appendix, Materials and Methods*.

Database Deposition Information. The sequences for *P.* sp. PS5- and *P.* sp. A757-derived bmp gene clusters have been deposited in GenBank under accession numbers KR011923 and KT808878, respectively. Structures for Mpy16, Bmp2, and Bmp2-TM are deposited in the Protein Data Bank (www.rcsb.org) under accession numbers 5BUK, 5BVA, and 5BUL, respectively.

Note. During the review and publication of this manuscript, the crystal structure of the flavin-dependent halogenase PltA was reported in the literature (31).

ACKNOWLEDGMENTS. We thank our colleague B. M. Duggan at University of California, San Diego for assistance in acquiring NMR data. This work was jointly supported by US National Science Foundation Grant OCE-1313747 (to B.S.M.) and US National Institutes of Health (NIH) Grants P01-ES021921 and R01-AI47818 (to B.S.M.) and R21-AI119311 (to K.E.W. and T.J.M.), the Mote Protect Our Reef Grant Program (POR-2012-3), the Dart Foundation, the Smithsonian Competitive Grants Program for Science (V.J.P.), the Howard Hughes Medical Institute (J.P.N.), NIH Marine Biotechnology Training Grant Predoctoral Fellowship T32-GM067550 (to A.E.), a Helen Hay Whitney Foundation Postdoctoral Fellowship (to V.A.), and a Swiss National Science Foundation Postdoctoral Fellowship (to S.D.).

1. Holmström C, Kjelleberg S (1999) Marine *Pseudoalteromonas* species are associated with higher organisms and produce biologically active extracellular agents. *FEMS Microbiol Ecol* 30(4):285–293.
2. Tebben J, et al. (2011) Induction of larval metamorphosis of the coral *Acropora millepora* by tetrabromopyrrole isolated from a *Pseudoalteromonas* bacterium. *PLoS One* 6(4):e19082.
3. Sneed JM, Sharp KH, Ritchie KB, Paul VJ (2014) The chemical cue tetrabromopyrrole from a biofilm bacterium induces settlement of multiple Caribbean corals. *Proc Biol Sci* 281(1786):20133086.
4. Neu AK, Månsson M, Gram L, Prol-García MJ (2014) Toxicity of bioactive and probiotic marine bacteria and their secondary metabolites in *Artemia* sp. and *Caenorhabditis elegans* as eukaryotic model organisms. *Appl Environ Microbiol* 80(1):146–153.
5. Gribble GW (2010) *Naturally Occurring Organohalogen Compounds: A Comprehensive Update* (Springer, Vienna).
6. Walsh CT, Garneau-Tsodikova S, Howard-Jones AR (2006) Biological formation of pyrroles: Nature's logic and enzymatic machinery. *Nat Prod Rep* 23(4):517–531.
7. Dorrestein PC, Yeh E, Garneau-Tsodikova S, Kelleher NL, Walsh CT (2005) Dichlorination of a pyrrolyl-*S*-carrier protein by $FADH_2$-dependent halogenase PltA during pyoluteorin biosynthesis. *Proc Natl Acad Sci USA* 102(39):13843–13848.
8. Yamanaka K, Ryan KS, Gulder TA, Hughes CC, Moore BS (2012) Flavoenzyme-catalyzed atropo-selective N,C-bipyrrole homocoupling in marinopyrrole biosynthesis. *J Am Chem Soc* 134(30):12434–12437.
9. Mantovani SM, Moore BS (2013) Flavin-linked oxidase catalyzes pyrrolizine formation of dichloropyrrole-containing polyketide extender unit in chlorizidine A. *J Am Chem Soc* 135(48):18032–18035.
10. Höfer I, et al. (2011) Insights into the biosynthesis of hormaomycin, an exceptionally complex bacterial signaling metabolite. *Chem Biol* 18(3):381–391.
11. Agarwal V, et al. (2014) Biosynthesis of polybrominated aromatic organic compounds by marine bacteria. *Nat Chem Biol* 10(8):640–647.
12. Whalen KE, Poulson-Ellestad KL, Deering RW, Rowley DC, Mincer TJ (2015) Enhancement of antibiotic activity against multidrug-resistant bacteria by the efflux pump inhibitor 3,4-dibromopyrrole-2,5-dione isolated from a *Pseudoalteromonas* sp. *J Nat Prod* 78(3):402–412.
13. Quadri LE, et al. (1998) Characterization of Sfp, a *Bacillus subtilis* phosphopantetheinyl transferase for peptidyl carrier protein domains in peptide synthetases. *Biochemistry* 37(6):1585–1595.
14. Agarwal V, et al. (2015) Chemoenzymatic synthesis of acyl coenzyme A substrates enables *in situ* labeling of small molecules and proteins. *Org Lett* 17(18):4452–4455.
15. Yeh E, Blasiak LC, Koglin A, Drennan CL, Walsh CT (2007) Chlorination by a long-lived intermediate in the mechanism of flavin-dependent halogenases. *Biochemistry* 46(5):1284–1292.
16. Dong C, et al. (2005) Tryptophan 7-halogenase (PrnA) structure suggests a mechanism for regioselective chlorination. *Science* 309(5744):2216–2219.
17. Zhu X, et al. (2009) Structural insights into regioselectivity in the enzymatic chlorination of tryptophan. *J Mol Biol* 391(1):74–85.
18. Zhang X, Parry RJ (2007) Cloning and characterization of the pyrrolomycin biosynthetic gene clusters from *Actinosporangium vitaminophilum* ATCC 31673 and *Streptomyces* sp. strain UC 11065. *Antimicrob Agents Chemother* 51(3):946–957.
19. Peschke JD, Hanefeld U, Laatsch H (2005) Biosynthesis of the marine antibiotic pentabromopseudilin. 2. The pyrrole ring. *Biosci Biotechnol Biochem* 69(3):628–630.
20. Jaremko MJ, Lee DJ, Opella SJ, Burkart MD (2015) Structure and substrate sequestration in the pyoluteorin type II peptidyl carrier protein PltL. *J Am Chem Soc* 137(36):11546–11549.
21. Gu L, et al. (2009) Metamorphic enzyme assembly in polyketide diversification. *Nature* 459(7247):731–735.
22. Diethelm S, Teufel R, Kaysser L, Moore BS (2014) A multitasking vanadium-dependent chloroperoxidase as an inspiration for the chemical synthesis of the merochlorins. *Angew Chem Int Ed Engl* 53(41):11023–11026.
23. Buedenbender S, Rachid S, Müller R, Schulz GE (2009) Structure and action of the myxobacterial chondrochloren halogenase CndH: A new variant of FAD-dependent halogenases. *J Mol Biol* 385(2):520–530.
24. Lang A, et al. (2011) Changing the regioselectivity of the tryptophan 7-halogenase PrnA by site-directed mutagenesis. *Angew Chem Int Ed Engl* 50(13):2951–2953.
25. Shepherd SA, et al. (2015) Extending the biocatalytic scope of regiocomplementary flavin-dependent halogenase enzymes. *Chem Sci (Camb)* 6(6):3454–3460.
26. Eustáquio AS, et al. (2003) Clorobiocin biosynthesis in *Streptomyces*: Identification of the halogenase and generation of structural analogs. *Chem Biol* 10(3):279–288.
27. Harris CM, Kannan R, Kopecka H, Harris TM (1985) The role of the chlorine substituents in the antibiotic vancomycin: Preparation and characterization of monodechlorovancomycin and didechlorovancomycin. *J Am Chem Soc* 107(23):6652–6658.
28. Neumann CS, Fujimori DG, Walsh CT (2008) Halogenation strategies in natural product biosynthesis. *Chem Biol* 15(2):99–109.
29. Blasiak LC, Drennan CL (2009) Structural perspective on enzymatic halogenation. *Acc Chem Res* 42(1):147–155.
30. Teufel R, Agarwal V, Moore BS (2016) Unusual flavoenzyme catalysis in marine bacteria. *Curr Opin Chem Biol* 31:31–39.
31. Pang AH, Garneau-Tsodikova S, Tsodikov OV (2015) Crystal structure of halogenase PltA from the pyoluteorin biosynthetic pathway. *J Struct Biol* 192(3):349–357.
32. Eichhorn E, van der Ploeg JR, Leisinger T (1999) Characterization of a two-component alkanesulfonate monooxygenase from *Escherichia coli*. *J Biol Chem* 274(38):26639–26646.
33. Costas AMG, White AK, Metcalf WW (2001) Purification and characterization of a novel phosphorus-oxidizing enzyme from *Pseudomonas stutzeri* WM88. *J Biol Chem* 276(20):17429–17436.

Supplementary information for

Biosynthesis of coral settlement cue tetrabromopyrrole in marine bacteria by a uniquely adapted brominase-thioesterase enzyme pair

Abrahim El Gamal, Vinayak Agarwal, Stefan Diethelm, Imran Rahman, Michelle Schorn, Jennifer M. Sneed, Gordon V. Louie, Kristen E. Whalen, Tracy J. Mincer, Joseph P. Noel, Valerie J. Paul, and Bradley S. Moore

This supplementary information section contains

Materials & Methods

Supplementary Figures S1–S20

Supplementary Tables S1 & S2

Supplementary References

MATERIALS AND METHODS

Genome sequencing

Genomic DNA was isolated from 5 mL overnight liquid cultures of *P.* sp. PS5 and *P.* sp. A757 inoculated in 5 mL Difco 2216 Marine Broth (BD 212185) from -80 ºC glycerol stocks and grown overnight at 30 ºC with shaking at 200 rpm. Genomic DNA was isolated using a DNeasy Blood & Tissue Kit (Qiagen) following the spin column protocol for extraction of genomic DNA from gram-negative bacteria. Next generation sequencing libraries were constructed from genomic DNA of *P.* sp. PS5 and *P.* sp. A757 using the Ion Plus Fragment Library Kit (Thermo Fisher Scientific). Sample preparation was done with the Ion PGM 400 OT2 Kit (Thermo Fisher Scientific). The library was sequenced on an Ion Torrent PGM platform (Thermo Fisher Scientific) using the Ion PGM Hi-Q Sequencing Kit on an Ion Torrent 318v2 sequencing chip (Thermo Fisher Scientific).

Genome assembly, annotation and verification of Bmp genes

De novo assemblies of raw reads of *P.* sp. PS5 and *P.* sp. A757 were performed using CLC Genomics Workbench (Qiagen) and SPAdes (1) assemblers, respectively, using default parameters for Ion Torrent PGM sequencing. Annotation of the draft genomes of *P.* sp. PS5 and *P.* sp. A757 was performed using the RAST server (2). The draft genome was queried with translated sequences of Mm_Bmp1–10 using BLAST in the SEED Viewer genome browser interface. *PS5_bmp* and *A757_bmp* gene sequences were verified by Sanger sequencing (SeqXcel, La Jolla, CA).

Cloning and heterologous expression of *PS5_bmp1–4*

PS5_bmp1–4 was PCR amplified from genomic DNA using PrimeStar Max DNA polymerase (Takara) standard protocol, and ligated into SacI/NotI (NEB) digested pETDuet (Novagen) using T4 DNA Ligase (NEB), followed by propagation in *E. coli* DH5α (NEB), Qiagen MiniPrep plasmid extraction, and Sanger sequencing verification (SeqXcel, La Jolla, CA). An open reading frame encoding an ACP synthase (AcpS) from *M. mediterranea* (3) (Genbank accession code: NC_015276.1) was amplified from genomic DNA and cloned into NdeI/XhoI digested pRSFDuet (Novagen) using the same protocol as before. Thus constructed pETduet-*PS5_bmp1–4* and pRSFduet-*acpS* were co-transformed into *E. coli* BL21-Gold(DE3) (Agilent) for expression. Five mL LB containing 50 µg/mL kanamycin and 100 µg/mL carbenicillin to maintain plasmids with and without 1 g/L KBr (final concentration) were each inoculated with 100 µL of overnight culture of *E. coli* BL21-Gold(DE3)/pETDuet-*PS5_bmp1–4*/pRSF-*acpS* grown at 30 ºC. The cultures were grown at 37ºC for 2 h with shaking, then transferred to 30 ºC and induced after 15 min with 50 µM IPTG (final concentration). Cultures were incubated for an additional 16 h at 30 ºC with shaking at 200 rpm. Cultures were subsequently extracted with two volumes of EtOAc. The organic layer was collected and solvent was removed *in vacuo*. The resulting residue was dissolved in 100 µL MeOH for LC/MS/MS analysis.

Analytical scale culturing and extraction of wildtype tetrabromopyrrole-producing bacterial strains

P. sp. PS5 and *P.* sp. A757 were cultured as previously described (4-5). Briefly, a Difco 2216 Marine Broth (BD 212185)/agar plates were inoculated from a -80 ºC glycerol stocks of *P.* sp. PS5 or *P.* sp. A757 and grown overnight at 30 ºC. Five mL Difco 2216 liquid broth were inoculated with a single colonies of *P.* sp. PS5 or *P.* sp. A757 and grown overnight at 30 ºC with shaking at 200 rpm. Fifteen mL Difco 2216 liquid broth supplemented with an additional 1 g/L KBr (final concentration) to increase production of brominated secondary metabolites (6) were inoculated with 100 µl of overnight cultures and incubated overnight at 30 ºC with shaking at 200 rpm. The cultures were subsequently extracted with two volumes of EtOAc. The organic layers were collected, and the solvent was removed *in vacuo.* The residues were dissolved in 100 µL MeOH each for LC/MS/MS analysis.

LC/MS/MS elution profile used for analysis of *in vivo* and *in vitro* extracts

Extracts were analyzed by LC/MS/MS using a reverse phase C_{18} column (Phenomenex Luna, 5 µm, 4.6 × 100 mm) operating on an Agilent 1260 HPLC in tandem to an Agilent 6530 Accurate Mass Q-TOF mass

spectrometer. Mass spectra were acquired in negative ionization mode. Data was acquired for blank runs between samples to prevent and exclude carry-over of bromopyrroles from one sample to the next. HPLC solvents used were water + 0.1 % formic acid (A) and MeCN + 0.1 % formic acid (B). The HPLC elution profile was as follows: (initial flow rate 0.5 mL/min) 10% B for 5 min, linear gradient to 70% B over 10 min, linear increase to 80% B over 10 min, (flow rate changed to 0.7 mL/min) linear increase to 100% B over 0.5 min, hold at 100% B for 3 min, linear decrease to 10% B over 0.5 min. Identical injection volumes were used within a given experiment.

Data analysis and plotting

LC/MS/MS data was analyzed using the Agilent MassHunter software package. Data was plotted using Microsoft Excel and OriginPro (OriginLab). Extracted ion chromatograms were called using the $[M-H]^{1-} \pm m/z$ 0.5 for the most abundant isotope as follows: **1** (*m/z* 381.67), **6** (*m/z* 301.76), and **7** (*m/z* 345.75). Chromatograms corresponding to sets of experiments (i.e., within a given figure panel) are normalized to the largest peak among spectra, while individual chromatograms are normalized to the largest peak within that chromatogram.

Cloning, protein expression and purification for *in vitro* assays

Cloning and expression of Mm_Bmp1-Bmp3 complex, Mm_Bmp2, Mm_Bmp4, Mm_Bmp1(ACP), and Mm_Bmp1(TE) were performed in a manner identical to previously reported (3). *B. subtilis* Sfp and *P. stutzeri* PtdH were also purified in an identical to that previously described (3). Expression of *E. coli* SsuE was performed according to a published protocol (7).

Mm_Bmp1(TE):S202A is new to this study, and was purified in an identical manner to that reported for wildtype recombinant proteins (3). Point mutagenesis of *Mm_bmp1(TE)* to generate the Ser202 to Ala mutant was performed by PCR mutagenesis using PrimeStar Max DNA Polymerase (Takara) standard protocol with pET28-N-His_6-*Mm_bmp1(TE)* as the template. Primers were designed with the motif 5′-[20 nucleotide sequence-modified overlap] [35 nucleotide primer region]-3′ followed by treatment with DpnI exonuclease, propagations in *E. coli* DH5α (NEB), Sanger sequencing verification (SeqXcel, La Jolla, CA), and transformation into *E. coli* Bl21-Gold(DE3) (Agilent) for expression.

Total *in vitro* enzymatic synthesis of 1 from L-proline

One mL reactions consisting 2 mM L-proline, 0.5 mM CoA, 2 mM $MgCl_2$, 50 mM KBr, 2 mM $NADP^+$, 0.1 mM FAD, 10 mM phosphite, 10 μM Mm_Bmp1-Bmp3 complex, 25 μM Mm_Bmp2, 1 μM Mm_Bmp4, 2 μM Sfp, SsuE, and PtdH were incubated for 12 h at 30 ºC with and without ATP in buffer consisting of 20 mM Tris-HCl (pH 8), 50 mM KCl, 10 % (v/v) glycerol. Reactions were extracted with 1.6 mL EtOAc. The organic layer was collected and solvent was removed *in vacuo*. The resulting residue was dissolved in 100 μL MeOH, and 30 μL were injected for LC/MS/MS analysis in the same manner as described for analysis of *in vivo* extracts.

Chemical synthesis

Chemicals and solvents. All chemicals were purchased from Acros, Aldrich, Fluka, or Alfa Aesar and used as such unless stated otherwise. For flash chromatography technical grade solvents were used without further purification. For reactions analytical grade solvents were purchased and used without further purification. Deuterated solvents were obtained from Sigma-Aldrich.

Reactions. All non-aqueous reactions were carried out using oven-dried glassware under an atmosphere of nitrogen unless otherwise stated. Reactions were magnetically stirred and monitored by TLC unless otherwise stated. Chromatographic purification was performed as flash chromatography (Alfa Aesar silica gel, 60 Å pore size) using the solvents indicated as eluent with 0.3-0.5 bar pressure. Thin layer chromatography (TLC) was performed on Merck silica gel 60 F_{254} TLC glass plates and visualized with UV light or stained in ceric ammonium molybdate or potassium permanganate solutions. The yields given refer to chromatographically purified and spectroscopically pure compounds unless otherwise stated.

Analysis. ^{1}H- and ^{13}C- NMR spectra were recorded on VARIAN Inova (500 MHz) or BRUKER Avance (600 MHz) spectrometers in the solvents indicated. All signals are reported in ppm with the internal chloroform signal at 7.26 ppm or 77.0 ppm, or the internal DMSO signal at 2.50 ppm or 39.52 ppm as standard. The data is being reported as (s=singlet, d=doublet, t=triplet, q=quadruplet, m=multiplet or unresolved, br=broad signal, coupling constant(s) in Hz, integration). HiRes-MS was carried out on an Agilent 1100 Series Instrument with diode-array and MS detectors on a Phenomenex Luna C_{18} 5µ 100 x 4.6 mm column.

Chemical syntheses of 1, 6, and 7

Synthetic standards of **1**, **6**, and **7** were prepared according to reported protocols. **1** was prepared according to literature procedures by halogenation of pyrrole using NBS (8). 2,3,4-tribromo-1H-pyrrole **6** was prepared according to a modified literature procedure (9). For the TIPS protection of pyrrole, sodium hydride was employed as a base instead of *n*-BuLi. **7** was prepared according to a slightly modified literature procedure (10): To a suspension of pyrrole-2-carboxylic acid (1g, 9 mmol) in $CHCl_3$ (10 mL) and AcOH (2 mL) was slowly added bromine (1.6 mL, 31.5 mmol). The reaction was warmed to 50 °C and stirred for 4 h. The mixture was diluted with $CHCl_3$ and water. The phases were separated and the organic phase was washed with water. The carboxylic acid was then extracted from the organic phase using 10% K_2CO_3. The basic solution was first washed twice with $CHCl_3$ and then acidified using 4M HCl. The resulting precipitate was collected by filtration and dried under vacuum to give **7**. **1**: ^{1}H-NMR (500 MHz, $CDCl_3$, for full spectrum see **Fig. S10**): δ 8.52 (bs, 1H, N*H*); HRMS (ESI) *m/z* calculated for C_4NBr_4 ($[M-H]^{1-}$) 377.6770, found 377.6759. **6**: ^{1}H-NMR (600 MHz, $CDCl_3$, values in good agreement with literature (11)): δ 8.46 (bs, 1H, NH), 6.86 (d, J = 3.1 Hz, 1H); HRMS (ESI) *m/z* calculated for C_4NBr_3 ($[M-H]^-$) 299.7665, found 299.7663. **7**: (300 mg, 0.86 mmol, 10%). R_f 0.15 (hexanes/EtOAc 4:1); ^{1}H-NMR (500 MHz, d_6-DMSO, for full spectrum see **Fig. S11**): δ 12.97 (bs, 1H, COO*H*), 11.71 (bs, 1H, N*H*); ^{13}C-NMR (150 MHz, d_6-DMSO, for full spectrum see **Fig. S12**): δ 159.4, 122.6, 106.7, 104.3, 103.4; HRMS (ESI) *m/z* calculated for $C_5H_3NO_2Br_3$ ($[M+H]^-$) 345.7708, found 345.7674.

Chemical synthesis of 3,4,5-tribromopyrrolyl-*S*-pantetheine probe 9

A synthetic scheme for **9** along with NMR spectra for intermediates and 2D NMR datasets for **9** are provided in the supplementary section (**Figs. S13-S19**). A flask was charged with previously prepared **7** (300 g, 0.86 mmol, 1 equiv.) and CH_2Cl_2 (10 mL). Oxalyl chloride (0.15 mL, 1.7 mmol, 2 equiv.) was added slowly and the mixture was allowed to stir for 1 h. The solvent was removed and the residue was taken up in CH_2Cl_2 (10 mL). *N*-Boc-2-amino ethanethiol (228 mg, 1.3 mmol, 1.5 equiv.) followed by triethylamine (0.24 mL, 1.7 mmol, 2 equiv.) were added and the reaction was allowed to stir at ambient temperature overnight. After removal of the solvent, the residue was subjected to flash column chromatography (hexanes/EtOAc 9:1 → 4:1) to give the respective thioester (260 mg, 0.51 mmol, 59%). R_f 0.30 (hexanes/EtOAc 4:1); ^{1}H-NMR (500 MHz, $CDCl_3$, n.b.- Due to rotamers at the Boc carbamate, some peaks are split. NH peaks are not reported. A full ^{1}H spectrum is given in **Fig. S13**): δ 3.45-3.14 (m, 3H), 2.78 (t, J = 6.6 Hz, 1H), 1.54-1.39 (m, 9H); HRMS (ESI) *m/z* calculated for $C_{12}H_{15}N_2O_3SBr_3Na$ ($[M+Na]^+$) 526.8246, found 526.8210. To a solution of this thioester (260 mg, 0.51 mmol) in EtOAc (4 mL) at 0 °C was added freshly prepared HCl in EtOAc (4 mL, 3 M in EtOAc)[1]. The solution was allowed to warm to ambient temperature and stirred for 15 min before use. The mixture was stirred at 0 °C for 30 min whereupon a white precipitate had formed. The solvent was removed under vacuum to afford hydrochloride salt **S1** (quant.). A flask was charged with acetonide **S2** (11) previously prepared (12) (64 mg, 0.25 mmol, 1.1 equiv.) and EDC (66 mg, 0.35 mmol, 1.5 equiv.). A suspension of **S1** (100 mg, 0.23 mmol, 1 equiv.) in CH_2Cl_2 (2 mL) was added followed by diisopropylethylamine (80 µL, 0.46 mmol, 2 equiv.). The mixture was stirred at ambient temperature overnight. The solvent was evaporated and the residue was directly subjected to flash column chromatography (hexanes/EtOAc 1:1 → EtOAc) to afford to corresponding amide product (64 mg, 0.10 mmol, 43%). The acetonide (10 mg, 0.015 mmol) was dissolved in AcOH/H_2O (1 mL, 2:1), and the solution was stirred for 5 h. The mixture was poured into a separatory funnel containing sat. $NaHCO_3$ and EtOAc. The phases were separated and the aqueous phase was extracted three times with EtOAc.

[1] To a mixture of EtOAc (2.4 mL) and EtOH (0.72 mL) at 0 °C was slowly added AcCl (0.85 mL).

The combined organic phases were washed with brine and dried over $MgSO_4$. The solvent was removed and the residue was purified by flash column chromatographs (CH_2Cl_2/MeOH 20:1) to give diol **9:** (7.5 mg, 0.012 mmol, 80%) R_f 0.45 (CH_2Cl_2/MeOH 9:1); ^{1}H-NMR (500 MHz, d_6-DMSO): δ 8.16 (t, *J* = 5.7 Hz, 1H, NH), 7.70 (t, *J* = 5.9 Hz, 1H, NH), 5.36 (bs, 1H), 4.45 (bs, 1H), 3.69 (s, 1H), 3.36-3.20 (m, 4H), 3.16 (d, *J* = 10.4 Hz, 1H), 3.09 (t, *J* = 6.7 Hz, 1H), 2.31-2.22 (m, 2H), 0.79 (s, 3H), 0.77 (s, 3H); ^{13}C-NMR (150 MHz, d_6-DMSO): δ 178.9, 173.0, 170.8, 129.3, 109.9, 104.4, 104.0, 75.1, 68.2, 48.7, 39.1, 38.2, 35.2, 34.9, 21.0, 20.4; HRMS (ESI) *m/z* calculated for $C_{16}H_{22}N_3O_5SBr_3Na$ ($[M+Na]^+$) 627.8723, found 627.8719.

Preparation and purification of 3,4,5-tribromopyrrolyl-*S*-Bmp1(ACP) 8 and pyrrolyl-*S*-Mpy15

E. coli CoA biosynthetic enzymes pantothenate kinase CoaA, phosphopantetheine adenyl transferase CoaD, and dephospho-CoA kinase CoaE were expressed and purified as previously described (12). To generate **8**, 10 reactions of 500 µL each consisting of 2 µM CoaA, 2 µM CoaD, 2 µM CoaE, 2 µM Sfp, 250 µM Bmp1(ACP), 1 mM 3,4,5-tribromopyrrolyl-*S*-pantetheine **9**, 10 mM $MgCl_2$, and 9 mM ATP in 50 mM HEPES (pH 7.9) buffer were incubated at 30ºC for 12 h. As a negative control, ATP was substituted with an appropriate volume of buffer in a single 100 µL scale reaction. Reactions were pooled and purified by size exclusion chromatography on a Superdex 75 10/300 GL (GE Life Sciences) column eluted isocratically with 20 mM HEPES-Na (pH 7.5) 100 mM KCl. Glycerol was add to pooled fractions containing product to a final concentration of 10% (v/v) followed by concentration. An identical procedure was used for generation and purification of pyrrolyl-*S*-Mpy15 with Mpy15 switched for Bmp1(ACP) and **9** switch for pyrrolyl-*S*-pantetheine synthesized as previously reported (12).

LC-MS/MS confirmation of chemo-enzymatically prepared pyrrolyl-*S*-ACPs

Loading reactions were confirmed by LC/MS/MS as previously described (3). Reactions with and without ATP were injected onto a C_4 column (Vydac 5 µm, 4.6 mm × 250 mm) operating on an Agilent 1260 HPLC in tandem to an Agilent 6530 Accurate Mass Q-TOF mass spectrometer. Mass spectra were acquired in positive ionization mode. HPLC solvents used were water + 0.1% formic acid (A) and MeCN + 0.1% (B). The elution profile was as follows (flow rate: 0.7 mL/min): 10% B for 10 min, linear increase to 30% B over 5 min, linear increase to 70% B over 40 min, linear decrease to 10% B over 5 min, linear increase to 100% B over 1 min followed by 2 min at 100% B, decrease to 10% B over 1 min, 10% B for 2 min and 5 min of post-time equilibration. Loading was assessed by extraction of the predicted acyl-(cylco)pantetheine MS2 fragments corresponding to the pantetheine arm of the holo-ACP as previously described (3). The mass and charge of the parent peptide were determined from the corresponding deconvoluted peptidic MS1 spectra, and the mass difference was confirmed between apo-ACP from the no ATP negative control and holo-ACP from the reaction with ATP (**Fig. S3**).

***In vitro* enzymatic synthesis of 1 from 8**

1 mL reactions consisting of 25 µM **8**, 50 mM KBr, 0.1 mM FAD, 2 mM $NADP^+$, SsuE, PtdH, 10 mM phosphite, 50 µM Mm_Bmp2, and 25 µM Mm_Bmp1(TE) or Mm_Bmp1(TE):S202A for 12 h at 30 ºC in buffer consisting of 20 mM Tris-HCl (pH 8), 50 mM KCl, and 10% (w/v) glycerol. For reactions where enzymes were excluded (-Bmp2 and -TE) an equivalent volume of buffer was substituted. Reactions were extracted with 1.6 mL EtOAc. The organic layer was collected and solvent was removed *in vacuo* and the resulting residue was dissolved in 100 µL MeOH. Samples (30 µL injections) were analyzed by LC/MS/MS using the same conditions as described for *in vivo* and Mm_Bmp1-4 *in vitro* extracts. To ensure no carryover from one injection to the next, reactions were analyzed in the order '-Bmp2', '-TE', 'S202A', and 'All', with data gathered for blank injections preceding and following each reaction extract.

Cloning, expression, purification, crystallization, and structure determination for Mm_Bmp2 and Mm_Bmp2-TM

Cloning, expression, and purification. P. sp. PS-5 Bmp2 was cloned into the pET28b(+) (Novagen) plasmid vector utilizing the NdeI and XhoI restriction sites to afford a thrombin cleavable hexa-histidine tag at

the N-terminus of the recombinant protein. Selection pressure was maintained by inclusion of 50 µg/mL kanamycin (final concentration) in all solid and liquid growth media. The insert was verified by restriction analysis and Sanger sequencing (SeqXcel, La Jolla, CA), and transformed in to *E. coli* BL21-Gold(DE3) (Agilent) cells for protein expression. 1 L terrific broth culture was grown to an OD_{600} ~ 0.6 at 30 ºC and protein expression was induced by the addition of IPTG to a final concentration of 0.3 mM. The temperature was adjusted to 18 ºC, and the culture was allowed to incubate for an additional 18 h. Cultures were harvested by centrifugation, the supernatant discarded, and the pellet resuspended in 20 mM Tris-HCl (pH 8.0), 500 mM NaCl, 10% glycerol buffer, and lysed by sonication. The supernatant was clarified by centrifugation and loaded on to a 5 mL His-Trap Ni-NTA column (GE Biosciences) equilibrated in harvest buffer. The column was extensively washed with 20 mM Tris-HCl (pH 8.0), 1 M NaCl, 30 mM imidazole buffer, and eluted by a linear gradient to 20 mM Tris-HCl (pH 8.0), 1 M NaCl, 200 mM imidazole buffer across 20 column volumes. Purity of eluted proteins was checked by SDS-PAGE, and thrombin was added to a final concentration of 1 unit/mg recombinant protein. Thus purified protein was then dialyzed overnight against 20 mM Tris-HCl (pH 8.9), 50 mM KCl buffer at 4 °C. The dialyzed protein was applied to a 5 mL ion exchange Q Sepharose FF column (GE Biosciences) equilibrated in dialysis buffer, and eluted using a linear gradient to 20 mM Tris-HCl (pH 8.9), 1 M KCl buffer.

Activity assays. For activity assays, protein was concentrated after ion exchange using Amicon centrifugal filters to a final volume of 2.5 mL and buffer was exchanged using PD-10 size exclusion columns (GE Biosciences) to 20 mM Tris-HCl (pH 8.0), 10% glycerol buffer. The protein concentration was measured using the Bradford assay, and protein was stored at -80 °C in 100 µL aliquots.

Crystallization. For crystallization, 4 mL of ion exchange-purified protein was applied to a Sephadex-75 size exclusion chromatography column (GE Biosciences) equilibrated in 20 mM HEPES-Na (pH 7.5), 100 mM KCl buffer and eluted isocratically. Protein purity was verified by SDS-PAGE, and pure fractions were pooled and concentrated using Amicon centrifugal filters to a final concentration of 100 µM. Sparse-matrix screening for crystal growth was performed using commercially available crystallization screens in hanging-vapor drop format at 9 °C. Initial conditions were optimized at 9 °C in hanging-vapor drop format to yield the following reproducible crystal growth condition for wild type Bmp2: 100 mM HEPES-Na (pH 7.5), 200 mM NaCl, 25% (w/v) PEG3350. Crystals appeared within 2 days and reached their maximum size by 5 days. The crystals were harvested and briefly dipped in 100 mM HEPES-Na (pH 7.5), 200 mM NaCl, 25% (w/v) PEG3350, 20% (v/v) ethylene glycol cryo-protectant prior to vitrification in liquid nitrogen.

Structure determination. X-ray diffraction were scaled and indexed using the HKL-2000 package (13) and unit cell composition determined (14). Bmp2 structure was determined by molecular replacement using Phaser (15) by a sequence-alignment based Ala model (16) of the PDB: 3E1T (17). Initial solution was extended manually using Coot (18) and computationally using ARP/wARP (19) in an iterative manner. Refinement was carried out using Phenix (20). Although clear density for FAD could be observed prior to refinement, the cofactor was manually built into the model only after the free *R* factor (21) dropped below 30%.

Mm_Bmp2-TM. Mm_Bmp2-TM was generated by PCR site-directed mutagenesis using *bmp2-wt* pET28b(+) plasmid vector as template. Mutations were verified using Sanger sequencing (SeqXcel, La Jolla, CA), and recombinant Mm_Bmp2-TM protein was expressed and purified in a manner identical to that described above. Mm_Bmp2-TM was prone to aggregation, and care was taken to minimize the time between purification and crystallization trials. Mm_Bmp2-TM crystallized in conditions similar to Bmp2-wt, albeit with different space group and unit cell dimensions, with the final optimized mother liquor being 100 mM HEPES-Na (pH 7.5), 200 mM ammonium sulfate, 20% (w/v) PEG3350, 5% (v/v) ethylene glycol. Crystals were briefly dipped in 100 mM HEPES-Na (pH 7.5), 200 mM ammonium sulfate, 20% (w/v) PEG3350, 25% (v/v) ethylene glycol cryo-protectant prior to vitrification in liquid nitrogen. Structure of Mm_Bmp2-TM was determined using the structure of Bmp2-wt as a molecular replacement search model.

Cloning, expression, purification, crystallization, and structure determination for Mpy16

Cloning, expression, and purification. Mpy16 was amplified from the genomic DNA of *Streptomyces* CNQ-418 (22) and cloned into a modified pET28-MBP vector that we have described previously (23). This vector affords a N-terminal hexa-histidine tag, followed by a maltose binding protein (MBP), and a TEV

protease cleavage site downstream of the MBP protein, followed by the translated recombinant protein. Culture growth conditions, and protein purification protocols are identical to those described above (TEV was used in place of thrombin to remove the purification tag), with an additional subtractive Ni-NTA chromatography step before ion exchange employed to remove the hexa-histidine bearing MBP tag subsequent to TEV digestion.

Crystallization and structural determination. Initial crystallization conditions for Mpy16 were identified as before for Bmp2, and optimized to 100 mM Tris-HCl (pH 8.0), 10% (w/v) PEG8000, 5% (v/v) glycerol. The crystals were briefly dipped in 100 mM Tris-HCl (pH 8.0), 10% (w/v) PEG8000, 30% (v/v) glycerol cryo-protectant prior to vitrification in liquid nitrogen. X-ray diffraction data was indexed and scaled as before for Bmp2, and molecular replacement solution identified using 3E1T as molecular replacement search model. Model building and refinement was carried out in a manner identical to that described above.

Co-expression of *Mm_bmp2* with *Mm_bmp1*, *Mm_bmp3*, and *Mm_bmp4*

A two-plasmid system in *E. coli* BL21 Gold (DE3) for the coexpression of *Mm_bmp1*, *Mm_bmp3*, and *Mm_bmp4* has been described previously for the *in vivo* production of pyrrolyl-*S*-Bmp1 (3). To this system was introduced a third plasmid, pETDuet (Novagen), bearing *Mm_bmp2* or *Mm_bmp2-TM* in the second cloning site (MCS-2) of the plasmid vector. 5 mL LB liquid cultures were grown in the presence of 50 μg/mL kanamycin, 50 μg/mL streptomycin, and 100 μg/mL ampicillin (final concentration) and supplemented with 1 g/L (final concentration) of KBr. At OD_{600} ~ 0.6, protein expression was induced by the addition of 0.3 mM IPTG (Promega, PAV3951) and growth was allowed at 30 °C for an additional 18 h. The culture was extracted twice with EtOAC and solvent removed *in vacuo*. The residue was dissolved in methanol, and analyzed LC/MS/MS as described previously.

***In vitro* assay of wild type Mm_Bmp2, Mm_Bmp2-TM, and Mpy16 with pyrrolyl-*S*-ACPs as substrates**

Pyrrolyl-*S*-Bmp1(ACP) and pyrrolyl-S-Mpy15 were prepared as described previously (12) and used as substrates in *in vitro* reactions. 50 μM pyrrolyl-*S*-ACP substrate was incubated with 20 μM halogenase catalyst in 20 mM HEPES-Na (pH 7.9) reaction buffer containing 200 mM halide (KCl or KBr), 1 mM NADP+, 20 μM FAD, 10 mM freshly made Na-phosphite, 5 mM TCEP, 10 μM PtdH and SsuE enzymes, and 10% v/v glycerol. Reactions were incubated at 30 C for 3 h, and 100 μL reaction was quenched by the addition of 50 μL of 2% formic acid. Precipitate was removed by centrifugation and assays analyzed by LC/MS/MS as reported previously (12). Abundance of acyl-(cyclo)pantetheine MS2 product ions were individually normalized for each assay as reported in Figures 6E–G.

SUPPLEMENTARY FIGURES

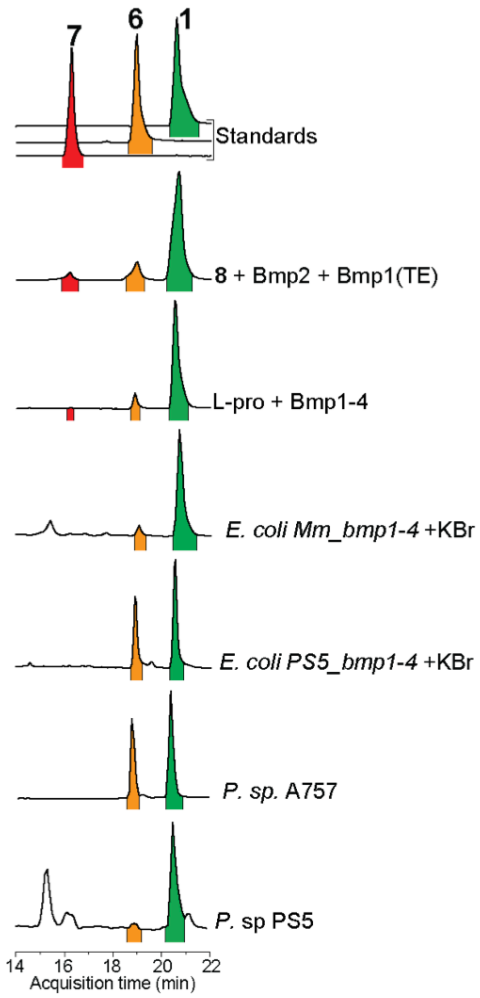

Figure S1. LC/MS comparisons of *in vivo* and *in vitro* EICSs to those of authentic standards of 1, 6, and 7. EICs for predicted $[M-H]^{1-}$ for the most abundant isotopic masses of **1** (*m/z* 381.67), **6** (*m/z* 301.76), and **7** (*m/z* 345.75). All traces are self-normalized.

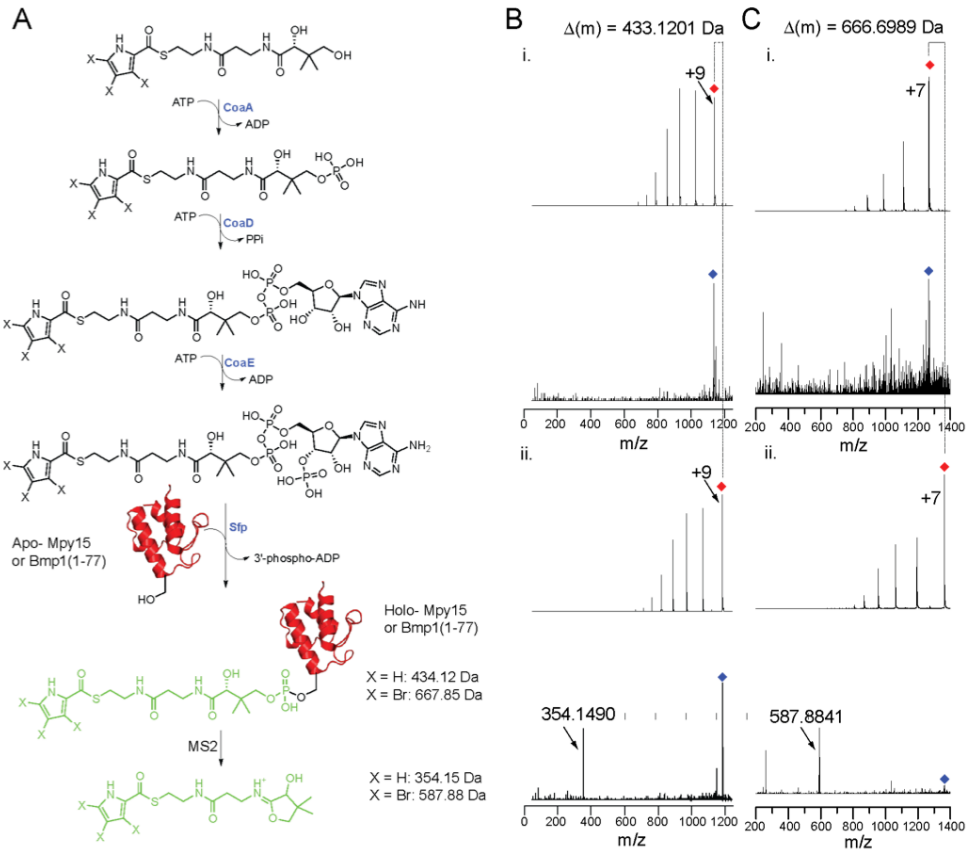

Figure S2. Confirmation of CoA extension and loading of pyrrole substrates onto ACPs. A. Scheme for CoA *in vitro* extension of chemically synthesized pyrrolyl-*S*-pantetheine precursor to pyrrolyl-*S*-CoA by *E. coli* CoA biosynthetic enzymes CoaA, CoaD, and CoaE. Upon completion of CoA synthesis, the substrate is loaded onto the catalytic serine of apo-ACP via *B. subtilis* phosphopantetheine transferase Sfp to generate "holo" pyrrolyl-*S*-ACP, resulting in a gain in mass specified to the right. To confirm substrate generation, the whole protein was analyzed by LC/MS/MS, resulting in a characteristic pantetheine MS2 fragments. Comparison to Apo-ACP from a negative control reaction in which ATP required for CoA enzymatic steps is excluded, demonstrates the expected mass shift between the parent ion and for apo- and holo- forms. B. i. MS1 and M2 for apo-Mpy15, ii. MS1 and MS2 for pyrrolyl-*S*-Mpy15. Red diamonds indicated the MS1 peptide masses while blue diamonds indicated peptide mass sampled for MS2. The pantetheine fragment mass is indicated in the MS2 spectrum. Charge is indicated to the right of the parent peptide. The corresponding mass shift between apo- and holo- Mpy15 is indicated by the dotted lines. C. Analogous scheme to 'B' for generation of 3,4,5-tribromopyrrolyl-*S*-Bmp1(ACP) **8** from chemically synthesized 3,4,5-tribromopyrrolyl-*S*-pantetheine **9**.

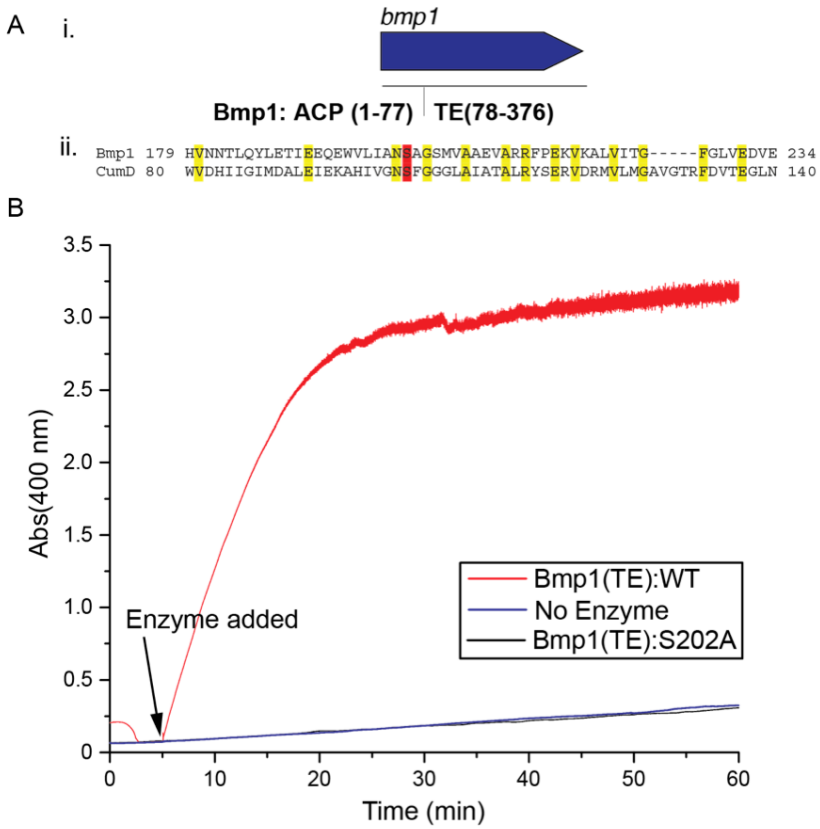

Figure S3. Bioinformatic identification and *in vitro* confirmation of catalytic Ser202 of Mm_Bmp1(TE) with a model chromogenic substrate, p-nitrophenyl acetate (pNPA).
A. i) Architecture of Bmp1 ACP-TE didomain, ii) BLAST query of the PDB database with the amino acid sequence of Mm_Bmp1 gives closest functionally and structurally characterized homolog CumD (44% similarity, 25% identity, 65% query coverage, e-value $7x10^{-14}$), a meta-cleavage product hydrolase from *Pseudomonas fluorescens* IP01 involved in the degradation cumene (isopropyl benzene); Bmp1:Ser202 aligns with confirmed catalytic Ser103 of CumD (24). B. 250 µM freshly prepared pNPA in 20 mM Tris-HCl (pH ~ 8), 50 mM KCl, 10% (v/v) glycerol was incubated with 5 µM Bmp1(TE), Bmp1(TE):S202A, or no enzyme. Upon addition of fresh substrate in DMSO to the buffer solution, the reaction was monitored spectrophotometrically at wavelength of 400 nm in a plastic UV cuvette. Enzyme was added 5 minutes after addition of the substrate. Measured absorbance is plotted versus time. Upon addition of Bmp1(TE), a steep absorbance increase was observed due to production of hydrolysis product p-nitrophenol. Loss of hydrolytic activity, identical to incubation without enzyme (blue curve), was observed when pNPA was incubated with Bmp1(TE):S202A (black curve).

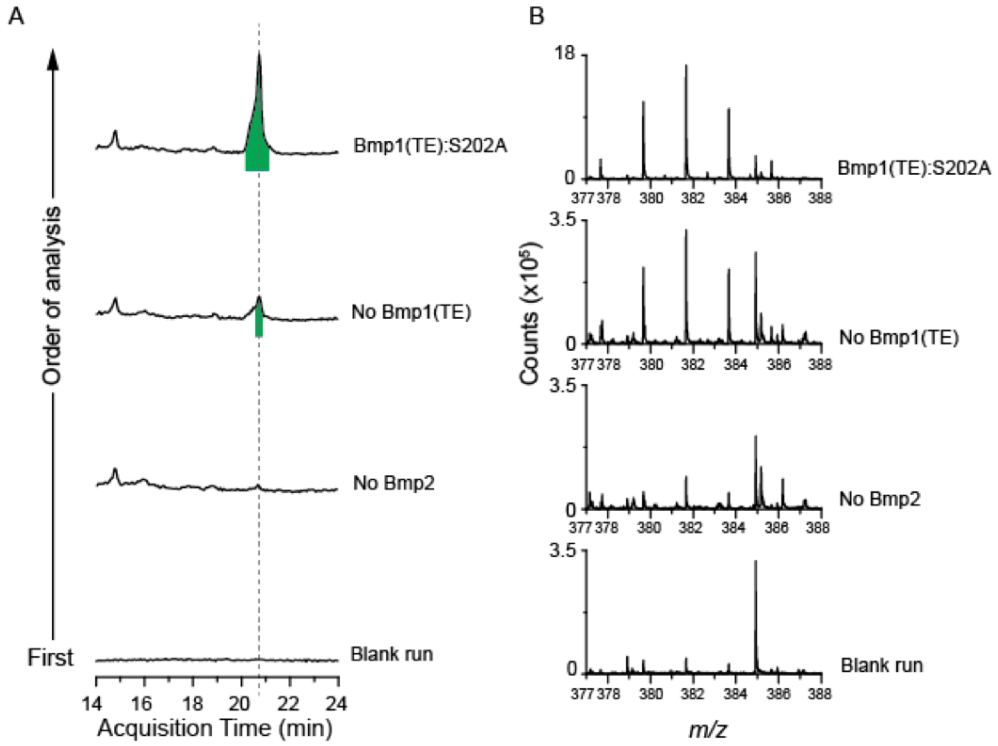

Figure S4. Non-enzymatic hydrolysis of proposed ACP-bound tetrabrominated intermediate yields 1. Extracted ion chromatograms (EICs) for 2,3,4,5-tetrabromo-1H-pyrrole (*m/z* 381.67) from incubations of 3,4,5-tribromopyrrolyl-*S*-ACP with various combination of Bmp1(TE) and Bmp2. All EICs are normalized to the largest peak (highlighted in green) in 'Bmp1(TE):S202A' EIC. Green highlight indicates presence of **1**. LC/MS analyses were performed sequentially with blank runs before and after each run in order to discount carry-over of substrate. Only the first blank run is shown, as **1** was not observed in the 'no Bmp2' reaction, and levels increased in the subsequent reactions. B. Mass spectral pattern at location of the dashed line in A; 'No Bmp1(TE)' and 'Bmp1(TE):S202A' reactions show *m/z* and isotopic distribution consistent with **1**.

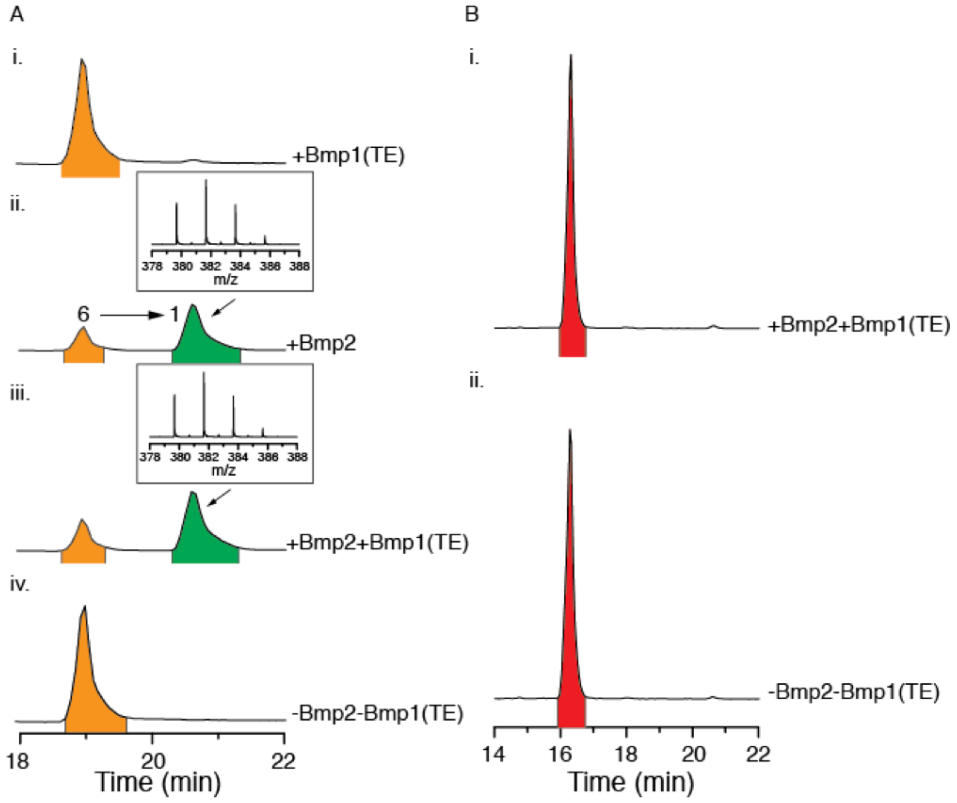

Figure S5. Interrogation of the potential of 2,3,4-tribromopyrrole 6 and 7 to serve as intermediates in the biosynthesis of 1. One mL reactions consisting of 25 µM **2** or **7** were incubated with 50 mM KBr, 0.1 mM FAD, 2 mM $NADP^+$, SsuE, PtdH, 10 mM phosphite including or excluding 50 µM Bmp2 and 25 µM Bmp1(TE, 78-376) in 20 mM Tris-HCl (pH 8) with 50 mM KCl and 10% (v/v) glycerol for 12 h at 30 ºC. Reactions were extracted with 1.6 mL EtOAc. Solvent was removed *in vacuo* and the resulting residue was dissolved in 100 µL MeOH. The extracts were analyzed by LC-MS/MS as previously described. A. Combined EICs for *m/z* 301.76 (**6**) and *m/z* 381.67 (**1**) reactions with substrate **6** (highlighted in orange) with i) Bmp1(TE) ii) Bmp2, iii) Bmp2 and Bmp1(TE), and iv) neither Bmp1(TE) nor Bmp2. Incomplete conversion to **1** (highlighted in green) was observed in ii)-iii). Mass spectra for products are shown above EICs for ii)-iii). All EICs are normalized to 'i'. B. Combined EICs for *m/z* 345.75 (**7**) and *m/z* 381.67 (**1**) for reactions with **7** (highlighted in red) as substrate with i) Bmp2 and Bmp1(TE) and ii) neither Bmp2 nor Bmp1(TE). No conversion was observed. EICs are normalized to 'i".

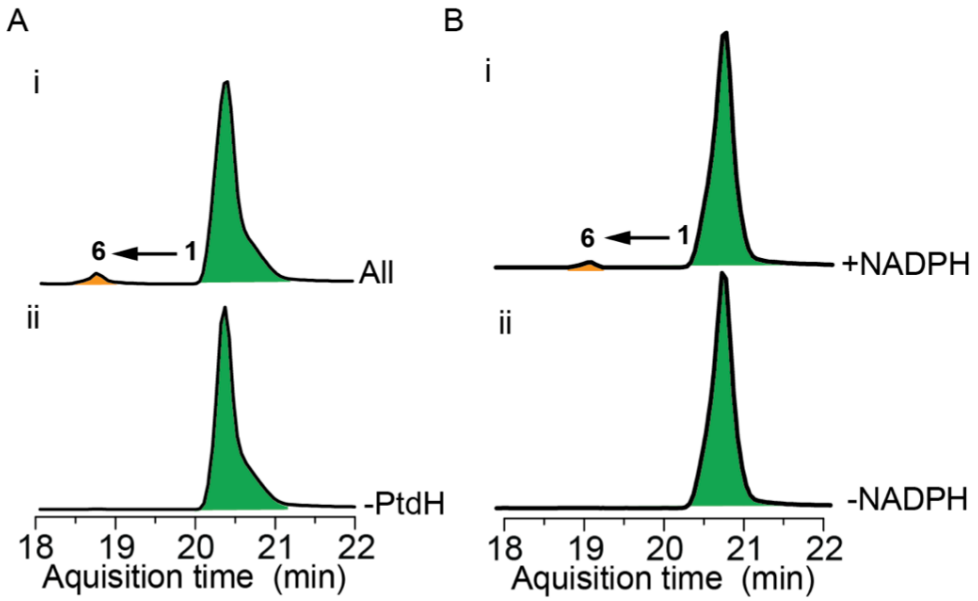

Figure S6. Reductive debromination of 1 by NADPH yields 6. A) EICs for **1** (*m/z* 381.67, shaded green) and **6** (*m/z* 301.76, shaded orange) for the organic extracts of 1 mL reactions incubated in 20 mM Tris-HCl (pH 8) with 50 mM KCl and 10% (v/v) glycerol for 12 h at 30 ºC consisting of 50 µM **1** with 2 mM $NADP^+$, 10 mM phosphite, and including or excluding PtdH (i.e., NADPH generation system with and without PtdH). (i) In the presence of the full NADPH generation system modest conversion of **1** to **6** is observed. (ii) When PtdH is eliminated from the reaction, no conversion of **1** to **6** is observed; $NADP^+$ is not reduced to NADPH in the absence of PtdH. B) EICs for **1** (*m/z* 381.67, shaded green) and **6** (*m/z* 301.76, shaded orange) for the organic extracts of 1 mL reactions incubated in 20 mM Tris-HCl (pH 8) with 50 mM KCl and 10% (v/v) glycerol for 12 h at 30 ºC consisting of 50 µM **1** with or without 1 mM NADPH. (i) In the presence of NADPH modest conversion of **1** to **6** is observed, consistent with the experiment shown in panel 'A' with the complete NADPH generation system. (ii) In the absence of NADPH no conversion of **1** to **6** is observed.

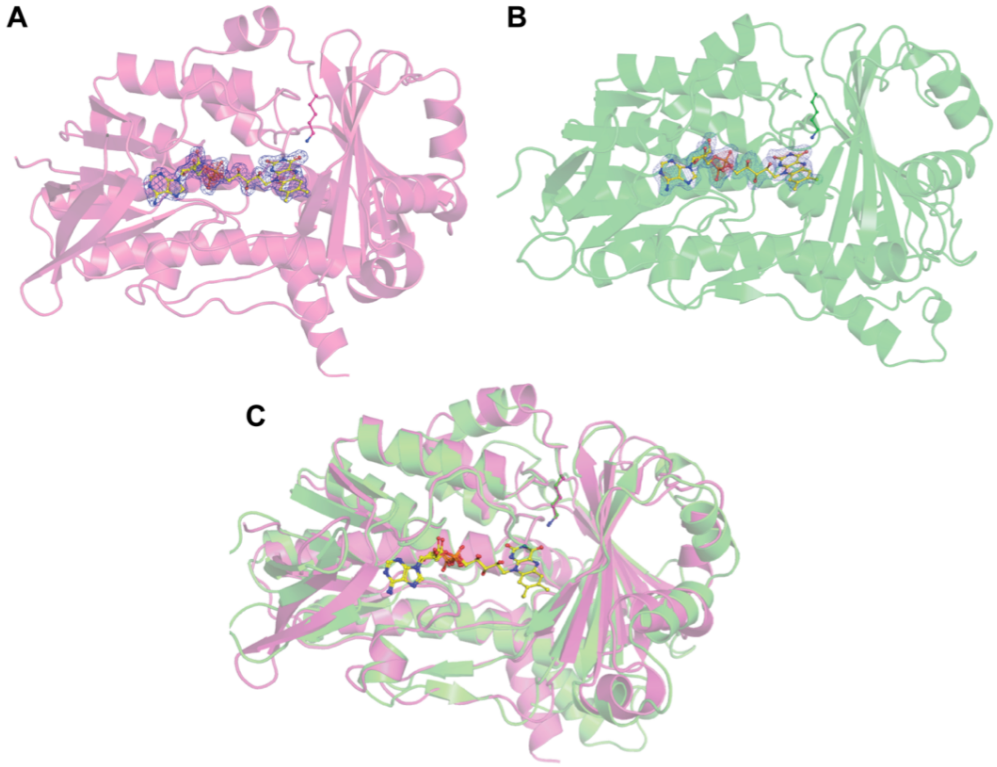

Figure S7. FAD-bound holo structures of pyrrolyl-*S*-ACP flavin-dependent halogenases from this study. (**A**) holo-Mm_Bmp2 structure. (**B**) holo-Mpy16 structure. (**C**) Superimposed Bmp2 (in pink) and Mpy16 (in green) structures. The flavin cofactors and the side chain of the catalytic lysine residues are shown in stick-ball representation.

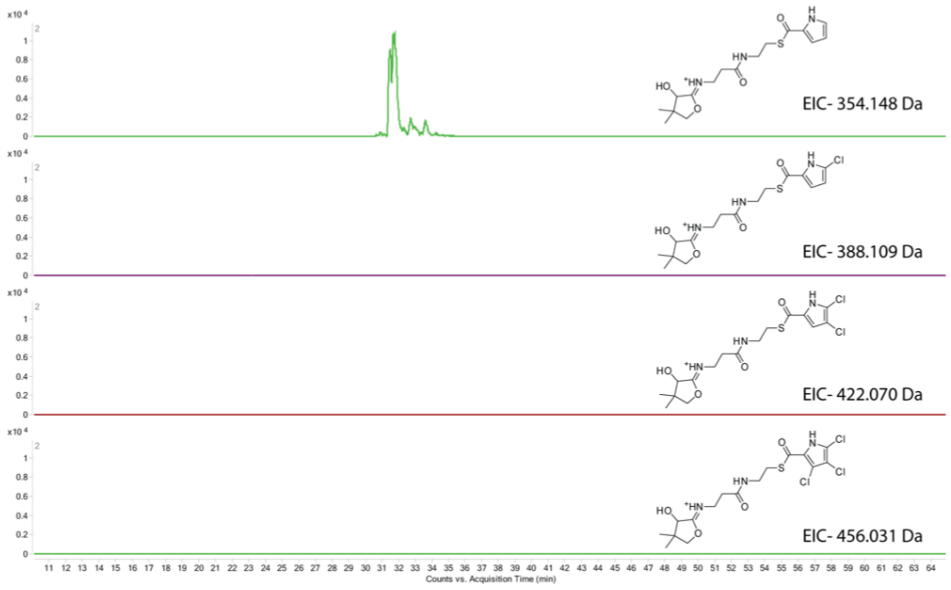

Figure S8. Lack of chlorination activity for Bmp2-TM. Halogenation reactions for Bmp2-TM were carried out as before, but in the absence of bromide, and in the presence of 200 mM chloride in the reaction. As can be seen from the EICs, no mono-, di-, or tri-chlorinated pyrrolyl-*S*-Bmp1(ACP) products can be detected.

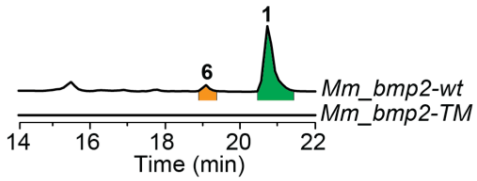

Figure S9. *In vivo* coexpression of *Mm_bmp1*, *Mm_bmp3*, and *Mm_bmp4* with wildtype *Mm_bmp2* (*Mm_bmp2-wt*) or *Mm_bmp2* triple mutant (*Mm_bmp2-TM*). Combined extracted ion chromatograms at $[M-H]^{1-}$ *m/z* 381.67 (**1**) and *m/z* 301.76 (**6**) corresponding to the dominant ions for the molecular formulae C_4NHBr_4 and $C_4NH_2Br_3$, respectively. Production of **1** and **6** can be observed when *Mm_bmp2-wt* is coexpressed with *Mm_bmp1*, *Mm_bmp3*, and *Mm_bmp4*, together with previously reported *M. mediterranea* MMB-1 phosphopantetheinyl transferase (GenBank locus tag: NC_015276.1) (3). However, neither production of **1** nor **6** is observed with *bmp2-wt* is substituted by *Mm_bmp2-TM* (expressing Bmp2-Y302S, F306V, A345W triple mutant).

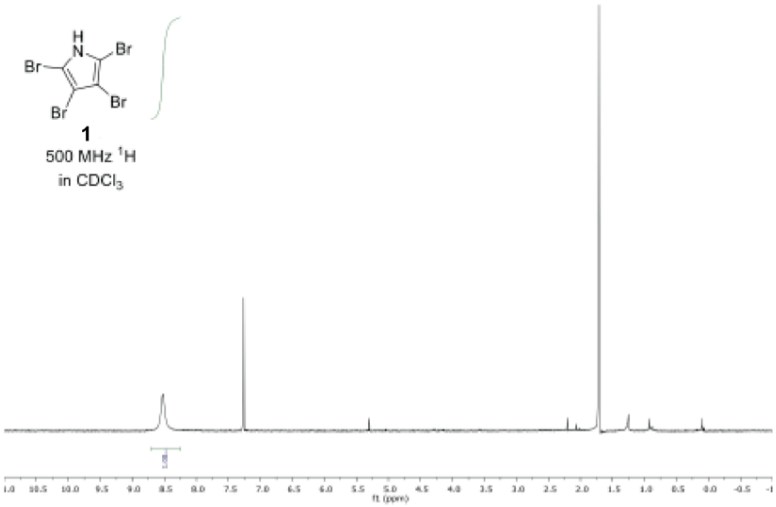

Figure S10. ^{1}H NMR spectrum of **1** ($CDCl_3$, 500 MHz).

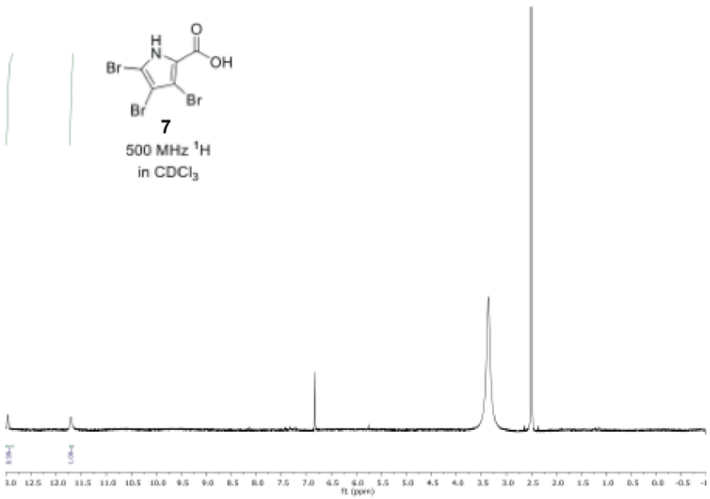

Figure S11. ^{1}H NMR spectrum of **7** ($CDCl_3$, 500 MHz).

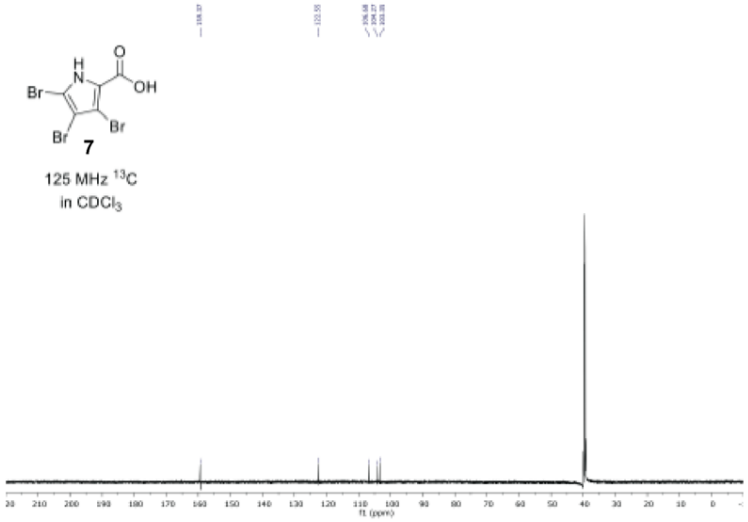

Figure S12. ^{13}C NMR spectrum of **7** ($CDCl_3$, 125 MHz).

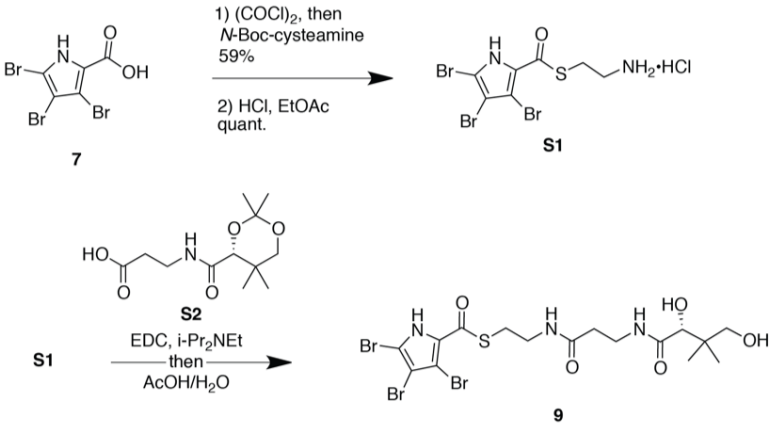

Figure S13. Scheme for the synthesis of **9**.

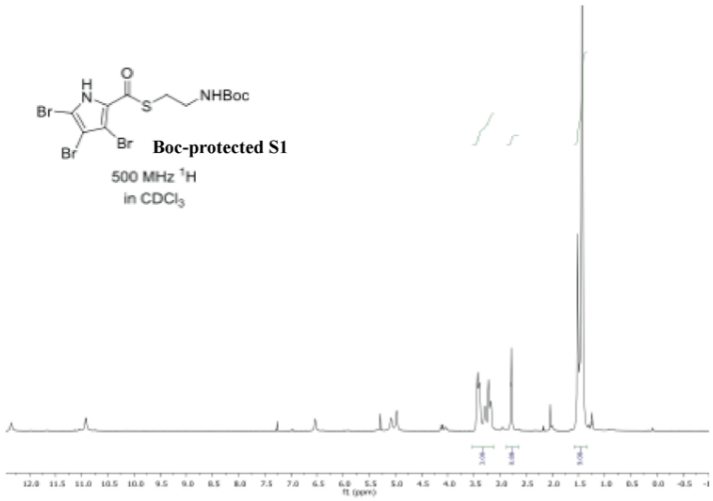

Figure S14. ^{1}H NMR spectrum of Boc-protected **S1** ($CDCl_3$, 500 MHz).

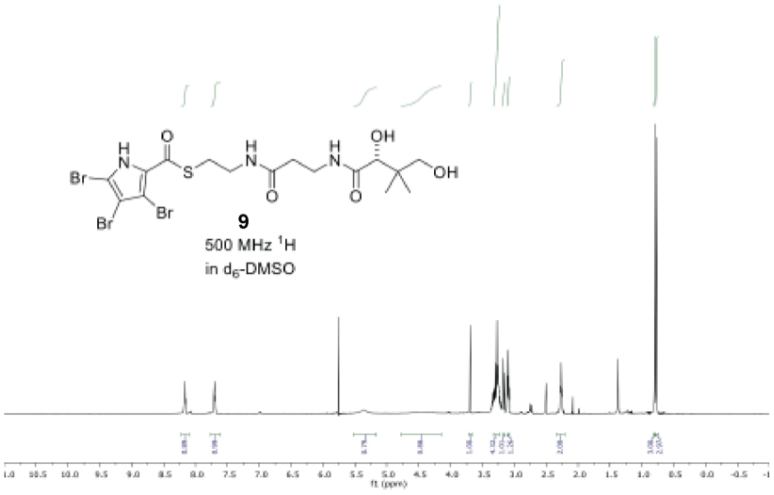

Figure S15. ^{1}H NMR spectrum of **9** (d_6-DMSO, 500 MHz).

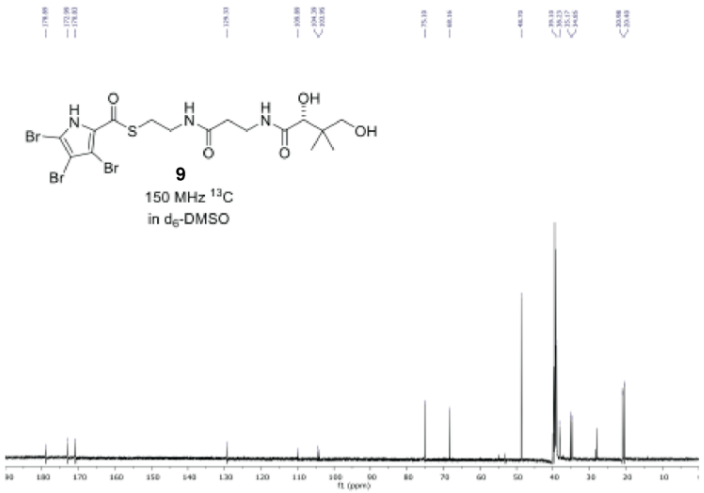

Figure S16. ^{13}C NMR spectrum of **9** (d_6-DMSO, 150 MHz).

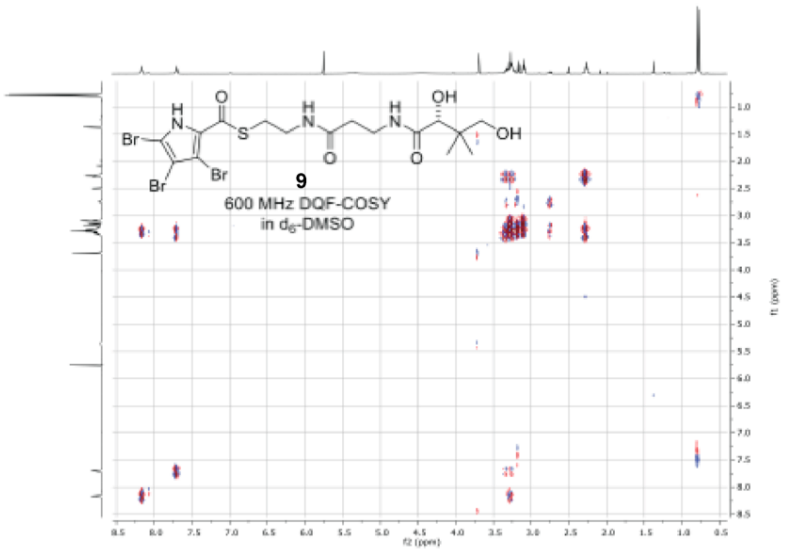

Figure S17. DQF-COSY spectrum of **9** (d_6-DMSO, 600 MHz).

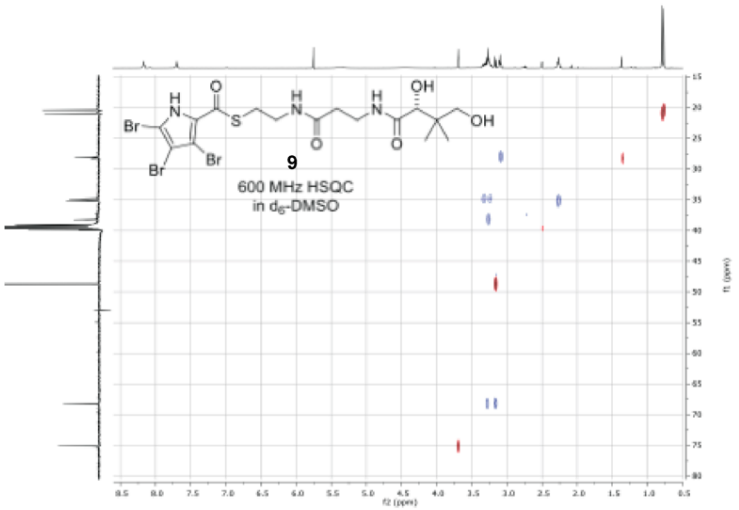

Figure S18. HSQC spectrum of **9** (d_6-DMSO, 600 MHz).

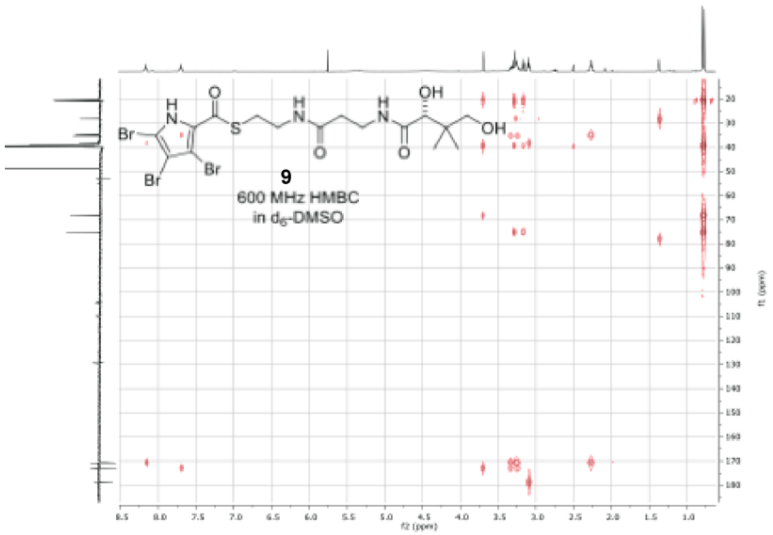

Figure S19. HMBC spectrum of **9** (d_6-DMSO, 600 MHz).

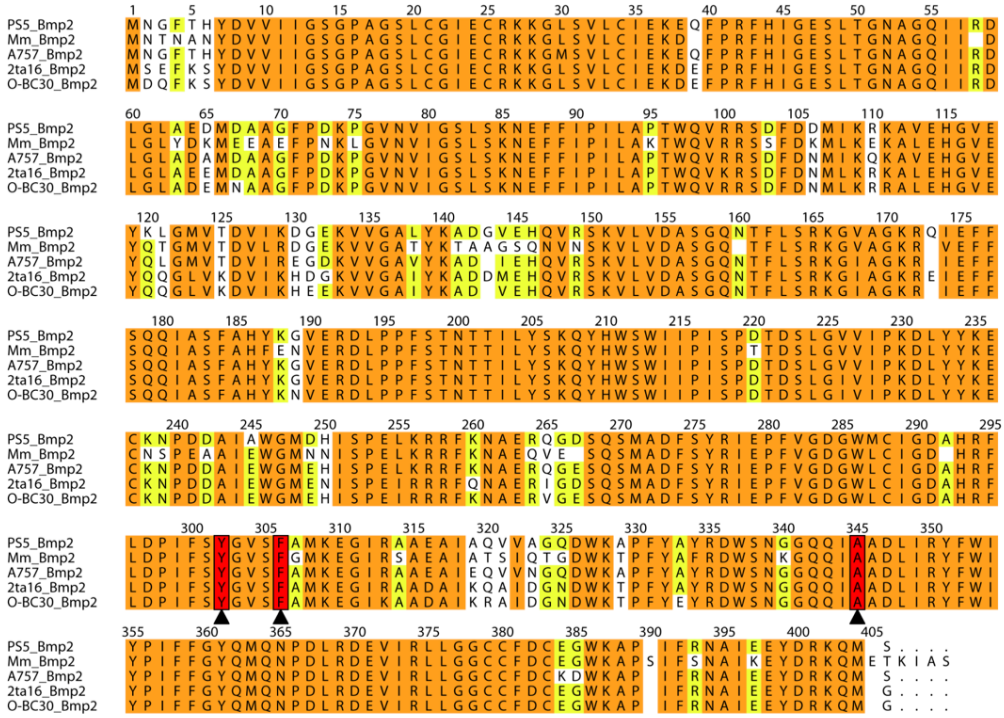

Figure S20. Sequence alignments of Bmp2 homologs. Sequence alignment of Bmp2 homologs from *Pseudoalteromonas* sp. PS5 (PS5_Bmp2), *Marinomonas mediterranea* MMB-1 (Mm_Bmp2), *Pseudoalteromonas* sp. A757 (A757_Bmp2), *Pseudoalteromonas luteoviolacea* 2ta16 (2ta16_Bmp2), and *Pseudoalteromonas phenolica* O-BC30 (O-BC30_Bmp2) showing conservation of Y302, F306, and A345 residues (numbering according to PS5_Bmp2 sequence).

SUPPLEMENTARY TABLES

Table S1. Bmp homology.

Protein name	Annotation	PS5 X Mm (% amino acid similarity/ identity)	PS5 X A757 (% amino acid similarity/ identity)
Bmp1	Acyl carrier protein(ACP)-thioesterase didomain	83/70	98/94
Bmp2	$FADH_2$-dependent pyrrolyl-*S*-ACP brominase	89/83	99/95
Bmp3	$FADH_2$-dependent prolyl-*S*-ACP dehydrogenase	84/76	97/93
Bmp4	L-proline adenylation domain	67/51	93/85
Bmp5	$FADH_2$-dependent p-hydroxbenzoate brominase/decarboxylase	No PS5 homolog found	-
Bmp6	Chorismate lyase	No PS5 homolog found	-
Bmp7	Bromo- pyrrole/phenol coupling cytochrome P450	No PS5 homolog found	-
Bmp8	Carboxymuconolactone decarboxylase/peroxidase	No PS5 homolog found	-
Bmp9	Ferredoxin	73/64	98/93
Bmp10	Ferredoxin reductase	61/42	82/69

Table S2. Data collection and refinement statistics for Mpy16, Bmp2, and Bmp2-TM structures.

	Mpy16	Bmp2	Bmp2-TM
Data collection			
Space group	$P2_1\,2_1\,2_1$	$P2_1\,2_1\,2$	$P2_1$
a, b, c (Å	62.83, 73.28, 189.72	82.97, 90.48, 57.92	49.23, 51.53, 77.06
α, β, γ	90.00, 90.00, 90.00	90.00, 90.00, 90.00	90.00, 100.89, 90.00
Rmerge (%)	0.09 (0.64) [1]	0.08 (0.94)	0.06 (0.49)
I/σ(I)	37.6 (3.0)	24.9 (1.9)	30.0 (8.5)
Completeness (%)	100.0 (99.8)	100.0 (100.0)	98.8 (99.5)
Total reflections	64779	36287	26147
Redundancy	12.0 (11.7)	7.0 (7.0)	6.3 (5.9)
Refinement			
Resolution (Å)	38.08 – 1.95	19.23 – 1.87	32.97 – 1.98
R_{work}/R_{free}	0.172/0.212	0.188/0.224	0.179/0.215
Number of atoms			
Protein	6825	3148	3096
Solvent	428	274	219
FAD	106	53	53
Average B values			
Protein	31.53	27.75	26.00
Solvent	35.77	33.99	31.77
FAD	23.14	19.49	16.09
R.m.s. deviations			
Bond lengths (Å)	0.007	0.007	0.007
Bond angles (°)	1.036	1.097	1.085

[1]Values for the highest resolution shell are reported in parentheses.

References

1. Bankevich A*, et al.* (2012) SPAdes: a new genome assembly algorithm and its applications to single-cell sequencing. *J Comput Biol* 19(5):455-477.
2. Aziz RK*, et al.* (2008) The RAST Server: rapid annotations using subsystems technology. *BMC Genomics* 9:75.
3. Agarwal V*, et al.* (2014) Biosynthesis of polybrominated aromatic organic compounds by marine bacteria. *Nat Chem Biol* 10(8):640-647.
4. Sneed JM, Sharp KH, Ritchie KB, & Paul VJ (2014) The chemical cue tetrabromopyrrole from a biofilm bacterium induces settlement of multiple Caribbean corals. *Proc Biol Sci* 281(1786).
5. Whalen KE, Poulson-Ellestad KL, Deering RW, Rowley DC, & Mincer TJ (2015) Enhancement of antibiotic activity against multidrug-resistant bacteria by the efflux pump inhibitor 3,4-dibromopyrrole-2,5-dione isolated from a *Pseudoalteromonas* sp. *J Nat Prod* 78(3):402-412.
6. Feher D, Barlow R, McAtee J, & Hemscheidt TK (2010) Highly brominated antimicrobial metabolites from a marine *Pseudoalteromonas* sp. *J Nat Prod* 73(11):1963-1966.
7. Eichhorn E, van der Ploeg JR, & Leisinger T (1999) Characterization of a two-component alkanesulfonate monooxygenase from *Escherichia coli*. *J Biol Chem* 274(38):26639-26646.
8. Gilow HM & Burton DE (1981) Bromination and Chlorination of Pyrrole and Some Reactive 1-Substituted Pyrroles. *J Org Chem* 46(11):2221-2225.
9. John EA, Pollet P, Gelbaum L, & Kubanek J (2004) Regioselective syntheses of 2,3,4-tribromopyrrole and 2,3,5-tribromopyrrole. *J Nat Prod* 67(11):1929-1931.
10. Wang MZ*, et al.* (2011) Design, synthesis and antifungal activities of novel pyrrole alkaloid analogs. *Eur J Med Chem* 46(5):1463-1472.
11. Jansen PA*, et al.* (2013) Discovery of small molecule vanin inhibitors: new tools to study metabolism and disease. *ACS Chem Biol* 8(3):530-534.
12. Agarwal V*, et al.* (2015) Chemoenzymatic synthesis of acyl coenzyme A substrates enables *in situ* labeling of small molecules and proteins. *Org Lett* 17(18):4452-4455.
13. Otwinowski Z, Borek D, Majewski W, & Minor W (2003) Multiparametric scaling of diffraction intensities. *Acta Crystallogr A* 59(Pt 3):228-234.
14. Kantardjieff KA & Rupp B (2003) Matthews coefficient probabilities: Improved estimates for unit cell contents of proteins, DNA, and protein-nucleic acid complex crystals. *Protein Sci* 12(9):1865-1871.
15. McCoy AJ*, et al.* (2007) Phaser crystallographic software. *J Appl Crystallogr* 40(Pt 4):658-674.
16. Stein N (2008) CHAINSAW: a program for mutating pdb files used as templates in molecular replacement. *J App Cryst* 41:641-643.
17. Buedenbender S, Rachid S, Muller R, & Schulz GE (2009) Structure and action of the Myxobacterial chondrochloren halogenase CndH: A new variant of FAD-dependent halogenases. *J Mol Biol* 385(2):520-530.
18. Emsley P & Cowtan K (2004) Coot: model-building tools for molecular graphics. *Acta Crystallogr D Biol Crystallogr* 60(Pt 12 Pt 1):2126-2132.
19. Perrakis A, Sixma TK, Wilson KS, & Lamzin VS (1997) wARP: improvement and extension of crystallographic phases by weighted averaging of multiple-refined dummy atomic models. *Acta Crystallogr D Biol Crystallogr* 53(Pt 4):448-455.
20. Zwart PH*, et al.* (2008) Automated structure solution with the PHENIX suite. *Methods Mol Biol* 426:419-435.
21. Kleywegt GJ & Brunger AT (1996) Checking your imagination: applications of the free R value. *Structure* 4(8):897-904.
22. Yamanaka K, Ryan KS, Gulder TA, Hughes CC, & Moore BS (2012) Flavoenzyme-catalyzed atropo-selective N,C-bipyrrole homocoupling in marinopyrrole biosynthesis. *J Am Chem Soc* 134(30):12434-12437.
23. Lee J*, et al.* (2013) Structural and functional insight into an unexpectedly selective N-methyltransferase involved in plantazolicin biosynthesis. *Proc Natl Acad Sci U S A* 110(32):12954-12959.

24. Fushinobu S, *et al.* (2002) Crystal structures of a meta-cleavage product hydrolase from *Pseudomonas fluorescens* IP01 (CumD) complexed with cleavage products. *Protein Sci* 11(9):2184-2195.

Chapter 3, in full, is a reprint of materials as it appears in "Biosynthesis of a coral chemical cue tetrabromopyrrole in marine bacteria by a uniquely adapted brominase-thioesterase enzyme pair" in *Proceedings of the National Academy of Sciences U.S.A.*, 2016. El Gamal A., Agarwal V., Diethelm S., Rahman I., Schorn M., Sneed J.M., Louie G.V., Whalen, K.E., Mincer T.J., Noel J.P., Paul V.J., and Moore B.S. The dissertation author was one of two equally contributing primary investigators and authors of this paper.

A.E., V.A., and B.S.M. designed research; A.E., V.A., S.D., I.R., and M.A.S. performed research; S.D., J.M.S., G.V.L., K.E.W., T.J.M., J.P.N., and V.J.P. contributed new reagents/analytic tools; A.E., V.A., S.D., and B.S.M. analyzed data; and A.E., V.A., and B.S.M. wrote the paper.

Chapter 4: An alkylhydroperoxidase-like debrominase is an enzymatic switch in the biosynthesis of pentabromopseudilin

4.1 Introduction

Halogenated organic compounds (organohalogens) are pervasive in the environment[2,23]. Efforts toward the bioremediation of anthropogenic organohalogen toxins have led to the identification of microbes and associated enzymes capable of dehalogenation through to complete mineralization of a wide range of man-made pollutants[71,83,84]. In particular, cobalamin-dependent reductive dehalogenases have been the focus of much study due to their ability to couple dehalogenation with microbial respiration in contaminated sediments [85]. Though considerable progress has been made in the study of their structure and mechanism, these oxygen-sensitive and often membrane-associated proteins have proven to be largely intractable to direct interrogation[86]. In addition to man-made organohalogens, is an astonishing diversity of organohalogens of natural origin ranging from simple aliphatic and aromatic molecules that resemble structures and sub-structures of man-made pollutants[23,70] to complex natural product scaffolds such as terpenoids, oligopeptides, alkaloids, and polyketides with diverse biological activities[1]. In line with the widespread distribution of natural organohalogens, emerging studies have suggested a native role for microbial dehalogenation as part of a biogeochemical halogen cycle in marine and terrestrial environments[20-22]. However, in contrast to the abundance of reported halogenated natural products (> 4,000 compounds)[2], the biochemical transformations leading to their natural formation and degradation remain largely unexplored, providing a potential untapped source of novel biocatalysts[2,20,23]. Moreover, an

example of a dedicated dehalogenase from the context of a confirmed microbial natural product biosynthetic pathway has yet to be reported.

The terminal reaction in biosynthesis of the highly brominated bacterial marine natural product pentabromopseudilin (**1**) by the Bmp pathway involves the coupling of asymmetric 2,3,4-tribromopyrrole (**2**) to 2,4-dibromophenol catalyzed by cytochrome P450(CYP450)-Bmp7 (**Fig. 4.1A,B**)[50]. This biosynthetic scheme is at odds with earlier isotope feeding studies that implied a symmetric intermediate in the biosynthesis of **1** due to shuffling of the ^{13}C-labeled 5-position of L-proline with respect C-C coupling of the L-proline-derived bromopyrrole moiety of **1** (**Fig. 4.1B**)[81]. In corroboration of these isotope experiments, we recently confirmed that symmetric 2,3,4,5-tetrabromopyrrole (**3**) (**Fig 4.1B**), which is not a substrate for Bmp7, is an intermediate in the biosynthesis of **1**[16,50]. Therefore, in order to reconcile these observations, **3** must undergo a dehalogenation to **2** via an unknown mechanism. Here we demonstrate that the transformation of **3** to **2** is catalyzed by a dedicated dehalogenase enzyme-Bmp8 encoded in the Bmp biosynthetic pathway utilizing a cofactor-independent thiolate redox mechanism. We probed (meta)genomic datasets and found hundreds of Bmp8 homologs from diverse genera and varied genetic contexts bearing a conserved catalytic triad, and demonstrate that a distant homolog of Bmp8 is also able to catalyze the dehalogenation of **3** via an analogous mechanism. To best of our knowledge Bmp8 is the first reported example of a bacterial cofactor-independent dehalogenase, as well as the first example of a dehalogenase enzyme from the context of a confirmed natural product biosynthetic pathway.

While we previously showed that degradation of **3** to **2** occurs in aqueous solution under reducing conditions (**Fig. S4.15**)[16], the fact that **1** is a major product of the Bmp pathway suggested a direct enzymatic route for the conversion of **3** to Bmp7 substrate **2**[50]. In search of a dehalogenase catalyzing the conversion of **3** to **2**, we re-examined the Bmp biosynthetic gene cluster for open reading frames (ORFs) possibly encoding dehalogenating enzymes. The Bmp biosynthetic gene cluster consists of modularly encoded bromopyrrole (Bmp1–4, Bmp_BrPy) and bromophenol (Bmp5–6, Bmp_BrPh) enzymes united by coupling CYP450-Bmp7 (**Fig. 4.1A,B**). In turn these modules are flanked by genes encoding Bmp7 redox partners Bmp9–10 (**Fig. 4.1A**). Upstream of *bmp9–10* is an additional ORF *bmp8* (**Fig. 4.1A**) putatively encoding a ~21 kDa protein that annotates as a member of the carboxymuconolactone decarboxylase superfamily (CMD), which takes its name from decarboxylases participating in the degradation of monocyclic aromatic molecules, but also includes alkylhydroperoxidase subunit D (AhpD) involved in intracellular defense against oxidative stress[87]. Bacteria that produce **3** and not **1** such as the biofilm-associated marine bacterium *Pseudoalteromonas* sp. PS5 possess only *Bmp_BrPy* and vestigial *bmp9–10* (Bmp7 is not present in these bacteria), while *bmp8* is notably absent in the genomes of these bacteria (**Fig. 4.1A**). Our previous studies confirmed the functions of Bmp1–7 along with Bmp9–10, but the role of Bmp8 remained speculative[50]. On the basis of primary sequence annotation as a "decarboxylase" we initially postulated that Bmp8 might play a role in the elimination of proline-derived alpha-carboxylate of a tribromopyrrolyl-*S*-acyl carrier protein(ACP) intermediate leading to **1** (**Fig. 4.1C**) [50]. Involvement of Bmp8 in the bromopyrrole biosynthesis was supported by

our observation that *in vivo* expression of *bmp8* with *bmp1–7* in *Escherichia coli* led to an increase in the heterologous production of **2** and **1** with a concomitant decrease in the level of **3** [50]. However, this proposal was challenged by our more recent finding that elimination of the prolyl alpha-carboxylate is mediated by a brominative mechanism catalyzed by pyrrole halogenase-Bmp2 and leading to **3** (**Fig. 4.1C**)[16]. Hence, we were presented with an alternate hypothesis that Bmp8 might be a reductive dehalogenase that converts **3** to **2** (**Fig. 4.1B**), consistent with its *in vivo* activity and distant homology to AhpD redox enzymes. Therefore, we sought to purify recombinant Bmp8 to interrogate its function *in vitro*.

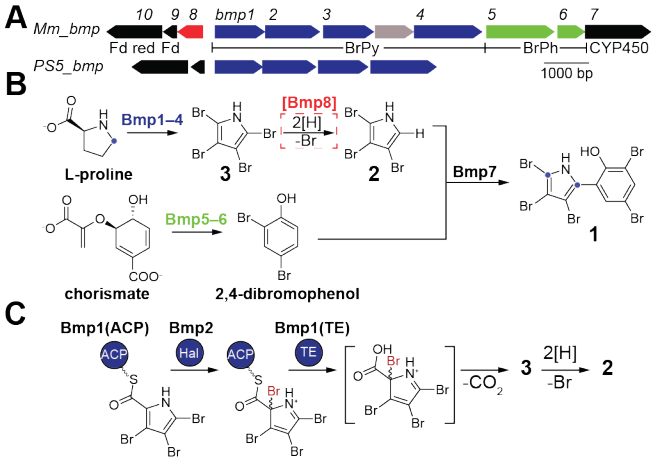

Figure 4.1: Bmp biosynthetic pathway. (**A**) Bmp gene clusters from *M. mediterranea* MMB-1 (*Mm_bmp*) and *P.* sp. PS5 (*PS5_bmp*); bromopyrrole (BrPy) and bromophenol (BrPh) biosynthetic modules are labeled below; *bmp9–10* encode CYP450-Bmp7 redox partners ferredoxin (Fd) and ferredoxin reductase (Fd Red), respectively. *Mm_bmp* features a putative permease (grey) inserted between *bmp3* and *bmp4* of the BrPy module. (**B**) Biosynthetic scheme for 1 including the hypothesized Bmp8-catalyzed dehalogenation of 3. The position of ^{13}C-isotope label from Ref. 14 is indicated by the blue circle at the 5-position L-proline and then again in 1. (**C**) Terminal reaction sequence leading to 3; 2 arises as an off-pathway reductive degradation product of 3.

4.2 Results and Discussion

Insolubility of Bmp8 had precluded previous functional characterization [50]. However, the fact that Bmp8 demonstrated *in vivo* activity in *E. coli* heterologously expressing the Bmp pathway implied that its soluble expression might rely on the co-expression of another component of the Bmp pathway. We recently showed that thioesterase domain of the ACP-thioesterase(TE) didomain-Bmp1, Bmp1(TE), catalyzes offloading of a tetrabrominated pyrrole from Bmp1(ACP) *en route* to **3** (i.e., the reaction sequence directly preceding proposed dehalogenation of **3**) (**Fig. 4.1C**)[16]. Fortuitously, co-expression of N-His_6-tagged-Bmp8 with untagged Bmp1(TE), lead to soluble expression of Bmp8 from the *Marinomonas mediterranea* MMB-1 Bmp gene cluster (**Fig. 4.1A**) as a stand-alone recombinant protein not in complex with Bmp(TE) following purification by affinity chromatography (**Fig. S4.1**). We subsequently performed proteolytic cleavage of the N-terminal His_6-tag prior to biochemical characterization of Bmp8.

With purified soluble Bmp8 in hand, we tested the hypothesis that Bmp8 catalyzes the dehalogenation of **3** to **2** (**Fig. 4.2A**, **S4.10**). Incubation of synthetically prepared **3** with equimolar Bmp8 as-purified lead to rapid and complete turnover to **2** (**Fig. 4.2B**). Pre-incubation of Bmp8 with EDTA did not alter activity, implying that Bmp8 does not utilize a metal cofactor (**Fig. 4.2B**). Addition of **3** in 2-fold excess to Bmp8 led to incomplete conversion to **2**, while turnover was achieved by the addition of glutathione, suggesting that Bmp8 undergoes oxidation in the course of the debromination of **3** and is rescued by an exogenous reducing agent (**Fig. 4.2A,B**). Slight conversion of **3** to **2** was also observed in the presence of glutathione and absence of Bmp8 (**Fig. 4.2B**), consistent with our previous observation that **3** is

labile to aqueous reductive degradation. A minor product with predicted molecular formula $C_4NH_3Br_2$ confirmed to be symmetric 3,4-dibromopyrrole (**4**) by ^{1}H-NMR was additionally observed in all reactions where Bmp8 was present indicating that **2** might also be a substrate for Bmp8 (**Figs. 4.2A,B** and **S4.10**). Consistent with this observation, incubation of Bmp8 with a 2-fold excess of **2** and glutathione lead to partial conversion of **2** to **4**, in contrast to complete conversion of **3** to **2** for the same incubation time (**Figs. 4.2B** and **S4.11**). Hence, Bmp8 regioselectively dehalogenates the symmetric 2/5-position of **3**. The loss in efficiency exhibited by the second dehalogenation is likely due to a change in the reactivity of the pyrrole upon elimination of an electron-withdrawing bromine atom. To explore halogen specificity, we incubated Bmp8 with the chlorinated analog of **3**, 2,3,4,5-tetrachloropoyrrole, and glutathione and observed partial conversion to a product with molecular formula $C_4NH_2Cl_3$ as determined by high resolution mass spectrometry (**Figs. S4.2** and **S4.9**). The difference in reactivity between the brominated and chlorinated substrates is likely explained by significant differences in bond dissociation energies between C-Cl and C-Br bonds ($\Delta\Delta H_f$ ~ 120 KJ/mol)[88]. Consistent with this observation, non-enzymatic dechlorination of 2,3,4,5-tetrachloropyrrole by glutathione was not observed (**Fig. S4.2**). Taken together these results indicate that Bmp8 is a cofactor-independent reductive dehalogenase that catalyzes a series of regioselective dehalogenations of halopyrroles that appears to be oxidized in the course of dehalogenation (**Fig. 4.2A**). In further support of loss of activity of Bmp8 due to oxidation, we showed that Bmp8 exhibits a loss of activity following extended pre-incubation in air (**Fig. S4.13**). Additionally, we showed that Bmp8 dialyzed after

treatment with excess **1** exhibits a loss of activity that can be recovered upon subsequent dialysis with a reducing agent (**Fig. S4.12**). We next investigated the mechanism of dehalogenation employed by Bmp8.

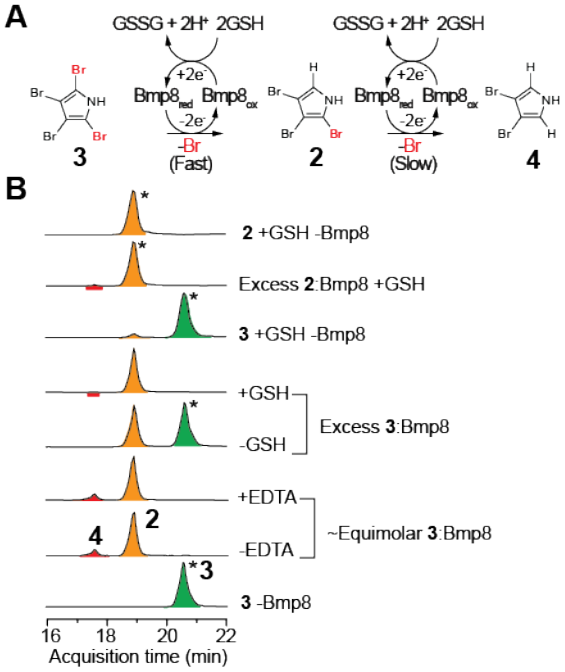

Figure 4.2: Debromination of bromopyrroles by Bmp8. (**A**) Scheme for reductive dehalogenation 3 and 2 and recycling of Bmp8 by glutathione (GSH). (**B**) Combined extracted ion chromatograms (EICs) for *m/z*'s corresponding to $[M\text{-}H]^{1-}$ ions for 3 (shaded green), 2 (shaded orange), and 4 (shaded red) for organic extracts of Bmp8 incubated with 3 or 2 at various ratios of substrate to enzyme with and without additives for a fixed reaction time (30 min); remaining starting material is indicated by an asterisk (*).

Due to the fact that the transformation of **3** to **2** is a net $2e^-$ reduction reaction, we inspected the primary sequence of Bmp8 for redox motifs. Bmp8 bears homology to the CMD superfamily member AhpD, whose primary function is that of a thioredoxin that reduces the side chain thiolate of the catalytic cysteine residue of the alkylperoxidase AhpC, but has also been shown to possess alkylhydroperoxidase

activity (ROOH to ROH and H_2O)[87,89]. AhpD contains a redox motif found among diverse classes of enzymes catalyzing disulfide exchange reactions (i.e., thioredoxins) consisting of two cysteine residues separated by two variable amino acid residues (CXXC) [90]. Consistent with its homology to AhpD, Bmp8 contains a CXXC motif (Bmp8-CXXC) comprised of amino acid residues Cys82 and Cys85 (**Fig. 4.3A**). Additionally, our query of publically available (meta)genomic datasets with the primary amino acid sequence of Bmp8 lead to the discovery of an expanded conserved CXYCXXH motif present among hundreds of homologs from genomic and marine environmental metagenomic sequences (**Fig. S4.3**). The Bmp8 homolog sequences for which genomic information was available represent diverse genera of marine bacteria, and the vast majority of these sequences are derived from genetic contexts other than the Bmp pathway (**Fig. S4.3**). We next explored the functional significance of the conserved CXYCXXH motif identified in our homology search.

We first investigated the role of the Bmp8-CXXC motif in the redox mechanism of Bmp8. In mechanisms described for CXXC-containing reductases, the substrate is first attacked by an electron-donating cysteine residue side chain thiolate to form a thioether, which is then resolved by attack of the thioether bond by the second cysteine side chain thiolate resulting in release of the reduced product and formation of an intramolecular disulfide bridge at the enzyme active site [90]. Hence we reasoned that the mechanism of Bmp8 might terminate in the formation of disulfide bridge between Bmp8-Cys82 and Bmp8-Cys85 (**Fig. 4.3B**). To investigate the role of Bmp8-CXXC in the Bmp8 reaction mechanism, we incubated fully reduced Bmp8 with a 2-fold excess of **3** or an equivalent volume of buffer and monitored the redox

state of the Bmp8-CXXC by mass spectrometric analysis of the trypsin-digested enzyme. For Bmp8 incubated with a 2-fold excess **3** we observed only one population corresponding to the oxidized Bmp8-CXXC-containing trypsin-digested fragment (-2H), while for the untreated sample we observed populations corresponding to both the oxidized and reduced fragments as anticipated due to increased susceptibility to oxidation of the cysteine residue side-chain thiols upon denaturation of the protein (**Fig. 4.3C**). To eliminate adventitious oxidation, we repeated the experiment, but quenched the intact enzyme with a thiol alkylating agent iodoacetamide prior to digestion. As expected, for the enzyme incubated with **3** we observed no alkylation of the trypsin-digested fragment containing the Bmp8-CXXC, while for the untreated protein we observed only the alkylated species (**Fig. 4.3D**). This binary result confirms oxidation of the Bmp8-CXXC in the course of dehalogenation of **3**, and also demonstrates that the enzyme as-purified is initially in its fully reduced state, which we also confirmed by alkylation of the intact enzyme at the starting point of the reaction (**Fig. S4.4**). Bmp8 homologs derived from the Bmp pathway context contain an additional two conserved cysteine residues corresponding to Cys57 and Cys163 in *M. mediterranea* Bmp8 (**Fig. S4.5**). Hence we also investigated the potential of these additional conserved Cys residues to participate in the redox mechanism of Bmp8. While mutagenesis of either residue lead to insolubility of the protein, levels of alkylation of the trypsin-digested fragments containing either Cys57 and Cys163 were comparable between both **3**-treated and untreated Bmp8, indicating that these additional conserved Cys residues are not involved in the redox reaction mechanism of Bmp8, but may instead serve a stabilizing role.

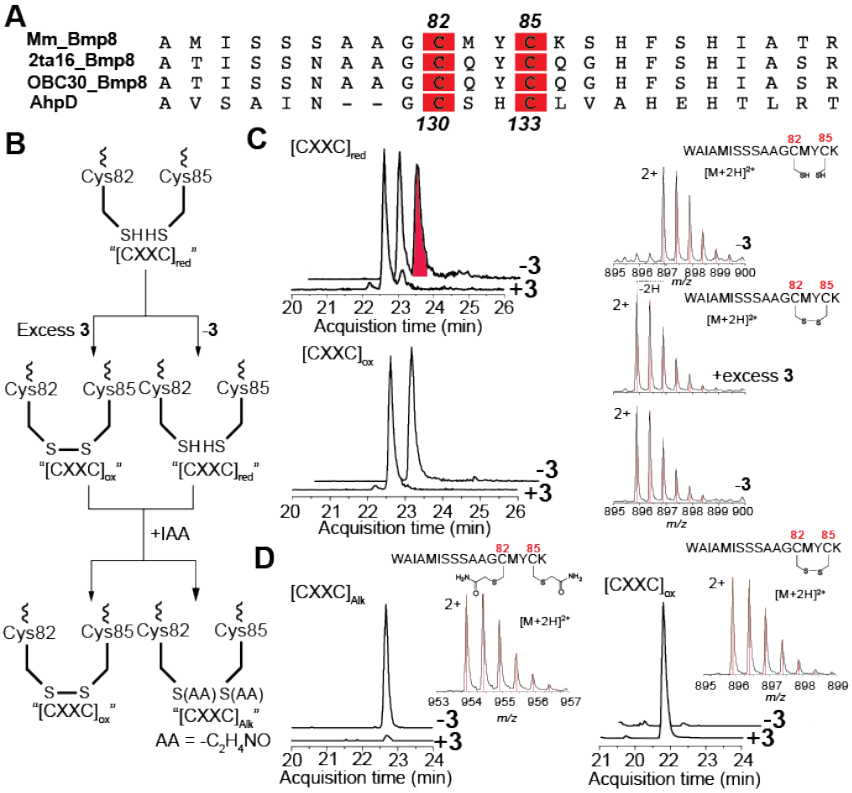

Figure 4.3: Redox state of Bmp8-CXXC. (**A**) Alignment (MAFFT) focusing on the region containing the conserved CXXC motif for Bmp8 from three marine bacteria harboring the Bmp pathway, *M. mediterranea* (Mm_Bmp8; 'Bmp8' in main text), *P. luteoviolacea* 2ta16 (2ta16_Bmp8), and *Pseudoalteromonas phenolica* O-BC30 (OBC30_Bmp8), in addition to functionally characterized bacterial alkylhydroperoxidase thioredoxin AhpD (*Mycobacterium tuberculosis* H37Rv, GenBank AAA86657.1); cysteine residues corresponding to the CXXC motif are highlighted in red with corresponding residue numbering indicated above for Mm_Bmp8 and below for AhpD. (**B**) Hypothesis scheme for redox state of the Bmp8-CXXC with and without treatment with a 2-fold excess of 3 and alkylation thereof with iodoacetamide (IAA). (**C**) EICs for the predicted *m/z*'s for $[M+2H]^{2+}$ ions for the trypsin-digested peptide fragment containing Bmp8-CXXC in the reduced state (top, left) and oxidized state (bottom, left). Due to overlap between the oxidized and reduced peptide isotopic masses, the oxidized peptide mass extracts with the reduced mass, therefore the peak corresponding to the reduced peptide is highlighted in red for clarity. To the right of EICs, mass spectra averaged over EIC peaks corresponding to reduced and oxidized fragments with the -2H shift indicated for the oxidized peptide spectrum with respect to the reduced peptide spectrum (only the spectra corresponding to oxidized fragment for '-3' is shown for the sake of space). Calculated isotope distributions are indicated by the red lines. (**D**) EICs for *m/z*'s for predicted $[M+2H]^{2+}$ ions for alkylated and oxidized trypsin digested Bmp8-CXXC-containing peptide fragments with corresponding mass spectra averaged over EIC peaks shown to the right; predicted peptide distributions are indicated by the red lines.

Having identified the electron-donating role of Bmp8-CXXC, we next sought to determine the individual roles of Bmp8-Cys82 and Bmp8-Cys85 in the Bmp8 reaction mechanism. The mechanism for 2-Cys peroxidases such as AhpD involves an "peroxidatic" Cys residue that is critical to peroxidase activity and performs the initial attack of the peroxide (ROOH) to form a sulfenic acid species (Cys-*S*-OH), which is then resolved by a second non-essential Cys residue side chain thiolate releasing water and forming a disulfide bridge; the function of the resolving Cys can be complemented by exogenous nucleophiles in 1-Cys peroxidases that lack a resolving Cys residue [91]. In the case of the peroxidase activity of Bmp8-homolog *M. tuberculosis* AhpD, Cys133 (corresponding to Bmp8-Cys85) serves the role of the peroxidatic residue, while Cys130 (corresponding to Bmp8-Cys82) provides the resolving thiolate and is not required for activity (**Fig. 4.3A**)[87]. To distinguish the roles of Bmp8-CXXC cysteine residues, Cys82 to Ala (Bmp8:C82A) and Cys85 to Ala (Bmp8:C85A) mutants were constructed and assayed for activity. Incubation of Bmp8:C82A with a 2-fold excess of **3** and glutathione lead to complete conversion to **2** and **4**, while no conversion was observed for Bmp8:C85A treated in the same manner (**Figs. 4.3A** and **4.4A**). Hence Cys85 is essential to activity, while Cys82 plays a non-essential role that appears to be complemented by an exogenous nucleophile.

To investigate the role of the glutathione thiolate as a complementary nucleophile, we monitored Bmp8:C82A incubated with glutathione by whole-protein spectrometry. Upon addition of a 2-fold excess of **3**, we observed a mass shift consistent with glutathionylation of Bmp8:C82A. By contrast no glutathionylation

was observed Bmp8:C85A, indicating that the observed modification takes place on the side chain thiolate of Bmp8-Cys85 (**Figs. 4.4B** and **S4.6**, **Table S4.1**). Hence, the glutathione thiolate appears to complement for the resolving role of Bmp8-Cys82 side chaine thiolate. Interestingly, addition of **3** to wildtype Bmp8 lead to positive mass shifts consistent with singly and doubly glutathionylated species, as well a negative mass shift that likely corresponds to the oxidized (-2H) form (**Figs. 4.4B** and **S4.6**, **Table S4.1**). This observation is consistent with the mechanism of disulfide bridge opening by glutathione, in which the glutathione thiolate would attack either the side chain sulfurs of Bmp8-Cys82 or Bmp8-Cys85 to form a disulfide bridge with one side chain thiol, while liberating the other. If the Bmp8-Cys82 side chain sulfur is the initial site of attack by the glutathione thiolate, then Bmp8-Cys85 would still be available to perform its catalytic function, leading to a second glutathionylation following an additional round of catalysis to afford doubly gluathionylated Bmp8, which we observed as the major gluathionylated species in the reaction with wildtype Bmp8 (**Figs. 4.4B** and **S4.6**, **Table S4.1**). On the other hand, if the Bmp8-Cys85 side chain were the initial site of attack, Bmp8 would have to be recycled back to its full reduced form before turnover could be restored, consistent with our observation of minor population of singly gluathionylated wildtype Bmp8 (**Figs. 4.4B** and **S4.6**, **Table S4.1**). Therefore, the fact that doubly gluathionylated species is the major species observed indicates a strong bias for nucleophilic attack on the side chain sulfur of Cys82, consistent with its resolving role. We further investigated whether adducts were formed upon incubation of Bmp8-Cys82 with **2** and **5**, and observed no change in mass, consistent with the relatively unproductive interaction of these

substrates with Bmp8 (**Fig. S4.16**). Having confirmed the mechanism for complementation of Cys82 by glutathione, we further sought to explore an evolutionary justification for conservation of the CXXC motif among Bmp8 homologs.

The proposed role for the resolving Cys residue in 2-Cys peroxiredoxins is to protect that attacking Cys thiol from over-oxidation (i.e. to sulfinic acid, Cys-*S*-O_2H), which leads to inactivation of the enzyme[92]. Hence, we reasoned that Bmp8-Cys82 may serve the evolutionary function of protecting Bmp8-Cys85 from over-oxidation. Moreover, if Bmp8-Cys85 is susceptible to over-oxidation Bmp8:C82A should be capable of multiple turnovers in the absence of an exogenous reducing agent, where water rather than glutathione might serve as the exogenous resolving nucleophile. Indeed, incubation of Bmp8:C82A as-purified with a 2-fold excess of **3** in the absence of glutathione lead to complete conversion to **2** and **4** in contrast to only partial conversion observed for the wildtype enzyme treated with a 2-fold excess of **3** (**Fig. 4.4A**). To verify the formation of a sulfinic acid species with side chain thiol of Bmp8-Cys85, we monitored Bmp8:C82A by whole-protein mass spectrometry before and after the addition of **3** in the absence of an exogenous reductant. Addition of **3** to Bmp8:C82A in the absence of glutathione lead to an observed mass shift consistent consistent with the formation of a sulfinic acid species (i.e., + 2[O]) (**Figs. 4.4C** and **S4.6, Table S4.1**). In contrast, pre-incubation of Bmp8:C82A with DTT (an alternative reductant to glutathione) lead to no change in mass upon addition of **3**, further supporting that the mass shift observed in the absence of reductant is due to over-oxidation (**Figs. 4.4A,C** and **S4.6**, **Table S4.1**). We additionally showed that the

Bmp8 mechanism does not involve molecular oxygen by perform the reaction under anaerobic conditions; hence the apparent addition of oxygen is likely due to hydroxylation by water rather than addition of molecular oxygen (**Fig. S4.14**). To resolve the site of proposed hydroxylation, we additionally monitored Bmp8:C85A and wildtype Bmp8 before and after addition of **3** in the absence an exogenous reductant. Upon addition of **3**, wildtype Bmp8 exhibited a subtle but significant downshift in mass likely due to disulfide bridge formation, while no mass shift was observed for Bmp8:C85A treated with **3**, coincident with its lack of activity (**Fig. 4.4C, Fig. S4.6, Table S4.1**). Hence we deduced that over-oxidation in Bmp8:C82A takes place on the side chain thiolate of Bmp8-Cys85. Taken together these results indicate that Bmp8-Cys85 is essential for activity, while Bmp8-Cys82 protects Bmp8-Cys85 from over-oxidation. We next explored the role of the His and Tyr residues of the CXYCXXH motif conserved among Bmp8 homologs.

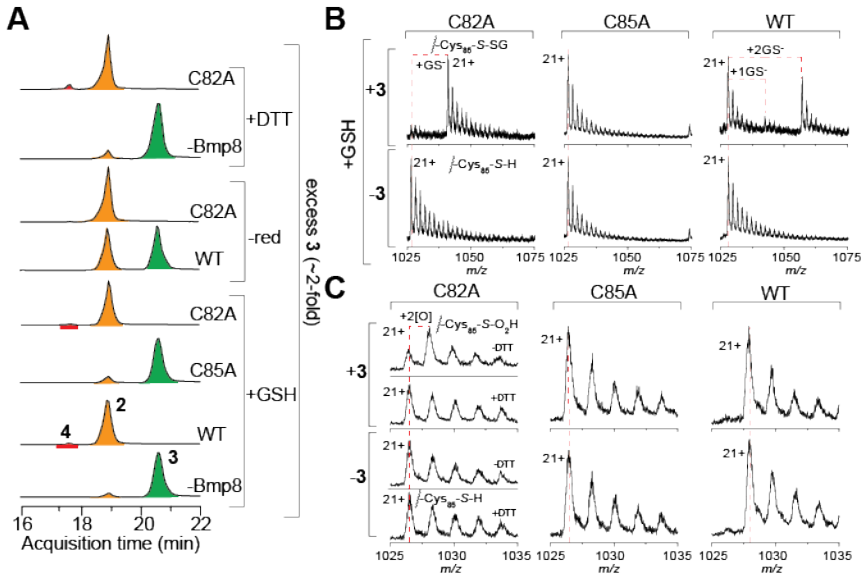

Figure 4.4: Biochemical interrogation of Bmp8-CXXC. (**A**) Combined EICs for predicted *m/*z's of $[M-H]^{1-}$ ions corresponding to 2 (highlighted orange), 3 (highlighted green), and 4 (highlighted red) for organic extracts of reactions consisting of Bmp8:C82A (C82A), Bmp:C85A (C85A), or wildtype Bmp8 (WT) incubated with a 2-fold excess of 3 and with reductants (GSH or DTT), and without reductants (-red); all reactions were quenched after a fixed incubation time of 30 min. (**B**)-(**C**) Mass spectra corresponding to the 21+ ion for Bmp8:C82A (C82A), Bmp:C85A (C85A), and wildtype Bmp8 (WT) incubated under various conditions before and after addition of a 2-fold excess of 3; red dashed lines indicated peak-to-peak alignments between treatments. Mass calculations for panels 'B' and 'C' are detailed in Fig. S6 and Table S1.

The YCXXH portion of the motif conserved among Bmp8 homologs suggests a potential Cys-Try-His catalytic triad essential to the reaction mechanism. To investigate the role of the conserved His residue, we performed site-directed mutagenesis of Bmp8-His88 to Val (Bmp8:H88V). Incubation of Bmp8:H88V with a 2-fold excess of **3** and glutathione led to no turnover, in support of its role in the Bmp8 reaction mechanism (**Fig. 4.5A,B**). Attempts to characterize the role of the conserved Tyr residue Bmp8-Tyr84 were precluded by insolubility of both Bmp8-Tyr84 to Phe and Ile mutants, perhaps supporting a stabilizing role for Tyr84. We further explored the relevance of the conserved CXYCXXH motif in predicting

bromopyrrole dehalogenation activity. Among the hits from our query of genomic databases with the sequence of Bmp8 was a distant *Pseudoalteromonas luteoviolacea* 2ta16 homolog (2ta16_Bmp8-H; 55% Mm_Bmp8) from the genetic context of ORFs putatively encoding enzymes involved in the electron transport, suggestive of a role in scavenging reactive oxygen species[93] (**Figs. 4.5A**, **S4.3**, and **S4.7**). Notably, *P. luteoviolacea* 2ta16 also contains a functional Bmp8 homolog from the context of the Bmp pathway (2ta16_Bmp8), which possesses even lower pairwise amino acid similarity to 2ta16_Bmp8-H than does *M. mediterranea* MMB-1 Bmp8 (48.5% for 2ta16_Bmp8 as compared to 55% for Mm_Bmp8) (**Fig. S4.8**). We expressed and purified ~22 kDa 2ta16_Bmp8-H and incubated the purified recombinant protein with a 2-fold excess of **3** and glutathione. Incubation of the reaction with 2ta16_Bmp8-H lead to partial conversion **3** to **2** for the same period in which full conversion was observed for incubation with Bmp8, while extended incubation time led to complete conversion of **3** to **2** and **4** (**Figs. 4.5B** and **S4.7**). Individual point mutagenesis of the the Cys and His residues of the CXYCXXH motif of 2ta16_Bmp8-H led to the same activity profile as exhibited for the corresponding Bmp8 mutants, implying an analogous dehalogenation reaction mechanism involving these conserved residues (**Fig. 4.5A,B**). Although lack of solubility precluded characterization of Bmp8-Y84F, the corresponding Tyr to Phe mutant of 2ta16_Bmp8-H (Bmp8-H:Y80F) was soluble, and demonstrated loss of activity with respect to dehalogenation of **3** (**Fig. 4.5B**). As Tyr and Phe only differ by a hydroxyl group, this result suggests a stabilizing hydrogen-bonding role for the conserved Tyr residue in 2ta16_Bmp8-H, and by proxy in Bmp8.

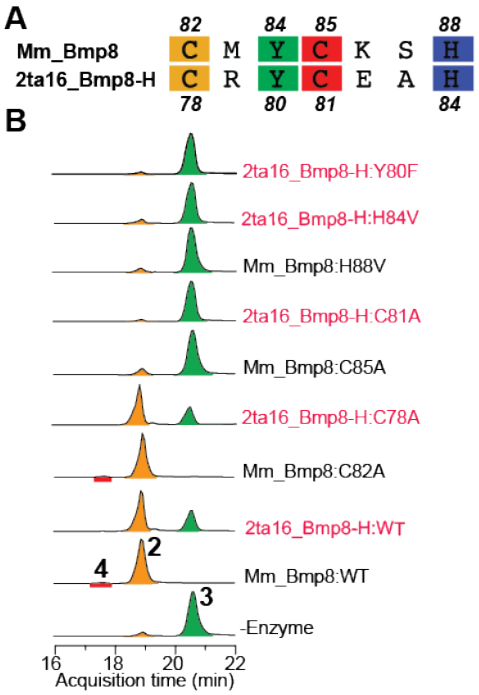

Figure 4.5: Biochemical interrogation of the conserved CXYCXXH of Mm_Bmp8 and a distant homolog 2ta16_Bmp8-H. (**A**) Alignment (MAFFT) of *M. mediterranea* Bmp8 (Mm_Bmp8) with a distant *P. luteoviolacea* 2ta16 Bmp8 homolog (2ta16_Bmp8-H; GenBank WP_023399179.1) conserved residues corresponding to catalytic triad highlighted in colors with corresponding residues. (**B**) Combined EICs for predicted *m/*z's of $[M-H]^{-1}$ ions corresponding to 2 (highlighted orange), 3 (highlighted green), and 4 (highlighted red) for Mm_Bmp8 ('Bmp8' in main text) and 2ta16_Bmp8-H (Bmp8-H, font colored red to distinguish from Bmp8) wild type enzymes (WT) and corresponding putative catalytic triad mutants for enzymes incubated with 3 and glutathione for a fixed reaction time (30 min); Bmp8-Y84F precluded is excluded due to insolubility of the recombinant enzyme.

Based on our mutagenesis experiments, we propose a mechanism for Bmp8 beginning with the shuttling of a proton from the thiol of Bmp8-Cys85 via Bmp8-His88 to the 2-position of **3** (**Fig. 16**). We next propose one of two mechanistic routes for dehalogenation **3** that each converge on the formation of a disulfide bridge between Bmp8-Cys82 and Bmp8-Cys85. In the first route ('i' in Fig. 4.6) the side chain thiolate of Bmp8-Cys85 would attack at the 2-position of **3**, resulting in

displacement of bromide and the formation of a stable thioether bond with the pyrrole. Bmp8-Cys82 would then perform a nucleophilic attack on the thioether resulting in liberation of **2** and formation of a disulfide bridge. This route is similar to that employed by the CXXC-containing disulfide bond exchange protein DsbB, whose Cys44 side chain thiolate forms a thioether bond with its charge-transfer partner ubiquinone that is displaced by nucleophilic attack by the side chain thiolate of Cys41[94]. This route is also analogous to that proposed for glutathione *S*-transferase reductive dehalogenases, which begins with a chloride-displacing glutathionylation of the substrate tetrachlorohydroquinone, followed by the release of the substrate via a disulfide-exchange reaction with a catalytic Cys residue in the enzyme active site[95,96]. The fact that glutathione is able to dehalogenate **3** non-enzymatically, may therefore lend support to this mechanistic route. The second route ('ii' in Fig. 4.6) is inspired by the mechanism for 2-Cys peroxiredoxins in which a sulfenic acid species (Cys-*S*-OH) is formed upon the initial attack of the catalytic cysteine residue side chain thiolate on the peroxide [91]. In this alternate route, Bmp8-Cys85 would directly attack bromine to form a Cys-*S*-Br species, with the concomitant release of **2**. Subsequent nucleophilic attack of the thioether by the Bmp8-Cys82 side chain thiolate would release bromide, leading to disulfide bond formation. An analogous mechanism to route 'ii' has been proposed in the mechanism peroxiredoxin-like selenoprotein thyroxine (thyroid hormone) deiodinases in which a redox active selenocysteine residue side chain selenol (in place of a cysteine side chain thiol) forms a putative transient selenyl-iodide adduct that is displaced by a resolving cysteine residue side chain thiolate[97]. While a selynyl-iodide intermediate has never been detected on a

deiodinase, formation of a selynyl-iodide intermediate has been detected in a sterically stabilized model organoselenol compound[98]. Unfortunately, we were unable to obtain evidence to decisively favor one route over another.

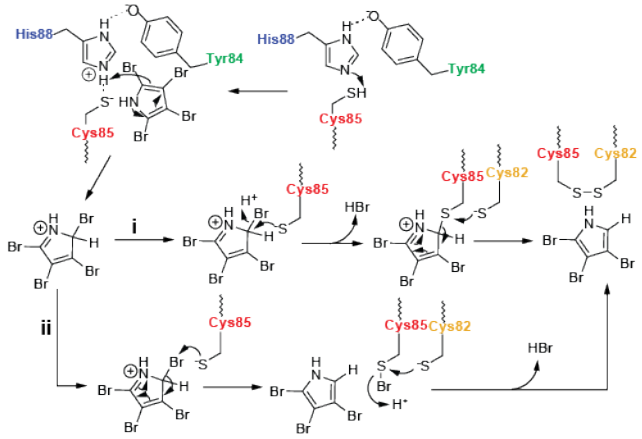

Figure 4.6: Bmp8 mechanistic proposal. Mechanistic proposal for dehalogenation of 3 by Bmp8; Mm_Bmp8 catalytic triad residues are color-coded according to panel 'A'. Conserved residues are color-coded according to the alignment shown in Fig. 5A.

In characterizing Bmp8 we demonstrate a rare example of a cofactor-independent reductive dehalogenase from a confirmed physiological context. While dehalogenation has been implied in the course of biosynthesis of natural products involving cryptic substrate-activating halogenation reactions[45,61,72,73], to the best of our knowledge Bmp8 is the first example of a dedicated tailoring dehalogenase enzyme from the confirmed context of a natural product biosynthetic pathway. Moreover, while a variety of enzymes have been identified based on their ability to dehalogenate man-made organohalogens[71,83,84], the physiological nature of these transformations is speculative. To best of our knowledge, the only other examples of dehalogenases for which a physiological context is known are transmembrane flavoprotein and selenoprotein deiodinases involved in the activation-inactivation and catabolism of thyroid hormone and thyroid hormone iodotyrosine biosynthetic

byproducts[7,74,99]. Of relevance to Bmp8, the selenoprotein deiodinases utilize a co-factor-independent reaction mechanism akin to 2-Cys peroxiredoxins in which an active site selenocysteine residue serves as the electron donor in places of a redox active cysteine residue [97]. Bmp8 bears no sequence homology to selenoprotein deiodinases, which are distantly related to 2-Cys peroxiredoxins, while Bmp8 bears homology to thioredoxins with peroxidase activity (e.g., AhpD). Therefore, the dehalogenation mechanism employed Bmp8 and selenoprotein deiodinases appears to be an example of convergent evolution. With respect to additional dehalogenases utilizing redox thiolate mechanisms, glutathione *S*-transferase-like enzymes involved in putative chlorophenol degradative pathway utilize a glutathione-dependent mechanism, as opposed to a mechanism that can be complemented by glutathione[95,100-103]. It is worth noting here that glutathione may not be the physiological or sole means of regenerating Bmp8. Indeed, the fact that we were able to observe stable glutathionylated forms of Bmp8, suggest that its mechanism for recycling is inefficient. While glutathione occurs at high (mM) intracellular concentrations in bacterial cells [104], and has been suggested as the redox partner for 1-Cys peroxidases that lack a resolving cysteine residue [91], alternative regeneration systems may also be employed in the *in vivo* regeneration of Bmp8. For example, peroxidase activity of *M. tubercuolosis* AhpD can be recycled by a surrogate electron donor NADPH-dependent flavoprotein thioredoxin reductase AhpF, an alternative electron donor for peroxiredoxin AhpC[87]. Although no dedicated thioredoxin reductase is encoded in the Bmp gene cluster, homologs of AhpF are present in the

genomes of strains harboring the Bmp pathway, and therefore may serve as opportunistic redox partners for Bmp8.

The importance of dehalogenation biocatalysts in bioremediation invites speculation on the biotechnological potential of Bmp8. The major class of reductive aromatic organohalogen dehalogenases studied to-date are transmembrane oxygen-sensitive cobalamin-dependent enzymes that, despite decades of study and identification of hundreds of homologs, have proved experimentally intractable [86]. By contrast, Bmp8 operates freely under aerobic conditions utilizing a simple cofactor-independent reaction mechanism that provides a promising platform for protein engineering. Indeed, we showed that a simple conserved CXYCXXH sequence motif is sufficient to predict bromopyrrole dehalogenase activity in a distantly related homolog, suggesting a potential for engineering of novel substrate scope by manipulation of the enzyme scaffold. Further, it has been shown that the simple alteration of the variable residues of CXXC motifs is sufficient for tuning the redox potential of the catalytic cysteine residue[105]. Our discovery of a tailoring dehalogenase from a natural product biosynthetic context further brings to light elucidation of organohalogen natural product biosynthesis as a paradigm for the elucidation of novel dehalogenation enzymology acting on diverse substrate scaffolds.

Our initial exploration of Bmp8 was initially motivated by its biosynthetic role, which is essentially that of an enzymatic switch that repurposes an otherwise dead-end product **3** into an intermediate **2** in the biosynthesis of **1**. In effect, Bmp8 delivers back-end regiocontrol following regiopromiscuous decarboxylative

halogenation by flavin-dependent halogenase-Bmp2. Further, given the well-defined ecological function of **3** as a chemoattractant settlement cue for coral larvae, it is interesting to consider the ecological consequence of Bmp8, which routes **3** into the considerably more energetically synthesis of **1**[80]. Indeed, producers of **3** such as *P.* sp. PS5 seem to harbor only the Bmp bromopyrrole biosynthetic module, and lack Bmp8 and hence the capacity to synthesize **2** enzymatically[16]. While both **1** and **2** have been shown to possess feeding deterrent and antimicrobial activities[75,106-108], it remains to be seen whether their ecological functions are redundant to or different from that of upstream **3**—an intriguing case of biosynthesis motivating ecology.

4.3 Supplementary Information

4.4.1 Materials & Methods

Preparation and characterization of halopyrroles. *Preparation:* 2,3,4,5-tetrabromopyrrole (**3**) and 2,3,4-tribromopyrrole (**2**) were synthesized as previously described [16]. 3,5-dibromopyrrole (**4**) was prepared enzymatically. Briefly, ten 1 mL reactions consisting of 10 μM Bmp8, 100 μM **3**, and 10 mM TCEP (to recycle Bmp8) were incubated in buffer (20 mM Tris-HCl pH 8 and 10% glycerol) for 12 h at 30 ºC. These conditions results in major production of a compound with molecular formula $C_4H_3Br_2N$ as determined by HRMS with trace intermediary **2** remaining. **4** was purified by HPLC using a reverse-phase C_{18} column (Phenomenex Luna, 5 μM particles size, 100 Å pore size, 250 mm x 10 mm) the following gradient with Buffer 'A' (H_2O + 0.1% TFA), Buffer 'B' (MeCN + 0.1% TFA): (initial flow rate 3 mL/min) 90% to 30 % A over 5 min, hold at 30% A for 5 min, (increase flow rate to 4 mL/min) to 0% A over 15 sec, hold at 0% A for 2 min, to 90% A over 15 sec, hold

at 90% 3 min. All halopyrroles were stored in DMSO at -20 ºC and were stable under repeated freeze-thaw. *Characteriziation*: The ^{1}H-NMR spectrum of **4** confirmed its symmetry, and the *J*-coupling constant of the symmetric C*H* of **4** matched to the literature value for the asymmetric *CH* of **2** [16], corroborating its assignment. **2,3,4,5-tetrachloropyrrole** was prepared in a manner analogous to **3**, using NCS in lieu of NBS [16]. The structure of the compound was confirmed by HRMS and ^{1}H-NMR. **4**: ^{1}H-NMR (600 MHz, CDCl3) delta 8.32 (bs, 1H, N*H*), 6.81 (d, J = 3 Hz, 2H), HRMS (ESI) $[M-H]^-$ *m/z* calculated for molecular formula $C_4H_3Br_2N$ 221.8599, found 221.8599; **2,3,4,5-tetrachloropyrrole**: ^{1}H-NMR (600 MHz, $CDCl_3$): 9.06 (bs, 1H, N*H*), HRMS (ESI) $[M-H]^-$ *m/z* calculated for molecular formula C_4HCl_4N is 201.8797, found 201.8790. The mass of the single product observed for incubation of 2,3,4,5-tetrachloropyrrole with Bmp8 was measured to be $[M-H]^-$ *m/z* 167.9162 (calculated for molecular formula $C_4H_2Cl_3N$ is 167.9180).

Cloning, expression, and purification of Mm_Bmp8. Expression of Bmp8 was achieved by co-expression of *Marinomonas mediterranea* MMB-1 *bmp8* (*Mm_bmp8*) along with *M. mediterranea* MMB-1 *bmp1(TE)* (*Mm_bmp1(TE)*). *Mm_bmp1(TE)* comprises residues 78-376 of Mm_Bmp1, previously identified as the thioesterase domain of ACP-TE didomain Bmp1 [16,50]. PCR-amplifed *Mm_bmp8* was ligated into the NdeI/XhoI sites of pET28a, which incorporates a N-terminal His_6-tag. *Mm_bmp1(TE)* was cloned into MCS-2 of pCDFDuet, which does not incorporate a His-tag. pET28-N-His_6-*Mm_bmp8* and pCDFDuet-*MM_bmp1(TE)* were co-transformed into *E. coli* BL21(GOLD). Expression was performed as by inoculation

of 1 L of terrific brother with 20 mL overnight culture with appropriate antibiotics. The culture was incubated for 6 h at 30 ºC with shaking at 200 rpm. Temperature was reduced to 18 ºC over 1 h followed by induced with 300 µL 1 M IPTG. The induced culture was incubated at 18 ºC for an additional 14 h. Cultures were harvested by centrifugation, the and the pellet was resuspended 20 mM Tris-HCl (pH 8.0), 500 mM NaCl, 10% glycerol buffer, and lysed by sonication. The supernatant was clarified by centrifugation and loaded on to a 5 mL His-Trap Ni-NTA column (GE Biosciences) equilibrated with harves buffer. The column was extensively washed with 20 mM Tris-HCl (pH 8.0), 1 M NaCl, 30mM imidazole buffer, and eluted by a linear gradient to 20 mM Tris-HCl (pH ~ 8.0), 1 M NaCl, 250 mM imidazole buffer across 20 column volumes. N-His_6-Bmp8 purified as a stand-alone purified protein, while Bmp1(TE) was observed in the flow through and wash by SDS-PAGE analysis. Purity of eluted proteins was checked by SDS-PAGE. To cleave the N-His_6 tag thrombin was added to purified N-His_6-Bmp8 to a final concentration of 1 unit/mg recombinant protein. The cleavage reaction mixture was transferred into dialysis tubing, and incubated overnight in 2 L 20 mM Tris-HCl (pH ~ 8.9), 50 mM KCl, 3 mM DTT buffer at 4 °C. The dialyzed protein was applied to a 5 mL ion exchange Q Sepharose FF column (GE Biosciences) equilibrated in dialysis buffer, and eluted using a linear gradient to 20 mM Tris-HCl (pH ~ 8.9), 1 M KCl buffer. Glycerol was added to the ion exchange fraction to a final concentration of 10% (w/v). Thrombin cleavage was verified by SDS-PAGE analysis (N-His_6-cleaved protein retains N-terminal-GSH after cleavage). Purifed Bmp8 was concentrated after ion exchange using an Amicon centrifugal filter with >10 kDA cut-off. Bmp8 mutants were

purified in the same way as for Bmp8. Bmp8-H was purified in the same manner as Bmp8, but without co-expression with Bmp1(TE).

Construction, expression, and purification of Mm_Bmp8 mutants. Expression constructs for Bmp8 mutants C57S, C82A, Y84F/I, C85A, H88V, and C163S were constructed by PCR point mutagenesis using pET28- *bmp8* as the template. Primers were designed with the motif 5′-[20 nucleotide sequence-modified overlap] [35 nucleotide primer region]-3′ followed by treatment with DpnI exonuclease, propagations in *E. coli* DH5✔ (NEB), Sanger sequencing verification (SeqXcel, La Jolla, CA), and transformation into *E. coli* BL21-Gold(DE3) (Agilent) for expression. Expression purification, and processing of Bmp8 mutants was performed in an identical manner as previously described for the purification of wild type Bmp8. Note that Bmp8 C57S, Y84F/I, and C163S were insoluble and therefore were not assayed.

Identification, cloning, mutagenesis, and expression of 2ta16_Bmp8-H and mutants. 2ta16_Bmp8-H (NCBI accession WP_023399179.1, 55% positives, expected value $2x10^{-35}$) was identified in the genome *Pseudoalteromonas luteoviolacea* 2ta16 by a BLASTP search of the genome-sequenced strains available in-house using *Marinomonas mediterranea* MMB-1 Bmp8 (Mm_Bmp8) as a query. Analogous residues to the proposed active site of Bmp8 were identified via a pairwise amino acid alignment using the EMBOSS Needle (EMBL-EBI) web tool. PCR-amplified *2ta16_bmp8-H* was cloned into the pET28a expression vector in identical manner to *Mm_bmp8* to afford pET28-*2ta16_bmp8-H*. Expression constructs for

Bmp8-H C78A, Y80F, H84V, and C81A we constructed by PCR mutagenesis of pET28-*bmp8-H* using the same methodology used for Bmp8 mutant constructs. N-His_6-tagged 2ta16_Bmp8-H and mutants expressed as soluble recombinant proteins without need for co-expression with a helper, but were otherwise expressed, purified, and processed in the same manner as previously described for Mm_Bmp8.

***In vitro* enzymatic activity assaying of Bmp8, 2ta16_Bmp8-H, and mutants.** Freshly purified Bmp8, Bmp8-H, or mutants thereof were assayed in 1 mL reactions with an incubation time of 30 min at 30 ºC in reaction buffer containing 20 mM Tris-HCl (pH 8), 50 mM KCl, and 10% glycerol. For reactions containing equimolar or excess substrate the enzyme concentration was set at 25 μM. To investigate metal-dependency, Bmp8 was pre-incubated with 1 mM EDTA at 30 ºC prior to the addition of substrate. Reactions with enzyme not pre-treated with EDTA were also pre-incubated for 1 h at 30 ºC prior to addition of substrate to account for loss of activity due to oxidation by molecular oxygen. Reactions with excess substrate were initiated by addition of **2** or **3** to a final concentration 50 μM (~ 2-fold excess to enzyme). The volumes of no-enzyme negative control reactions were adjusted with an appropriate concentration of reaction buffer and substrate was added to the same concentration as for the corresponding enzymatic reaction. Enzymes were recycled by addition of glutathione to a final concentration of 1 mM (40-fold excess to enzyme). Reactions were quenched by addition of the whole reaction to 1.9 mL EtOAc followed by mixing by vortex mixing and separation by centrifugation. The organic layer was collected and the solvent removed *in vacuo* at 30 ºC. The resulting residue was dissolved in 100 μL MeOH for LC/MS analysis.

LC/MS analysis of *in vitro* enzyme assays. Extracts of *in vitro* enzyme assays were analyzed by LC/MS 30 μL of sample (in MeOH) on a reverse phase C_{18} column (Phenomenex Luna, 5 μm, 4.6 × 100 mm) operating on an Agilent 1260 HPLC in tandem to an Agilent 6530 Accurate Mass Q-TOF mass spectrometer. Mass spectra were acquired in negative ionization mode. HPLC solvents used were water + 0.1 % formic acid (A) and MeCN + 0.1 % formic acid (B). The HPLC elution profile was as follows: (initial flow rate 0.5 mL/min) 10% B for 5 min, linear gradient to 70% B over 10 min, linear increase to 80% B over 10 min, (flow rate changed to 0.7 mL/min) linear increase to 100% B over 0.5 min, hold at 100% B for 3 min, linear decrease to 10% B over 0.5 min. Identical injection volumes were used within a given experiment.

Mass spectrometric analysis of trypsin-digested Bmp8-CXXC. Reactions consisting of Bmp8 (50 μM) and **3** (100 μM) or an equivalent of reaction buffer (20 mM Tris-HCl pH ~ 8, 50 mM KCl, 10 % glycerol) in a total volume of 100 μL reaction buffer. Reactions were incubated for 1 h at 30 ºC, flash frozen in an acetone/dry ice bath, and stored at -80 ºC prior to analysis. To minimize ambient oxidation, reactions were thawed immediately prior to injection of 15 μL of the sample onto a C_4 column (Higgins Analytical PROTO 300, 5 μm, 250 x 4.6 mm) operating on an Agilent 1260 HPLC in tandem to an Agilent 6530 Accurate Mass Q-TOF mass spectrometer. Mass spectra were acquired in positive ionization mode. HPLC solvents used were water + 0.1% formic acid (A) and MeCN + 0.1% (B). The

elution profile was as follows (flow rate: 0.7 mL/min): 10% B for 10 min, linear increase to 30% B over 5 min, linear increase to 70% B over 40 min, linear decrease to 10% B over 5 min, linear increase to 100% B over 1 min followed by 2 min at 100% B, decrease to 10% B over 1 min, 10% B for 2 min and 5 min of post-time equilibration. Fragment of interest were search using the extracted ion chromatogram feature in Agilent MassHunter software searching for MS1 masses predicted for predicted trypsin-digest fragments (ExPASy PeptideMass web tool) of interest in a range of ± *m/z* 0.1.

Mass spectrometric analysis of trypsin-digested alkylated Bmp8-CXXC. Reactions consisting of Bmp8 (50 μM) and **3** (100 μM) or an equivalent of reaction buffer (20 mM Tris-HCl pH ~ 8, 50 mM KCl, 10 % glycerol) in a total volume of 100 μL reaction buffer. To check the initial redox state of the Bmp8-CXXC, one of two reactions without **3** was immediately quenched with 10 μL of 1 M iodoacetamide, incubated for 30 min at 30 ºC, then flash frozen in acetone/dry ice and store at -80 ºC prior to further work-up. The additional reactions with and without **3** were were incubated for 1 h at 30 ºC then quenched with 10 μL 1 M iodoacetamide, incubated for an additional 30 min at 30 ºC, flash frozen, and stored at -80 ºC. Thawed reactions were digested with 1 μg of proteomics grade trypsin (Sigma) for 1 h, then flash frozen and stored at -80 ºC prior to analysis. LC/MS analysis was performed as previously described above for the analysis of trypsin-digested Bmp8-CXXC without alkylation.

Whole-protein mass spectrometric analysis. Reactions consisting of wildtype Bmp8, Bmp8:C82A, or Bmp8:C85A (50 μM) in buffer (20 mM Tris-HCl pH ~ 8, 50 mM KCl, 10% glycerol, and 1 mM GSH or DTT for reactions containing reductants) were analyzed before and immediately after addition of **3** (100 μM). Additional reactions without **3** were incubated in parallel and analyzed at the end of each sequence to ensure that any modifications to the proteins were due to the addition of **3** rather than the result of extended incubation. Reactions were analyzed by direct injection of 60 μL of the reaction onto an Agilent 1260 HPLC in tandem to an Agilent 6530 Accurate Mass Q-TOF mass spectrometer at an injection speed of 1 mL/min maintaining a flow of water (+0.1 % formic acid) at flow rate of 0.7 mL/min held over 2 min.

Data analysis and plotting. LC/MS data was analyzed and visualized using the Agilent MassHunter software package. For enzyme activity assays, extracted ion chromatograms were called using the calculated *m/z* for the $[M-H]^{1-}$ ± 0.1 for the most abundant M+2 isotope corresponding to a give halogenated pyrrole species. For peptides extracted ion chromatograms were extracted survey for the most abundant species predicted *m/z* for $[M+ZH]^{Z+}$ surveyed over a range of charges Z (integer > 0). Whole protein mass spectra were extracted by average over the elution peak over a fixed interval. Mass spectral isotope predictions were obtained using the Agilent Isotope Distribution Calculator tool, which is part of the MassHunter software suite. Data was exported from MassHunter and re-plotted in OriginPro (OriginLab), and figures were assembled in Adobe Illustrator (Adobe). Chromatograms corresponding

to sets of experiments are normalized to the largest peak among spectra, while individual chromatograms are normalized to the largest peak within a given chromatogram.

4.4.2 Supplementary Figures

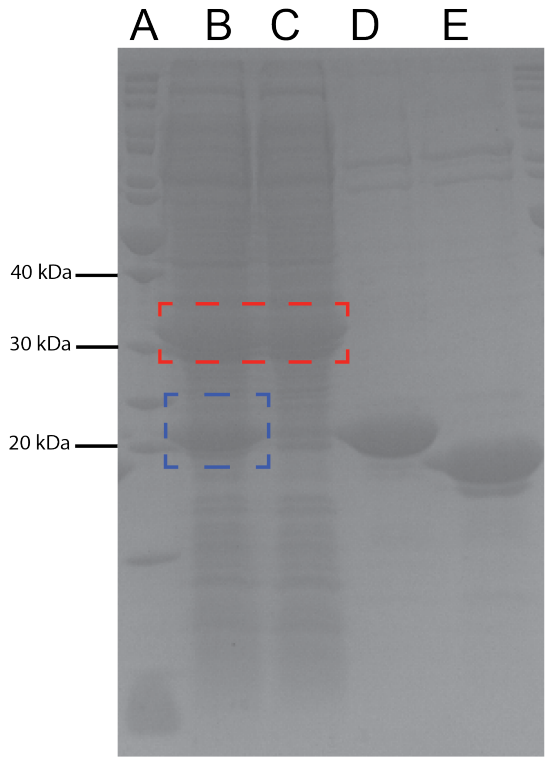

Figure S4.1: Affinity purification of N-His$_6$-Bmp8 by co-expression with Bmp1(TE), and cleavage of N-His$_6$ affinity tag. Bmp8 analyzed by SDS-PAGE gel. Expected molecular weights are as follows: Bmp1(78-376, TE)-33.442 kDa, N-His$_6$-Bmp8-23.086 kDa, and N-GSH-Bmp8-21.566 kDA (N-terminal GSH remains post-cleavage). SDS-PAGE lanes are as follows: (**A**) Protein molecular weight ladder (Fisher Scientific BP3602), (**B**) Crude lysate of *E. coli* co-expressing N-His$_6$-Bmp8 (band boxed in blue) and Bmp1(TE) (band boxed in red), (**C**) Pre-wash flow-through from Ni^+-affinity column, (**D**) Purified N-His$_6$-Bmp8, (**E**) Ion-exchange-purified N-His$_6$-tag-cleaved N-GSH-Bmp8.

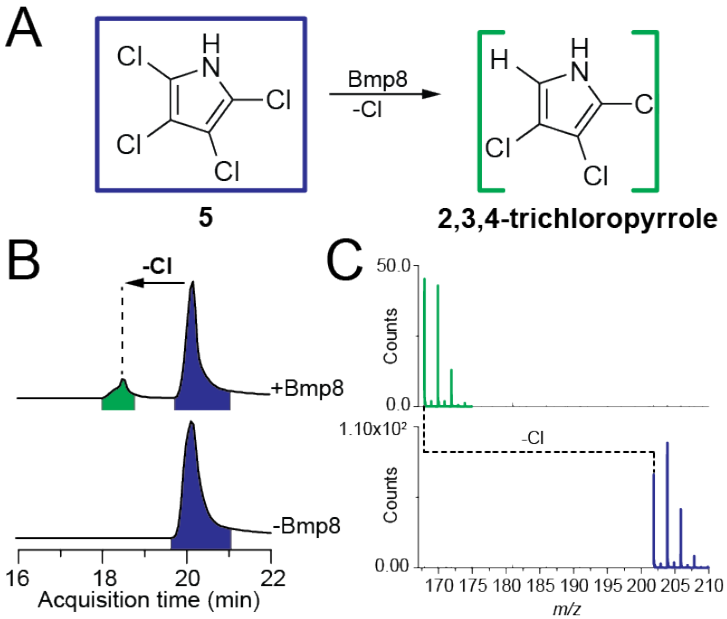

Figure S4.2. Dechlorination of 2,3,4,5-tetrachloropyrrole catalyzed by Bmp8. (**A**) Scheme for dechlorination 5 to 2,3,4-trichloropyrrole (regiospecificity inferred from dehalogenation of **3**). (**B**) Combined EICs for predicted *m/z* $[M-H]^-$ ions corresponding to molecular formulae C_4NHCl_4 (**5**) and trichloropyrrole ($C_4NH_2Cl_3$) for reactions consisting of synthetically prepared **5** (100 µM) incubated with and without excess glutathione (2 mM) with and without Bmp8 (25 µM) in reaction buffer (20 mM Tris-HCl pH ~ 8, 50 mM KCl, 10% glycerol) for 30 min. at 30 ºC. (**C**) Mass spectra corresponding to the shaded peaks shown in panel 'B' exhibiting the anticipate isotopic distribution for tetra- and tri- chlorinated compounds, and illustrating the peak-to-peak mass difference corresponding to loss of chlorine.

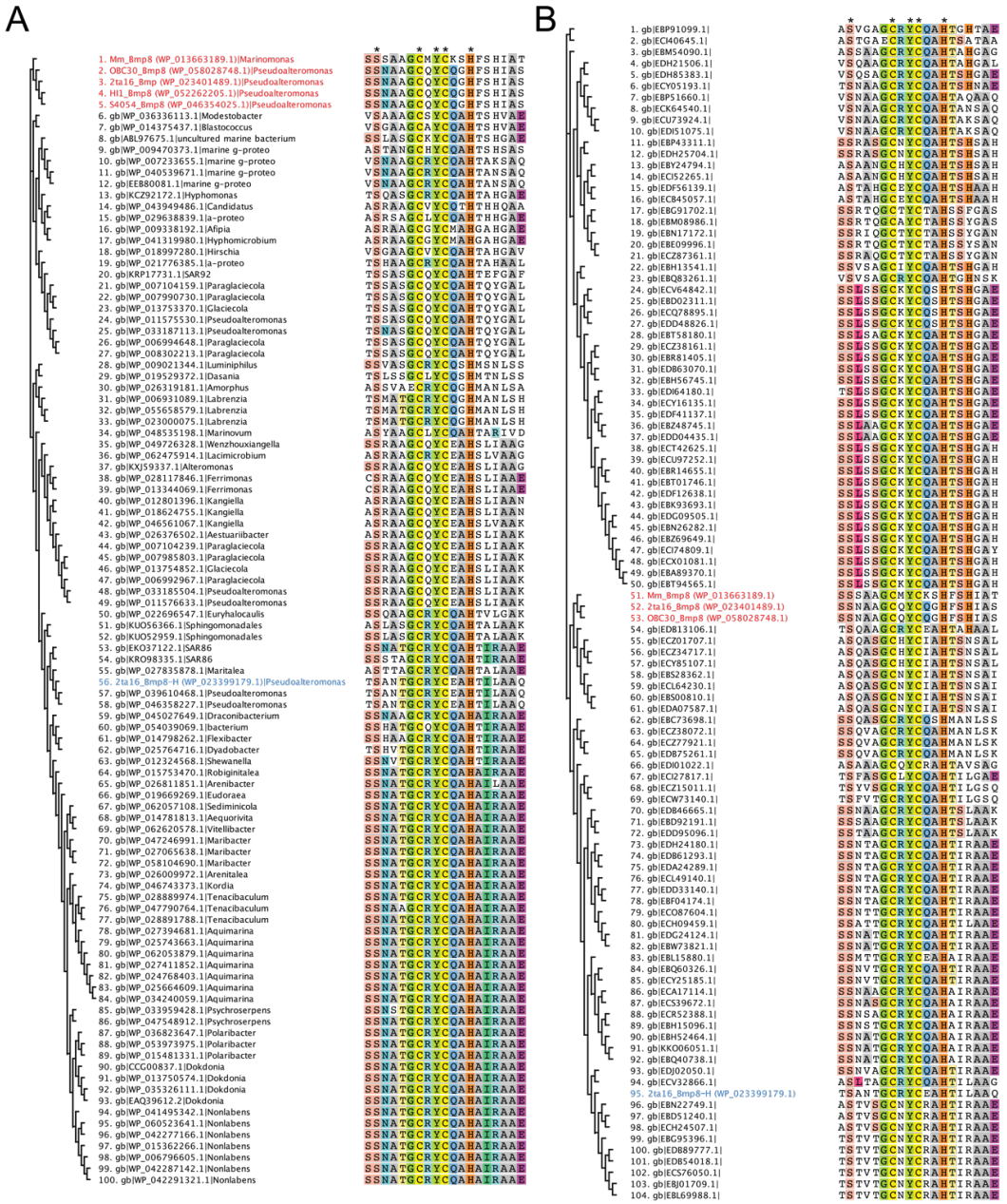

Figure S4.3: Bmp8 homologs from (meta)genomic datasets. Alignment (MAFFT) focusing on conserved residues in the vicinity of the active site of Bmp8 ('*' above indicates residues conserved in this region for all sequences) with reference distance trees (Geneious, Jukes-Cantor, Neighbor-Joining) for top ~100 query hits (BLASTP, expected value cut-off of 10, default parameters) for query *M. mediterranea* MMB-1 Bmp8 (Mm_Bmp8) from (**A**) GenBank non-redundant protein database (nr) and (**B**) Genbank environmental metagenomics database (env_nr). Bmp8 homologs found in the genetic context of the whole or partial Bmp gene locus are labeled in red and included for reference with the metagenomics hits in panel 'B'. Bmp-harboring *P. luteoviolacea* 2ta16 includes a second non-Bmp Bmp8 homolog 2ta16_Bmp8-H highlighted in blue and also included in panel 'B'. Sequences are labeled with GenBank accession numbers, and, in panel 'A' are labeled with derivative genera.

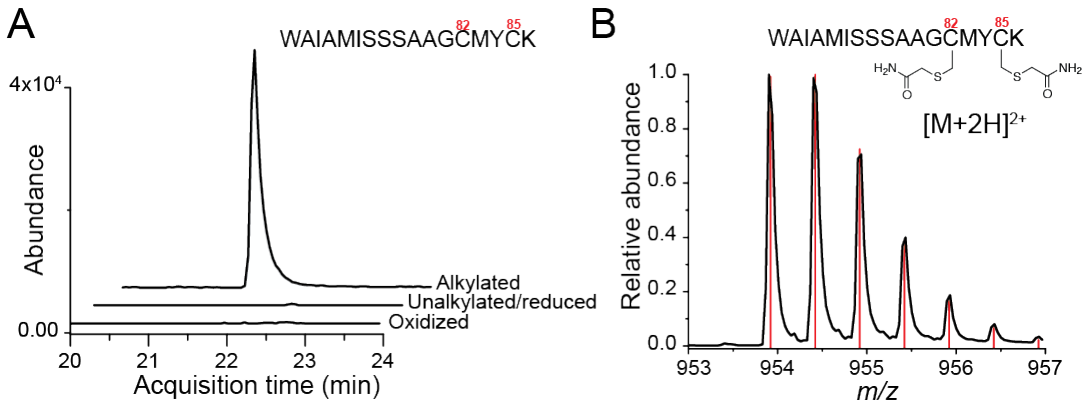

Figure S4.4: Bmp8-CXXC is reduced in enzyme as-purified. To verify that the initial redox state of Bmp8-CXXC, intact Bmp8 was treated with iodoacetamide then trypsin-digested, as described in the 'Materials and Methods.' (**A**) EICs for the trypsin digested fraction containing Bmp8-CXXC for the *m/z* predicted for the $[M+2H]^{2+}$ of the oxidized, unalkylated/reduced, and alkylated fragments. Only the alkylated fragment was detected demonstrating that Bmp8-CXXC is in the fully reduced state as-purified, and that alkylation of the Bmp8-CXXC of intact Bmp8 goes to completion. (**B**) Mass spectrum corresponding to the depicted $[M+2H]^{2+}$ of the alkylated Bmp8-CXXC-containing digested fragment averaged over the correspond EIC peak in panel 'A' (black). The predicted isotope distribution is indicated by the red lines.

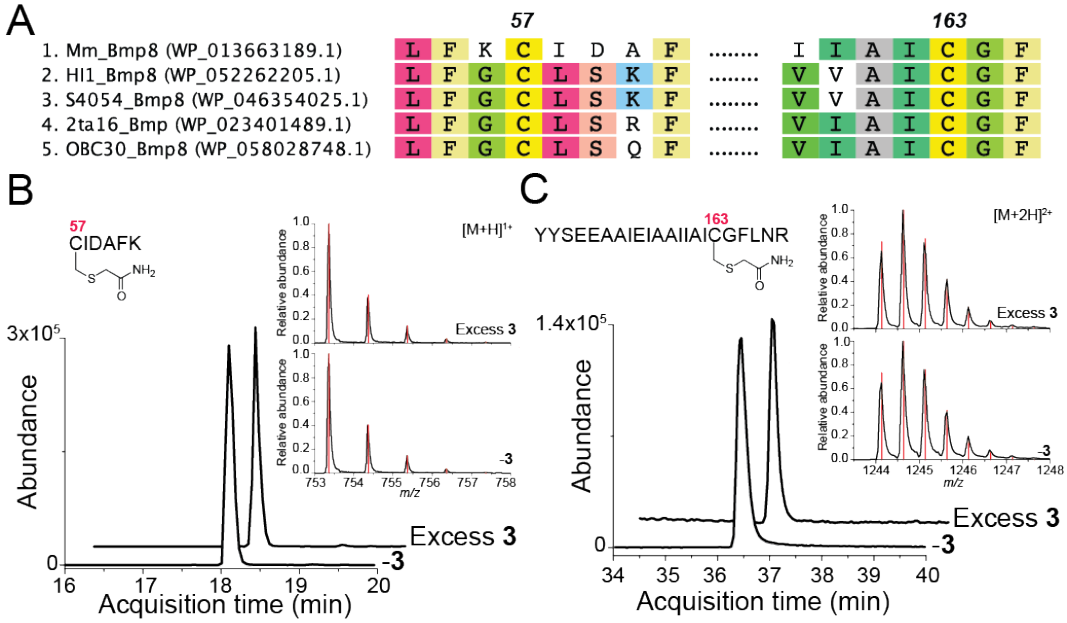

Figure S4.5: Conserved Bmp8 Cys57 and Cys163 do not play a direct role in Bmp8 reaction mechanism. The state of the additional Bmp cysteine residues, Cys57 and Cys163 was investigated for Bmp8 incubated with and without 3, alkylated, and trypsin-digested as described in the 'Materials and Methods.' (**A**) Alignment (MAFFT) of Bmp8 homologs found in the genetic context of the Bmp pathway with conserved Mm_Bmp8-Cys57 and Cys163 indicated above. (**B**) EICs for the predicted *m/z* of the $[M+2H]^{2+}$ ion corresponding to the alkylated trypsin-digested fragment containing Bmp8-Cys57 for Bmp8 incubated with and without **3** with corresponding mass spectra averaged over EIC peaks (black) with predicted isotope distributions indicated by the red lines. (**C**) EICs for predicted *m/z* of the $[M+H]^{1+}$ ion corresponding to alkylated trypsin-digested fragment containing Bmp8-Cys163 for Bmp8 incubated with and without **3** and corresponding mass spectra averaged over EIC peaks (black) with predicted isotope distributions indicated by the red lines.

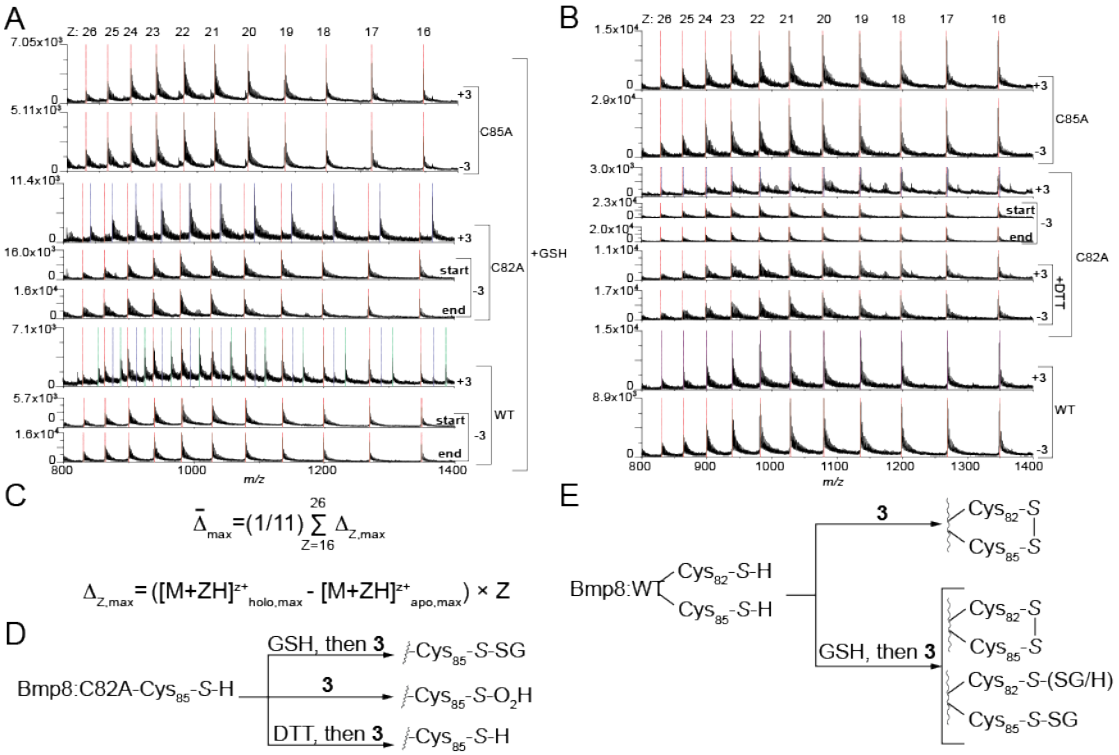

Figure S4.6: Whole-protein mass spectra for wildtype Bmp8 and Bmp8 Cys to Ala mutants under various conditions. (**A**)-(**B**) Mass spectra for Bmp8-WT (WT), Bmp8-C82A (C82A), and Bmp8-C85A (C85A) before and after treatment with **3**. For spectra labeled with 'start' or 'end', 'start' refers to the sample before addition of 3, while 'end' refers to a separate reaction without 3 incubated in parallel as a negative control intended to demonstrate that observed mass shifts are due to the addition of **3** as opposed to extended incubation times. Charge states corresponding to each population are indicated at the top of panels 'A' and 'B', while masses predicted for the maximum isotope for each $[M+ZH]^{Z+}$ ion are indicated by the red lines for the 'apo' form, and blue lines for the 'holo' adduct-bound (+SG or +2[O]) forms; the +2SG predicted mass for 'WT +**3**' is indicated in green. (**C**) Calculation of the mean peak-to-peak difference ($\bar{\Delta}_{max}$) between 'holo' adduct-bound Bmp8-C82A and 'apo' Bmp8-C82A taken as the mean of differences for a given charge Z ($\Delta_{max,Z}$) over Z = 16 to 26; values are shown in Table S1. (**D**)-(**E**) Proposed adducts formed with Bmp8:C82A and Bmp8:WT for different treatments based on calculated $\bar{\Delta}_{max}$ in Table S1.

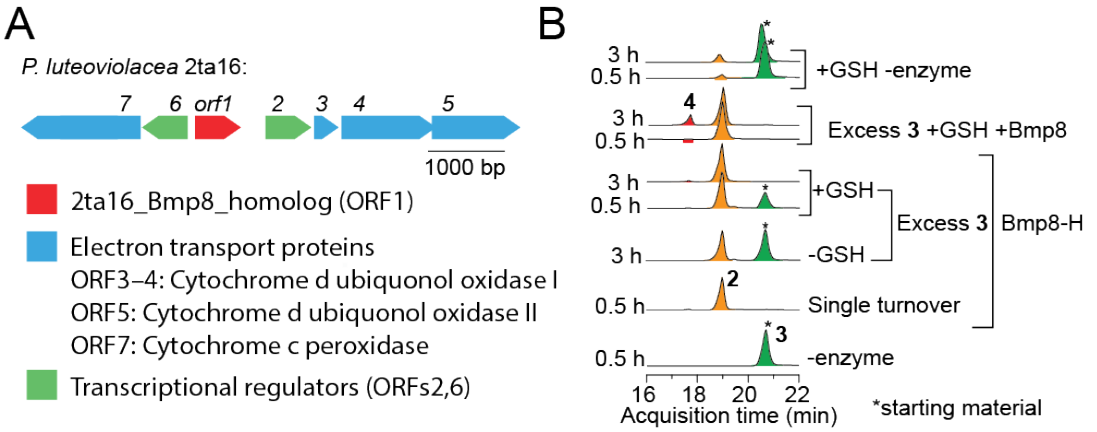

Figure S4.7: A distant Bmp8 homolog from *P. luteovioalcea* 2ta16, 2ta16_Bmp-H. (**A**) Genetic context for the 2ta16_Bmp8_homolog (2ta16_Bmp8-H) from *P. luteoviolacea* 2ta16 (GenBank WP_023399179.1). (**B**) 2ta16_Bmp8-H and Mm_Bmp8 were incubated with 3 as described in the 'Materials and Methods' and reactions were quenched by extraction with two volumes at EtOAc after incubation for 0.5 or 3 h. The figure shows combined EICs for predicted of *m/z*'s of $[M-H]^{1-}$ ions for **2**, **3**, and **4** for extracts analyzed as described in the 'Materials and Methods.'

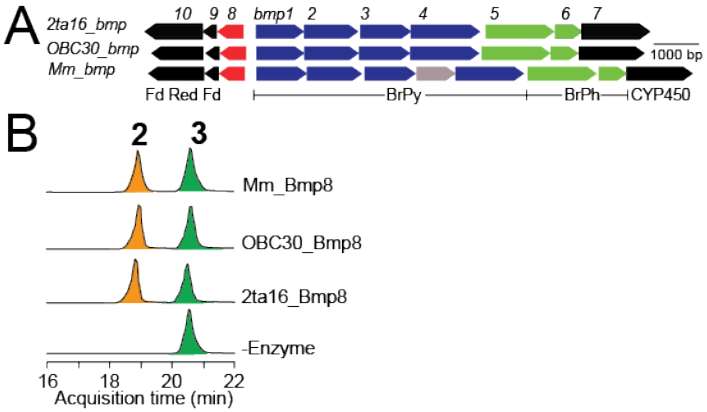

Figure S4.8: Functional characterization for Bmp8 homologs from Bmp pathways harbored by two additional marine bacteria. (**A**) Bmp gene cluster from *P. luteoviolacea* 2ta16 (*2ta16_bmp*), *P. phenolica* O-BC30 (*OBC30_bmp*), and *M. mediterranea* (*Mm_bmp*). (**B**) Activity of Bmp8 homologs expressed and purified as described for Mm_Bmp8 in the materials and methods for enzyme incubated with ~2-fold excess of 3 for a reaction time of 30 min. Traces represent combined EIC's for the predicted $[M-H]^{1-}$ for 3 (peak shaded green) and 2 (peak shaded orange).

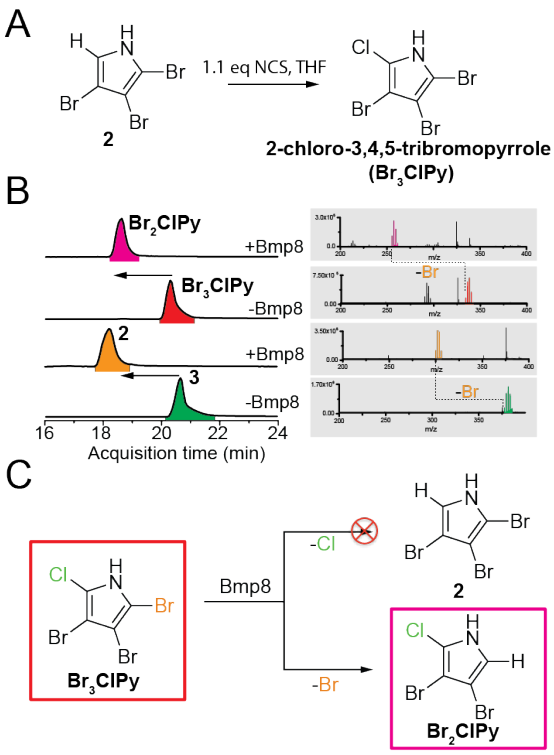

Figure S4.9: Bmp8 selectively debrominates a differentially halogenated pyrrole substrate. (**A**) Route for the synthesis of 2-chloro-3,4,5-tribromopyrrole (Br_3ClPy) from **2**. Briefly, to 2 (10 mg) in 15 mL THF was added 1.1 eq. NCS while stirring. The reaction was stirred for 3 h at room temperature, and solvent was removed *in vacuo*. The residue was dissolved in minimal hexane and purified by silica gel chromatography. The predicted *m/z* for $[M-H]^{-1}$ ion for C_4NHBr_3Cl (Br_3ClPy) is 333.7275, measured is 333.72120. (**B**) EICs for reactions containing Bmp8 incubated with equimolar substrate (Br_3ClPy or 3 as a positive control) in the same manner as described for *in vitro* enzyme assays in 'Materials and Methods'. The top two traces are combined EICs for predicted *m/z* for $[M-H]^{-1}$ ions corresponding to **2**, Br_3ClPy, and Br_2ClPy. The bottom two traces or EICs for predicted *m/z* for $[M-H]^{-1}$ corresponding to **2** and **3**. To the right of traces are mass spectra averaged over the respective highlighted peaks in EICs consistent with expected M+2 Cl/Br isotopic distributions. Only a single with *m/z* 255.8165; predicted *m/z* for the $[M-H]^{1-}$ ion for the singly debrominated product (i.e. with molecular formula $C_4NH_2Br_2Cl$) is 255.8169. (**C**) Scheme illustrating selective dehalogenation of Br_3ClPy by Bmp8.

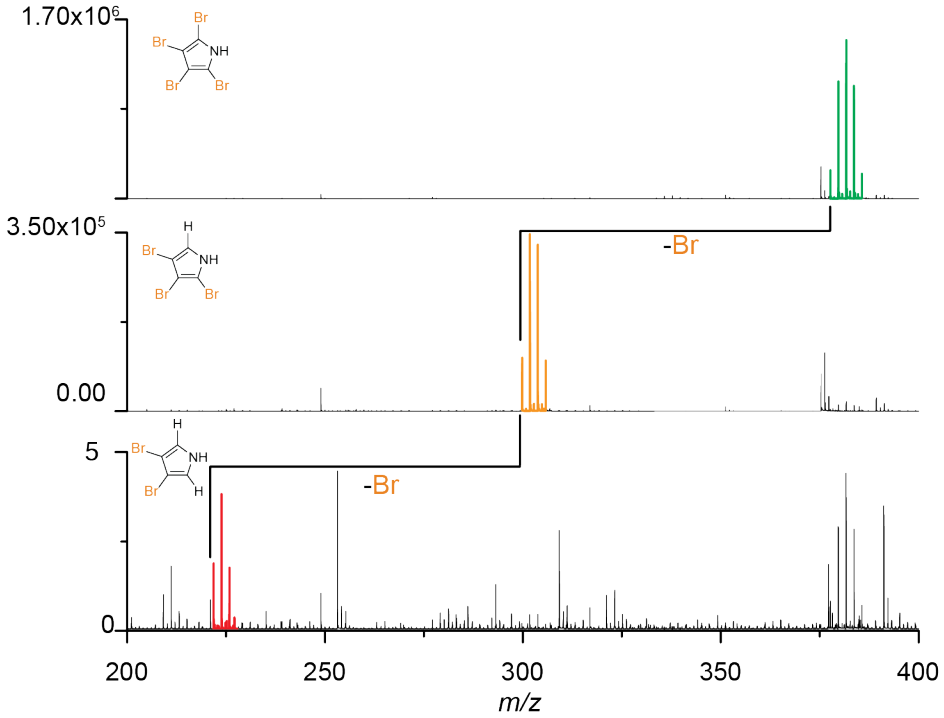

Figure S4.10: Mass spectra for Bmp8 products. Mass spectra showing debromination of **3** (tetrabromopyrroles) to **2** (tribromopyrrole), and **2** to **4** (dibromopyrrole).

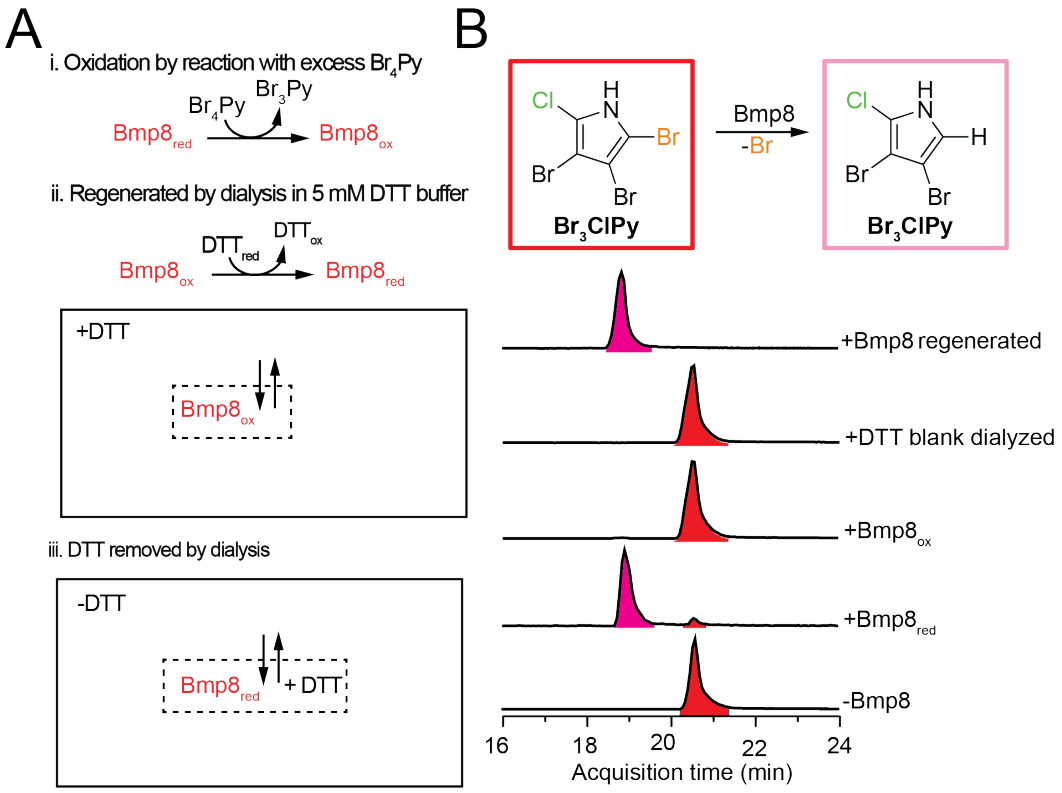

Figure S4.11: Regeneration of Bmp8. (**A**) Scheme for oxidation and reduction of Bmp8. i. Bmp8 as-purified was treated with an excess of tetrabromopyrrole (Br_4Py, **1**) for 3 h, followed by ii. dialysis in buffer (20 mM Tris-HCl pH ~ 8, 50 mM KCl, 10% glycerol) containing dithiothreitol (+DTT) to regenerate the enzyme, and then iii. removal of DTT from the buffer by dialysis in the same buffer not containing DTT (-DTT). 2-chloro-3,4,5-tribromopyrrole (Br_3ClPy) was used as a substrate in case of carryover of Br_4Py used in excess to oxidize Bmp8, and, in principle, removed by dialysis. Br_3ClPy (equimolar to enzyme) was incubated with for 3 h at 30 ºC with regenerated Bmp8 ('+Bmp8 regenerated'), a blank buffer control treated in the same manner as regenerated Bmp8 ('+DTT blank dialyzed'), dialyzed not regenerated Bmp8 (i.e., dialyzed twice in –DTT buffer instead of once in +DTT buffer and once in –DTT buffer, '+$Bmp8_{ox}$'), an as-purified Bmp8 positive control ('+$Bmp8_{red}$'), or no Bmp8 ('-Bmp8'). (**B**) Extracted ion chromatograms (EICs) for organic extract of reactions for predicted *m/z*'s of Br_3ClPy and '-Br' 2-chloro-3,4-tribromopyrrole (Br_2ClPy). Reactions were extracted and analyzed in the same manner as described in the Materials and Methods section.

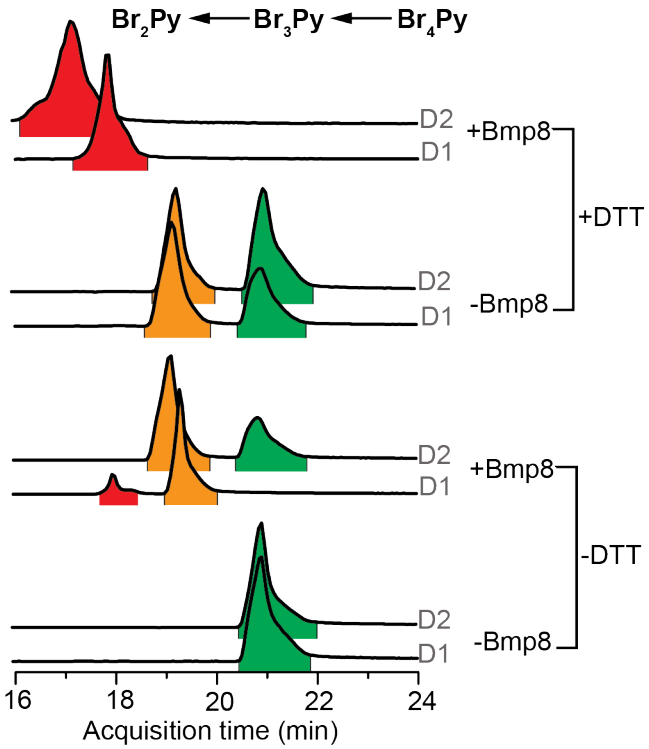

Figure S4.12: Oxygen sensitivity of Bmp8. Extracted ion chromatograms (EICs) for the predicted m/z's [M-H]- for tetrabromopyrrole (Br4Py, **3**) and tribromopyrrle (Br3Py, **2**), and dibromopyrrole (Br2Py, **4**). Reactions with equimolar Br4Py to with Bmp8 as-purified ('D1') and incubated overnight in a vial with the lid left open to allow for equilibration with air ('D2') with and without dithiothreitol (DTT). Reactions were incubated for 6h at 30 ºC, and extracted and analyzed as previously described.

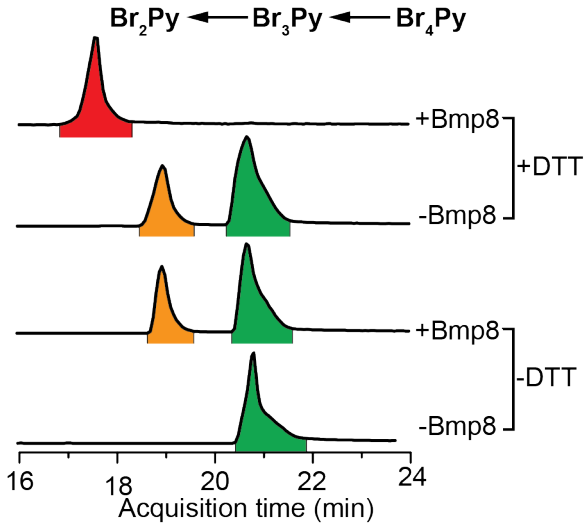

Figure S4.13: Reductive dehalogenation of tetrabromopyrrole (Br_4Py, 3) by Bmp8 under anaerobic conditions with and without dithiothreitol (DTT). Extracted ion chromatograms (EICs) for the predicted *m/z*'s $[M-H]^-$ for Br_4Py and tribromopyrrle (Br_3Py, **2**), and dibromopyrrole (Br_2Py, **4**). Bmp8 and Br_4Py (~2-fold excess to enzyme) were incubated for 12 h in open vials in anaerobic chamber to evacuate the solutions of molecular oxygen. Solutions were then combined while still under anaerobic conditions and incubated for an additional 6 h at ambient temperature in the same anaerobic chamber (~25 ºC). Reactions were extracted in the anaerobic chamber using the same reaction procedure as described in the Materials and Methods sections. Reaction conditions and analysis are the same as described in Material and Methods section.

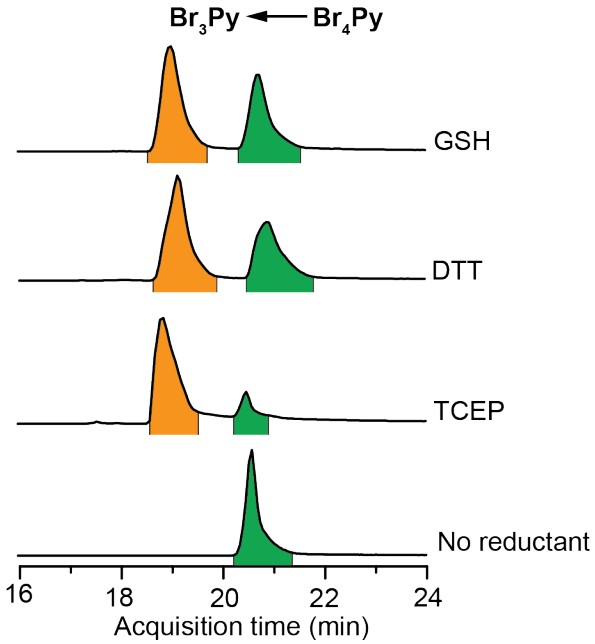

Figure S4.14: Non-enzymatic aqueous reductive dehalogenation of tetrabromopyrrole (Br_4Py, 3) by reducing agents. Extracted ion chromatograms (EICs) for the predicted *m/z*'s $[M-H]^-$ for Br_4Py,tribromopyrrle (Br_3Py, **2**), and dibromopyrrole (not observed). Br_4Py (100 μM) was incubated for 12 h at 3 ºC in aqueous buffer (20 mM Tris-HCl pH ~ 8, 50 mM KCl, 10% glycerol) with 2 mM of reductants (glutathione, GSH; dithiotreitol, DTT; tris(2-carboxyethyl)phosphine, TCEP) or no reductant. Reactions were extracted and analyzed as described in the Material & Methods section (above).

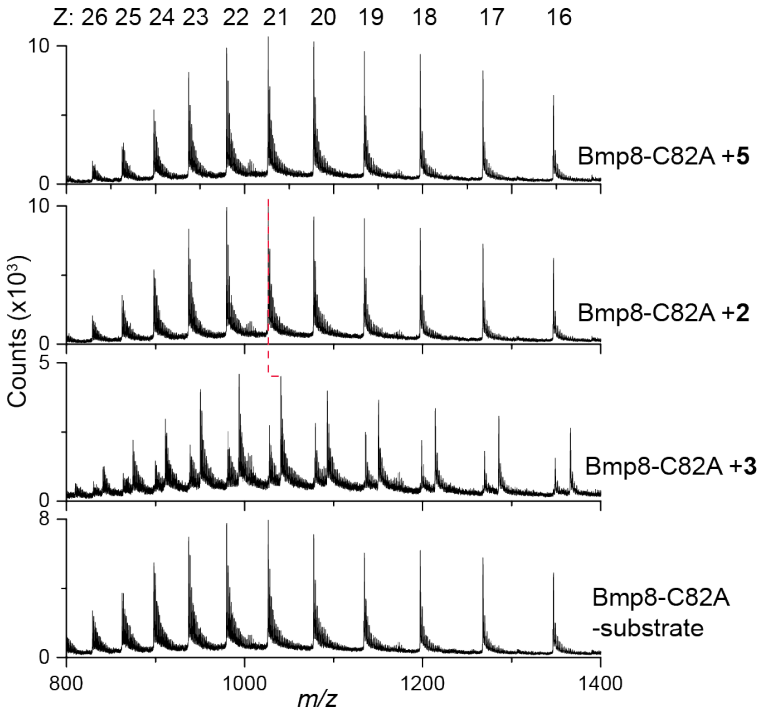

Figure S4.15: Whole-protein mass spectrometry of Bmp8-C82A with other halogenated pyrrole substrates. Bmp8-C82A was incubated with additional Bmp8 substrates **2** and **5**. A mass shift is only observed upon addition of **3**, consistent with slow turnover of **2** and **5** by Bmp8. The procedure for whole-protein mass spectrometric experiments is described in the Material and Methods.

4.4.3 Supplementary Tables

Table S4.1. Mass shift calculation from whole-protein mass spectrometry analysis.

Description	*Calculated neutral protein mass* (Da)*	*Expected neutral mass for 'apo' protein* (Da)	*Difference from 'start'* (Da)	*Mass shift assignment*	*Expected shift* (Da)	*Mean peak-to-peak difference* (Da)**
Bmp8:WT						
No reductant						
no **3** start	21,565.77±0.27	21,566.40	-	-	-	-
after **3**	21,563.13±1.62	-	-2.64	-2H	-2.02	-2.64±1.57
no **3** end	21,565.57±0.26	21,566.40	-0.20	No shift	0	-0.20±0.36
GSH						
no 3 start	21,567.75±0.22	21,566.40	-	-	-	-
after **3** peak 1	21,565.68±0.5	-	-2.07	-2H	-2.02	-2.07±0.57
after **3** peak 2	21,872.66±1.37	-	304.92	$+GS^-$	305.07	304.92±1.38
after **3** peak 3	22,178.09±0.84	-	610.34	$+2GS^-$	610.14	610.34±0.83
no **3** end	21,567.71±0.32	21,566.40				-0.04±0.34
Bmp8:C82A						
No reductant						
no **3** start	21,534.32±0.19	21,534.40	-	-	-	-
after **3**	21,566.33±0.58	-	32.61	+2[O]	31.99	32.61±0.70
no **3** end	21,534.04±0.15	-	-0.28	No shift	0	-0.28±0.23
GSH						
no **3** start	21,535.04±0.23	21,534.40	-	-	-	-
after **3**	21,840.23±0.23	-	305.20	$+GS^-$	305.07	305.20±0.33
no **3** end	21,534.65±0.43	21,534.40	-0.38	No shift	0	-0.38±0.42
DTT						
no **3** start	21,535.08±0.13	21,534.40	-	-	-	-
after **3**	21,535.24±1.07	-	0.15	No shift	0	0.15±1.08
no **3** end	21,534.91±0.25	21,534.40	-0.18	No shift	0	-0.18±0.12
Bmp8:C85A						
No reductant						
no **3** start	21,534.07±0.21	21,534.40	-	-	-	-
after **3**	21,533.85±0.20	-	-0.22	No shift	0	-0.22±0.3
no **3** end	21,533.95±0.20	21,534.40	-0.13	No shift	0	-0.13±0.34
GSH						
no **3** start	21,534.72±0.07	21,534.40	-	-	-	-
after **3**	21,534.68±0.12	-	-0.04	No shift	0	-0.04±0.10
no **3** end	21,534.63±0.13	21,534.40	-0.09	No shift	0	-0.09±0.15

* Calculated as the average of $Zx([M+ZH]^{Z+})$-ZxH over Z=[16,26]. **Calculation shown in Fig. S6.

Chapter 4, in full, is currently being prepared for submission of the material. El Gamal A., Agarwal V., Rahman I., and Moore B.S. The dissertation author is the primary investigator and author of this paper.

A.E. designed and carried out experiments, analyzed data, and wrote the paper; V.A., I.R., and B.S.M provided feedback on the paper and experimental design.

Chapter 5: Opportunities in halopyrrole biosynthesis

5.1 Lessons from pentabromopseudilin biosynthesis: the halopyrrole biosynthetic handle

The elucidation of the brominated marine pyrrole/phenol (Bmp) biosynthetic pathway is a testament to the tremendous opportunities presented by the study of marine bromination. Indeed, awaiting discovery in the biosynthetic pathway of pentabromopseudilin were three new enzymes catalyzing transformations involving halogens, including the first two examples of brominases from a confirmed biosynthetic context, as well as the first example of a tailoring dehalogenase. Reflecting on the process for the discovery of the Bmp gene cluster, it is worth highlighting how an established halopyrrole biosynthetic logic proved a powerful tool for teasing out a basis for associated bromophenol biosynthesis. One of the main challenges in mining for biosynthetic gene clusters encoding the biosyntheses of non-canonical natural products (i.e. neither NRPS nor PKS) is the lack of a biosynthetic "handle" for genome mining. Hence, the success in applying this halopyrrole probe begs the question of what other opportunities await. One area of great potential lies in unlocking the biosynthesis of the fabled bromopyrrole-containing pyrrole imidazole alkaloid (PIA) class of sponge natural products for which more than 150 structures have been described over the past forty years, and which have captivated the imaginations of synthetic chemists and pharmacologists alike[82]. Feeding studies have shown incorporation of radiolabeled L-proline into the structure of the proposed PIA building block-oroidin. Hence, it would appear that the halopyrrole biosynthetic logic could strike again this time in unlocking the biosynthesis of the amino imidazole

moiety of oroidin, and thereby providing access to an entire class of natural products. The remainder of this chapter is dedicated to a description of the state-of-the-art and challenges in the elucidation of PIA biosynthesis along with an original example of sponge metagenome mining toward elucidation of a PIA gene locus.

5.2 A foray into pyrrole-imidazole alkaloid biosynthesis

5.2.1 Background and Introduction

Pyrrole-imidazole alkaloids (PIAs) are a diverse class of marine sponge secondary metabolites with promising bioactivities, including cytoxic, anti-microbial, and anti-feedant properties[82,109]. Among the over 150 PIAs described to date are the anti-microbial sceptrins, anti-fungal and anti-tumor palau'amine, and anti-tumor agelastatins, found in the sponge genera *Agelas, Stylissa, Stylotella, Axinella*, and *Hymeicaedon* (**Fig. 5.1**)[110]. Despite their promising potential as drug leads, access to complex PIAs has been a bottleneck to their development as drugs.

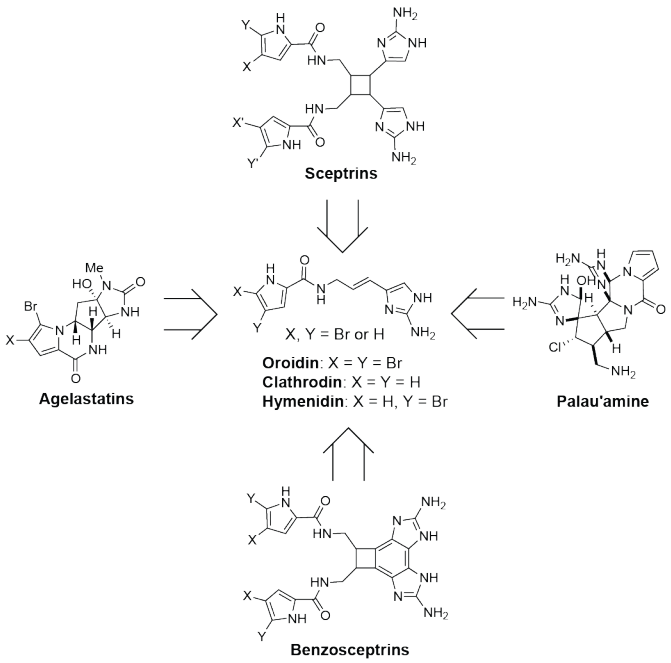

Figure 5.1: Packing a punch with parsimony. Complex PIAs are thought to arise from universal achiral building blocks.

Exemplifying biosynthetic parsimony, complex multi-stereocenter PIAs are proposed to originate from one of three achiral PIA building blocks, namely, oroidin, hymenidin, and clathrodin, which differ only in the nature of the substitution of the 4 and 5 positions of the pyrrole moiety (**Fig. 5.1**)[110]. For example, palau'amine isolated from the sponge *Stylotella agminata*, whose hexacyclic structure features eight contiguous stereocenters, is a proposed dimer of achiral clathrodin (**Figs. 5.1** and **5.2**)[111,112]. Moreover, biomimetic studies employing cell-free assays from crude sponge enzyme preparations from tissues of the Caribbean sponge species *Agelas sceptrum* and *Stylissa caribica* demonstrated oroidin as a precursor to the more complex bioactive PIA benzosceptrin C [113]. Furthermore, the biogenetic precursors of the pyrrole moiety of oroidin is posited from feeding studies to be the amino acid L-proline, while L-homoarginine via L-lysine (or L-histidine) is proposed as the

precursor of the aminopropylimidazole moiety[114]. As in the identification of the *bmp* gene cluster (Chapter 2), the L-proline adenylation domain provides a facile basis for mining for potential PIA biosynthetic gene clusters.

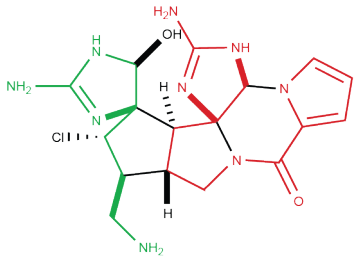

Figure 5.2: Palau'amine: simplicity in complexity. As per biosynthetic proposal, clathrodin moiety (red) and clathrodin sub-unit 3-amino-1-(2-amino imidazolyl) prop-1-ene moiety (green).

Understanding of PIA biosynthesis has progressed slowly over the last decades due to inherent limitations associated with traditional approaches of study. Indeed, the state-of-the-art in the study biosynthesis of PIAs has until now relied on indirect chemical techniques such as *in vivo* isotope tracer experiments, and *in vitro* crude enzyme assays [110,113,115,116]. While these studies have suggested the chemical building blocks involved in higher PIA biosynthesis, they fall short in addressing the genetic and biochemical bases for their production. Moreover, despite monumental successes in the total syntheses of many complex PIAs such as palau'amine, synthetic chemistry has thus far proven an impractical mean for gaining access to PIA material[117-120]. A conclusive molecular basis for PIA biosynthesis is key not only to the discovery of new enzymes, but also to gaining access to these valuable molecules through exploitation of nature's synthetic toolkit.

5.2.2 Approach

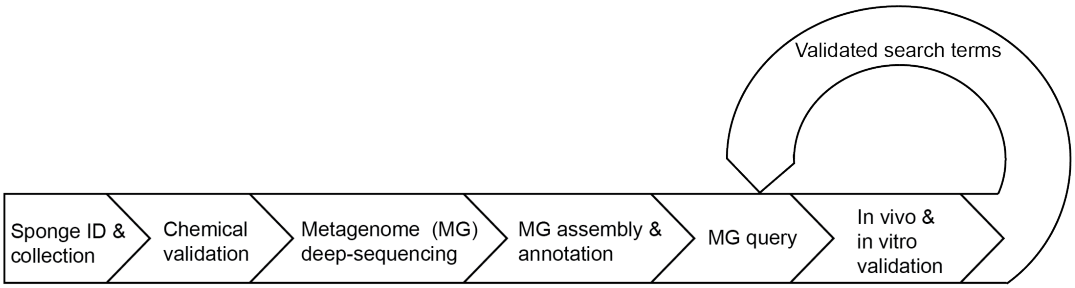

Figure 5.3: Scheme for metagenomic approach for elucidation of PIA biosynthesis. Experimental validation will afford a handle to accelerate the rate of discovery of new pathways.

Sponges harbor complex microbiomes that are thought to account for the majority of their secondary metabolism[121]. At least a portion of sponge microbiota are known to be vertically transferred from adult sponges to their offspring during spawning[122]. Hence, it is this core microbiome that likely gives rise to the highly reproducible chemotypes observed within sponge species[123,124]. Nonetheless, it cannot be excluded that the sponge itself might also possess the capacity to produce natural products, or at least modify the natural products produced by its microbiome. Hence, a deep-sequencing metagenomics approach which examines the entire genetic content of the sponge organism may provide the best first-pass approach for gaining a holistic understanding of the biosynthetic capacities of these organisms[125]. The initial workflow described in 'Fig. 5.3' (above) begins with identification and collection of sponges known to harbor PIAs, followed by chemical verification to confirm presence of PIAs. Validated specimens are then subjected to whole-animal metagenomic DNA extraction and deep-sequencing. Sequencing data is then assembled and annotated, and queried using candidate amino acid sequences based on retro-biosynthetic hypotheses. Upon identification of candidate gene loci, one might

proceed to validate targets through a combination of *in vivo* heterologous expression of a full gene cluster, and *in vitro* interrogation of individual biochemical transformations through the cloning and expression of individual enzymes. The verification of the first PIA biosynthetic pathway promises to accelerate the discovery of many more PIA pathways (**Fig. 5.3**). The remainder of this section will discuss preliminary findings utilizing this approach.

5.3 Preliminary work

5.3.1 Collection of marine sponges harboring PIAs

The two fundamental questions motivating an initial study of PIA biosynthesis are, firstly, the origin of oroidin, and, secondly, whether more complex "higher" PIAs are derived from oroidin. Hence, we initially sought a sponge harboring oroidin, and another sponge harboring the simplest of the higher PIAs, the oroidin dimer sceptrin (**Fig. 5.1**). Moreover, sponges from distinct geographical locations were sought with the rationale that a core microbiome, independent of environment, might be derived via comparison of these two metagenomes thus focusing the search for candidate biosynthetic gene loci. To this end, the sponge *Stylissa massa* known to produce oroidin and cyclooroidin derivatives[126] was collected in Guam by a team lead by Dr. Vinayak Agarwal of the Moore Laboratory in the summer of 2014, while the Caribbean sponge *Agelas tubulata* shown to harbor sceptrins was obtained from collaborators at Sirenas Marine Discovery in La Jolla, CA. Hence, the rationale for choosing initial target sponges for investigation is born of a "simple-to-complex" strategy.

5.3.2 Chemical validation

Initial chemical validation of samples was performed by liquid chromatography tandem mass spectrometry (LC-MS) analysis of methanol extracts of *A. tubulata* and *S. massa*. Extracts of *S. massa* were confirmed to harbor masses consistent with anticipated oroidin and cyclooroidin derivatives (**Figs. 5.4** and **5.5**), while extracts of *A. tubulata* were confirmed to contain masses consistent with the oroidin dimer sceptrin (personal correspondence with Eduardo Esquinazi, Sirenas Marine Discovery).

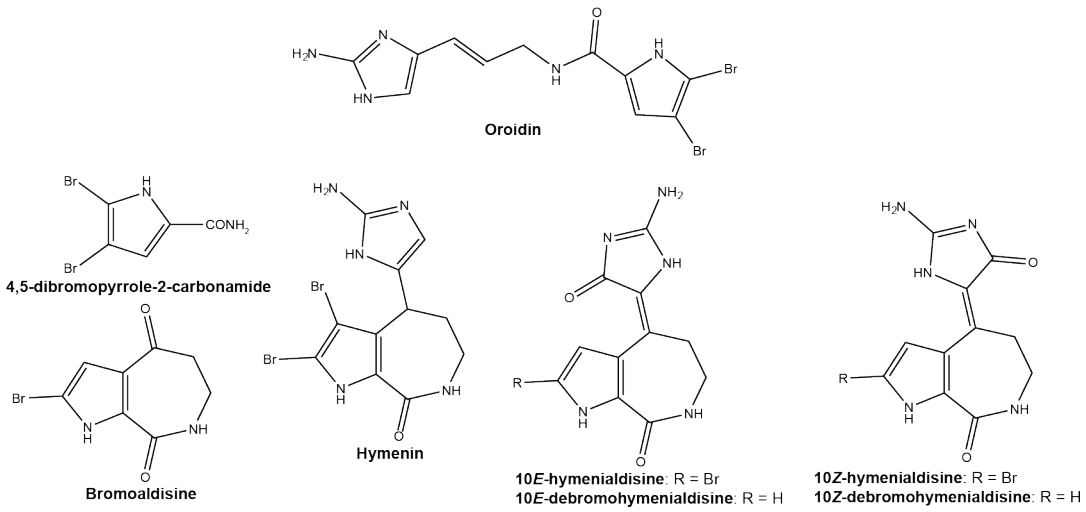

Figure 5.4: Chemical diversity of *S. massa*. Representative structure of alkaloids furnished by extracts of the sponge *S. massa*[126].

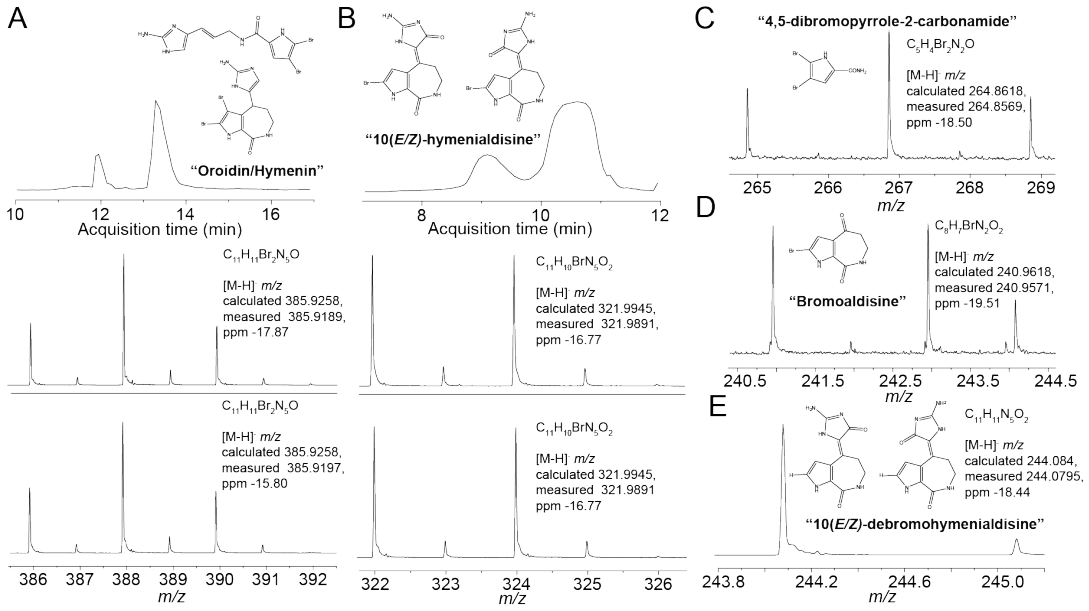

Figure 5.5: LC-MS validation of production of oroidin and cylcooroidin compounds from *S. massa* collected in Guam. (A)-(E) Mass spectra with associated molecular formulae and proposed structures (also shown in Fig. 4) based on previous isolation work with *S. masssa*[126]. Extracted ion chromatograms are shown to the tops of panels (A)-(B) for compounds with identical molecular formulae, and for which two peaks were present. Multiple known structures fit to the mass spectrum shown in panel 'E'. The vertical axis is relative abundance. Structural assignments are entirely speculative based on predicted molecular formulae.

5.3.3 Metagenomes

Whole sponge metagenomic DNA was prepared from tissue of *A. tubulata* and *S. massa* using a protocol described by Brady *et al.*[127] Metagenomes were deep-sequenced using the Illumina HiSeq sequencing platform. The resulting metagenomes were assembled and uploaded onto the JGI server for annotation. These metagenomes both exhibited remarkable microbial diversity. Comparison of the *S. massa* and *A. tubulata* prokaryotic diversity (Bacteria and Archaea) showed that the metagenomes were highly similar at a phylum level (**Fig. 5.6**).

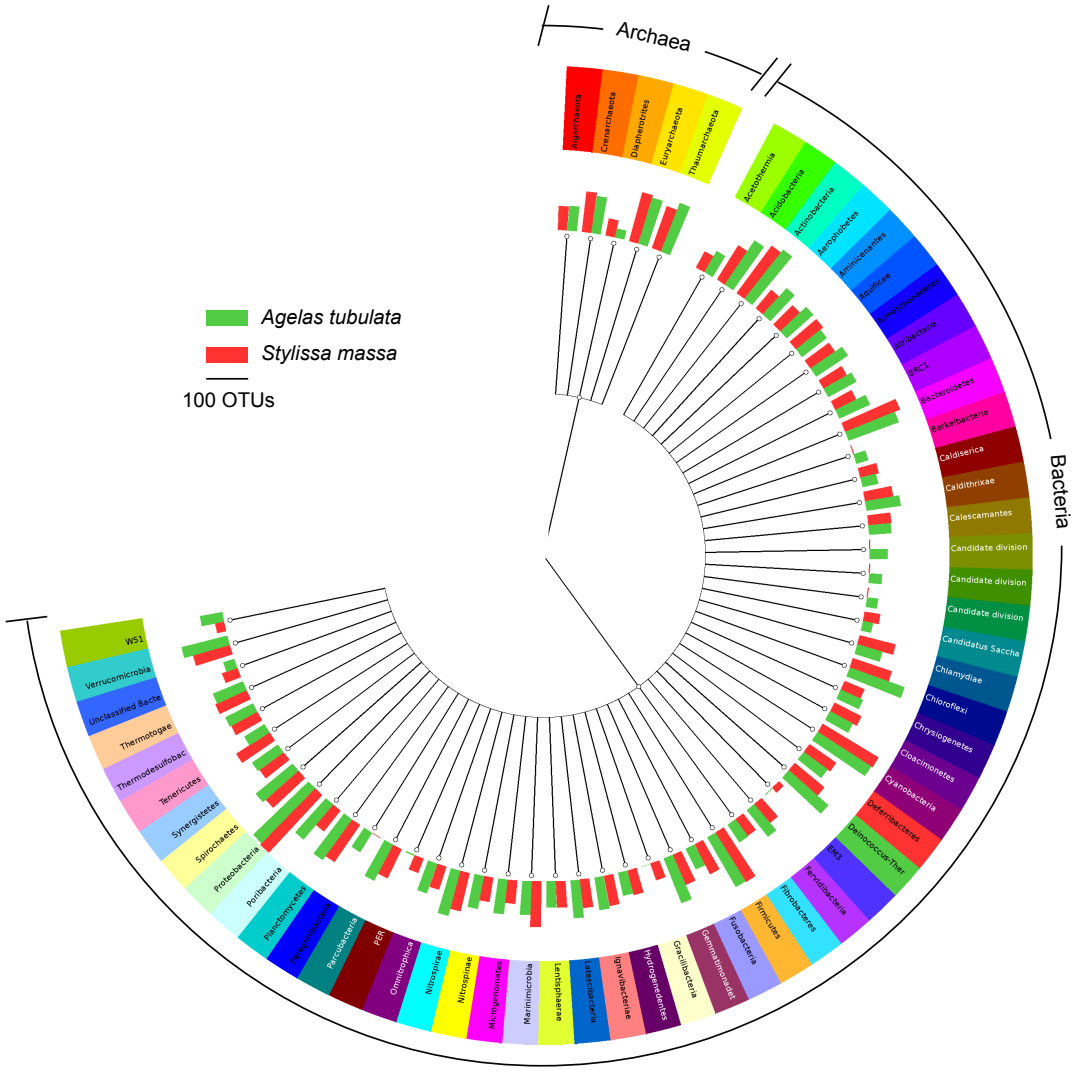

Figure 2. Comparison of phylum-level prokaryotic diversity of *A. tubulata* and *S. massa*. Radial phylogenetic tree[128] showing the phylum-level diversity based on 16S metagenomics reads. Bars associated with nodes show the abundance of operational taxonomic units (OTUs) for the respective metagenome.

5.3.4 Metagenomic query

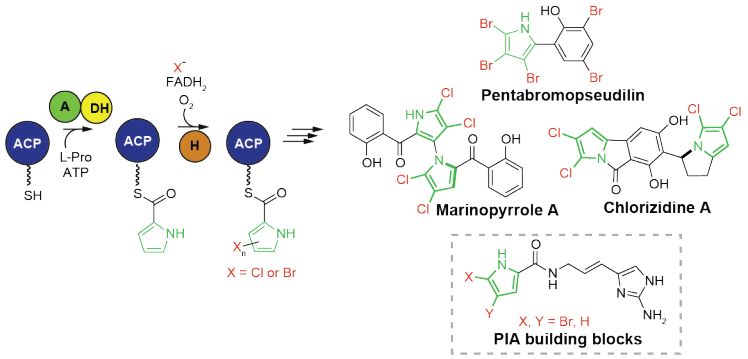

Figure 5.7: Return of the halopyrrole biosynthetic handle. L-proline is thought to be the precursor in the biosynthesis of the halopyrrole moiety, therefore canonical halopyrrole biosynthetic motifs might be used to mine sponge metagenomes for PIA biosynthetic loci.

Based on reports of incorporation of radiolabeled L-proline into the structure of oroidin[114], it was hypothesized that the halopyrrole moiety of PIAs is derived via the same conserved halopyrrole biosynthetic logic used to mine bacterial genomes for the Bmp gene locus (Chapter 2) (**Fig. 5.7**). Therefore, proline adenylation domains and pyrrole halogenases were employed as a two-pronged hook to search for potential PIA clusters. Mining the metagenome of *S. massa* lead to the identification of several short contigs containing putative proline adenylation domains, while no homologs to pyrrole halogenases could be identified. A search of the *A. tubulata* metagenome similarly revealed several proline adenylation domains, but, likewise, their context could not be ascertained due the brevity of the contigs on which they were found. Unlike the metagenome of *S. massa*, the metagenome of *A. tubulata* returned some twenty homologs of flavin-dependent pyrrole halogenases. The most closely related homolog showed greater sequence homology to halogenases that act on thiotemplated rather than free substrates (**Fig. 5.8**). Further, a search of publically available genomic

databases using the putative pyrrole halogenase sequence from *A. tubulata* returned partial sequences for putative flavin-dependent halogenases amplified from metagenomes of sponges known to harbor PIAs in an earlier study[129].

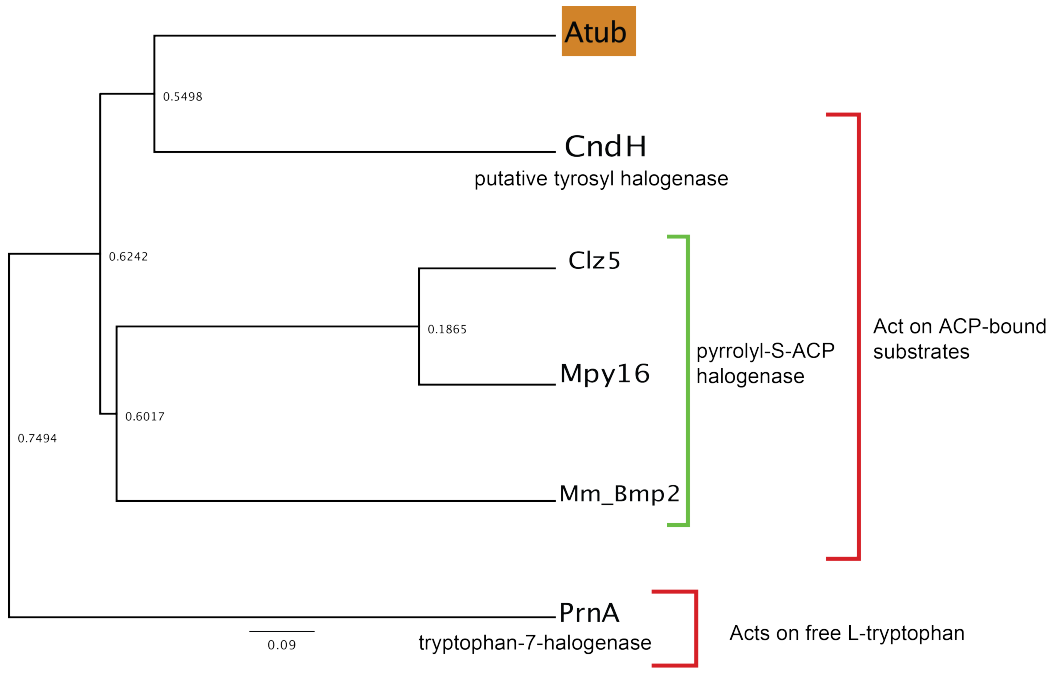

Figure 5.8: Phylogeny of putative *A. tubulata* pyrrole halogenase. An unrooted distance tree was constructed (Jukes-Cantor, Neighbor-Joining, Geneious) for flavin-dependent halogenases including a pyrrole halogenase homolog from the metagenome of *A. tubulata* ('Atub', highlighted orange); the genetic context for 'Atub' is shown in 'Fig. 25'.

Inspection of the gene neighborhood for the putative *A. tubulata* halogenase revealed a gene annotating as a CoA-ligase, which could serve in place of an adenylation domain (**Fig. 5.9**). Also present in the gene neighborhood were several genes encoding for enzymes catalyzing redox and radical chemistry (**Fig. 5.9**). Resistance mechanisms for natural products are often encoded their biosynthetic gene clusters[130]. In addition to apparent biosynthetic enzymes, the cluster from *A. tubulata*

also encodes for putative topoisomerase IV. Interestingly, analogs of oroidin have been shown to be inhibitors of DNA topoisomerase IV[131]. As a thought exercise, a cursory biosynthetic scheme for oroidin (the putative precursor of sceptrin harbored by *A. tubulata*) was constructed based on the annotations found in the genetic context of the putative *A. tubulata* halogenase (**Fig. 5.9**). Indeed, many biosynthetic steps leading to the formation of sceptin, let alone oroidin, are apparently absent from the annotated genetic context captured by the ~21 kb contig shown in Figure 8. Additionally, the cluster contains many ORFs that lack annotations due dissimilarity from known enzymes. Therefore, before proceeding with detailed investigation of this gene cluster it the experimental validation of key transformations is advised. Several approaches for biochemical validation are described briefly in the following section.

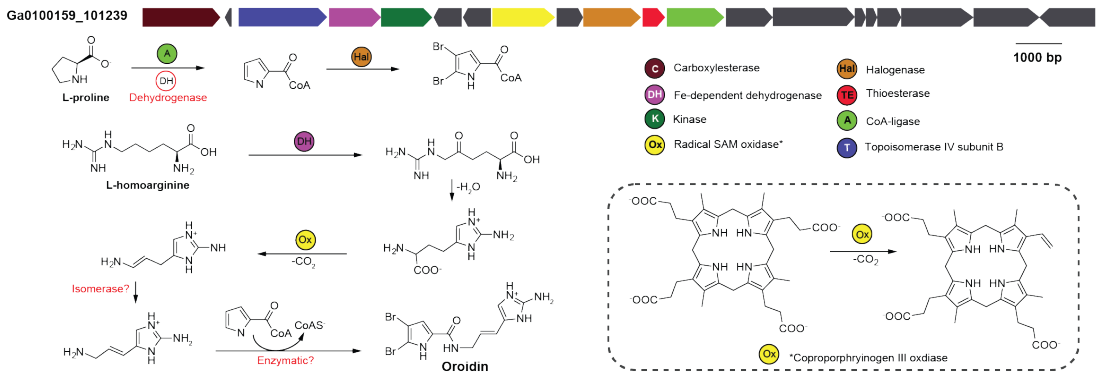

Figure 5.9: Putative "PIA" cluster from the *A. tubulata metagenome*. The top of the figure shows the ~21 kb contig containing a putative *A. tubulata* pyrrole halogenase (orange) chosen for its promising genetic context. Annotations for apparent biosynthetic and resistance genes are shown according to the coloring scheme used in the gene map. ORFs shaded are annotated to encode "hypothetical proteins." Based on these annotations a rough biosynthetic proposal was constructed for oroidin (note that *A. tubulata* harbors a putative oroidin dimer sceptrin). Red font indicates implicit transformations that could not be accounted for by gene annotations. The biosynthetic scheme is inspired by that shown in ref. 7. The transformation associated with the annotation "coproporhyinogen III oxidase-like radical SAM enzyme" is shown in the dashed box (bottom, right). Note this biosynthetic scheme is included as a thought experiment, and is not experimentally validated.

5.3.4 Validation

Thus far a metagenomics approach has failed to reveal a viable PIA biosynthetic gene cluster for heterologous expression. Nonetheless, despite lack of sufficient genetic context in many cases, one might begin to screen candidate pyrrole halogenases using the methodology described in Chapter 3 of this thesis to study the reaction catalyzed by pyrrole brominase Bmp2. Moreover, the specificity of candidate proline adenylation domains can be assayed[132].

5.4 Future directions

In light of the challenge thus far in identifying a high-confidence PIA biosynthetic gene locus via a metagenomics strategy, it is worth revisiting the

assumptions driving the present approach. The first assumption is that the halopyrrole moiety of PIAs derives from a conserved biosynthetic logic. This proposal is based on past studies showing incorporation of radiolabeled L-proline into oroidin[114]. However, adherence to convention comes with the risk of turning a blind eye to alternative strategies. Indeed, the *A. tubulata* metagenome-derived gene cluster used as an example in this chapter appears to possess a halogenase and CoA-ligase, but lacks an open reading frame (ORF) annotating as an acyl carrier protein (ACP) despite a substantial (~21 kb) genetic context. Hence, for the sake of argument, the biosynthesis of the halopyrrole moiety of oroidin might arise via an ACP-independent pathway, which is without precedent in halopyrrole biosynthesis[133]. The second assumption is that the sponge microbiome, rather than the sponge itself is the producer of the major chemistry present in the sponge. The enormous capacity for secondary metabolism of host-associated microorganisms has been demonstrated from marine invertebrates[134,135]. Nonetheless, if the sponge itself is responsible for whole or part of the biosynthesis of PIAs, a transcriptomic approach such as used to identify dispersed biosynthetic enzymes in plants by correlative gene expression might be more appropriate[136]. As little is known about sponge enzymes, and relatively few genomes of marine invertebrates have been sequenced, relying on annotations to identify biosynthetic genes could pose an additional challenge[137]. In light of the inherent risk involved in the pursuit of unknowns, the assumptions going into the approach to PIA biosynthesis should be thoroughly vetted. While the success of high risk research often hinges on a degree of chance, chance certainly favors a well-rationalized approach.

This chapter does not mean to suggest that a metagenomics approach to the elucidation of PIA biosynthesis is destined to failure, but that improvements can be made to increase the odds of success. It is apparent from initial sequencing efforts, that the metagenomes generated for *A. tubulata* and *S. massa* are exceedingly complex. Hence, a strategy that reduces the complexity of DNA samples prior to sequencing could dramatically increase the efficiency of downstream steps in the workflow. One strategy could be a single-cell genomics approach as has previously been used to identify sponge symbionts with enormous biosynthetic potential[135]. Assuming limiting sequencing and computational resources, a single-cell approach would require a means of prioritizing amplified genomes for sequencing. In turn, this would hinge on confidence in the retrobiosynthetic proposal for oroidin which would word serve as the basis for designing degenerate nucleic acid probes for initial screening of single microbial cells. An additional strategy for simplifying metagenomes would be to sequence metagenomes of sponge eggs or larvae, which would ostensibly be enriched for vertically rather than horizontally transferred microbiota, hence increasing chances of capturing intact genomic information for the producing microbial symbiont. Despite evidence for vertical transfer of sponge symbionts, a metagenomics approach has never been taken to study this phenomenon[122,124,138]. A traditional biochemical approach that casts a wider net in screening for crude enzyme activity coupled with a modern genomics approach could also serve to inform and specify a broader view on oroidin biosynthesis. Indeed, crude sponge protein extracts have been used to generate circumstantial evidence in support of the role of oroidin as a precursor to higher PIAs[113]. Based on the dipeptide-

like structure of oroidin, it is reasonable to assume that its building blocks derive from amino acid precursors, hence, screening protein fractions for modification of a cocktail of amino acids utilizing a mass spectrometry networking approach is a highly feasible prioritization scheme toward the generation of protein sequence search tags. The study of the biosynthesis of PIAs is a daunting task, however any progress toward the identification of a genetic biosynthetic signature for a PIA molecule promises to crack open the biosynthesis of a class of over 150 natural products, whose bioactivities have amazed pharmacologists, and inspired synthetic chemists[82].

5.5 Acknowledgements

Many thanks to Dr. Vinayak Agarwal, Michelle Schorn, Dr. Valerie J. Paul (Smithsonian Marine Station), and Prof. Jason Biggs (University of Guam) for collecting *Stylissa massa* from Guam, to Dr. Sheila Podell and Prof. Eric Allen for sequencing and assembly of the metagenome of *A. tubulata*, to Dr. Zhenjian Lin and Prof. Eric Schmidt (University of Utah) for sequencing and assembly of the metagenome of *S. massa*, and to Dr. Eduardo Esquinazi and colleagues at Sirenas Marine Discovery (La Jolla, CA) for collection and chemical analysis of *A. tubulata*

References

1 Gribble, G. W. Naturally occurring organohalogen compounds--a comprehensive survey. *Fortschr Chem Org Naturst* **68**, 1-423 (1996).

2 Gribble, G. W. *Naturally Occurring Organohalogen Compounds – A Comprehensive Update*. Vol. 91 (Springer, 2010).

3 Eustaquio, A. S., Gust, B., Luft, T., Li, S. M., Chater, K. F. & Heide, L. Clorobiocin biosynthesis in Streptomyces: identification of the halogenase and generation of structural analogs. *Chem Biol* **10**, 279-288 (2003).

4 Harris, C. M., Kannan, R., Kopecka, H. & Harris, T. M. The Role of the Chlorine Substituents in the Antibiotic Vancomycin - Preparation and Characterization of Monodechlorovancomycin and Didechlorovancomycin. *J Am Chem Soc* **107**, 6652-6658 (1985).

5 Bister, B., Bischoff, D., Nicholson, G. J., Stockert, S., Wink, J., Brunati, C., Donadio, S., Pelzer, S., Wohlleben, W. & Sussmuth, R. D. Bromobalhimycin and chlorobromobalhimycins--illuminating the potential of halogenases in glycopeptide antibiotic biosyntheses. *Chembiochem* **4**, 658-662 (2003).

6 Groll, M., Huber, R. & Potts, B. C. Crystal structures of Salinosporamide A (NPI-0052) and B (NPI-0047) in complex with the 20S proteasome reveal important consequences of beta-lactone ring opening and a mechanism for irreversible binding. *J Am Chem Soc* **128**, 5136-5141 (2006).

7 Bianco, A. C., Salvatore, D., Gereben, B., Berry, M. J. & Larsen, P. R. Biochemistry, cellular and molecular biology, and physiological roles of the iodothyronine selenodeiodinases. *Endocr Rev* **23**, 38-89 (2002).

8 Kale, A. J., McGlinchey, R. P., Lechner, A. & Moore, B. S. Bacterial self-resistance to the natural proteasome inhibitor salinosporamide A. *ACS Chem Biol* **6**, 1257-1264 (2011).

9 Wang, J., Sanchez-Rosello, M., Acena, J. L., del Pozo, C., Sorochinsky, A. E., Fustero, S., Soloshonok, V. A. & Liu, H. Fluorine in pharmaceutical industry: fluorine-containing drugs introduced to the market in the last decade (2001-2011). *Chem Rev* **114**, 2432-2506 (2014).

10 O'Hagan, D. & Harper, D. B. Fluorine-containing natural products. *J Fluorine Chem* **100**, 127-133 (1999).

11 Weber, T., Blin, K., Duddela, S., Krug, D., Kim, H. U., Bruccoleri, R., Lee, S. Y., Fischbach, M. A., Muller, R., Wohlleben, W., Breitling, R., Takano, E. & Medema, M. H. antiSMASH 3.0-a comprehensive resource for the genome mining of biosynthetic gene clusters. *Nucleic Acids Res* **43**, W237-243 (2015).

12 Bachmann, B. O., Van Lanen, S. G. & Baltz, R. H. Microbial genome mining for accelerated natural products discovery: is a renaissance in the making? *J Ind Microbiol Biot* **41**, 175-184 (2014).

13 Neumann, C. S., Fujimori, D. G. & Walsh, C. T. Halogenation strategies in natural product biosynthesis. *Chemistry & Biology* **15**, 99-109, doi:Doi 10.1016/J.Chembiol.2008.01.006 (2008).

14 Blasiak, L. C. & Drennan, C. L. Structural Perspective on Enzymatic Halogenation. *Accounts of Chemical Research* **42**, 147-155, doi:Doi 10.1021/Ar800088r (2009).

15 Vaillancourt, F. H., Yeh, E., Vosburg, D. A., Garneau-Tsodikova, S. & Walsh, C. T. Nature's inventory of halogenation catalysts: oxidative strategies predominate. *Chem Rev* **106**, 3364-3378 (2006).

16 El Gamal, A., Agarwal, V., Diethelm, S., Rahman, I., Schorn, M. A., Sneed, J. M., Louie, G. V., Whalen, K. E., Mincer, T. J., Noel, J. P., Paul, V. J. & Moore, B. S. Biosynthesis of coral settlement cue tetrabromopyrrole in marine bacteria by a uniquely adapted brominase-thioesterase enzyme pair. *Proc Natl Acad Sci U S A* (2016).

17 Frese, M. & Sewald, N. Enzymatic halogenation of tryptophan on a gram scale. *Angew Chem Int Ed Engl* **54**, 298-301 (2015).

18 Brown, S. & O'Connor, S. E. Halogenase Engineering for the Generation of New Natural Product Analogues. *Chembiochem* **16**, 2129-2135 (2015).

19 Chen, X. & van Pee, K. H. Catalytic mechanisms, basic roles, and biotechnological and environmental significance of halogenating enzymes. *Acta Biochim Biophys Sin (Shanghai)* **40**, 183-193 (2008).

20 Leri, C. A., Hakala, J. A., Marcus, M. A., Lanzirotti, A., Reddy, C. M. & Myneni, S. C. B. Natural organobromine in marine sediments: New evidence of biogeochemical Br cycling. *Global Biogeochem Cy* **24**, doi:10.1029/2010GB003794 (2010).

21 Oberg, G. The natural chlorine cycle--fitting the scattered pieces. *Appl Microbiol Biotechnol* **58**, 565-581 (2002).

22 Ahn, Y. B., Rhee, S. K., Fennell, D. E., Kerkhof, L. J., Hentschel, U. & Haggblom, M. M. Reductive dehalogenation of brominated phenolic compounds by microorganisms associated with the marine sponge *Aplysina aerophoba*. *Appl Environ Microbiol* **69**, 4159-4166 (2003).

23 Gribble, G. W. The natural production of organobromine compounds. *Environ Sci Pollut Res Int* **7**, 37-47 (2000).

24 Emerson, S. & Hedges, J. in *Chemical Oceanography and the Marine Carbon Cycle* 3-32 (2008).

25 Dembitsky, V. M. Biogenic iodine and iodine-containing metabolites. *Nat Prod Commun* **1**, 139-175 (2006).

26 Hager, L. P., Morris, D. R., Brown, F. S. & Eberwein, H. Chloroperoxidase. II. Utilization of halogen anions. *J Biol Chem* **241**, 1769-1777 (1966).

27 Clutterbuck, P. W., Mukhopadhyay, S. L., Oxford, A. E. & Raistrick, H. Studies in the biochemistry of micro-organisms. *Biochem J* **34**, 664-677 (1940).

28 Johnson, S. M., Paul, I. C., Rinehart, K. L. & Srinivas.R. Absolute Configuration of Caldariomycin. *J Am Chem Soc* **90**, 136-& (1968).

29 Hofrichter, M. & Ullrich, R. Heme-thiolate haloperoxidases: versatile biocatalysts with biotechnological and environmental significance. *Appl Microbiol Biotechnol* **71**, 276-288 (2006).

30 van Pee, K. H., Dong, C. J., Flecks, S., Naismith, J., Patallo, E. P. & Wage, T. Biological halogenation has moved far beyond haloperoxidases. *Adv Microbiol* **59**, 127-157 (2006).

31 Wever, R., Plat, H. & Deboer, E. Isolation Procedure and Some Properties of the Bromoperoxidase from the Seaweed *Ascophyllum-Nodosum*. *Biochim Biophys Acta* **830**, 181-186, doi:Doi 10.1016/0167-4838(85)90026-3 (1985).

32 Butler, A. & Walker, J. V. Marine Haloperoxidases. *Chem Rev* **93**, 1937-1944 (1993).

33 Petty, M. A. An introduction to the origin and biochemistry of microbial halometabolites. *Bacteriol Rev* **25**, 111-130 (1961).

34 Rutledge, P. J. & Challis, G. L. Discovery of microbial natural products by activation of silent biosynthetic gene clusters. *Nat Rev Microbiol* **13**, 509-523 (2015).

35 Keller, S., Wage, T., Hohaus, K., Holzer, M., Eichhorn, E. & van Pee, K. H. Purification and Partial Characterization of Tryptophan 7-Halogenase (PrnA) from *Pseudomonas fluorescens Angew Chem Int Ed Engl* **39**, 2300-2302 (2000).

36 Dong, C. J., Flecks, S., Unversucht, S., Haupt, C., van Pee, K. H. & Naismith, J. H. Tryptophan 7-halogenase (PrnA) structure suggests a mechanism for regioselective chlorination. *Science* **309**, 2216-2219, doi:Doi 10.1126/Science.1116510 (2005).

37 Hohaus, K., Altmann, A., Burd, W., Fischer, I., Hammer, P. E., Hill, D. S., Ligon, J. M. & vanPee, K. H. NADH-dependent halogenases are more likely to be involved in halometabolite biosynthesis than haloperoxidases. *Angew Chem Int Edit* **36**, 2012-2013 (1997).

38 Yeh, E., Blasiak, L. C., Koglin, A., Drennan, C. L. & Walsh, C. T. Chlorination by a long-lived intermediate in the mechanism of flavin-dependent halogenases. *Biochemistry* **46**, 1284-1292, doi:Doi 10.1021/Bi0621213 (2007).

39 Flecks, S., Patallo, E. R., Zhu, X. F., Ernyei, A. J., Seifert, G., Schneider, A., Dong, C. J., Naismith, J. H. & van Pee, K. H. New Insights into the Mechanism of Enzymatic Chlorination of Tryptophan. *Angewandte Chemie-International Edition* **47**, 9533-9536 (2008).

40 Zehner, S., Kotzsch, A., Bister, B., Sussmuth, R. D., Mendez, C., Salas, J. A. & van Pee, K. H. A regioselective tryptophan 5-halogenase is involved in pyrroindomycin biosynthesis in *Streptomyces rugosporus* LL-42D005. *Chem Biol* **12**, 445-452 (2005).

41 Milbredt, D., Patallo, E. P. & van Pee, K. H. A tryptophan 6-halogenase and an amidotransferase are involved in thienodolin biosynthesis. *Chembiochem* **15**, 1011-1020 (2014).

42 Heemstra, J. R., Jr. & Walsh, C. T. Tandem action of the O2- and FADH2-dependent halogenases KtzQ and KtzR produce 6,7-dichlorotryptophan for kutzneride assembly. *J Am Chem Soc* **130**, 14024-14025 (2008).

43 Shepherd, S. A., Menon, B. R., Fisk, H., Struck, A. W., Levy, C., Leys, D. & Micklefield, J. A Structure-Guided Switch in the Regioselectivity of a Tryptophan Halogenase. *Chembiochem* (2016).

44 Dorrestein, P. C., Yeh, E., Garneau-Tsodikova, S., Kelleher, N. L. & Walsh, C. T. Dichlorination of a pyrrolyl-S-carrier protein by FADH2-dependent halogenase PltA during pyoluteorin biosynthesis. *Proc Natl Acad Sci U S A* **102**, 13843-13848 (2005).

45 Yamanaka, K., Ryan, K. S., Gulder, T. A., Hughes, C. C. & Moore, B. S. Flavoenzyme-catalyzed atropo-selective N,C-bipyrrole homocoupling in marinopyrrole biosynthesis. *J Am Chem Soc* **134**, 12434-12437 (2012).

46 Mantovani, S. M. & Moore, B. S. Flavin-linked oxidase catalyzes pyrrolizine formation of dichloropyrrole-containing polyketide extender unit in chlorizidine A. *J Am Chem Soc* **135**, 18032-18035 (2013).

47 Heide, L., Westrich, L., Anderle, C., Gust, B., Kammerer, B. & Piel, J. Use of a halogenase of hormaomycin biosynthesis for formation of new clorobiocin analogues with 5-chloropyrrole moieties. *Chembiochem* **9**, 1992-1999 (2008).

48 Lin, S., Van Lanen, S. G. & Shen, B. Regiospecific chlorination of (S)-beta-tyrosyl-*S*-carrier protein catalyzed by SgcC3 in the biosynthesis of the enediyne antitumor antibiotic C-1027. *J Am Chem Soc* **129**, 12432-12438 (2007).

49 Buedenbender, S., Rachid, S., Muller, R. & Schulz, G. E. Structure and Action of the Myxobacterial Chondrochloren Halogenase CndH: A New Variant of FAD-dependent Halogenases. *Journal of Molecular Biology* **385**, 520-530, doi:Doi 10.1016/J.Jmb.2008.10.057 (2009).

50 Agarwal, V., El Gamal, A. A., Yamanaka, K., Poth, D., Kersten, R. D., Schorn, M., Allen, E. E. & Moore, B. S. Biosynthesis of polybrominated aromatic organic compounds by marine bacteria. *Nat Chem Biol* **10**, 640-647 (2014).

51 Hofer, I., Crusemann, M., Radzom, M., Geers, B., Flachshaar, D., Cai, X., Zeeck, A. & Piel, J. Insights into the biosynthesis of hormaomycin, an exceptionally complex bacterial signaling metabolite. *Chem Biol* **18**, 381-391 (2011).

52 Winter, J. M. & Moore, B. S. Exploring the chemistry and biology of vanadium-dependent haloperoxidases. *J Biol Chem* **284**, 18577-18581 (2009).

53 Winter, J. M., Moffitt, M. C., Zazopoulos, E., McAlpine, J. B., Dorrestein, P. C. & Moore, B. S. Molecular basis for chloronium-mediated meroterpene cyclization - Cloning, sequencing, and heterologous expression of the napyradiomycin biosynthetic gene cluster. *J Biol Chem* **282**, 16362-16368 (2007).

54 Bernhardt, P., Okino, T., Winter, J. M., Miyanaga, A. & Moore, B. S. A stereoselective vanadium-dependent chloroperoxidase in bacterial antibiotic biosynthesis. *J Am Chem Soc* **133**, 4268-4270 (2011).

55 Diethelm, S., Teufel, R., Kaysser, L. & Moore, B. S. A multitasking vanadium-dependent chloroperoxidase as an inspiration for the chemical synthesis of the merochlorins. *Angew Chem Int Ed Engl* **53**, 11023-11026 (2014).

56 Orjala, J. & Gerwick, W. H. Barbamide, a chlorinated metabolite with molluscicidal activity from the Caribbean cyanobacterium *Lyngbya majuscula*. *J Nat Prod* **59**, 427-430 (1996).

57 Argoudelis, A. D., Herr, R. R., Mason, D. J., Pyke, T. R. & Zieserl, J. F. New amino acids from Streptomyces. *Biochemistry* **6**, 165-170 (1967).

58 Vaillancourt, F. H., Yin, J. & Walsh, C. T. SyrB2 in syringomycin E biosynthesis is a nonheme FeII alpha-ketoglutarate- and O2-dependent halogenase. *Proc Natl Acad Sci U S A* **102**, 10111-10116 (2005).

59 Ueki, M., Galonic, D. P., Vaillancourt, F. H., Garneau-Tsodikova, S., Yeh, E., Vosburg, D. A., Schroeder, F. C., Osada, H. & Walsh, C. T. Enzymatic generation of the antimetabolite gamma,gamma-dichloroaminobutyrate by NRPS and mononuclear iron halogenase action in a streptomycete. *Chem Biol* **13**, 1183-1191 (2006).

60 Galonic, D. P., Barr, E. W., Walsh, C. T., Bollinger, J. M., Jr. & Krebs, C. Two interconverting Fe(IV) intermediates in aliphatic chlorination by the halogenase CytC3. *Nat Chem Biol* **3**, 113-116 (2007).

61 Neumann, C. S. & Walsh, C. T. Biosynthesis of (-)-(1S,2R)-allocoronamic acyl thioester by an Fe(II)-dependent halogenase and a cyclopropane-forming flavoprotein. *J Am Chem Soc* **130**, 14022-14023 (2008).

62 O'Hagan, D., Schaffrath, C., Cobb, S. L., Hamilton, J. T. & Murphy, C. D. Biochemistry: biosynthesis of an organofluorine molecule. *Nature* **416**, 279 (2002).

63 Eustaquio, A. S., Pojer, F., Noe, J. P. & Moore, B. S. Discovery and characterization of a marine bacterial SAM-dependent chlorinase. *Nat Chem Biol* **4**, 69-74 (2008).

64 Dong, C. J., Huang, F. L., Deng, H., Schaffrath, C., Spencer, J. B., O'Hagan, D. & Naismith, J. H. Crystal structure and mechanism of a bacterial fluorinating enzyme. *Nature* **427**, 561-565 (2004).

65 Smith, D. R. M., Gruschow, S. & Goss, R. J. M. Scope and potential of halogenases in biosynthetic applications. *Curr Opin Chem Biol* **17**, 276-283 (2013).

66 Leao, P. N., Nakamura, H., Costa, M., Pereira, A. R., Martins, R., Vasconcelos, V., Gerwick, W. H. & Balskus, E. P. Biosynthesis-assisted structural elucidation of the bartolosides, chlorinated aromatic glycolipids from cyanobacteria. *Angew Chem Int Ed Engl* **54**, 11063-11067 (2015).

67 Tibrewal, N. & Tang, Y. Biocatalysts for Natural Product Biosynthesis. *Annu Rev Chem Biomol* **5**, 347-366, doi:10.1146/annurev-chembioeng-060713-040008 (2014).

68 Butler, A. & Carter-Franklin, J. N. The role of vanadium bromoperoxidase in the biosynthesis of halogenated marine natural products. *Nat Prod Rep* **21**, 180-188, doi:10.1039/b302337k (2004).

69 Liu, M., Hansen, P. E. & Lin, X. K. Bromophenols in Marine Algae and Their Bioactivities. *Mar Drugs* **9**, 1273-1292 (2011).

70 Vetter, W. Marine halogenated natural products of environmental relevance. *Rev Environ Contam Toxicol* **188**, 1-57 (2006).

71 Janssen, D. B., Oppentocht, J. E. & Poelarends, G. J. Microbial dehalogenation. *Curr Opin Biotechnol* **12**, 254-258 (2001).

72 Vaillancourt, F. H., Yeh, E., Vosburg, D. A., O'Connor, S. E. & Walsh, C. T. Cryptic chlorination by a non-haem iron enzyme during cyclopropyl amino acid biosynthesis. *Nature* **436**, 1191-1194 (2005).

73 Gu, L., Wang, B., Kulkarni, A., Geders, T. W., Grindberg, R. V., Gerwick, L., Hakansson, K., Wipf, P., Smith, J. L., Gerwick, W. H. & Sherman, D. H. Metamorphic enzyme assembly in polyketide diversification. *Nature* **459**, 731-735 (2009).

74 Rokita, S. E., Adler, J. M., McTamney, P. M. & Watson, J. A. Efficient use and recycling of the micronutrient iodide in mammals. *Biochimie* **92**, 1227-1235 (2010).

75 Burkholder, P. R., Pfister, R. M. & Leitz, F. H. Production of a pyrrole antibiotic by a marine bacterium. *Appl Microbiol* **14**, 649-653 (1966).

76 Unson, M. D., Holland, N. D. & Faulkner, D. J. A Brominated Secondary Metabolite Synthesized by the Cyanobacterial Symbiont of a Marine Sponge and Accumulation of the Crystalline Metabolite in the Sponge Tissue. *Mar Biol* **119**, 1-11 (1994).

77 Teuten, E. L., Xu, L. & Reddy, C. M. Two abundant bioaccumulated halogenated compounds are natural products. *Science* **307**, 917-920 (2005).

78 Technical Fact Sheet –Polybrominated Diphenyl Ethers (PBDEs) and Polybrominated Biphenyls (PBBs). (2014).

79 Kimbrough, K. L., Johnson, W. E., Lauenstein, G. G., Christensen, J. D. & Apeti, D. A. An Assessment of Polybrominated Diphenyl Ethers (PBDEs) in Sediments and Bivalves of the U.S. Coastal Zone. 87 (Silver Spring, MD, 2009).

80 Sneed, J. M., Sharp, K. H., Ritchie, K. B. & Paul, V. J. The chemical cue tetrabromopyrrole from a biofilm bacterium induces settlement of multiple Caribbean corals. *Proc Biol Sci* **281** (2014).

81 Peschke, J. D., Hanefeld, U. & Laatsch, H. Biosynthesis of the marine antibiotic pentabromopseudilin. 2. The pyrrole ring. *Biosci Biotechnol Biochem* **69**, 628-630 (2005).

82 Al-Mourabit, A., Zancanella, M. A., Tilvi, S. & Romo, D. Biosynthesis, asymmetric synthesis, and pharmacology, including cellular targets, of the pyrrole-2-aminoimidazole marine alkaloids. *Nat Prod Rep* **28**, 1229-1260 (2011).

83 Smidt, H. & de Vos, W. M. Anaerobic microbial dehalogenation. *Annu Rev Microbiol* **58**, 43-73, doi:10.1146/annurev.micro.58.030603.123600 (2004).

84 Copley, S. D. Evolution of efficient pathways for degradation of anthropogenic chemicals. *Nat Chem Biol* **5**, 559-566, doi:10.1038/nchembio.197 (2009).

85 Nijenhuis, I. & Kuntze, K. Anaerobic microbial dehalogenation of organohalides-state of the art and remediation strategies. *Curr Opin Biotechnol* **38**, 33-38, doi:10.1016/j.copbio.2015.11.009 (2016).

86 Jugder, B. E., Ertan, H., Lee, M., Manefield, M. & Marquis, C. P. Reductive Dehalogenases Come of Age in Biological Destruction of Organohalides. *Trends Biotechnol* **33**, 595-610, doi:10.1016/j.tibtech.2015.07.004 (2015).

87 Hillas, P. J., del Alba, F. S., Oyarzabal, J., Wilks, A. & Ortiz De Montellano, P. R. The AhpC and AhpD antioxidant defense system of *Mycobacterium tuberculosis*. *J Biol Chem* **275**, 18801-18809, doi:10.1074/jbc.M001001200 (2000).

88 Darwent, B. d. in *National Standard Reference Data Series* (ed National Bureau of Standards) (1970).

89 Clarke, T. E., Romanov, V., Chirgadze, Y. N., Klomsiri, C., Kisselman, G., Wu-Brown, J., Poole, L. B., Pai, E. F. & Chirgadze, N. Y. Crystal structure of alkyl hydroperoxidase D like protein PA0269 from *Pseudomonas aeruginosa*: homology of the AhpD-like structural family. *BMC Struct Biol* **11**, 27, doi:10.1186/1472-6807-11-27 (2011).

90 Fomenko, D. E. & Gladyshev, V. N. Identity and functions of CxxC-derived motifs. *Biochemistry* **42**, 11214-11225, doi:10.1021/bi034459s (2003).

91 Poole, L. B. The catalytic mechanism of peroxiredoxins. *Subcell Biochem* **44**, 61-81 (2007).

92 Knoops, B., Loumaye, E. & Van Der Eecken, V. Evolution of the peroxiredoxins. *Subcell Biochem* **44**, 27-40 (2007).

93 Dubbs, J. M. & Mongkolsuk, S. Peroxiredoxins in bacterial antioxidant defense. *Subcell Biochem* **44**, 143-193 (2007).

94 Inaba, K. & Ito, K. Structure and mechanisms of the DsbB-DsbA disulfide bond generation machine. *Biochim Biophys Acta* **1783**, 520-529, doi:10.1016/j.bbamcr.2007.11.006 (2008).

95 McCarthy, D. L., Navarrete, S., Willett, W. S., Babbitt, P. C. & Copley, S. D. Exploration of the relationship between tetrachlorohydroquinone dehalogenase and the glutathione *S*-transferase superfamily. *Biochemistry* **35**, 14634-14642, doi:10.1021/bi961730f (1996).

96 Warner, J. R., Lawson, S. L. & Copley, S. D. A mechanistic investigation of the thiol-disulfide exchange step in the reductive dehalogenation catalyzed by tetrachlorohydroquinone dehalogenase. *Biochemistry* **44**, 10360-10368, doi:10.1021/bi050666b (2005).

97 Schweizer, U., Schlicker, C., Braun, D., Kohrle, J. & Steegborn, C. Crystal structure of mammalian selenocysteine-dependent iodothyronine deiodinase suggests a peroxiredoxin-like catalytic mechanism. *Proc Natl Acad Sci U S A* **111**, 10526-10531, doi:10.1073/pnas.1323873111 (2014).

98 Goto, K., Sonoda, D., Shimada, K., Sase, S. & Kawashima, T. Modeling of the 5'-deiodination of thyroxine by iodothyronine deiodinase: chemical corroboration of a selenenyl iodide intermediate. *Angew Chem Int Ed Engl* **49**, 545-547, doi:10.1002/anie.200905796 (2010).

99 Schweizer, U. & Steegborn, C. New insights into the structure and mechanism of iodothyronine deiodinases. *J Mol Endocrinol* **55**, R37-R52, doi:10.1530/Jme-15-0156 (2015).

100 Fortin, P. D., Horsman, G. P., Yang, H. M. & Eltis, L. D. A glutathione *S*-transferase catalyzes the dehalogenation of inhibitory metabolites of polychlorinated biphenyls. *J Bacteriol* **188**, 4424-4430, doi:10.1128/JB.01849-05 (2006).

101 Anandarajah, K., Kiefer, P. M., Jr., Donohoe, B. S. & Copley, S. D. Recruitment of a double bond isomerase to serve as a reductive dehalogenase during biodegradation of pentachlorophenol. *Biochemistry* **39**, 5303-5311 (2000).

102 Xun, L., Topp, E. & Orser, C. S. Purification and characterization of a tetrachloro-*p*-hydroquinone reductive dehalogenase from a *Flavobacterium* sp. *J Bacteriol* **174**, 8003-8007 (1992).

103 Kohler-Staub, D. & Leisinger, T. Dichloromethane dehalogenase of *Hyphomicrobium* sp. strain DM2. *J Bacteriol* **162**, 676-681 (1985).

104 Masip, L., Veeravalli, K. & Georgiou, G. The many faces of glutathione in bacteria. *Antioxid Redox Signal* **8**, 753-762, doi:10.1089/ars.2006.8.753 (2006).

105 Chivers, P. T., Prehoda, K. E. & Raines, R. T. The CXXC motif: a rheostat in the active site. *Biochemistry* **36**, 4061-4066, doi:10.1021/bi9628580 (1997).

106 John, E. A., Pollet, P., Gelbaum, L. & Kubanek, J. Regioselective syntheses of 2,3,4-tribromopyrrole and 2,3,5-tribromopyrrole. *J Nat Prod* **67**, 1929-1931, doi:10.1021/np0498399 (2004).

107 Emrich, R., Weyland, H. & Weber, K. 2,3,4-Tribromopyrrole from the Marine Polychaete *Polyphysia Crassa*. *Journal of Natural Products* **53**, 703-705, doi:DOI 10.1021/np50069a028 (1990).

108 Neu, A. K., Mansson, M., Gram, L. & Prol-Garcia, M. J. Toxicity of Bioactive and Probiotic Marine Bacteria and Their Secondary Metabolites in *Artemia* sp and *Caenorhabditis elegans* as Eukaryotic Model Organisms. *Appl Environ Microb* **80**, 146-153, doi:10.1128/Aem.02717-13 (2014).

109 Forte, B., Malgesini, B., Piutti, C., Quartieri, F., Scolaro, A. & Papeo, G. A submarine journey: the pyrrole-imidazole alkaloids. *Mar Drugs* **7**, 705-753, doi:10.3390/md7040705 (2009).

110 Stout, E. P., Wang, Y. G., Romo, D. & Molinski, T. F. Pyrrole aminoimidazole alkaloid metabiosynthesis with marine sponges *Agelas conifera* and *Stylissa caribica*. *Angew Chem Int Ed Engl* **51**, 4877-4881 (2012).

111 Lanman, B. A., Overman, L. E., Paulini, R. & White, N. S. On the structure of Palau'amine: Evidence for the revised relative configuration from chemical synthesis. *J Am Chem Soc* **129**, 12896-12900, doi:Doi 10.1021/Ja074939x (2007).

112 Ma, Z. Q., Lu, J. M., Wang, X. & Chen, C. Revisiting the Kinnel-Scheuer hypothesis for the biosynthesis of palau'amine. *Chem Commun* **47**, 427-429, doi:Doi 10.1039/C0cc02214d (2011).

113 Stout, E. P., Morinaka, B. I., Wang, Y. G., Romo, D. & Molinski, T. F. De novo synthesis of benzosceptrin C and nagelamide H from 7-15N-oroidin: implications for pyrrole-aminoimidazole alkaloid biosynthesis. *J Nat Prod* **75**, 527-530, doi:10.1021/np300051k (2012).

114 Genta-Jouve, G. & Thomas, O. P. Biosynthesis in marine sponges: the radiolabelling strikes back. *Phytochemistry Reviews* **12**, 425-434, doi:Doi 10.1007/S11101-012-9225-9 (2013).

115 Genta-Jouve, G., Cachet, N., Holderith, S., Oberhansli, F., Teyssie, J. L., Jeffree, R., Al Mourabit, A. & Thomas, O. P. New Insight into Marine Alkaloid Metabolic Pathways: Revisiting Oroidin Biosynthesis. *Chembiochem* **12**, 2298-2301, doi:Doi 10.1002/Cbic.201100449 (2011).

116 Wang, Y. G., Morinaka, B. I., Reyes, J. C., Wolff, J. J., Romo, D. & Molinski, T. F. Synthesis of 7-(15)N-Oroidin and evaluation of utility for biosynthetic studies of pyrrole-imidazole alkaloids by microscale (1)H-(15)N HSQC and FTMS. *J Nat Prod* **73**, 428-434, doi:10.1021/np900638e (2010).

117 Lansdell, T. A., Hewlett, N. M., Skoumbourdis, A. P., Fodor, M. D., Seiple, I. B., Su, S., Baran, P. S., Feldman, K. S. & Tepe, J. J. Palau'amine and Related Oroidin Alkaloids Dibromophakellin and Dibromophakellstatin Inhibit the Human 20S Proteasome. *J Nat Prod* **75**, 980-985, doi:Doi 10.1021/Np300231f (2012).

118 Seiple, I. B., Su, S., Young, I. S., Nakamura, A., Yamaguchi, J., Jorgensen, L., Rodriguez, R. A., O'Malley, D. P., Gaich, T., Kock, M. & Baran, P. S. Enantioselective Total Syntheses of (-)-Palau'amine, (-)-Axinellamines, and (-)-Massadines. *J Am Chem Soc* **133**, 14710-14726, doi:Doi 10.1021/Ja2047232 (2011).

119 Seiple, I. B., Su, S., Young, I. S., Lewis, C. A., Yamaguchi, J. & Baran, P. S. Total Synthesis of Palau'amine. *Angew Chem Int Edit* **49**, 1095-1098, doi:Doi 10.1002/Anie.200907112 (2010).

120 Kock, M., Grube, A., Seiple, I. B. & Baran, P. S. The pursuit of Palau'amine. *Angew Chem Int Edit* **46**, 6586-6594, doi:Doi 10.1002/Anie.200701798 (2007).

121 Hentschel, U., Piel, J., Degnan, S. M. & Taylor, M. W. Genomic insights into the marine sponge microbiome. *Nat Rev Microbiol* **10**, 641-U675 (2012).

122 Bright, M. & Bulgheresi, S. A complex journey: transmission of microbial symbionts. *Nat Rev Microbiol* **8**, 218-230 (2010).

123 Noyer, C. & Becerro, M. A. Relationship between genetic, chemical, and bacterial diversity in the Atlanto-Mediterranean bath sponge *Spongia lamella*. *Hydrobiologia* **687**, 85-99 (2012).

124 Schmitt, S., Tsai, P., Bell, J., Fromont, J., Ilan, M., Lindquist, N., Perez, T., Rodrigo, A., Schupp, P. J., Vacelet, J., Webster, N., Hentschel, U. & Taylor, M. W. Assessing the complex sponge microbiota: core, variable and species-specific bacterial communities in marine sponges. *Isme J* **6**, 564-576 (2012).

125 Gurgui, C. & Piel, J. Metagenomic Approaches to Identify and Isolate Bioactive Natural Products from Microbiota of Marine Sponges. *Metagenomics: Methods and Protocols* **668**, 247-264, doi:Doi 10.1007/978-1-60761-823-2_17 (2010).

126 Tasdemir, D., Mallon, R., Greenstein, M., Feldberg, L. R., Kim, S. C., Collins, K., Wojciechowicz, D., Mangalindan, G. C., Concepcion, G. P., Harper, M. K. & Ireland, C. M. Aldisine alkaloids from the Philippine sponge Stylissa massa are potent inhibitors of mitogen-activated protein kinase kinase-1 (MEK-1). *J Med Chem* **45**, 529-532 (2002).

127 Brady, S. F., Simmons, L., Kim, J. H. & Schmidt, E. W. Metagenomic approaches to natural products from free-living and symbiotic organisms. *Nat Prod Rep* **26**, 1488-1503 (2009).

128 Keegan, K. P., Glass, E. M. & Meyer, F. *MG-RAST, a Metagenomics Service for Analysis of Microbial Community Structure and Function*. Vol. 1399 (2016).

129 Bayer, K., Scheuermayer, M., Fieseler, L. & Hentschel, U. Genomic Mining for Novel FADH(2)-Dependent Halogenases in Marine Sponge-Associated Microbial Consortia. *Marine Biotechnol* **15**, 63-72 (2013).

130 Tang, X., Li, J., Millan-Aguinaga, N., Zhang, J. J., O'Neill, E. C., Ugalde, J. A., Jensen, P. R., Mantovani, S. M. & Moore, B. S. Identification of Thiotetronic Acid Antibiotic Biosynthetic Pathways by Target-directed Genome Mining. *ACS Chem Biol* **10**, 2841-2849, doi:10.1021/acschembio.5b00658 (2015).

131 Tomasic, T., Katsamakas, S., Hodnik, Z., Ilas, J., Brvar, M., Solmajer, T., Montalvao, S., Tammela, P., Banjanac, M., Ergovic, G., Anderluh, M., Peterlin Masic, L. & Kikelj, D. Discovery of 4,5,6,7-Tetrahydrobenzo[1,2-d]thiazoles as Novel DNA Gyrase Inhibitors Targeting the ATP-Binding Site. *J Med Chem* **58**, 5501-5521, doi:10.1021/acs.jmedchem.5b00489 (2015).

132 Geladopoulos, T. P., Sotiroudis, T. G. & Evangelopoulos, A. E. A Malachite Green Colorimetric Assay for Protein Phosphatase-Activity. *Anal Biochem* **192**, 112-116 (1991).

133 Walsh, C. T., Garneau-Tsodikova, S. & Howard-Jones, A. R. Biological formation of pyrroles: nature's logic and enzymatic machinery. *Nat Prod Rep* **23**, 517-531 (2006).

134 Tianero, M. D., Kwan, J. C., Wyche, T. P., Presson, A. P., Koch, M., Barrows, L. R., Bugni, T. S. & Schmidt, E. W. Species specificity of symbiosis and secondary metabolism in ascidians. *Isme J* **9**, 615-628 (2015).

135 Wilson, M. C. & Piel, J. Metagenomic approaches for exploiting uncultivated bacteria as a resource for novel biosynthetic enzymology. *Chem Biol* **20**, 636-647 (2013).

136 Nutzmann, H. W. & Osbourn, A. Gene clustering in plant specialized metabolism. *Curr Opin Biotechnol* **26**, 91-99 (2014).

137 Srivastava, M., Simakov, O., Chapman, J., Fahey, B., Gauthier, M. E., Mitros, T., Richards, G. S., Conaco, C., Dacre, M., Hellsten, U., Larroux, C., Putnam, N. H., Stanke, M., Adamska, M., Darling, A., Degnan, S. M., Oakley, T. H., Plachetzki, D. C., Zhai, Y., Adamski, M., Calcino, A., Cummins, S. F., Goodstein, D. M., Harris, C., Jackson, D. J., Leys, S. P., Shu, S., Woodcroft, B. J., Vervoort, M., Kosik, K. S., Manning, G., Degnan, B. M. & Rokhsar, D. S. The Amphimedon queenslandica genome and the evolution of animal complexity. *Nature* **466**, 720-726 (2010).

138 Lee, O. O., Chui, P. Y., Wong, Y. H., Pawlik, J. R. & Qian, P. Y. Evidence for vertical transmission of bacterial symbionts from adult to embryo in the Caribbean sponge *Svenzea zeai*. *Appl Environ Microbiol* **75**, 6147-6156 (2009).